MAX-PLANCK-INSTITUT FÜR QUANTENOPTIK

# Optical Second-Harmonic Investigations of the Kinetics of Elementary Surface Reactions on Si(001) and Si(111)

Markus B. Raschke

**MPQ-Report**
**246**

MPQ 246 Mai 1999

Max-Planck-Institut für Quantenoptik
85740 Garching, Bundesrepublik Deutschland

MAX-PLANCK-INSTITUT FÜR QUANTENOPTIK

# Optical Second-Harmonic Investigations of the Kinetics of Elementary Surface Reactions on Si(001) and Si(111)

Markus B. Raschke

MPQ 246

Mai 1999

*Let every student of nature take this as his rule that whatever the mind seizes upon with particular satisfaction is to be held in suspicion.*

Francis Bacon

# Summary

Resonant enhancement of optical second-harmonic generation (SHG) from silicon surfaces by dangling-bond-derived surface states makes this technique a very sensitive and versatile *in situ* monitor for surface coverage of hydrogen and other adsorbates. The ability to monitor hydrogen adsorption in real time allowed to distinguish between different reaction channels for dissociative adsorption of $H_2$ on vicinal Si(001) and Si(111) surfaces in the temperature range between 450 and 650 K. Whereas the presence of steps on Si(111) leads only to a moderate increase in reactivity, the initial sticking coefficients for step adsorption on misoriented Si(001) exceed those determined for terrace adsorption by several orders of magnitude. For double height-steps on Si(001) the values increase from $10^{-8}$ to $10^{-4}$ in the investigated temperature range from 90 to 600 K. In contrast to terrace adsorption this is a weak dependence on temperature and corresponds to an activation energy of 0.09 eV. The pronounced rise of the sticking coefficient from below $10^{-10}$ at 400 K to nearly $10^{-4}$ at 1000 K for the terrace sites indicates the presence of an adsorption barrier of at least 0.75 eV. Within the range of misorientations investigated the sticking coefficients attributed to terrace adsorption and their temperature dependence agree with each other and with previously reported values from the flat surface. Density functional theory calculations of Kratzer, Pehlke, and Scheffler indicate the presence of a direct adsorption path for monohydride formation, but with a dramatically reduced barrier for step adsorption due to efficient rehybridization of dangling-bond orbitals.

Both the independence of the sticking coefficients from step density, and the observation that the adsorbed hydrogen atoms are rather immobile up to surface temperatures of $\sim$600 K rule out reaction mechanisms in which hydrogen adsorption on the terraces proceeds via steps or other static defect sites. These results together with high-flux supersonic molecular-beam experiments provide strong evidence of a direct mechanism within the framework of phonon-assisted sticking. In addition, the existence of two new inter-dimer reaction pathways could be verified which provide an important contribution to the understanding of the underlying forces which govern both, dissociative adsorption and recombinative desorption from the Si(001) surface.

Hydrogen diffusion on silicon surfaces was investigated by making use of the intrinsic chemical properties of vicinal Si(001). These allowed for the formation of a periodic non-equilibrium hydrogen concentration profile, taking advantage of the different adsorption energy barriers for the step as compared with terrace adsorption.

Monitoring the transition to thermal equilibrium of the surface coverage an activation barrier for step-to-terrace diffusion of $1.7 \pm 0.15$ eV was determined. In the context of these diffusion experiments, a promising new method for studying mass transport diffusion of strongly bound chemisorbates was established utilizing of rare-gas templates for formation of monolayer gratings and detection with linear optical diffraction.

From measurements of the equilibrium hydrogen coverage the steps are found to be energetically favored with a $H_2$ chemisorption energy difference of $\sim 0.2$ eV between step and terrace sites. The preferred binding of the hydrogen atoms to the rebonded silicon step edge atoms is in accordance with density functional calculations of Pehlke and Kratzer.

The binding energy of hydrogen with a well-defined silicon surface was determined for the first time by a novel experimental approach. A bakeable UHV quartz apparatus was used to establish thermal equilibrium between the gas phase and Si(111)7×7 at $H_2$ pressures of $10^{-5} - 1$ mbar and temperatures of 770 - 980 K. The resulting isotherms measured *in situ* with SHG allowed precise determination of the hydrogen binding energy and its dependence on surface coverage. For H/Si(111)7×7 in the investigated coverage range between 0.05 ML and 0.3 ML the bond energy increases from 2.9 to 3.15 eV. These values are compatible with the large barrier for phonon-assisted sticking of $H_2$/Si. The Si–H bond is thus found to be considerably weaker than hydrogen bonding in silanes (3.7 to 3.9 eV).

As an example of the applicability of SHG for addressing elementary reaction steps in the case of adsorbates which interact with the surface in a more complex way, isothermal desorption of SiO from Si(001) was investigated. The desorption kinetics could be studied over a wide range of desorption rates ($10^{-1}$ to $10^{-6}$ ML $s^{-1}$). From their temperature dependence between 780 and 1000 K an activation energy of $E_A = 3.4 \pm 0.2$ eV and pre-exponential factor of $\nu_0 = 10^{16\pm1} s^{-1}$ were obtained. A pronounced decrease of the first-order rate constants was observed with an increase of initial coverage from 0.02 to 0.6 ML. These results were interpreted in terms of coverage-dependent oxygen-binding configurations, which influence the stability of the oxide layer.

# Contents

# Chapter 1

# Introduction

The investigation of the chemistry of single-crystal silicon surfaces has been a significant driving force in surface science and still attracts great interest in both basic and applied research. In particular, microscopic understanding of semiconductor surface reactions might play an increasingly important role in the future for the fabrication of electronic devices, where, in going to miniature surface structures, atomic level properties will assume a greater role. In this respect the interaction of hydrogen with silicon surfaces has been of ongoing scientific interest since the early days of surface science [1–19].

Many of the chemical reactions applied in silicon wafer processing leave hydrogen on the surface, making the desorption of $H_2$ a possible rate-limiting step in epitaxial growth or chemical vapor deposition [20–23]. From a fundamental point of view, hydrogen on silicon serves as a prototype for studying elementary reaction steps of covalently bound adsorbates. Hydrogen is the simplest possible chemisorbate and the (001) and (111) single crystal faces of silicon are the best characterized semiconductor surfaces. In the monohydride state, a single hydrogen atom binds to one silicon surface atom and the local geometry and electronic structure have been studied intensively and are well understood today [2–8].

Investigations of the kinetical and dynamical properties of hydrogen on silicon have just begun in recent years and a number of phenomena that are in various respect different from that typical for metal surfaces have been discovered experimentally [9–14]. Whereas the focus of these studies mainly was on recombinative desorption and surface diffusion, the issue which has attracted particular interest recently, concerns the dissociative adsorption of molecular hydrogen. The corresponding sticking probabilities on well-ordered single crystal surfaces have long been considered to be unmeasureably small for gas at room temperature with upper limits put forth between $10^{-6}$ and $10^{-8}$ [1,24,25]. Making use of the high sensitivity of the technique of optical second-harmonic generation (SHG) the dissociative adsorption could first be detected by our group and the extremely small sticking coefficients were measured [14,26,27]. The reaction was found to be characterized by a pronounced dependence on surface temperature. This observation indicated that strong dynamic lattice distortions are important for the dissociation process and confirmed corresponding theoretical pre-

dictions [28,29]. The proposed model of phonon-assisted sticking, however, has been questioned on the basis of ab initio cluster calculations and unresolved quantitative discrepancies between the results of dynamical studies using *ab initio* potential energy surfaces and the experiments prevailed [15,18,19,30,31]. In addition, experiments performed simultaneously by another group using molecular beam techniques were at variance with the SHG measurements [32].

On the basis of this status of the experimental and theoretical work it has not been possible to give a definite answer concerning the different reaction mechanisms proposed. In particular for Si(001), the influence of steps and defects or subtle electronic effects have been discussed. This led to an ongoing debate concerning the influence of surface minority sites, hydrogen surface diffusion, and energy balance between adsorption and desorption - issues which are addressed in this work.

The presence of steps and defects provides an experimental challenge to separate the chemistry of these minorities from the chemical properties of the pristine surface. Although scanning tunneling microscopy (STM) has the ideal capability for studying atom-resolved reactions of isolated adsorption sites, kinetic information about the reaction is not easily obtained. Measurements of the temporal behavior of reactions over a wide range of rates and surface temperatures are not accessible with STM, particularly due to its limited time resolution. Here the properties of SHG – *in situ* applicability, high adsorbate sensitivity, non-destructive character, and symmetry selectivity – make it an advantageous technique compared with other surface probes to investigate the kinetics of surface chemical processes.

The first part of this work therefore reports on investigations focussed on the reaction of molecular hydrogen with deliberately created steps and defects on Si(001) and Si(111), which will be compared with flat, well-ordered surfaces. The assumption of enhanced reactivity of the steps is intuitively tempting, but not convincing due to the unchanged coordination number of step edge atoms compared to terrace sites. Strikingly, however, up to six orders of magnitude higher reactivities for double-height steps could be observed for Si(001) and explained with a barrier-free adsorption pathway found on the basis of density functional theory (DFT) calculations, performed in close collaboration with the experiments.

An important aspect concerning equilibrium properties of an adsorbate is surface diffusion. Due to the large diffusion barriers associated with covalently bound adsorbates, experiments are in general difficult to perform. Here both the creation of a lateral adsorbate concentration gradient and its *in situ* detection could be realized using vicinal surfaces. The difference in reactivity between the step and terrace sites implies creation of the non-equilibrium distribution of hydrogen on the stepped surface under certain reaction conditions. In combination with a special choice of incident polarization that enables site-selective determination of the hydrogen distribution, the kinetics of the hydrogen diffusion from the steps onto the terraces could be investigated. From the final equilibrium distribution the difference in binding energy between the step and terrace sites could be determined and compared with first principles calculations.



Despite its importance as a fundamental quantity describing the H/Si system, the hydrogen bond energy with single crystal silicon surfaces has not yet been determined. Thermodynamic measurements would provide a view of the chemisorption complementary to measurements of the kinetic parameter governing the reaction. Independent determination of the binding energy would therefore allow to check for consistency of the energetics established with the energy barriers determined from adsorption and desorption. The experimental difficulty arises from the high adsorption barrier which requires high temperatures to establish equilibrium. This could be realized in a novel experiment by performing hydrogen adsorption measurements in a high-temperature (1200 K) quartz-UHV-chamber – using SHG as the ultimate probe. These measurements of the adsorption isotherms necessary for determining the heat of the reaction take place under ambient reaction conditions virtually inaccessible by other than optical probes.

Having used SHG as the major probe for studying the elementary reaction steps of hydrogen on silicon, one is tempted to apply this technique also as a quantitative probe for chemisorbates which interact with the surface in a more complex way. After performing an adequate calibration the isothermal desorption of SiO from oxidized silicon surfaces has been studied over a wide dynamical range of rates. Despite the technological importance of oxygen on silicon and the vast number of studies which have been devoted to this system, this study brings new insight into the desorption mechanism.

The first chapter of this thesis gives a background overview of clean silicon surfaces and their reaction dynamics with hydrogen. Then the technique of second-harmonic generation is introduced. In the chapter which follows, the experimental setup and methods used are described. In chapter 4 and the ensuing chapters the experimental results of the interaction of molecular hydrogen with defects and steps will be addressed. Different inter-dimer reaction pathways for terrace adsorption and their implications are discussed. The hydrogen diffusion on stepped surfaces and the determination of the binding energy difference between step and terrace sites is presented. The isosteric heat of adsorption measurements are discussed in chapter 5. The last chapter deals with the isothermal desorption of SiO. In the appendix a new linear optical diffraction and rare-gas template technique is demonstrated and its applicability to perform surface diffusion measurements is discussed.

# Chapter 2

# Hydrogen on silicon and second-harmonic generation

Few experimental techniques have contributed to evaluation of the kinetics and dynamics of hydrogen interaction with silicon surfaces to the same extent as optical second-harmonic generation (SHG). This chapter reviews the principal properties of both the system under investigation and SHG as the major probe.

## 2.1 Clean silicon surfaces

Group IV semiconductors crystallize in a diamond structure and cleaving these covalent crystals leaves broken tetrahedral bonds at the surface. These bonds - commonly referred to as dangling bonds (db) - are highly directional with electrons localized both spatially and energetically. In recent years, in particular the field of electronic structure calculations has contributed significantly to determining the equilibrium configurations of clean semiconductor surfaces. This led to a high degree of understanding of their structural and electronic properties.

The various silicon surface planes have been the subject of comprehensive book chapters [33,34] and reviews [35–37] and therefore only the basic properties of Si(001) and Si(111) surfaces are summarized here to the extent required for understanding the results of this work.

### Planar Si(001)2×1

The nominally flat Si(001) surface with its square unit cell reconstructs in a 2×1 or more complex superlattice structure. This proceeds by pairing of neighboring silicon atoms into dimers via formation of a $\sigma$-bond reducing the dangling bond density from two to one per surface atom, leading to the formation of rows of dimers along the [110] direction [38,39]. A ball-and-stick model of the Si(001)2×1 surface is shown in Fig. 2.1.

The dimer bond length is about 2.3 Å, slightly shorter than the Si–Si distance of 2.35 Å in the bulk [34,37]. The dangling bonds are comparatively close together and

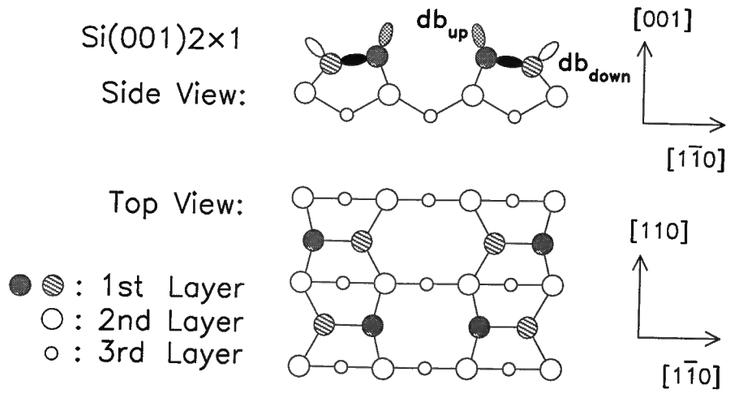


**Fig. 2.1:** Schematic of arrangement of dimer pairs on the 2×1 reconstructed Si(001) surface (side and top views). If neighboring dimer rows buckle in the opposite direction, this results in a c(4×2) superstructure.

are the origin of narrow bands of surface states localized in the energy gap separating the valence from the conduction band. The surface can further lower its energy by relaxation, similar to Jahn-Teller distortion, in which the symmetric dimers become asymmetric. This opens an energy gap between the highest-occupied and lowest-unoccupied surface states which gives rise to an insulating as opposed to a metallic surface. The calculated dangling bond bands originating from the asymmetric dimers are plotted in Fig. 2.2. The resulting surface gap of 0.7 eV is in good agreement with experimental results ranging from 0.44 to 0.9 eV [37].

The dimers are tilted at an angle of $\sim 19°$, which lowers their energy by $\sim 0.14$ eV compared with symmetric 2×1 dimers [42]. In the ground state of the surface the dimers are alternatingly buckled because of elastic coupling in the second and lower layers. The resulting c(4×2) structure (antiferromagnetic ordering) was found to be energetically favored by 0.05–0.07 eV per dimer over the p(2×1) reconstruction. Due to this small energy, however, this superstructure is only stable at low temperatures [43] and already at room temperature the dimers dynamically flip between their two asymmetric configurations [44–46].

Electronically the Si atom that is raised adopts a puckered $sp^3$ configuration, increasing the $s$-state character of the dangling bond. In contrast, the lowered one takes a nearly planar $sp^2$-like configuration which increases the $p$-state character of its db. The resulting energy difference leads to a net charge transfer from the lower $p$-like db, increasing the occupation of the db at the upper Si atom. Calculated contour plots are shown in Fig. 2.3 for the valence charge density (left) and valence charge



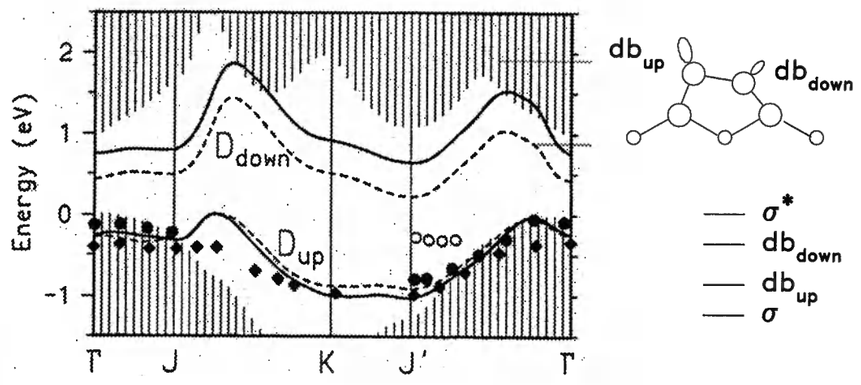


**Fig. 2.2:** Calculated GWA (solid lines) and LDA (dashed lines) dangling-bond band structure for asymmetric 2×1 dimers on Si(001). The symbols refer to photoemission data [40,41] (from Ref. [37]).

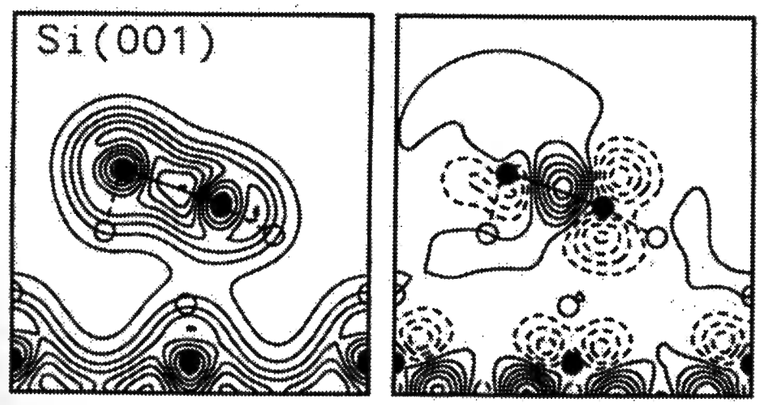


**Fig. 2.3:** Contour plot of the total charge density (left) and differences between a superposition of atomic valence charge densities (right) for Si(001)2×1 (from Ref. [42]).

density difference compared with a superposition of the atomic values (right). The extended $sp^3$-like orbital at the upper Si atom is able to concentrate charge, leaving depletion at the lower Si atom. This asymmetric charge distribution could be observed experimentally by scanning tunneling spectroscopy [47]. The two corresponding states can then only weakly interact compared with the $\pi$-bond that would be formed if the two Si atoms take the same height. The stabilization energy has been found to be in the range of 0.2 to 0.4 eV, determined both experimentally [11] and theoretically [48–50].

### Defects

Steps and defects are the most common types of surface irregularities and various types have been identified on silicon surfaces [39,43,51]. Even on well-prepared Si(001) defects seem to amount to a density of a few per cent [52]. Whereas adatom defects are rarely observed on silicon surfaces, vacancy defects prevail with the most common type being referred to as the 'a-type' defect, interpreted as a dimer vacancy. Another type is called 'c-type'. It corresponds to two missing silicon atoms from the same side of adjacent Si-dimers in the same row.

The defects are found to alter the electronic structure of the surface locally [53,54]. In addition, they can exert a long-range strain field which can effect the surface geometry. The vacancy defects, for instance, are found to stabilize the buckling in adjacent dimers [43,47]. STM investigations found, however, that the true defect density is smaller since many of the apparent defects are not due to missing atoms but rather represent contaminants [53,55,56]. Calculations suggest that a perfectly ordered surface is only slightly favored energetically in relation to a surface containing dimer vacancies [57]. Under experimental conditions a certain, but non-equilibrium, defect distribution in annealed samples is therefore expected. However, there is also a strong extrinsic component for defect formation. For Si(001), which in general is more reactive than Si(111), it is known that exposing the surface to monovalent adsorbates such as hydrogen or chlorine at elevated temperatures can reduce the defect concentration [8,58].

### Vicinal Si(001)

Crossing a single layer height step, the directions of the dangling bonds rotate by 90° because of the tetrahedral bonding of silicon. As a result the dimer rows of consecutive terraces are oriented perpendicular to each other. Four different types of steps are distinguished on Si(001), including the double-layer-height steps created for larger miscut angles. These configurations are shown in Fig. 2.4 and denoted according to the nomenclature introduced by Chadi [59]. $S$ and $D$ represent single- and double-layer-height steps respectively, with the subscripts A and B indicating whether the dimer bonds are perpendicular (A) or parallel (B) to the step edge. The $S_A$ step is lowest in energy since it does not lead to the formation of large strain or extra dangling bonds. This explains why in STM observation the $S_A$ steps are straight whereas the $S_B$ steps in general are rough and meander [51]. Kinks in these $S_B$ steps create energetically favorable $S_A$ segments.

The presence of steps is an intrinsic property of the Si(001) surface because the anisotropic stress (tensile stress parallel to the surface dimers and compressive stress in the perpendicular direction) of the 2×1 reconstructed surface would cause a perfectly flat surface to break up in alternating 2×1 and 1×2 domains [60,61]. Although the $S_A$-type step has the lowest energy, $D_B$ steps prevail on the surface for sufficiently large



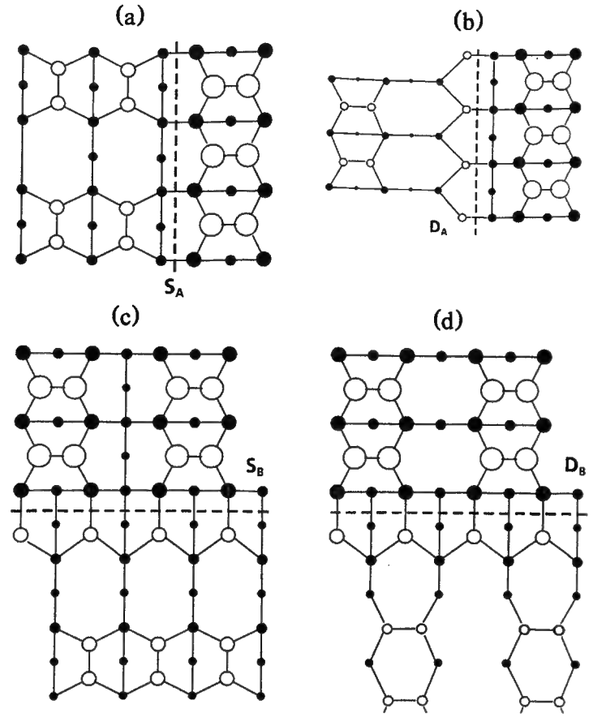


**Fig. 2.4:** Schematic top views of $S_A$, rebonded $D_A$, $S_B$, and $D_B$ steps, respectively ((a)–(d)). The surface normal is tilted from the (001) direction towards [$\bar{1}$10] ((a) and (b)) or [110] ((c) and (d)). Please note that all dimers are asymmetric (from Ref. [59]).

miscut angles since they are energetically favored over $S_A$+$S_B$ and $D_A$ steps [59,60]. If the surface misorientation is then accommodated by double-layer steps, the periodicity becomes primitive and the surface exhibits single-domain orientation. The regular arrays of the $D_B$ steps on vicinal Si(001) have been observed with low-energy electron diffraction (LEED) and STM [62,63]. The continuous transition between single-layer and double-layer steps has been calculated to occur between $\alpha_c \approx 1.2° - 2.5°$ [60,64] in agreement with the limits between 1° and 3.5° found experimentally [62,65,66]. In principle, two types of step edge structures are possible, but only the "rebonded-edge" configurations as shown in Fig. 2.4 with the additional step edge atom bound to the upper terrace is realized.

**Si(111)7×7**

The (111) face of silicon is the natural cleavage plane with the lowest surface tension. In this [111] direction the silicon crystal has a double layer structure. Therefore, and in contrast to the dimer pairing reconstruction of the Si(001) surface, the Si(111) surface exhibits different and more complex reconstructions, with the 7×7 being the most important one. The 7×7 reconstruction forms irreversibly after cleaving and annealing the crystal [38,67], and is explained with the dimer-adatom stacking fault (DAS) model [68]. This structure is the most stable of a series of ($n$×$n$) ($n$ odd) DAS reconstructions [36]. Top and side view of the structure of the unit cell are shown in Fig. 2.5.

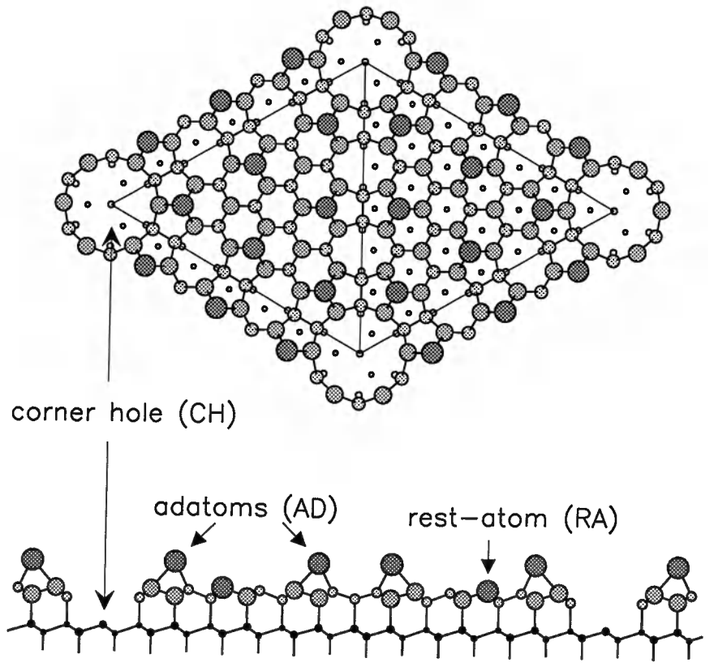


**Fig. 2.5:** Model of the Si(111)-7×7 surface (top and side views) with its double-layer structure. Circles of decreasing size indicate different heights.

This massive reconstruction leads to reduction of the initially 49 dangling bonds to 19 with formation of three structurally different sites – 12 located at atoms of the outer adatom layer, 6 at the corresponding rest-atom layer and one db-site at the silicon atom in the corner hole. The number of dangling bonds is therefore only 19/49 of the density of surface atoms. With a minimum distance of over 4 Å between the db's, this value is much greater than on the Si(001) surface.



As a result of the inward (outward) relaxation of the surface adatom (rest-atom) layer the dangling bond states become more $p_z$-($s$-) like. The surface Si-atom back-bonds result in additional surface state bands below and within the valence band. The charge transfer from the adatoms to the rest-atoms leaves the corresponding dangling bonds almost completely empty and filled, respectively [69]. Since atoms move away from their ideal position, this relaxation induces additional strain.

## 2.2 Hydrogen interaction with silicon surfaces

Whereas the basic properties concerning the hydrogen bonding geometry are already well understood, the dynamical aspects of hydrogen interaction have become the subject of extensive experimental and theoretical efforts. As a result of the work of the past decade, it is now well established that the spatially localized electronic states on silicon surfaces give rise to a reaction behavior in various respects different from that typical for metal surfaces. One manifestation is the occurrence of strong dynamic lattice distortions in diffusion, recombinative desorption and dissociative adsorption. A detailed understanding of the underlying microscopic phenomena is therefore highly desirable from a fundamental point of view.

This chapter briefly reviews what is known about surface structure after hydrogen termination, followed by a discussion of the present understanding of the kinetics and dynamics of surface diffusion, recombinative desorption and dissociative adsorption. For general reviews concerning the hydrogen-terminated surface see Ref. [4,8]. Further details concerning the dynamic properties see Ref. [7,15–18].

### 2.2.1 Hydrogen-terminated silicon surfaces

The Si–H bond is the prototype of a chemical bond with a semiconductor surface and the structural aspects of hydrogen-terminated Si(001) and Si(111) surfaces are well understood today [4,8,33].

Hydrogen-terminated silicon surfaces can be produced preferably by exposure to atomic hydrogen produced by predissociation of $H_2$ or wet chemical etching in HF solution [70,71]. On Si(001) in the monohydride phase each surface silicon atom is terminated with one hydrogen atom, i.e. the 2×1 reconstruction is preserved. This can be achieved preferably by exposure at surface temperatures around 600 K. Since the Si–H bond is considerably stronger than that of Si–Si, higher hydrides can be formed by extended exposure at reduced temperatures. In the dihydride phase e.g., where the dimer bond is broken, two hydrogen atoms reside on one Si atom.

In its atomic form hydrogen chemisorbs on all silicon surfaces with a high sticking probability. The silicon dangling bonds easily interact with singly occupied H-1$s$ orbital and rehybridize, resulting in covalent Si–H bond formation. This reaction removes the dangling-bond surface state from the band gap region and produces new

hydrogen-induced $\sigma$-bonding and $\sigma^*$-antibonding states at lower and higher energies, respectively [4]. As a consequence the buckling of the dimers on Si(001)2×1 is released. Due to the loss of the stabilization energy between the dangling bonds, the SI-dimer bond length becomes slightly longer compared with the clean surface. In addition, as a result of the new surface relaxation the backbond surface states are indirectly modified.

### 2.2.2 Recombinative desorption and hydrogen diffusion

Hydrogen desorbs molecularly from silicon surfaces and one might expect a process wherein two atoms diffuse and recombine at random to be second-order in surface coverage. This was observed by Reider *et al.* applying SHG to perform isothermal desorption measurements for Si(111)7×7 and the activation energy was found to be 2.4±0.1 eV [10]. This value is in agreement with the desorption barriers found by others from the analysis of temperature-programmed desorption (TPD) and laser-induced thermal desorption (LITD) experiments [24,72–75]. Both the isothermal technique together with the high sensitivity of SHG at low coverages allowed a detailed analysis of the reaction kinetics over a wide range of temperatures and coverages. From the temporal behavior of coverage below 0.1 ML noninteger order behavior was observed and has been attributed to two types of inequivalent adsorption sites (adatoms/rest-atoms), having different binding energies [10,74]. This two-site model was supported recently by *ab initio* calculations [76,77] which found a fairly good agreement with the proposed value of $\Delta E \simeq 0.15$ eV.

In contrast, desorption of $H_2$ from Si(001)2×1 obeys first-order kinetics, with an activation barrier of $2.5 \pm 0.1$ eV [9,11,73,78]. This behavior could be explained by assuming that it would be energetically favorable for the two hydrogen atoms to reside on the same Si-dimer rather than exist independently on the surface [11,48]. This pairwise occupation of the same dimer would be due to the weak $\pi$-like interaction between the dangling bonds of unoccupied dimers and has been observed with STM [79,80]. For low hydrogen coverages the entropy gain, however, would favor a random distribution and the kinetics would change to second order. In isothermal desorption experiments Höfer *et al.* were able, again using SHG, to accurately determine the desorption kinetics down to $\sim 0.003$ ML [11]. From the observed deviations from first-order for coverages below 0.05 ML a pairing energy of $0.25 \pm 0.05$ eV could be derived [11]. This paring energy has been suggested on the basis of early cluster calculations [81,82] and reproduced accurately on the basis of *ab initio* slab calculations [50,83]. Recent theoretical investigations suggest that there are additional interactions between adjacent dimers and for instance found an interaction energy of $\sim$0.3 eV between neighboring single-occupied dimers of the same orientation [49,84]. Besides the reaction mechanism where the hydrogen would desorb in a concerted fashion from its paired configuration from the dimer, other mechanisms have been proposed involving



dihydride intermediates formed at steps and single-atom defects, and the different models will be discussed below.

Measurements of hydrogen diffusion on Si(111)7×7 found a barrier of 1.5 eV, which is equivalent to nearly 2/3 of the desorption barrier and about half of the expected binding energy [12]. This is in contrast to metal surfaces, where the barrier heights are typically less than 20% of the desorption barrier [85]. This large lateral corrugation is due to the localized Si–H bond and could be well reproduced in recent theoretical investigations [76,86]. However, only in conjunction with a concerted displacement of the silicon adatom, are the hydrogen atoms able to diffuse from one site to the other. In that case, one of the three adatom backbonds is nearly broken when the H reaches the transition state with the neighboring rest-atom site. In contrast, assuming a static lattice the Si–H bond would have to be almost broken, leading to much higher barriers [87]. Similarly, calculations for hydrogen diffusion on Si(001)2×1 indicate a strong effect of silicon atom distortions on the energetics of the process [88–90]. These results already suggest that lattice relaxations also play a crucial role in explaining the results of recombinative desorption and dissociative adsorption.

### 2.2.3 Considerations of detailed balance in adsorption and desorption

In contrast to atomic hydrogen, which readily reacts with silicon dangling bonds [1], the small sticking probabilities of $\leq 10^{-6}$ for $H_2$ with this limit put forth early [24,25], imply that dissociative adsorption is an activated process with a barrier of $E_a \geq 0.5$ eV [1,13,14,26,32]. This activation barrier for $H_2$ adsorption is due to a large separation of Si dangling bonds and the near rare-gas-type electronic configuration of the $H_2$ molecule. Detailed balance requires the energy distribution of the desorbing

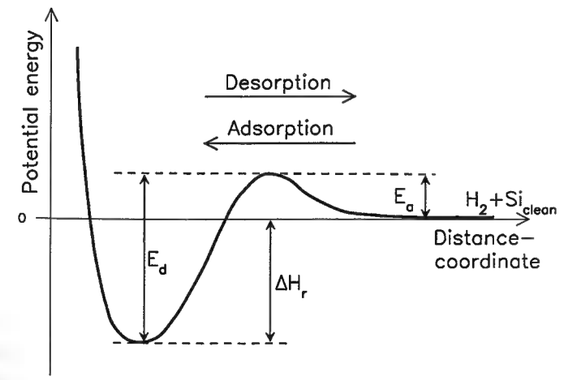


**Fig. 2.6:** Schematic energy diagram for adsorption and desorption.

molecules to be consistent with the activation barrier height for adsorption. This is illustrated in Fig. 2.6 in the form of a one-dimensional potential energy diagram. However, laser-induced desorption (LID) experiments showed that the total rotational, vibrational, and translational energy of the desorbing molecules did not substantially exceed the value expected for thermal equilibrium with the surface [13,91–94]. Theses findings would only be compatible with $E_a \leq 0.1$ eV. In addition, the similar results for Si(111)7×7 compared to Si(001)2×1 indicate that the dynamics is quite insensitive to the surface structure.

In order to explain this asymmetry between adsorption and desorption, Brenig and co-workers developed a model assuming that excess energy, if not deposited in the desorbing molecule, must be left in the selvage [28]. A two-dimensional potential energy surface (PES) has been proposed with one coordinate corresponding to a surface oscillator and the other to the distance of the molecule from the surface, as shown in Fig. 2.7.

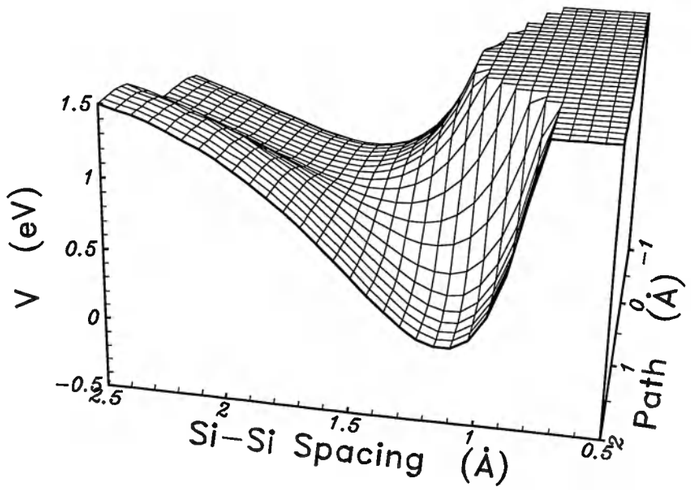


**Fig. 2.7:** Model potential for the interaction of molecular hydrogen with the silicon surface as seen from the gas phase side. The Si–Si spacing represents lattice distortions such as dimer stretch or tilt on Si(001) (from Ref. [28]).

From this view from the gas phase side it can be seen that the saddle point of the potential energy surface with the transition state for desorption is shifted with respect to the lattice equilibrium distance. With this transition state chosen to be nearly on an equipotential with the desorbed state the lattice has to be distorted. Therefore, upon desorption the excess energy is to a large extent released into silicon phonons [28]. Conversely, if the lattice is in its equilibrium configuration the incoming



molecule would experience a large barrier for adsorption. However, thermal excitation of lattice vibrations can decrease the effective dissociation barrier for the incident $H_2$ molecule [28]. With strong lattice excitations governing the reaction, this model is similar to that invoked for explaining the diffusion process.

To test for the prediction of phonon-assisted sticking Bratu *et al.* have performed adsorption experiments as a function of surface temperature. Making use of the *in situ* applicability of SHG and its high surface sensitivity, sticking coefficients down to $10^{-9}$ could be measured quantitatively both for Si(111)7×7 [14] and Si(001)2×1 [26]. Similar for both surface orientations, the sticking coefficients were found to increase by four orders of magnitude in the investigated temperature range from 550 to 1050 K, reaching values up to $10^{-5}$. These measurements provided strong evidence for a large adsorption barrier and the increase with surface temperature could be described by an activation barrier of $0.9 \pm 0.1$ eV for Si(111)7×7 [26] and $0.75 \pm 0.1$ eV for Si(001)2×1 [26]. These results demonstrated the decisive role of the lattice degrees of freedom in the reaction dynamics and fully support the phonon-assisted sticking model [17,27]. Parallel to the experiments of Bratu *et al.* [14,26] the adsorption of $D_2$ on Si(001)2×1 was investigated by Kolasinski *et al.* [95] who exposed the surface with a supersonic molecular beam and subsequently determined the surface coverage with TPD. Although the results of these experiments were also interpreted in terms of a dependence of the adsorption barrier on the lattice configurations [15,32,95] the absolute magnitude of the reported sticking coefficients were up to three orders of magnitude higher with a comparatively weak surface temperature dependence. The experimental conditions of both experiments (adsorption from a molecular beam vs. thermal gas) are not directly comparable, nevertheless, the large quantitative discrepancies between the observed sticking coefficients could not be explained. As will be discussed in section 4.1 of this work the high sticking coefficients observed are most likely caused by adsorption at steps and defects on the surface.

### 2.2.4 Microscopic reaction mechanism

In order to specify the microscopic nature of the surface excitation process, efforts were taken to make *ab initio* calculations based on density-functional theory for both Si(001)2×1 and Si(111)7×7. In spite of the complexity of the 7×7 reconstruction of Si(111), the theory was able to describe consistently the experimental findings concerning both adsorption and desorption [96,97]. The most recent study found good quantitative agreement between the activation energies for both adsorption and desorption by treating the full 7×7 unit cell numerically [97]. The interaction was then dominated by the dangling bonds of the adatoms and rest-atoms, and similar to the model describing the surface diffusion, distorted adatom facilitate a transition state for dissociation and recombination, as has been proposed by Bratu *et al.* [27].

Slab-type *ab initio* quantum dynamical calculations have been applied to the

Si(001)2×1 surface by Kratzer *et al.* considering an intra-dimer reaction pathway [98,99]. Here, coupling of the barrier height with the buckling modes of the Si-dimers was found and the minimum reaction path is shown in Fig. 2.8. The hydrogen molecule

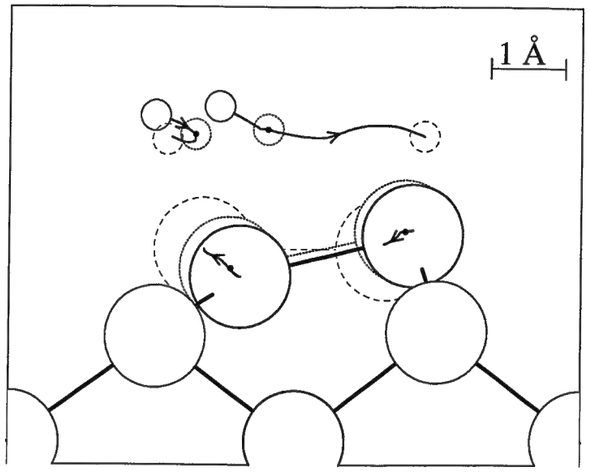


**Fig. 2.8:** Calculated reaction pathway for molecular hydrogen interaction with the Si-dimer of Si(001)2×1 (from Ref. [99]).

can minimize its repulsion with the surface by approaching the charge depleted dangling bond at the lower Si atom. Since the buckling of the dimer is accompanied by charge transfer between the dangling bonds and re-hybridization of the corresponding orbitals as described above, this could explain the dependence of the barrier on the buckling angle. Heating the surface would excite the dimer transiently into a less buckled configuration for which a reduced barrier was calculated, and thus promote sticking. The desorption was found to proceed directly from the paired monohydride state via the asymmetric transition state depicted in the figure following the reverse adsorption path. For this reaction path a desorption activation energy of 2.5 eV was calculated and found to be in excellent agreement with the experiments [11]. Surface phonons will take up part of the energy released after passing the desorption barrier. Although qualitatively consistent with the experimental observations, the coupling strength to the lattice, however, was not sufficient to give a conclusive quantitative explanation for the observed asymmetry between adsorption and desorption [30,31,100].

On the other hand, various *ab initio* cluster calculations were performed for hydrogen on Si(001)2×1 by several groups employing different theoretical methods [18,19,81–83,89,101–111]. In the case of desorption from single dimers the resulting activation barriers, ranging between 3.4 and 4.1 eV, were much higher than the 2.5 eV



observed experimentally [81,82,102,103,106,111]. In view of these discrepancies, alternative models for the reaction mechanism were proposed where both $H_2$ adsorption and desorption are two-step processes. The reaction would then not occur directly via doubly occupied dimers, but rather involve steps or single-atom defects. These defects would facilitate the creation of dihydride intermediate without an appreciable barrier and thus not lead to translational heating. Once a dihydride has been formed, the calculated desorption barrier seems consistent with the experimental values. In the early models proposed, diffusion-limited desorption from single-atom defects would occur [89,102,109,110]. Similarly the increase in sticking probability would be due to activated diffusion of hydrogen from the reaction centers across the surface. More recently refined models have been proposed including defect formation at steps and successive migration across the terraces [103,106,109]. This is illustrated schematically in Fig. 2.9.

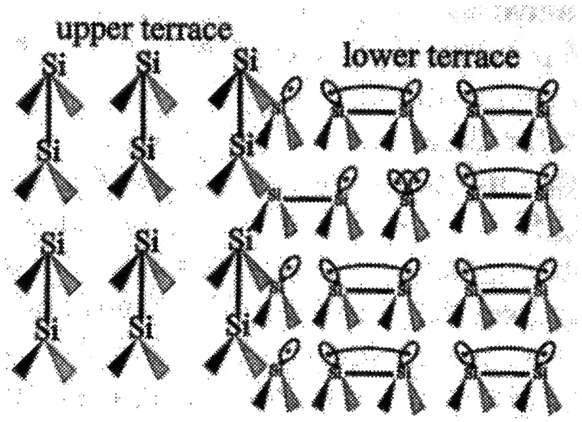


**Fig. 2.9:** Creation of isolated Si-defect at $S_B$-type steps on Si(001)2×1. The successive migration across the terraces would mediate both adsorption and desorption via formation of a silicon-dihydride (from Ref. [103]).

The isolated atom defect would react with the monohydride to form a Si-dimer and $SiH_2$. With the barrier for such defect migration found to be only 0.61 eV [103] this process could also explain the observed temperature dependence of the sticking coefficient. Alternatively their possible temperature dependent concentration on the surface would have a similar effect.

On the basis of the experimental and theoretical work described, it has not yet been possible to give a definite answer to which of the proposed microscopic reaction mechanisms is at work. Since it is difficult to assess the absolute accuracy of the different theoretical methods used [19,107,112], experiments are required.

## 2.3 Second-harmonic generation at silicon surfaces

Quite a number of optical techniques have been adopted for surface studies over the past two decades, of which second-harmonic generation (SHG) and the more general case of sum-frequency generation (SFG) have received much attention because of their surface sensitivity and specificity [113–115]. Both methods are capable of non-detrimental, *in situ* remote sensing and mapping of the surface composition. For the purpose of the experiments described here, SHG has been applied and a brief account of the underlying theory is given; for further details the reader is referred to the literature [116–121].

### Phenomenological description

Via the nonlinear response an incident electric field $\boldsymbol{E}(t) = \boldsymbol{E}(\omega)\exp(-i\omega t)$ induces a nonlinear polarization in the medium, which can be expressed as

$$\boldsymbol{P}^{(2)}(\Omega) = \boldsymbol{\chi}^{(2)}(\Omega = \omega + \omega) : \boldsymbol{E}(\omega)\boldsymbol{E}(\omega), \tag{2.1}$$

with $\Omega = 2\omega$ and the second-order nonlinear susceptibility tensor $\boldsymbol{\chi}^{(2)}$. This equation shows that if the medium has inversion symmetry, i.e. the fields $\boldsymbol{E}(\omega)$ and $-\boldsymbol{E}(\omega)$ induce dipoles of $\boldsymbol{P}(\Omega)$ and $-\boldsymbol{P}(\Omega)$ respectively, this implies that $\boldsymbol{\chi}^{(2)} \equiv 0$ in the electric-dipole approximation. At a surface or at an interface the inversion symmetry is broken and the nonlinear polarization induced in the sheet at the interface (see Fig. 2.10) is given by

$$\boldsymbol{P}(\boldsymbol{r}, t) = \boldsymbol{P}_s \delta(z) e^{i(\boldsymbol{k}_{\parallel}(\Omega)\boldsymbol{r} - \Omega t)}. \tag{2.2}$$

The radiation field $\boldsymbol{E}(\Omega)$ generated by $\boldsymbol{P}$ is obtained from the solution of the wave equation. With the proper boundary conditions one arrives at the final result for the SH output intensity in the reflected direction:

$$I(2\omega) = \frac{8\pi^3\Omega^2\sec^2\theta_{2\omega}}{\hbar c^3 \epsilon_1(\omega)\sqrt{\epsilon_1(2\omega)}} \left|\boldsymbol{e}(\Omega)\cdot\boldsymbol{\chi}_s^{(2)} : \boldsymbol{e}(\omega)\boldsymbol{e}(\omega)\right|^2 I_1^2(\omega). \tag{2.3}$$

In this expression the quantities $\boldsymbol{e}(\Omega)$ and $\boldsymbol{e}(\omega)$ correspond to the unit polarization vectors $\hat{\boldsymbol{e}}(\Omega)$ and $\hat{\boldsymbol{e}}(\omega)$ after the appropriate Fresnel correction, e.g. $\boldsymbol{e}(\omega) \equiv \boldsymbol{F}(\omega)\hat{\boldsymbol{e}}(\omega)$; $I_1(\omega)$ denotes the irradiance of the input laser beam. If the surface has the structure of a polar layer, this electric-dipole contribution of the surface dominates the signal over additional, e.g. bulk electric-quadrupole terms.

In the case of SHG the nonlinear susceptibility $\boldsymbol{\chi}_s^{(2)}$ is a third-rank tensor with 18 elements $\chi_{s,ijk}^{(2)}$. However, in most cases the number of independent, non-vanishing elements is greatly reduced dictated by the symmetry of the interfacial layer. With



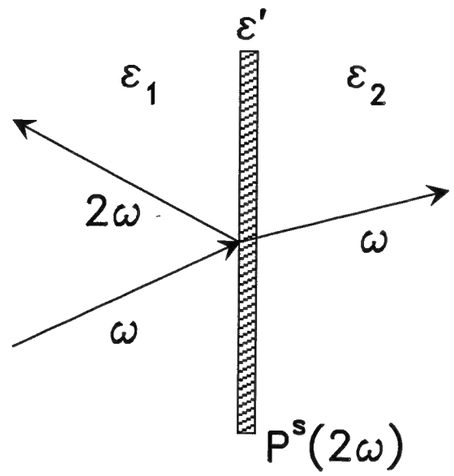


**Fig. 2.10:** Geometry of second-harmonic generation from an interface in the reflected direction. The polarization sheet with dielectric constant $\epsilon'$ is imbedded between the two media of inversion symmetry with dielectric constants $\epsilon_1$ and $\epsilon_2$.

different combinations of input and output beam polarizations the individual components can be isolated.

Microscopically, SHG corresponds to a sequence of electronic transitions from an initially occupied state $|g\rangle$, via two intermediate states $|n'\rangle$ and $|n\rangle$ induced by absorption of two pump photons $\hbar\omega$, followed by the emission of the SH photon $\hbar\Omega$ when returning from $|n\rangle$ to the initial state $|g\rangle$. The corresponding expression for $\boldsymbol{\chi}_s^{(2)}$ in the dipole approximation consists of eight terms of the form [117]

$$\chi_{s,ijk}^{(2)}(2\omega) = -N\frac{e^3}{\hbar^2}\sum_{g,n,n'}\left[\frac{\langle g|r_i|n\rangle\langle n|r_j|n'\rangle\langle n'|r_k|g\rangle}{(\Omega - \omega_{ng} + i\Gamma_{ng})(\omega - \omega_{n'g} + i\Gamma_{n'g})} + \cdots\right]\rho_g^{(0)}. \tag{2.4}$$

The quantities $\omega_{n^{(\prime)}g}$ and $\Gamma_{n^{(\prime)}g}$ are the energy difference and line widths for the transitions between the different quantum states, and $\rho_g^{(0)}$ denotes the population of the ground state $|g\rangle$. Resonant enhancement thus occurs whenever the frequency of the transition matches that of the pump beam or the SH frequency. For a quantitative evaluation of this expression, however, a detailed knowledge of the energies and transition moments of the material system would be required.

### SHG from silicon surfaces

The form of the nonlinear susceptibility tensor reflects the symmetry of the surface plane of the silicon crystal. The Si(111)7×7 surface has $C_{3v}$ symmetry and the corre-

sponding nonlinear susceptibility tensor can be written as

$$\chi^{(2)}_{s,ijk} = \begin{pmatrix} 0 & 0 & 0 & 0 & \chi_{\parallel\perp\parallel} & -\chi_{\xi\xi\xi} \\ -\chi_{\xi\xi\xi} & \chi_{\xi\xi\xi} & 0 & \chi_{\parallel\perp\parallel} & 0 & 0 \\ \chi_{\perp\parallel\parallel} & \chi_{\perp\parallel\parallel} & \chi_{\perp\perp\perp} & 0 & 0 & 0 \end{pmatrix}. \tag{2.5}$$

With respect to an isotropic surface, there is one additional independent non-zero tensor element $\chi_{\xi\xi\xi}$. This anisotropic component gives rise to only in-plane polarizations and therefore their contribution is strongest for normal incidence of the pump when the electric field oscillates in the surface plane. In the case of Si(001)2×1 the isotropic elements are the same. Here the surface exhibits an overall $C_{4v}$ symmetry because the two different domains with $C_{2v}$ symmetry, each, are rotated by 90° with respect to one another. This surface does not exhibit anisotropy and the corresponding term is zero.

The surface states in the bulk band gap enable resonant optical transitions in the visible and near-infrared spectral regions. Besides the dangling-bond-derived states, the distorted reconstruction-induced bonds provide additional filled and unfilled states. In the wavelength range between 700 and 1200 nm investigated in SH spectroscopy experiments, both the Si(111)7×7 and Si(001)2×1 surfaces reveal two resonant structures [17,122–124]. The sharp peak at low wavelengths has been attributed to the $E_1$-transition at 3.4 eV between the valence and conduction bands of bulk silicon. A broad extended feature for wavelengths above 800 nm is due to the dangling-bond states shown in Fig. 2.2 and found to be qualitatively similar for both Si(111)7×7 and Si(001)2×1. Hydrogen adsorption thus quenches the SH signal below a photon energy of 1.5 eV. The weak nonlinear response found for the bulk is in leading order due to electric-quadrupole and magnetic-dipole interactions. Calculations for Si(111) [125,126] and Si(001) [127] could provide a microscopic formulation of these nonlinear optical phenomena observed experimentally.

### SHG from vicinal surfaces

The presence of regular steps on the surface reduces the overall symmetry of the system and thus SHG is very sensitive to the miscut angle [128,129]. In the case of Si(001) tilted towards [110], the single-domain surface preserves the $C_{2v}$ symmetry of the individual terraces macroscopically and, due to the presence of the steps, the surface has only $C_{1v}$ symmetry with the mirror plane perpendicular to the steps. For small miscut angles the electronic structure of the terraces will be very little affected by the steps. The total dangling-bond resonant nonlinear response can then be approximated as the sum of independent contributions from the steps and the terraces and a nonresonant term:

$$\boldsymbol{P}^{(2)}(2\omega) = x_\alpha \boldsymbol{P}_s^{step} + (1 - x_\alpha)\boldsymbol{P}_s^{terr} + \boldsymbol{P}_s^{NR}. \tag{2.6}$$



Both the non-resonant and terrace polarizations depend on the miscut angle $\alpha$. $x_\alpha$ is the fraction of step edge atoms with respect to the number of terrace atoms. The

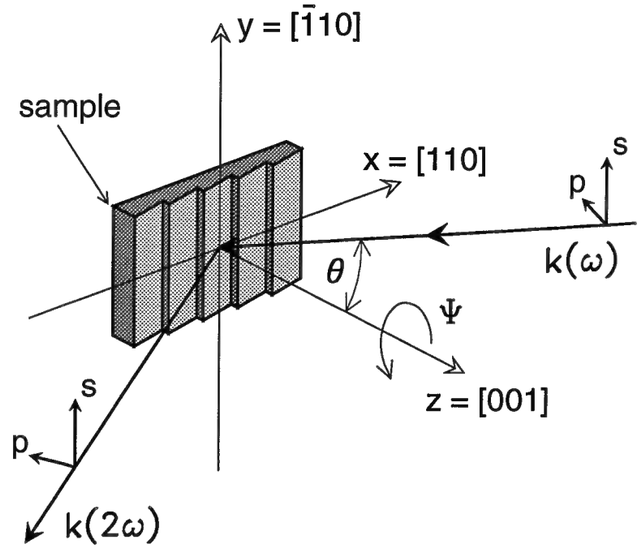


**Fig. 2.11:** Experimental geometry for SHG experiments on vicinal silicon surfaces.

relative contributions of these terms to the net surface nonlinear response can be adjusted by varying the polarization and plane of incidence of the pump light. As can be seen from Fig. 2.11 with the geometry depicted schematically, for p-polarized input one would obtain contributions from both the steps and terraces since for both the symmetry is broken. Increasing the angle of incidence for p-polarized input the terrace contributions would increase with respect to the steps. By rotating the sample by 90° the signal would be dominated by the steps for s-polarized input. This enables one to obtain different sensitivities towards the step sites compared with the terrace sites, which will be employed in particular in the experiments described in chapter 5.

# Chapter 3

# Experimental setup and procedures

The following sections provide a self-contained account of the basic experimental setup common to most of the experiments. More details about special experimental requirements will be given in conjunction with the description of the corresponding measurements.

## 3.1 The ultra-high vacuum system

The main components of the ultra-high vacuum (UHV) system used for most of the experiments described here were designed and built by P. Bratu [130] and Ch. Wittenzellner [131]. The original setup used for a number of previous studies [14,26,27,130–132] was modified to meet the requirements of the new experiments. In particular, the repeated dosing of molecular hydrogen up to the mbar range without built-up of contaminants in the chamber requires highly purified dosing gas, efficient pumping, and very clean UHV conditions. The last issue is particularly crucial since replacement reactions of the dosing gas at the chamber walls can introduce water and oxygen, which react orders of magnitude more readily with silicon compared to the dissociative adsorption of molecular hydrogen. The improved UHV system consists of three major components as shown schematically in Fig. 3.1: a small ($V \simeq 23\,l$, $\varnothing = 20\,cm$) spherical UHV chamber, a large pumping unit with various pumps, and a separately pumped gas-handling system.

The sample preparation chamber is equipped with a quadrupole mass spectrometer (Balzers, QMS 125) and a combined retarding-field LEED/Auger instrument (Omicron, Spectaleed). The mass spectrometer with a stainless-steel "Feulner Cap" [133,134] around the ionizer is mounted on a translational stage and can be placed reproducibly in front of the sample (typical distance 5 mm). This enables precise temperature-programmed desorption (TPD) measurements.

All parts of the system, including the sample manipulator and the gas-handling system can be fully baked at 160°C. During bakeout sample and sample holder are degassed at 350°C. After two days of bakeout a base pressure of $\leq 4 \times 10^{-11}$ mbar is obtained for the main chamber. For the dosing system a pressure in the lower $10^{-10}$ mbar range is reached.

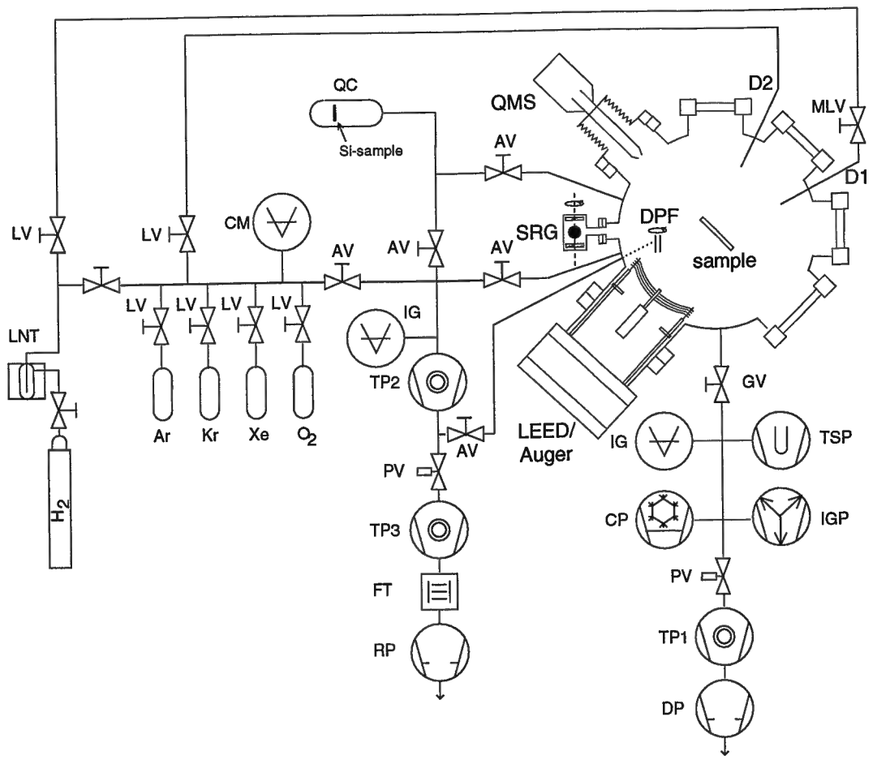


**Fig. 3.1:** Schematic representation of the vacuum system. The abbreviations are explained in Tab. 3.1.

The sample holder designed for mounting single-crystal silicon cut from commercial wafers has already been described in detail [130]. The samples ($9 \times 45$ mm$^2$) are clamped with spring-loaded molybdenum brackets onto two copper bars. Additional silicon spacers isolate the sample from both copper and molybdenum. The two copper blocks are attached to a liquid-nitrogen-cooled cryostat via an insulating sapphire plate. The high cooling efficiency of this setup allows a base temperature of $\sim 80$ K to be reached within less than two minutes after introducing liquid nitrogen. During sample preparation with surface temperatures exceeding 1200 K the temperature of the copper blocks does not exceed 100 K.

The silicon sample temperature is controlled via direct resistive heating. For a given current a constant sample temperature within $\pm(1-2)$ K is achieved. The large samples with thickness $<1$ mm ensure a homogeneous temperature distribution across the surface. For the temperature measurements a NiCr/NiAl thermocouple



| | |
|---|---|
| TP1, TP2, TP3 | Turbomolecular pump, 180 l/s, 170 l/s, 60 l/s |
| IGP | Ion getter pump, Star Cell (Varian), 220 l/s |
| CP | Cryogenic pump, 800 l/s |
| TSP | Titanium sublimation pump |
| RP, DP | Rotary vane pump, dry pump |
| LNT,FT | Liquid nitrogen trap, foreline trap |
| DPF | Differentially pumped feedthrough |
| IG | Ionization gauge |
| SRG, CM | Spinning rotor gauge, capacitance manometer |
| LV, MLV | Leak valve, motorized leak valve |
| AV, GV | Angle valve CF40, gate valve CF200 |
| PV | Pneumatic protection valve |
| D1 | Doser with tungsten filament |
| D2 | Doser with capillary array plate, $\varnothing = 25$ mm, $\varnothing_{porous} = 5\,\mu$m |
| QC | Quartz chamber, see chapter 6 |

**Tab. 3.1:** List of vacuum components abbreviated in the schematic of the vacuum system shown in Fig. 3.1.

is cemented onto the rear side of the sample with a ceramic glue (Ultra Temp 516, T-E-Klebetechnik, Hannover, Germany) and allows temperature measurements in the range between 20 and 1600 K [135]. The thermocouple contact is fully embedded in this zirconium-oxide-based material and thus the wires do not directly touch the sample. It has been verified that even for high annealing temperatures no contaminants, in particular nickel, diffuse onto the front side of the sample. Carefully controlled temper cycles lead to inherent contact of the ceramic with the sample. As verified with an infrared pyrometer (Optix, Keller), the thermocouple reproduces the surface temperature accurately up to $T_s \approx 800$ K. For higher surface temperatures the thermocouple reading is slightly lower than the actual surface temperature and was calibrated with the pyrometer. This allows temperature determination with an absolute accuracy of $\pm 15$ K. Within one set of experiments with the same sample the relative uncertainty was estimated to be $\pm 5$ K.

The sample holder is mounted on a 360°-rotatable manipulator which allows 100 mm motion in the vertical direction and $\pm 25$ mm in the x- and y-directions (Omniax, Vacuum Generators). The high mechanical stability of this manipulator allows precise repositioning without the necessity for realigning the optical setup, e.g. after temperature-programmed desorption experiments.

The chamber can be separated from the pumping unit located underneath via a 200 mm gate valve. A turbomolecular pump, an ion-getter pump, a Ti-sublimation pump and a closed-cycle He-refrigerated cryogenic pump are attached to a six-way crossing. Using this combination of pumps ensures that all inert and reactive gases of

different masses are efficiently pumped. Without the Ti-sublimation pump the total pumping speed for molecular hydrogen adds up to $\sim$1400 ls$^{-1}$. The system pressure is recorded with a Bayard-Alpert gauge. The gas-handling system, which is pumped independently of the main system with a turbomolecular pump, is attached to the chamber via an angle valve. Two leak valves lead to the chamber, one for hydrogen dosing, the other connecting the gas manifold with four glass bulbs for various gases. A capillary array doser is utilized for oxygen and rare-gas dosing.

The low sticking coefficients of molecular hydrogen on silicon require highly purified gas. For this reason 6.0 hydrogen (AGA, $H_2$+$D_2 \geq$ 99.9999 Vol.%, $D_2$ $\sim$150 ppm) is used and the residual traces of the major contaminants - in particular water ($\leq$ 1 ppm, specified) - are further reduced with a liquid-nitrogen-cooled trap. The trap consists of a spiral tube immersed in liquid nitrogen. Possible contaminants remaining, mainly rare gases and nitrogen, would not affect the measurements. Although oxygen ($\leq$1 ppm, specified) might not be efficiently trapped at liquid nitrogen temperatures, after this treatment the impurity level is found to be below the detection limit of the mass spectrometer. A very sensitive test for oxygen contamination on the surface is described in chapter 4 together with the discussion of the measurements.

For hydrogen exposure the chamber is shut off from the pumping unit and is backfilled with molecular hydrogen. The pressure is recorded with a spinning rotor gauge (MKS Instruments, absolute error $\leq$10 %) and a calibrated capacitance manometer (MKS, Baratron, Model 615A). Whereas the spinning rotor gauge serves as an absolute pressure gauge, the Baratron can track fast pressure changes, but is less accurate. To maintain a constant pressure, the right-angle valve to the turbo-pump of the gas-handling system is opened for a fractional turn and a closed loop electronic feedback is set up with the Baratron and the servomotor-driven leak valve (MKS, Model 245). This controls the pressure above $10^{-3}$ mbar; below $10^{-3}$ mbar manual dosing was performed. After hydrogen exposure the chamber is first pumped through the dosing system down to below $10^{-8}$ mbar. Then the main gate valve is opened to the pumping unit, where the UHV base pressure has been maintained during the dosing procedure. After that the valve to the gas handling system is closed again to avoid backstreaming due to the pressure gradient. With this two-stage pumping process, the system pressure reaches the $10^{-11}$ mbar range within 30 s after dosing even 1 mbar hydrogen for a few hundred seconds. The key factors for this performance are the combination of a small chamber, together with the two-step pumping process, keeping the backfilled volume to a minimum, and the high pumping efficiency of the cryo-pump.

A related advantage of the system is that sample changing is greatly simplified because all pumps can be keep operating with the gate valve closed when venting the chamber. The system is then first pumped with the turbomolecular pump of the dosing system and the gate is only opened after the bakeout commences. This procedure ensures very clean vacuum conditions.

For the rare-gas adsorption experiments described in the appendix a second sample



holder was built and mounted on a liquid-He evaporation cryostat. The cryostat, designed according to the criteria given in [134], consists of two tubes stacked into each other, thermally insulated from the environment via an additional evacuated outer tube. Liquid helium is introduced into the inner tube, is cooled by the backstreaming helium, and flows through lamellar silver blocks at the lower end. The sample holder is similar to the one described above but is about half the size for 6×25 mm$^2$ samples. It is mounted onto the polished silver end (Ø=25 mm) of the cryostat via a sapphire plate.

The temperature control below 50 K via direct resistive heating becomes difficult because of the low intrinsic defect carrier density of silicon. The rear side of the sample was therefore vacuum-sputtered with a thin layer of tantalum, with the layer thickness adjusted to the intrinsic sample conductivity at room temperature. Due to the inverse temperature dependence of the resistivity of the metal film compared with silicon, this enables both accurate temperature control at low sample temperatures and high temperature annealing. A sample base temperature of 20 K could be obtained and the temperature was calibrated with Ar, Kr, and Xe rare-gas TPD experiments, using the data given in [134] as reference.

## 3.2 Silicon surface preparation

As discussed in detail in chapter 4, the sample preparation scheme is of crucial importance for producing a well-ordered surface with few structural defects. It is known from low-energy electron diffraction (LEED) and scanning tunneling microscopy (STM) imaging that the preparation of silicon surfaces with long-range ordered superstructure and small defect concentrations is quite sensitive to both duration and maximal values of the high-temperature annealing and cooling rates. This is particularly the case for Si(001), where extended annealing even leads to surface roughening [52]. As discussed in chapter 1, Si(001) has an intrinsic tendency towards defect formation and in general defect densities are above the 1% level [8,136].

The different types of Si(001) and Si(111) samples used for the various experiments were cut with a diamond scribe from commercial 3" wafers (Virginia Semiconductor, Inc.). The single-crystal material was Czochralski (Cz) grown, n-type phosphorus-doped material ($n\sim5\times10^{14}$ cm$^{-3}$, $\rho$ = 6–12 Ωcm), single-side polished with a thickness of 0.5–0.6 mm. The nominally flat Si(001) and Si(111) surfaces were oriented to within ±0.25° along the principal axis. In addition, Si(001) miscut by 3.0° towards [010] (1.4 – 1.7 Ωcm) and Si(111) miscut by 5.0° towards [1$\bar{1}$0] (0.25 – 5.0 Ωcm) was used. For a systematic study of the reaction behavior of steps Si(001) misoriented towards [110] by different angles of misorientation of 2.5, 5.5, and 10° were used. Furthermore, experiments using a highly As-doped ($n\simeq2.5\times10^{19}$ cm$^{-3}$, $\rho$=0.003 Ωcm) crystal were performed. This sample was self-cut and polished from a 2" single crystal (Wacker,

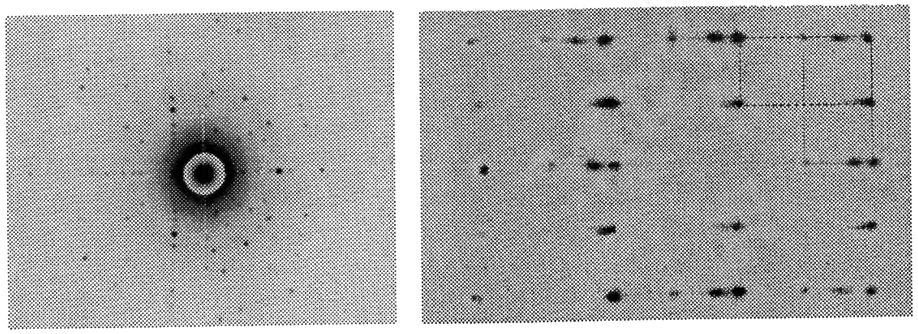

**Fig. 3.2:** Laue X-ray diffraction and low-energy electron diffraction (LEED) pattern of Si(001)5.5° → [110]. The dashed and dotted boxes drawn in the LEED pattern indicate the 2×1 and 1×2 domains and the corresponding diffraction spots with high and low intensity, respectively.

Siltronics)[1] with miscut of ∼1° predominantly towards [010].

With the exception of the highly doped silicon, the samples were mounted directly in UHV after rinsing in methanol and carefully checking for dust residues or scratches. In the case of the 0.003 Ωcm sample an additional *ex situ* chemical cleaning procedure was performed. Following the approach given in Ref. [137], after degreasing the sample, repetitive cycles of oxidation in $HNO_3$ and successive removal of this oxide in dilute HF solution were performed prior to insertion in UHV. For commercial wafers high-quality thermal oxide layers are grown under very clean process environments that protect the silicon from contamination. No further treatment is therefore required for these crystals since after outgassing of the sample the thermal decomposition of the oxide in UHV will remove the oxide together with the contaminants.

For the initial preparation the native oxide layer is removed by repetitive heating in steps of 50 K to a maximal temperature of 1250 K for Si(001), and 1350 K in the case of Si(111). A cooling rate of $2-3\,\mathrm{Ks}^{-1}$ was applied for the planar samples. In order to prepare well-ordered steps on the vicinal surfaces a slower cooling procedure of $\sim 1-2\,\mathrm{Ks}^{-1}$ is applied. Thorough outgassing of the sample and sample holder ensured that the chamber pressure stayed below $1\times10^{-9}$ mbar during the annealing cycles. After these procedures the surface impurity levels of oxygen and carbon were below the detection limit of the retarding-field Auger spectrometer.

The crystallographic orientations of the samples were checked *ex situ* with Laue X-ray diffraction and *in situ* following the sample cleaning procedure via LEED. Representative in Fig. 3.2 both the Laue pattern and corresponding LEED image of Si(001)5.5° → [110] are shown. The off-normal shift of the zeroth-order X-ray

[1] M. Stutzmann, Walter Schottky Institute (Garching), is gratefully acknowledged for providing the crystal rod.



diffraction spot directly relates to the miscut angle towards the [110] direction. The LEED pattern taken at a primary electron energy of 50 eV reflects the periodicities of the atomic configurations of both the terraces and the steps. The straight double-atomic height steps and the dimers are oriented perpendicular to the horizontal direction and give rise to the observed single-domain (1×2) structure. From the ratio of the (1×2) to (2×1) spot intensities the single-domain quality is estimated to be better than 90%.

The origin of the spot splitting can be understood with the help of the Ewald construction shown in Fig. 3.3 [138,139]. Due to the finite size of the terraces the cor-

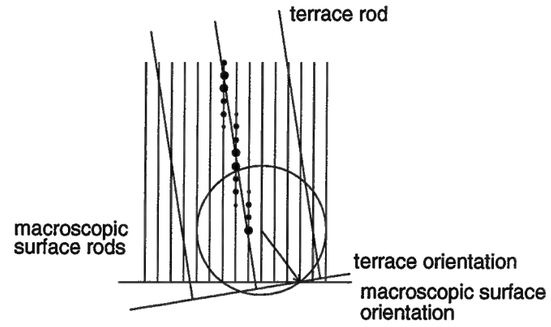


**Fig. 3.3:** Ewald-sphere construction of a stepped surface.

responding reciprocal lattice rods from the terraces have a non-zero width. Therefore, any surface beam that falls near the terrace rods has a strong intensity resulting in the replacement of each integral-order beam by two or three closely spaced spots at distance $\Delta K$. With the terraces composed of $M+1$ dimers separated by the distance $l$ the ratio of the corresponding spot distances is approximately given by

$$\frac{l}{M\cdot l}=\frac{\Delta K}{k_{10}}. \tag{3.1}$$

In this equation $k_{10}$ denotes the reciprocal lattice vector that corresponds to the silicon dimer separation along [110]. From the LEED image an average terrace width of ∼6.5 dimers can be derived. With the known miscut angle of $\alpha\approx5.5°$ the step height can thus be calculated with $h=\tan\alpha(M+1)2\sqrt{2}\cdot a_0$ to 2.7 Å using $a_0=5.4$ Å, the lattice constant of silicon. This value is compatible with the double-layer spacing of silicon [63].

## 3.3 Optical setup

This section deals with the basic considerations concerning the optical setup of the experiments with SHG from the silicon surfaces in the UHV chamber. In general,

the pump radiation from a pulsed laser is directed onto the surface and the reflected harmonic light is detected. From eq. 2.3 the generated second-harmonic output in the reflected direction from a vacuum/solid interface can be calculated. For a pulse duration $\tau$ of the pump (frequency $\omega$) with energy $E$ and cross-section $A$ the number of photons generated per pulse with frequency $2\omega$ is given by

$$S(2\omega) = \frac{32\pi^3\omega\sec^2\theta}{c^3\hbar\epsilon(\omega)\sqrt{\epsilon(2\omega)}}\left|\chi_s^{(2)}\right|^2\frac{E^2}{A\tau}, \tag{3.2}$$

where $\theta$ is the angle of incidence of the incoming laser beam and $\epsilon(\omega)$ is the dielectric constant of the material at frequency $\omega$.

With typical values of $\chi_s^{(2)}$ of the order of $10^{-15}$ esu·cm for silicon, a 1064-nm pump pulse incident at $\theta = 45°$ with $E = 30\,\text{mJ}$, $A = 0.2\ \text{cm}^2$, and $\tau = 3.5$ ns will generate $\sim 10^3$ photons per pulse. In the detection system, the reflected fundamental light therefore has to be suppressed by a factor better than $10^{15}$, which is accomplished with dielectric mirrors (used as interference filters) and color glass filters.

The basic experimental setup established in our group over the past years [17,130] is shown schematically in Fig. 3.4. The pump radiation at a wavelength of 1064 nm is provided by the Q-switched Nd:YAG laser (Infinity, Coherent) in the form of 3.5 ns pulses of variable repetition rate up to 100 Hz. This laser consists of a Q-switched, diode-pumped single-frequency ring laser as a master oscillator (8–10 ns pulses at 30 $\mu$J). These pulses are amplified in a two-rod double-pass chain containing a special combination of relay imaging and a phase-conjugated reflector. This results in a wide dynamic range enabling one to operate from single-shot to 100 Hz repetition rate with minimal change in pulse energy (maximal IR energy: 500 mJ) and beam quality. A top-hat near-field intensity profile is achieved with diameter 5.5 mm containing 95% of the pulse energy. With this homogeneous energy density and high energy stability (pulse-pulse noise 1% rms), the system is ideal for nonlinear optical experiments and greatly exceeds the performance of conventional Nd:YAG lasers.

The operation of the laser was continuously monitored by generating SH light on a GaAs crystal surface in air with a 4% fraction of the pump light split off the incident beam with a glass slide. With this reference channel the signal from the silicon sample can be normalized to compensate for potential long-term drifts in laser intensity. The internal IR energy monitor was found to control accurately for a constant output power.

The uncollimated laser beam with its diameter apertured to 5 mm hits the surface after passing through a set of two half-wave plates ($\lambda/2$) with a polarizer (P) in between. This allows the incident power and polarization to be tuned. In addition, a color glass filter (RG715, Schott) in front of the entrance window removes any residual SH light originating from the laser or the optical components in between. It was verified that the pyrex-glass windows of the UHV chamber neither generate harmonic light of detectable intensities nor alter the beam polarization. The monochromator



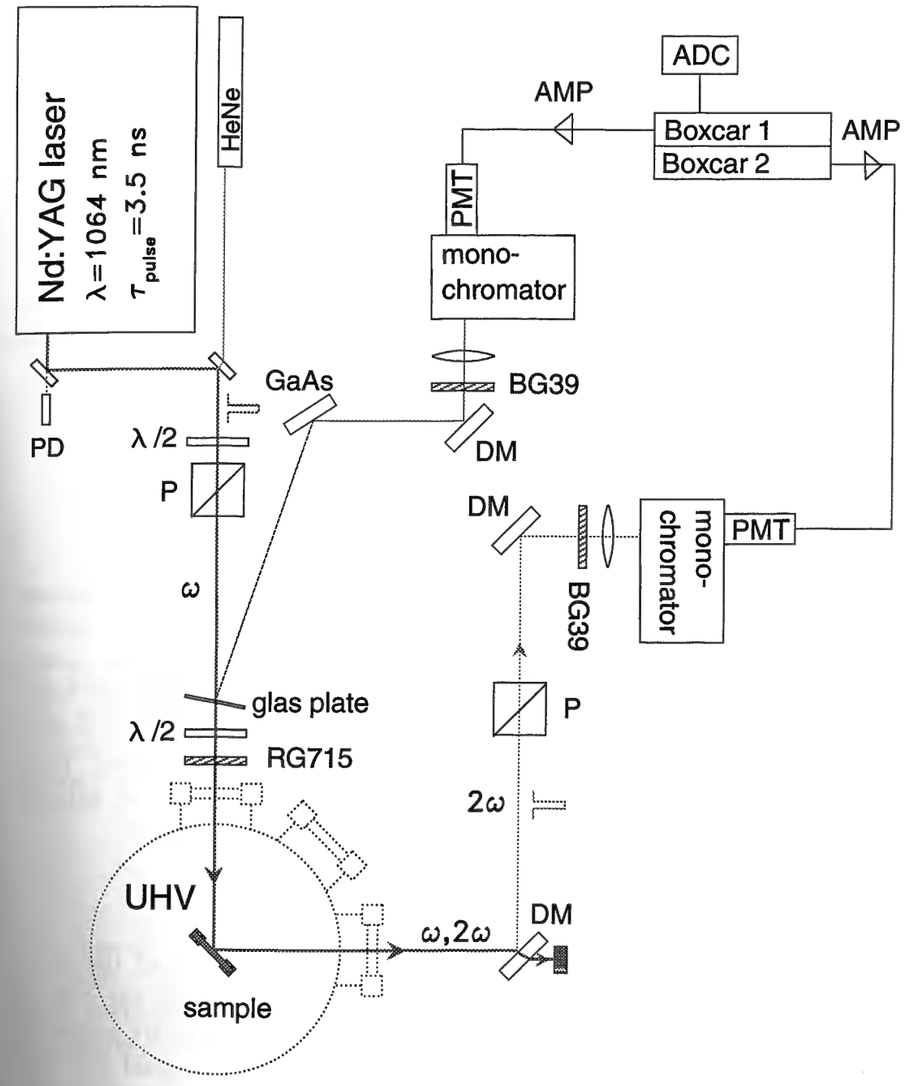


**Fig. 3.4:** Experimental arrangement for second-harmonic generation with a pulsed Nd:YAG laser at silicon surfaces in UHV.

suppresses stray light and the signal at 532 nm is detected by means of a photomultiplier tube (R928, Hamamatsu, quantum efficiency 15%). The amplified signal (gain = 1, time constant 1 $\mu$s) is fed into a box-car and integrated over a 150 ns time window that is gated on the laser pulse with a photodiode (PD).

For the purpose of the experiments the surface was irradiated with a laser fluence

of typically 30 mJ/cm$^2$ at a repetition rate of 30 Hz. The photon energy of $E_{h\nu} = 1.17$ eV of the laser is below the direct band-gap of silicon with 3.4 eV. The absorption coefficient is therefore small and the cw heating of the surface is only about 2−3 K and does not influence the reactivity of the surface. With the small transient temperature rise of ∼ 30 K during the pulse one can see that ns pulses are quite advantageous compared with the use of tightly focussed, high-repetition, unamplified sub-ps pulses from Ti-sapphire lasers [124], which on average lead to a substantial temperature rise.

In the case of Si(111)7×7 the dominant anisotropic $\chi^{(2)}_{s,\xi\xi\xi}$ component was monitored by choosing $s$ input and output polarization. For Si(001)2×1, where the SH efficiency is weaker, the input polarization was arbitrarily set in order to maximize the signal intensity recorded without a polarizer in the exit channel.

## 3.4 SHG measurements of adsorbate kinetics

### 3.4.1 Surface coverage calibration

As discussed in section 2.3, the SH response from silicon surfaces exhibits resonant enhancement for wavelengths above 900 nm with the dangling-bond-derived surface states. The corresponding signal is thus quenched upon interaction of the surface with chemisorbates, leading to a high adsorbate sensitivity [17,124,140]. Since quantitative kinetic measurements rely on accurate real-time monitoring of the surface coverage, calibration of the SH response with adsorbate coverage is required. Here, the previously established calibration for hydrogen adsorption is described, followed by a discussion of the procedure applied for oxygen adsorption on Si(001).

#### Hydrogen adsorption

In the case of hydrogen adsorption on both Si(111)7×7 and Si(001)2×1 the correlations of $\chi^{(2)}_s$ with surface coverage were previously established with the help of temperature-programmed desorption experiments [14,26]. The procedure applied is shown in Fig. 3.5 for the case of H/Si(001)2×1 [26]. Here, the SH signal $I^{(2\omega)}$ was recorded during exposure to a continuous flux $\Phi$ of atomic hydrogen created by dissociation of $H_2$ at a hot tungsten filament (inset: top). The surface temperature was kept at 600 K, where the monohydride is the only stable adsorbate state. These data were then converted with the help of a series of TPD experiments for discrete exposures (inset: bottom). The resulting calibration curve $\chi^{(2)}_s(\theta) \propto \sqrt{I^{(2\omega)}}$ is shown in the main panel with the hydrogen coverage of 1 ML defined as the number of dangling bonds of the 2×1 reconstructed surface ($n = 0.68 \times 10^{15}$ cm$^{-2}$). For $\theta < 0.2$ ML, $\chi^{(2)}_s$ has an approximately linear coverage dependence

$$\chi^{(2)}_s(\theta) \approx \chi^{(2)}_{s,0}(1 - \alpha\theta) \tag{3.3}$$



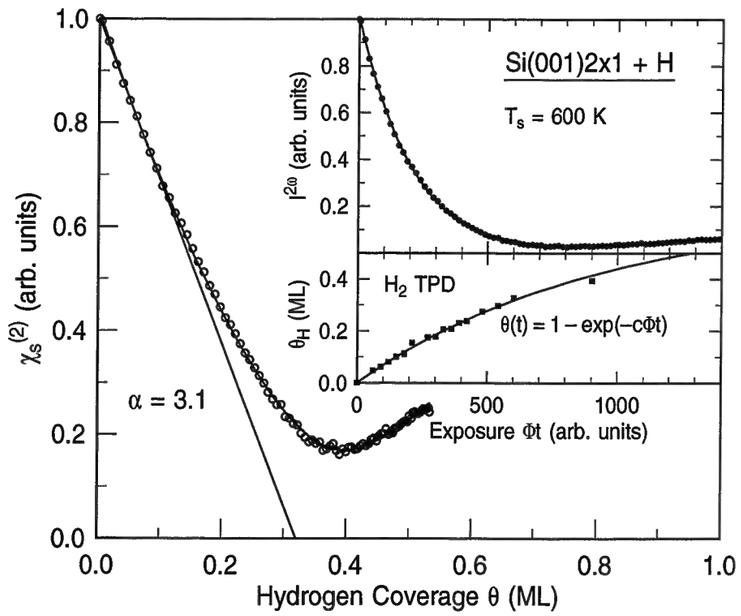


**Fig. 3.5:** Calibration of the SH response for Si(001) as a function of the hydrogen coverage (data from Ref. [26]). Inset: decrease of the SH intensity during exposure with atomic hydrogen for constant flux (top); coverage after discrete exposures determined with TPD (bottom).

with slope $\alpha \simeq 3.1$ ML$^{-1}$ (straight line) [26]. Similarly in the case of Si(111)7×7 using $\alpha \simeq 1.3$ ML$^{-1}$, the linear relation was found to describe the behavior for $\theta < 0.4$ ML [14]. Again the coverage is referred to the density of dangling bonds with 1 ML = $0.3 \times 10^{15}$ H atoms/cm$^2$.

These relations were applied in the previous studies addressing the hydrogen reaction kinetics in adsorption [14,26,27], desorption [10,11], and surface diffusion [12] on both Si(111) and Si(001). Similarly, throughout most of the hydrogen adsorption, desorption, and diffusion experiments described here this calibration is used. With TPD it was verified that the calibration is also valid for describing the terrace adsorption on the vicinal surfaces. In addition, molecular hydrogen was adsorbed to near full monolayer coverage by exposing the sample to high pressure. The observed signal dependence during exposure, including the transition through the minimum at higher coverages, reproduces what one expects from adsorbing atomic hydrogen.

### Oxygen adsorption

In principle, the use of SHG as a probe for surface kinetic processes is not restricted to simple chemisorbates such as hydrogen. Although SHG has been applied in a number of studies addressing the interaction of oxygen with silicon surfaces, as will be discussed in chapter 6, the relationship of the nonlinear susceptibility to coverage has not yet been established. The behavior is expected to differ from that found for hydrogen since oxygen not only strongly interacts with the silicon dangling bonds, but also breaks the Si-Si bonds.

Similarly to the procedure described above, the changes of the nonlinear susceptibility $\chi_s^{(2)}$ of Si(001)2×1 were related to the oxygen coverage by a comparison of TPD and SHG experiments. In this case the SH signal $\left(I^{(2\omega)} \propto |\chi_s^{(2)}|^2\right)$ was recorded before and after the sample was exposed to a desired dose of $O_2$. Background dosing was performed with research grade 99.998 vol.% molecular oxygen at pressures of $\sim 10^{-7}$ mbar recorded with an uncalibrated ion gauge. Then the resulting relative oxygen coverages were determined from the areas of the SiO corresponding TPD peaks. TPD

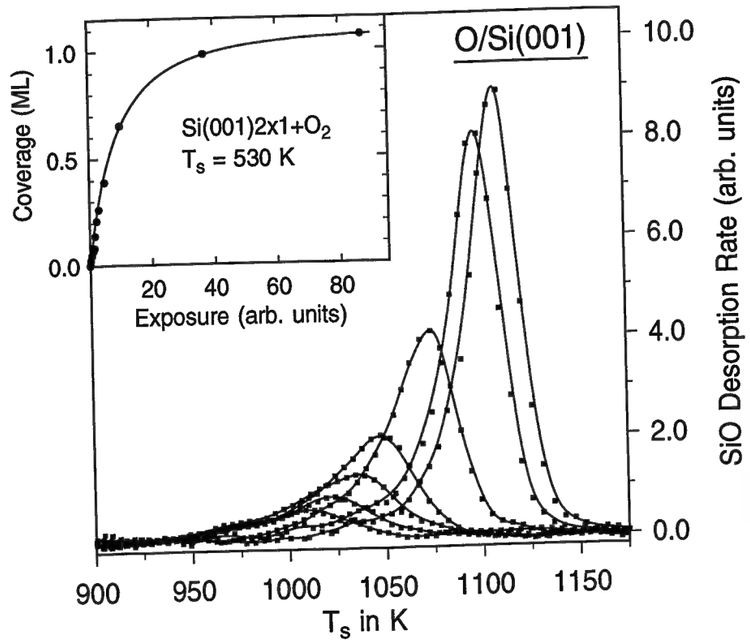


**Fig. 3.6:** Thermal desorption traces for SiO from Si(001) for coverages of 0.14, 0.21, 0.26, 0.39, 0.65, 0.98, and 1.07 ML (heating rate $\sim 14\,\mathrm{Ks}^{-1}$). Inset: oxygen coverage of Si(001) versus $O_2$ exposure at $T_s = 530$ K. The origin of the pronounced shift in peak temperature is due to the inhomogeneous decomposition of the oxide layer and is addressed in chapter 6.



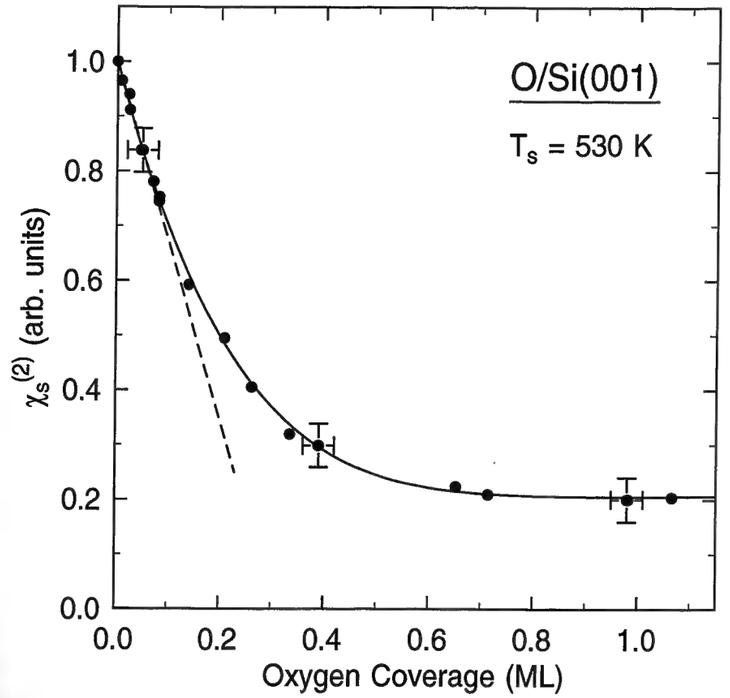


**Fig. 3.7:** Decrease of the nonlinear susceptibility $\chi_s^{(2)}$ for Si(001) with oxygen coverage determined from TPD data. For coverages $< 0.15$ ML, the dependence is approximately linear. The solid line represents the best fit to the model function eq. 3.5.

data and the observed adsorption behavior as a function of exposure $\Phi \cdot t$ are therefore plotted in Fig. 3.6. The adsorption process is characterized by fast initial uptake followed by a regime of slow oxide growth. The solid line in the inset is the fit to a modified Langmuir isotherm resulting from a sticking probability of the form

$$s(\theta) = \frac{\mathrm{d}\theta}{\mathrm{d}t \cdot \Phi} = s_0 \left(1 - \frac{\theta}{\theta_{\mathrm{sat}}}\right)^d . \tag{3.4}$$

This functional dependence accounts for the fact that after the initial uptake up to 1 ML the surface is not truly saturated and will continue to adsorb oxygen for extended exposures [141,142]. With an apparent saturation coverage of $\theta_{\mathrm{sat}} = 1.1$ ML and parameter $d = 1.5$ the experimental data can be described quite accurately.

The resulting coverage dependence of the absolute magnitude of $\chi_s^{(2)}$ is given in Fig. 3.7. For coverages $\theta < 0.15$ ML the signal decrease is approximately linear $\chi_s^{(2)}(\theta) \simeq \chi_{s,0}^{(2)}(1 - \alpha\theta)$ with $\alpha \approx 3\,\mathrm{ML}^{-1}$ (dashed line), similarly to the case of hydrogen adsorption. However, for higher coverages the dependence deviates markedly from

the corresponding hydrogen adsorption behavior.

### 3.4.2 Model for SH-coverage dependence

In modeling the dependence of $\chi_s^{(2)}$ over the full coverage range it is important to take into account the nonlocal influence exerted by one adsorbed species on its neighboring dangling bonds. This effects the electronic structure and decreases their relative contributions to $\chi_s^{(2)}$ [17]. By analogy with a model used to describe the local field corrections in SHG theory [143], a suitable analytical form for $\chi_s^{(2)}(\theta)$ is given by

$$\chi_s^{(2)}(\theta) = \chi_{s,db}^{(2)} \left(1 - \frac{\alpha\theta}{(1+\beta\theta^{3/2})^3}\right) + \chi_{s,NR}^{(2)}. \qquad (3.5)$$

Besides the dominant contribution given by the dangling-bond-derived near resonant term $\chi_{s,db}^{(2)}$, the term $\chi_{s,NR}^{(2)}$ describes the non-resonant background originating from the two-photon resonance at 3.4 eV and additional bulk contributions [17]. Although $\chi_{s,NR}^{(2)}$ has been found to depend on coverage [123], its overall contribution to the measured SH response is comparatively weak. For the purpose of parameterization it is therefore assumed to be constant. For small coverages ($\theta \ll \beta^{-2/3}$), this equation takes the linear form $\chi_s^{(2)}(\theta) \approx \chi_{s,0}^{(2)}(1-\alpha'\theta)$ similar to eq. 3.3 with $\alpha' = \alpha\chi_{s,db}^{(2)}/(\chi_{s,db}^{(2)} + \chi_{s,NR}^{(2)})$. The dependence on $\beta\theta^{3/2}$ originates from the dipole-dipole interaction depending on $1/r^3$, with $r$ being the average distance between neighboring adsorbates proportional to $1/\theta^{1/2}$.

Since both $\chi_{s,db}^{(2)}$ and $\chi_{s,NR}^{(2)}$ are complex quantities, $\chi_s^{(2)}(\theta)$ is determined by four parameters, viz. the relative magnitude and phase difference of $\chi_{s,db}^{(2)}$ and $\chi_{s,NR}^{(2)}$ and the proportionality constants $\alpha$ and $\beta$. $\left|\chi_{s,db}^{(2)}\right|$ and $\left|\chi_{s,NR}^{(2)}\right|$ can be taken directly from the data at zero and 1 ML coverage, respectively. In addition, since in contrast to H/Si(001) the signal does not go through a minimum, restricting the phase shift to $\phi \approx 90°$, only two free parameters $\alpha$ and $\beta$ remain. The solid line in Fig. 3.7 shows the result of the best fit of eq. 3.4 to the measured data points with $\chi_{s,db}^{(2)}/\chi_{s,NR}^{(2)} = 4.9 \times \exp(i93.4°)$, $\alpha = 3.7$, $\beta = 0.59$.

Similarly to the calibration procedure shown in the case of hydrogen on Si(001), the TPD-derived uptake curve (inset in Fig. 3.6) can be used to convert the *in-situ*-recorded adsorption traces for a constant oxygen flux to a calibration curve. An example for O/Si(001) and a surface temperature of 530 K is shown in the inset in Fig. 3.8. The converted data for Si(001) are plotted in the main panel of that figure and are found to be in excellent agreement with the fit using the model function discussed above.

For comparison, in the same figure the coverage dependence is shown for O/Si(111) 7×7. Although no direct TPD calibration was performed the exposure data taken from Ref. [130] could be converted by comparing with X-ray photoelectron spectroscopy



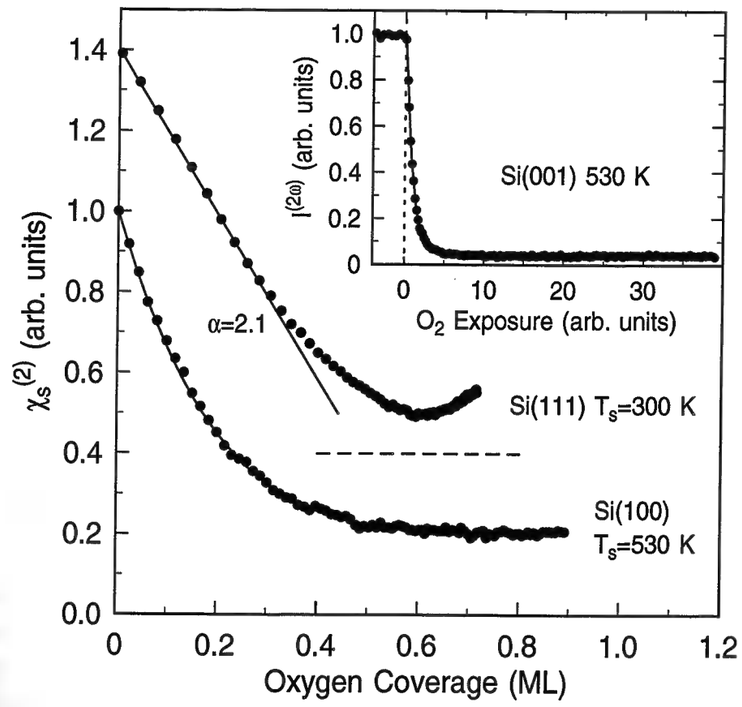


**Fig. 3.8:** Nonlinear susceptibility $\chi_s^{(2)}$ of Si(001)2×1 (this work) and Si(111)7×7 (data from Ref. [130]) as a function of oxygen coverage. The calibration curve $\chi_s^{(2)}(\theta) \propto \sqrt{I^{(2\omega)}}$ was obtained by converting the exposure into a coverage scale using the TPD uptake measurements.

(XPS) experiments [144,145]. In contrast to Si(001), the Si(111) data exhibit a pronounced minimum of $\chi_s^{(2)}$ at a coverage of ~0.6 ML. One ML is defined here as the density of surface atoms of unreconstructed Si(111)1×1 ($n = 0.78 \times 10^{15}\text{cm}^{-2}$). The minimum of the nonlinear susceptibility observed in the cases of hydrogen on both Si(001)2×1 and Si(111)7×7 and oxygen on Si(001)2×1 arises from a phase shift of $\phi > 90°$ between the two main contributions to $\chi_s^{(2)}$. This is shown representatively for the hydrogen adsorption in Fig. 3.5, where the model function with the parameters $\chi_{s,db}^{(2)}/\chi_{s,NR}^{(2)} = 2.8 \times \exp(i162°)$, $\alpha$=2.4 and $\beta$=0.32 well reproduces the data.

### 3.4.3 Adsorption and desorption kinetics

By studying gas surface reaction systems from the derived kinetic parameter a reaction model can be proposed. This together with the whole set of theoretical methods – from simple transition state theory arguments to very refined *ab initio* calculations –

can help to infer the underlying dynamics.

In the experiments described here, from measurements of the temporal change of surface coverage $\theta(t)$ during gas exposure or desorption it is possible to deduce the kinetic parameter from the following equation:

$$\frac{\mathrm{d}\theta}{\mathrm{d}t} = k_{\mathrm{ads}}(\theta, t, T_{\mathrm{s}}, ...) + k_{\mathrm{des}}(\theta, t, T_{\mathrm{s}}, ...). \tag{3.6}$$

In general, the rate of adsorption $k_{\mathrm{ads}}$ can be written as

$$k_{\mathrm{ads}} = \Phi(t)s(\theta), \tag{3.7}$$

where $\Phi(t)$ is the flux of particles onto the surface and $s(\theta)$ the coverage-dependent sticking coefficient. For direct dissociative adsorption,

$$s(\theta) = s_0(1-\theta)^2, \tag{3.8}$$

with $s_0$ the sticking coefficient at zero coverage. The validity of this functional form requires thermal equilibrium of the surface with a random distribution between identical, non-interacting adsorption sites [146]. These conditions are, however, rarely the case for the systems under investigation here. In most cases discussed below initial sticking coefficients are therefore derived from small changes in surface coverage, where the coverage dependence of $s$ is negligible [17].

For the rate of desorption and its dependence on coverage one has

$$k_{\mathrm{des}} = \theta^m \nu_{\mathrm{des}}, \tag{3.9}$$

with $m$ the order of the reaction and $\nu_{\mathrm{des}}$ the desorption rate constant.

For the purpose of data evaluation one has to solve the general equation 3.6. This is done numerically, preferably with $s_0$ and $\nu_{\mathrm{des}}$ as the only free parameters. In the case of conditions of negligible desorption during adsorption (low surface temperature) or vice versa (small background pressure) the two processes can be separated, enabling one to address the kinetic parameter independently.

If both $s_0$ and $\nu_{\mathrm{des}}$ are assumed to obey an Arrhenius expression, then one has

$$s(\theta) = s_0 \exp\left(-\frac{E_{\mathrm{ads}}}{k_{\mathrm{B}}T_{\mathrm{s}}}\right) \tag{3.10}$$

and

$$\nu(\theta) = \nu_0 \exp\left(-\frac{E_{\mathrm{des}}}{k_{\mathrm{B}}T_{\mathrm{s}}}\right), \tag{3.11}$$

where $s_0$, $\nu_0$ and $E_{\mathrm{ads}}$, $E_{\mathrm{des}}$ are the pre-exponential factors and activation energies for adsorption and desorption, respectively.

In the case of hydrogen adsorption the primary goal has been to determine sticking coefficients for dissociative adsorption for different surface temperatures. For that



purpose both the measured SH signal and recorded $H_2$ pressure $p$ as a function of time enter a fitting algorithm solving the differential equation 3.6 [14]. The fit routines used minimize the weighted sum squared $R = \sum_i g_i[f(x_i) - y_i]^2$ for the model function $f(x_i)$ and the data points $y_i$ (i.e. $\chi_{\mathrm{s}}^{(2)}$ and $p$) at position $x_i$ (i.e. time) via a gradient method [147,148]. The hydrogen pressure $p$ is related to the impinging particle flux $\Phi$ by $\Phi = p\,(2\pi m_{\mathrm{H_2}} k T_{\mathrm{gas}})^{-1/2}$.

The advantage of the *in situ* measurements is that sticking coefficients are accessible for temperatures above the onset of desorption. The desorption rates can also be deduced independently of the same set of data from the recovery of the SH signal after the gas flux is turned off. Although it has been shown in previous studies that the reaction order in desorption is coverage-dependent, for practical reasons both in the case of Si(111) and Si(001) for coverages $\theta < 0.15$ ML, a fractional order $m = 1.5$ was used to describe the desorption behavior sufficiently accurate [10,11].

The procedure is simplified in the case of constant $\Phi$ and negligible desorption, which leads to a constant SH signal decrease, and the initial sticking coefficient is then proportional to the slope of $\chi_{\mathrm{s}}^{(2)}$ according to $\Delta\theta_{\mathrm{H}}/\Delta t = \Phi s_0$, with $\Phi$ in units of $\mathrm{MLs}^{-1}$. Most of the experiments described in the following chapters were performed in the low-coverage regime and the linear relations established between $\theta$ and $\chi_{\mathrm{s}}^{(2)}$ can be used. Only in the case of the oxygen desorption experiments from Si(001) for coverages of up to 0.6 ML was the full calibrated functional dependence was taken into account.

The sticking coefficient or probability $s$ is defined as the ratio of the rate of capture of an atom or molecule in the chemisorbed state to the rate of collision of the gaseous particles with the surface [149]. Unless otherwise noted the sticking coefficient specified throughout this thesis are given with respect to this definition. In the case of the presence of different adsorption sites such as steps, which exhibit different reactivities compared to the terraces, the sticking probability scales with the step density. Provided that the density of the different sites is known, in order to be able to directly compare the reactivities of e.g. different types of steps, a site-specific reactivity is defined as $\hat{s} = s_0\theta_{\mathrm{site}}^{-1}$. Here $s_0$ would be the sticking coefficient and $\theta_{\mathrm{site}}$ denotes the concentration of the reactive site.

# Chapter 4

# Hydrogen interaction with vicinal silicon surfaces

It has been known since the early days of surface science that defects and more open, rough surfaces can markedly increase the adsorption probability [150,151]. In addition to a reduced adsorption barrier, compared to well ordered terrace sites, steps and defects tend to bind adsorbates more strongly and give rise to increased diffusion barriers. Although these effects strongly influence the adsorbate kinetics, detailed knowledge of the underlying processes is scarce.

In the case of silicon, the chemical properties of steps have gained considerable practical interest because they play a central role for homo- and heteroepitaxial growth, chemical vapor deposition (CVD), and the wet chemical preparation of surfaces [20,23,152,153]. Although progress has been made over the years in improving the process conditions on an empirical basis, the underlying microscopic processes are poorly understood. In the formation of epitaxial layers in CVD which proceeds via the step-flow growth mode the reactivity of the steps plays a central role, making knowledge of the chemical properties of step sites highly desirable [8]. In the aqueous and non-aqueous chemical preparation of surfaces with extremely low defect densities the etch rate depends on the local surface morphology. Since silicon adspecies or clusters are susceptible to attack from all sides, they are readily etched, which tends to planarize the surface [8,70,71,154].

This structure sensitivity of the reaction has been attributed to the reduced coordination number of the defect or step edge atoms on metal surfaces [149,150]. However, this argument is not applicable to steps on semiconductor surfaces. Here, for most of the different types of defects and, in particular, steps and kinks, there is a threefold coordination similar to the reconstructed terrace atoms [59]. All single crystal surfaces, even if prepared with the greatest possible care, contain at least some small amounts of steps and other imperfections. On Si(001), which, in general, has a higher affinity towards interaction with chemisorbates compared with Si(111) one could imagine that this is the result of the higher intrinsic defect concentration known from STM investigations [8]. In the extreme case, as already mentioned in chapter 2, for the interaction of molecular hydrogen with silicon surfaces in general and Si(001)

in particular, models are under debate which attribute the $H_2$ surface chemistry to be defect-mediated.

The first part of this chapter presents experiments dealing with various aspects concerning the dissociative adsorption of molecular hydrogen on Si(001)2×1 and Si(111)7×7 samples with different types of deliberately created steps and defects. The results are discussed in terms of different microscopic models to describe the underlying reaction dynamics. This is followed by a systematic investigation of the hydrogen interaction with $D_B$ steps on Si(001)2×1. These experiments are discussed with the help of theoretical investigations on the basis of the *ab initio* density functional theory (DFT) approach, which could provide insight into the underlying microscopic origins of the observed reaction behavior. Similar reaction mechanisms for dissociative adsorption on the terrace sites along inter-dimer dissociation pathways are presented thereafter. In the proceeding study the enhanced reactivity of the steps was used to create non-equilibrium hydrogen distributions on the vicinal Si(001) surface. This enabled investigations of surface diffusion in the presence of steps and of the hydrogen energetics in equilibrium.

## 4.1 Influence of steps and defects on the reaction of molecular hydrogen with silicon surfaces[1]

### 4.1.1 Motivation

The microscopic reaction mechanisms proposed to describe the reaction dynamics of $H_2$ with the Si(001)2×1 silicon surface are contradictory in various respects as discussed in chapter 2. On the one hand, the DFT-based slab-type calculations predict a direct, one step adsorption and desorption mechanism with a substantial coupling of the barrier heights to the dimer buckling (compare Fig. 2.8) [84,98,100]. Although this mechanism is in qualitative agreement with the phonon-assisted sticking model proposed by Brenig *et al.* [27,28], it differs quantitatively from the experimental results. Alternatively, as a result of *ab initio* cluster calculations, it was suggested, that single-atom defects mediate hydrogen adsorption and desorption [103,105,106,111]. These defects would facilitate the creation of dihydride intermediates without an appreciable adsorption barrier. The presence of such sites would thus not lead to translational heating in desorption whereas the sticking probability would be determined by their temperature-dependent concentration. The active sites were discussed to be either intrinsic defect and step sites or transiently created minority sites. Whereas DFT contains possible uncontrolled approximations, the cluster approach has inherent difficulties to account for lattice degrees of freedom.

[1] Most of the results discussed in this section were published as an article in Applied Physics: M. B. Raschke and U. Höfer, *Appl. Phys. B* **68**, 649 (1999).



This issue is accessible experimentally and the independent study of the kinetics of the hydrogen interaction with both the ordered Si-dimers as well as with minority sites on the surface is presented here. For that purpose hydrogen adsorption experiments are performed on crystal faces that contain minority sites deliberately created at concentrations above the 1% level.

In addition to the inconsistencies of the theoretical models, there are discrepancies between earlier SHG experiments [26,27] and supersonic molecular beam experiments [32] concerning both absolute values and temperature dependence of the sticking probabilities on Si(001). This issue will also be addressed here.

### 4.1.2 Hydrogen adsorption at steps and defects

#### Planar and vicinal Si(001)2×1

The first experiments deal with the highly doped 0.003-Ωcm Si(001) sample misoriented by ∼1° predominantly towards [010]. By measuring hydrogen uptake curves the corresponding adsorption kinetics and sticking coefficients can be derived. For that purpose the SH response is monitored as a function of time during hydrogen exposure, which is shown in Fig. 4.1. The clean surface is kept at a constant temperature $T_s$=575 K and at $t$=0 the hydrogen pressure is increased to the desired value, leading to a signal decrease as a result of dissociatively adsorbed hydrogen. Apparently, the adsorption behavior is characterized by two time constants: a fast initial drop of the nonlinear susceptibility right after the beginning of hydrogen exposure which saturates quickly is followed by a comparably slow decrease. After the $H_2$ flux is turned off, the signal stays constant or would increase for surface temperatures where desorption is appreciable ($T_s > 700$ K). From the desorption behavior it can be verified that the recorded changes of $\chi_s^{(2)}$ are solely due to adsorbed hydrogen [26]. For that purpose after each adsorption experiment the sample temperature is increased to about 900 K within a few seconds. The hydrogen desorbs almost instantaneously ($\nu_{des} \sim 10\,s^{-1}$) and the SH signal quickly rises to the value as measured for the initially clean sample for that surface temperature. In contrast, in the presence of oxygen or water - the possible major contaminants in the dosing gas, which would readily adsorb on silicon - the signal would only recover slowly due to the comparatively small desorption rate of SiO ($\nu_{des} \simeq 10^{-2}\,s^{-1}$) for that temperature (see also chapter 6).

The fast reaction saturates long before saturation coverage is reached and we therefore attribute this process to the interaction with minority sites such as the steps and other kinds of defects present on the surface. The slow adsorption process could, in principle, be caused by hydrogen diffusion onto the terraces and rapid refilling of the depleted minority sites. Interrupting the hydrogen exposure right after saturation of the first adsorption regime (see also Fig. 4.4) indicates, however, that the observed behavior can be attributed to two distinct reaction channels. Diffusion would be

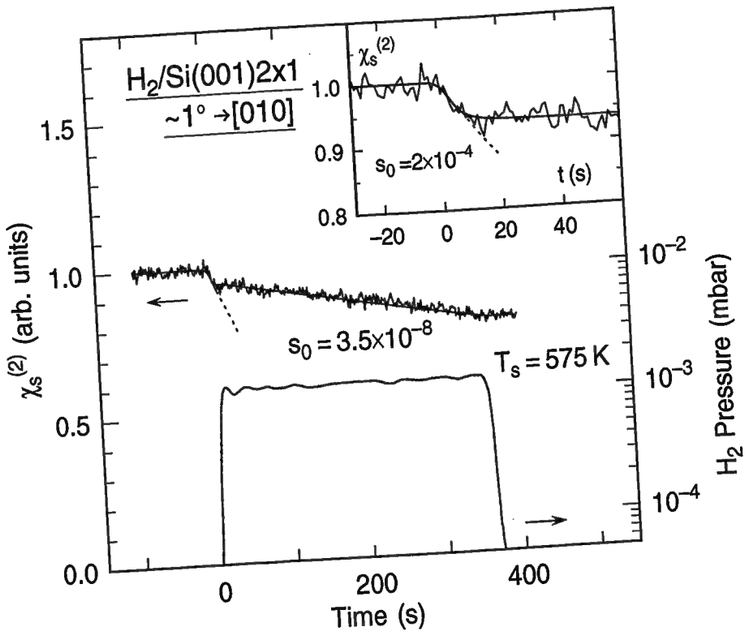


**Fig. 4.1:** Nonlinear response $\chi_s^{(2)}$ of Si(001)2×1 slightly misoriented by ∼1° towards [010] with $\rho = 0.003\,\Omega$cm during $H_2$ exposure for a substrate temperature $T_s = 575$ K. Inset: blow-up of the initial signal decrease right after hydrogen exposure.

visible as a fast secondary signal drop after resuming hydrogen dosing due to sticking at the depleted step sites, which is not observed for these surface temperatures.

The corresponding sticking coefficients $s_0$ are determined from the temporal change of both the nonlinear susceptibility and the recorded hydrogen pressure following the procedure described earlier with $s_0$ as the only free parameter. The proportionality factor $\alpha = 3.1\,\mathrm{ML}^{-1}$ from the coverage calibration is applied for the terrace adsorption. For the steps the solid line shown in the inset is the result of a numerical fit using $\alpha = 1\,\mathrm{ML}^{-1}$ and second-order Langmuir kinetics, which will be rationalized in the next chapter. The fast adsorption at the minority sites after the beginning of the hydrogen exposure corresponds to a site specific sticking coefficient of $2\times10^{-4}$. For the slow adsorption process the sticking coefficient is found to be $3.5\times10^{-8}$. With four orders of magnitude higher reactivity for the steps compared with the terrace sites the two adsorption rates are sufficiently distinct to allow their independent determination.

For comparison, the reaction with orientationally flat 10-Ωcm Si(001) was investigated. The hydrogen adsorption performed under similar experimental conditions compared with those described above is shown in Fig. 4.2. Apparently, the hydrogen uptake of this surface can be described by just one adsorption rate constant resulting



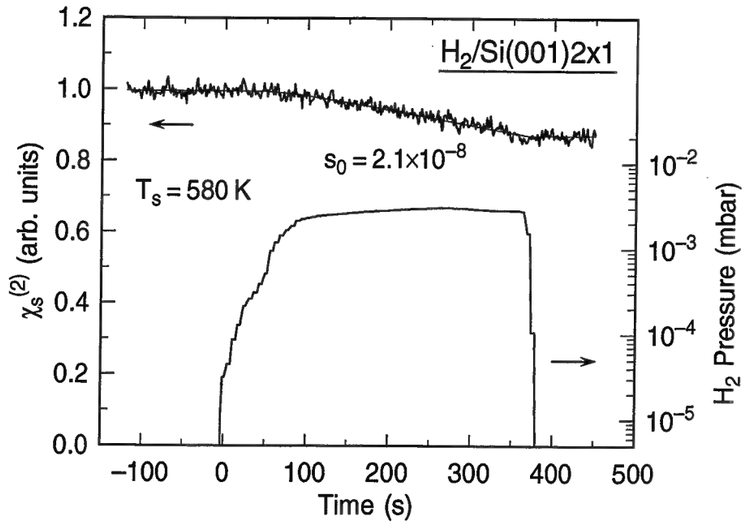


**Fig. 4.2:** Temporal change of $\chi_s^{(2)}$ for the orientationally flat Si(001)2×1 with $\rho = 10\,\Omega$cm for a substrate temperature $T_s = 580$ K during hydrogen exposure.

in a sticking coefficient of $2.1\times10^{-8}$. The slow adsorption process which corresponds to these small sticking coefficients can thus be identified as the adsorption of hydrogen on the terraces. With the same sticking coefficients for the flat and misoriented surfaces for this surface temperature, the reaction is not influenced by the presence of the steps and defects.

In Fig. 4.3 adsorption experiments are shown for higher surface temperatures for the stepped surface. Up to about 600 K the adsorption on the terraces can be monitored independently of the step adsorption and the derived values for the sticking coefficients match those determined for flat Si(001). For higher temperatures, however, hydrogen diffusion becomes increasingly significant. This can be seen from the measurement shown for $T_s = 660$ K. Here the saturation of the step sites and diffusion of hydrogen onto the terraces leads to an enhanced hydrogen uptake of the surface. This results in a higher effective sticking coefficient for terrace adsorption compared with the direct adsorption process as measured on well prepared planar Si(001). The dashed line shows the behavior expected if no diffusion would occur. For temperatures in excess of 760 K, however, the direct adsorption mechanism starts to compete with the step adsorption/diffusion mechanism as a result of the surface-temperature-dependent increase in the sticking coefficients for the terraces. This can be seen in the adsorption behavior at 800 K where the sticking coefficient of $2.7\times10^{-6}$ is already undistinguishable from orientationally flat Si(001).

It has been mentioned in the previous chapters that the occurrence of at least a

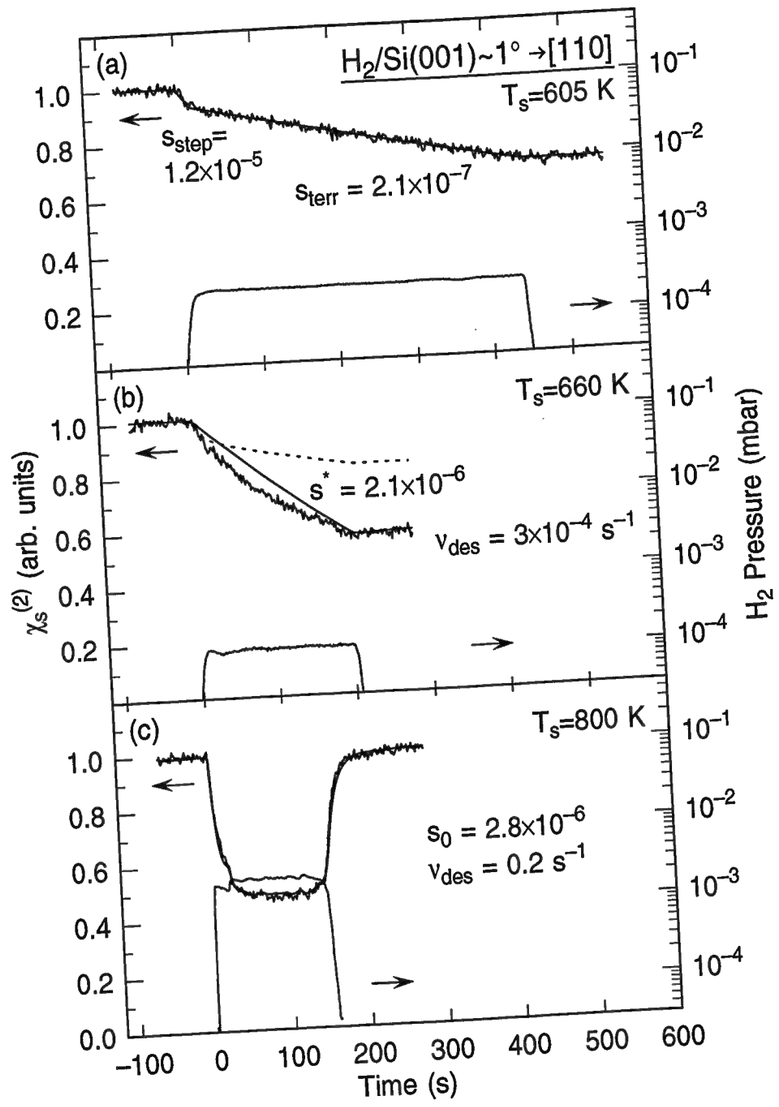


**Fig. 4.3:** Data describing the adsorption behavior of Si(001)2×1 slightly misoriented towards [010] for different surface temperatures of 605, 660, and 800 K. For $T_s > 620$ K the onset of desorption has been taken into account in the numerical fit. In the temperature range between 620 K and 760 K enhanced, diffusion-mediated hydrogen uptake is observed. The dashed line in (b) represents the adsorption behavior one would expect in the absence of diffusion.



small number of steps and defects during sample preparation is an intrinsic property of the Si(001) crystal face. However, not all types of defects might exhibit an enhanced reactivity. From the SH signal drop in the experiments on the planar surface such as that shown in Fig. 4.2, one can conclude that the number of reactive defects is below 0.5% ML. However, it could not be ruled out *a priori* that SHG might be insensitive to some types of possibly reactive minority sites. TPD experiments were performed after $H_2$ exposure just until the onset of a detectable SH signal decrease. With the TPD experiment optimized to be sensitive to the sub-1% hydrogen coverage level, it has been verified that within the accuracy of the experiment no hydrogen uptake occurs which is not associated with a corresponding SH signal decrease.

The following experiments show that the sample preparation scheme has a dramatic effect on the concentration of the number of chemically active minority sites on the surface. It is known that especially under annealing conditions shear stress leads to edge dislocations by the slipping of one crystal plane with respect to another, which would result in additional steps on the surface. A sample was mounted on slightly misaligned copper rods of the sample holder. As a result of this external strain the sample surface was slightly bent into a concave shape, as seen from He-Ne laser reflection. This led to adsorption behavior very similar to that of the slightly miscut sample with a small amount of hydrogen adsorbed at a comparatively high rate, as can be seen in Fig. 4.4. In this experiment the initial hydrogen uptake was measured at a reduced $H_2$ pressure in order to determine the corresponding sticking probability accurately. Performing TPD measurements after saturation of the fast adsorption regime, the corresponding hydrogen coverage was found to be $\sim 4\%$ ML. Both the resulting sticking coefficients of $1.9 \times 10^{-4}$ and $5.6 \times 10^{-8}$ for the adsorption at the minority sites and terrace adsorption, respectively, are in excellent agreement with the measurements described above. These experiments also show that the reaction behavior as observed for the 0.003-Ωcm sample is not specific to the high dopant level. The fact that the reaction behavior is independent of the interruption of the $H_2$ exposure again indicates the absence of hydrogen diffusion.

Another way of creating steps and defects on the surface is to perform several cycles of oxygen adsorption and desorption. The decomposition of the oxide layer as volatile SiO leads to inhomogeneous etching of the topmost surface layers with roughening and pit formation up to several atomic layers deep, as will be discussed in detail in chapter 6. This treatment was performed on the originally well-prepared surface used for the experiments shown in Fig. 4.3. Even after annealing of this surface to 1250 K its original flatness could not be recovered and reaction behavior towards hydrogen very similar to that described for the strained or misoriented surface is found.

Judging from the similar relative SH signal decrease for all the cases discussed so far where a comparably fast initial reaction channel was found, it can be assumed that the corresponding density of these highly reactive sites is similar to the strained surface where the hydrogen adsorption was characterized with TPD. Scaling the derived value

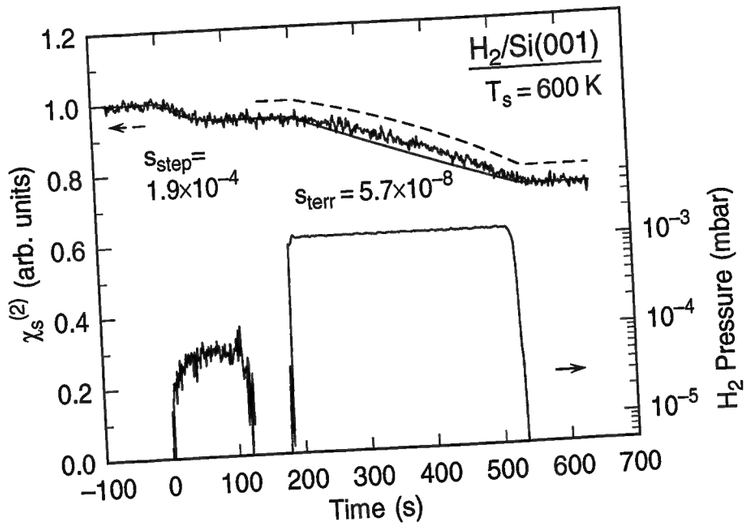


**Fig. 4.4:** Nonlinear response $\chi_s^{(2)}$ of flat Si(001)2×1 mounted under external strain during $H_2$ exposure. The initial signal drop due to adsorption at the steps/defects is not followed by hydrogen diffusion from these minority sites. The dashed line represents a numerical fit (vertically shifted by 0.05 for better distinction) to a reaction model for terrace adsorption discussed in section 4.3.

of the sticking probability for the steps and defects with the hydrogen saturation coverage of the corresponding sites, one obtains the sticking coefficient with respect to the total number of available adsorption sites (i.e. step/defect and terrace sites) of the surface. With the concentration of the minority sites of 4–6%, the initial sticking coefficients for these surfaces containing step or defects are found to be very similar, ranging between $6\times10^{-6}$ and $2\times10^{-5}$, as deduced from these and other measurements.

In Fig. 4.5 the reaction of Si(001) with a misorientation of 3° towards [010] with hydrogen is shown for a sample temperature of 580 K. Due to the larger angle of miscut the higher number of step sites leads to a more pronounced decrease of the corresponding SH signal upon hydrogen adsorption. The step adsorption can be described with a sticking coefficient of $4.5\times10^{-5}$. No terrace adsorption can be observed in this particular experiment because of the low dosing pressure used.

The [010] direction forms an angle of 45° with respect to the dimer row orientation. Although under these conditions one does not expect the formation of straight regular steps, the use of this crystallographic face was motivated by a recent hydrogen adsorption study performed on that surface [155]. In that investigation no two distinct reaction channels were observed and the reported high sticking probabilities for this surface of up to 0.1 for temperatures between 570 and 730 K are at clear variance with the measurements described here. Possible reasons explaining these discrepancies will



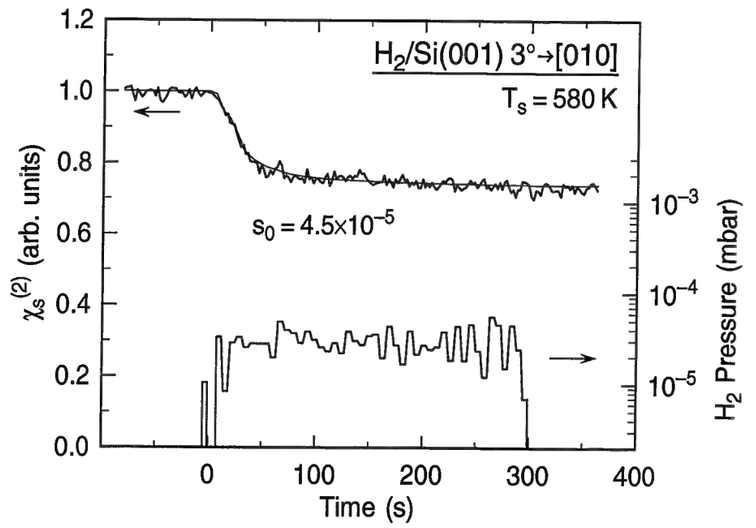


**Fig. 4.5:** Hydrogen adsorption at the steps of Si(001)2×1 misoriented by 3° towards [010] at a surface temperature $T_s = 580\,\mathrm{K}$ leading to a pronounced signal decrease due to the larger number of step sites. The low hydrogen pressure and sample temperature lead to only negligible hydrogen uptake on the terraces.

be discussed below.

### Vicinal Si(111)7×7

Whereas the reactivity of the minority sites on vicinal Si(001)2×1 exceeds the corresponding value for terrace adsorption by several orders of magnitude, the effect of misorientation on the sticking of $H_2$ was found to be much weaker in the case of the Si(111)7×7 5° → [1$\bar{1}$0] surface investigated. This surface is comprised of wide terraces with 7×7 structure separated by facets oriented ∼ 20° off the [111] direction [52,156]. Measurements of the extremely small sticking coefficients determined for that surface for temperatures of 520 and 580 K are shown in Fig. 4.6. Compared with vicinal Si(001), the sticking coefficients at the minority sites are three to four orders of magnitude lower for surface temperatures between 500 and 600 K. With a sticking coefficient of $5\times10^{-9}$ the reaction with the steps is only one to two orders of magnitude higher than the corresponding terrace adsorption for these surface temperatures. Despite this small value, the experiments shown clearly demonstrate that two separable reaction channels exist: After saturation of the "fast" sticking reaction (a) at the steps further hydrogen uptake can only be observed after either increasing the surface temperature (b) or hydrogen pressure (c). At $T_s = 520$ K the sticking coefficient ultimately drops to a value as low as $4\times10^{-11}$. This extremely low

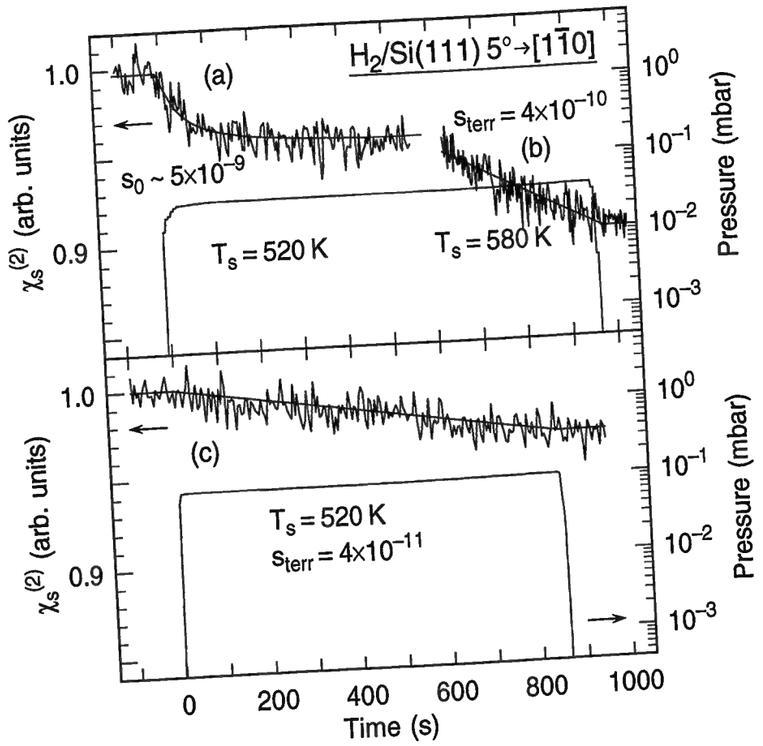


**Fig. 4.6:** Nonlinear response $\chi_s^{(2)}$ of Si(111)7×7 misoriented by 5° towards [1$\bar{1}$0]. Top: adsorption at the minority sites ($\sim 0.06$ ML) at $T_s = 520$ K with a sticking coefficient of $5\times10^{-9}$ (a); adsorption continues on the terraces if the sample temperature is increased (b) ($s_0 = 4\times10^{-10}$ for $T_s = 580$ K). Bottom: sticking coefficient of $4\times10^{-11}$ for terrace adsorption at $T_s = 520$ K (c): A gas flux of almost $10^6$ ML s$^{-1}$ is required for the adsorption of 0.03 ML in 15 min. (1 ML = $0.30\times10^{15}$ atoms cm$^{-2}$).

sticking coefficient can be measured reproducibly and the absence of contaminants could be seen from the hydrogen desorption behavior at $T \simeq 900$ K. To illustrate this exceedingly small value, it should be noted that in order to achieve the observed 0.03 ML hydrogen uptake a total exposure of $9\times10^8$ ML (flux $10^6$ ML s$^{-1}$ during a 15 min exposure time) was required. This finding together with the results on Si(001) indicate that a specific step structure is required to effectively dissociate molecular hydrogen on silicon surfaces, apparently not present on this type of misorientation on Si(111).

Similar to the adsorption on vicinal Si(001), for the reaction of $H_2$ with Si(111) 5° → [1$\bar{1}$0] Hansen *et al.* found surprisingly high sticking coefficients [155]. Values as high as $\sim 0.01-1$ in the temperature range between 540 and 660 K were reported.



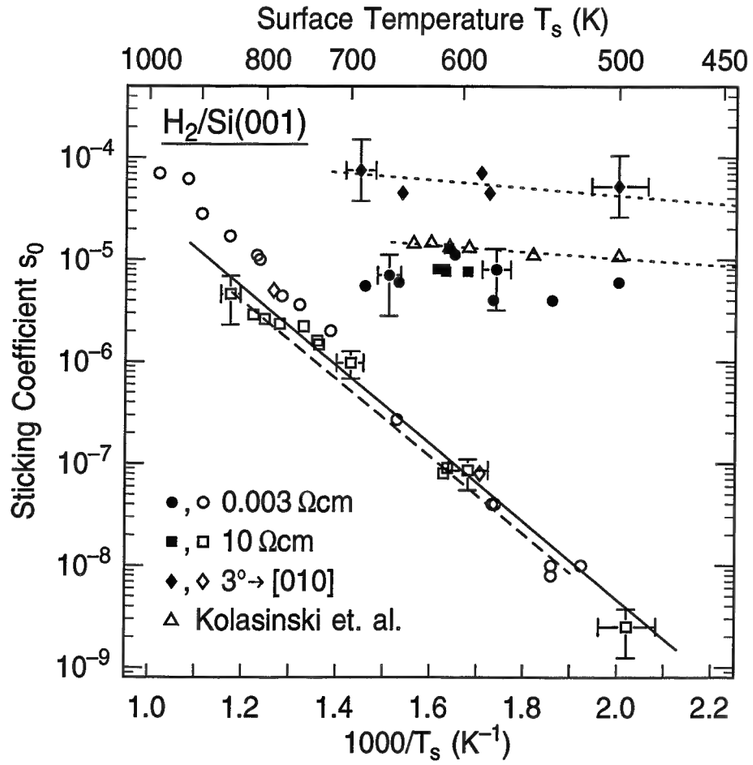


**Fig. 4.7:** Arrhenius plot of the initial sticking coefficients $s_0$ for dissociative adsorption of $H_2$ on flat and misoriented Si(001) surfaces. The solid line denotes a numerical fit to an exponential temperature dependence for the values derived from terrace adsorption. The dashed line represents the fit to the data for flat Si(001) taken from [26]. The open triangles are the values determined by Kolasinski *et al.* [32] for $D_2$/Si(001).

Although no convincing explanations can currently be given to interpret the discrepancies of about nine orders of magnitude with the study of Hansen and Seebauer, it should be mentioned that the sensitivity of their experiment was very limited as a result of non-resonant SH pump-wavelength, hydrogen purity, and gas handling.

### Arrhenius parameter

The reaction of hydrogen with the different samples was investigated for various surface temperatures, and the resulting sticking coefficients for both step and terrace adsorption on Si(001) are summarized in Fig. 4.7 in the form of an Arrhenius plot. In the investigated temperature range from 440 to 900 K the sticking coefficients vary

over nearly five orders of magnitude with a substantially different temperature dependence of the terrace compared with the step adsorption. The sticking coefficients associated with the terrace adsorption are all well aligned for the different surfaces investigated and show a very pronounced temperature dependence. With the behavior described by an Arrhenius law, $s_0 = A \times \exp(-E_A/k_B T_s)$, the obtained activation energy $E_A = 0.76 \pm 0.1$ eV and prefactor $A = 0.2$ are in excellent agreement with the results previously reported for the flat surface [26], shown as a dashed line for comparison.

A 30% and a 50% error were assigned for the sticking coefficients for the terraces and steps, respectively. This was assessed both from the accuracy of the measured experimental parameters such as surface temperature and hydrogen pressure and from the variations of values determined from experiments performed under seemingly identical conditions. The absolute accuracy in the low-temperature regime is limited by the presence of mainly oxygen and water in the chamber or the dosing gas. The absence of contaminants on the surface after the hydrogen adsorption experiments could be verified from the desorption experiments at 900 K, as mentioned above. In addition, the agreement of the determined parameters of the hydrogen desorption kinetics in the temperature range between 650 and 800 K with those obtained by dosing atomic hydrogen [11] excludes the presence of adsorbates other than hydrogen on the surface. For temperatures in excess of 650 K the adsorption kinetics of the steps can no longer be distinguished from terrace adsorption due to the comparatively fast hydrogen diffusion at these temperatures. The values determined should therefore be regarded as effective sticking coefficients including step and terrace contributions. For temperatures above 800 K the large rates of hydrogen desorption do not allow independent determination of adsorption and desorption kinetics. The desorption rates are obtained from extrapolating the Arrhenius behavior for desorption determined for lower temperatures. This procedure imposes the limit on obtaining accurate sticking probabilities at high temperatures.

### 4.1.3 Defect-mediated terrace adsorption

The experiments presented above clearly indicate that for surface temperatures below 600 K, the adsorption on the terraces occurs through a reaction channel that is independent of the steps. The observation of the less efficient reaction channel of the steps is possible because the barriers for hydrogen diffusion are quite large and prevent rapid migration of hydrogen from the steps and defects onto the terraces. However as already indicated above, and as will be shown quantitatively in the diffusion experiments presented in section 4.4, for $T_s > 600$ K migration becomes appreciable on the time scale of the adsorption experiments. This can be seen in Fig. 4.3 (b) where for $T_s = 660$ K the terrace hydrogen uptake via the minority sites already became more efficient than direct adsorption. For a quantitative description the terrace hydrogen



uptake can be approximated for negligible desorption and small coverages as

$$\frac{d\theta_H}{dt} = \Phi s_{terr} + n_{H,step}\theta_{step}\nu_d. \tag{4.1}$$

This equation is an expansion of eq. (3.7) with a second term taking the diffusion of atomic hydrogen with rate $\nu_d$ from the step sites into account. $n_{H,step}$ is the corresponding relative hydrogen coverage of the steps with density $\theta_{step}$. Assuming equilibrium between the depletion of the steps onto the terraces and refilling from the hydrogen gas phase, one can calculate the equilibrium step coverage $\bar{n}_{H,step}$. With first-order adsorption kinetics and neglecting back-migration to the steps from

$$\bar{n}_{H,step}\nu_d = \Phi s_{step}\left(1 - \bar{n}_{H,step}\right), \tag{4.2}$$

one obtains

$$\bar{n}_{H,step} = \frac{\Phi \hat{s}_{step}}{\nu_d + \Phi \hat{s}_{step}}. \tag{4.3}$$

Note that $\hat{s}_{step}$ is the site-specific reactivity given by $\hat{s}_{step} = s_{0,step}\theta_{step}^{-1}$. The effective sticking coefficient $s^*$ for step-mediated adsorption would then be given by

$$s^* = \frac{\hat{s}_{step}\nu_d}{\nu_d + \Phi \hat{s}_{step}}\theta_{step}. \tag{4.4}$$

The two limiting cases

$$\Phi \hat{s}_{step} \ll \nu_d: \quad s^* = \hat{s}_{step}\theta_{step} = s_{0,step}, \tag{4.5}$$

$$\Phi \hat{s}_{step} \gg \nu_d: \quad s^* = \frac{\nu_d \theta_{step}}{\Phi} \tag{4.6}$$

show that the sticking coefficient $s^*$ will be determined by the reactivity of the minority sites $\hat{s}_{step}$ for high temperatures (4.5) and by the diffusion rate $\nu_d$ for low temperatures (4.6). To illustrate the transition to step-mediated adsorption, a measurement for Si(001) containing $D_B$ steps is shown in Fig. 4.8. These surfaces, which will be the topic of the next chapter, contain steps which are well characterized and therefore more suitable for a quantitative consideration than the experiment shown in Fig. 4.3 (b). Both saturation of the step sites and diffusion of hydrogen onto the terraces are clearly visible at the temperature of 640 K and an effective sticking coefficient for the terraces of $s^* = 1.4 \times 10^{-6}$ can be determined. The upper line indicates the behavior one would expect for the measured sticking coefficient of $2 \times 10^{-7}$ for terrace adsorption in the absence of diffusion. The parameters describing adsorption and diffusion on this surface ($\Phi = 450\,\mathrm{ML\,s^{-1}}$, $\theta_{step} = 0.12$, $s_{step} = 4 \times 10^{-4}$, $\nu_d = 4.2 \times 10^{-3}\mathrm{s^{-1}}$) can be used to simulate the adsorption behavior of this experiment. This would result in an apparent sticking coefficient $s^* = 1.1 \times 10^{-6}$, which is in excellent agreement with the measured value after taking also the direct terrace adsorption into account i.e. adding the terrace sticking coefficient determined for flat Si(001) for that surface temperature.

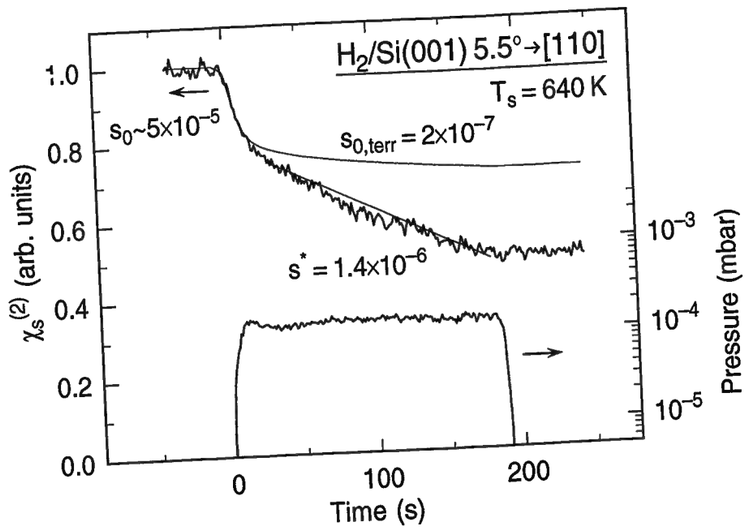


**Fig. 4.8:** Adsorption of hydrogen on the terraces of vicinal Si(001) mediated by $H_2$ dissociation at the $D_B$ steps. The fast drop is due to the sticking at the steps with a sticking probability of $\sim 5\times10^{-5}$. The subsequent decrease corresponds to an adsorption rate of $7\times10^{-4}$ ML s$^{-1}$.

In the low-temperature limit given by eq. (4.6), the defect-mediated channel can be suppressed with respect to the direct adsorption by applying a higher hydrogen flux $\Phi$ during exposure. Therefore, a defect-induced mechanism would in general manifest itself in a $1/p$ hydrogen pressure dependence of the apparent sticking coefficient. For flat Si(001)2×1 and a surface temperature of 600 K sticking coefficients were determined from the observed SH signal decrease recorded for different hydrogen pressures. The resulting values are plotted in Fig. 4.9 as a function of inverse pressure in the range from $2\times10^{-4}$ to $6\times10^{-2}$ mbar.

The observed behavior is not compatible with a defect-mediated adsorption process. With the expected value of $\nu_d \simeq 10^{-3}$ s$^{-1}$ for that surface temperature and a defect density of 1% ML, for instance, one would arrive at a coverage dependence represented by the dotted line. Only assuming unrealistically high diffusion rates or defect densities, one would get closer to the experimental values but still not reproduce their functional dependence (dashed line: $\theta_{step}=0.2$ ML).

For a direct sticking mechanism no coverage dependence would be expected. The observed decrease of the measured sticking coefficient with increasing pressure is likely a consequence of the liquid-nitrogen-cooled sample holder. From the empirical equation $1\times10^{-2}=\lambda(\text{cm})\times\text{p(mbar)}$ [157] describing the relation between mean free path of the hydrogen molecules and pressure it can be seen that with increasing pressure cold



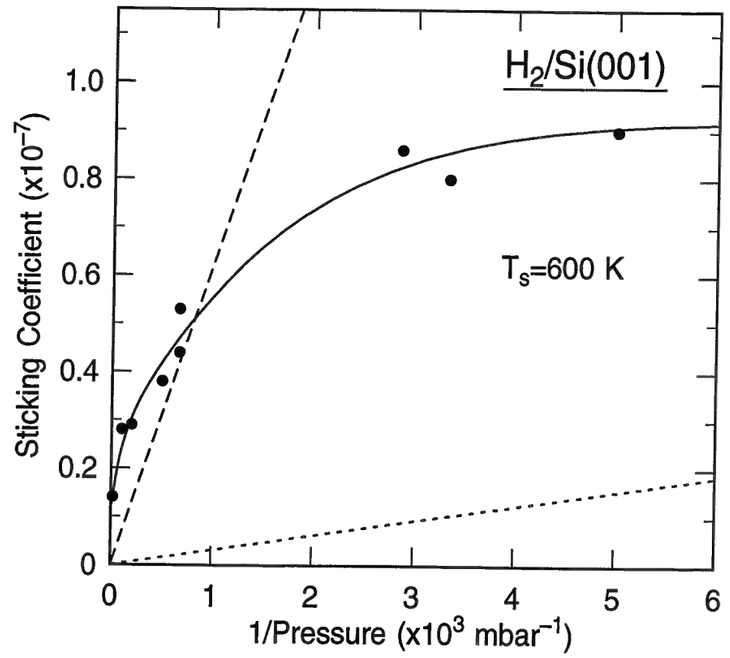


**Fig. 4.9:** Variation of the sticking coefficients for flat Si(001) determined from different adsorption experiments using different hydrogen pressures. The dotted (dashed) lines represent the behavior one would expect if the adsorption would solely be defect mediated with a diffusion rate $\nu_d=10^{-3}$s$^{-1}$ and a defect density of 0.01 ML (0.2 ML). The solid line through the data is drawn as a guide to the eye.

molecules in the vicinity of the sample cannot thermally equilibrate with the walls of the chamber before reaching the silicon sample. Both the decreasing impingement rate and the reduced kinetic energy of these hydrogen molecules would lead to a decrease in the measured sticking coefficient.

### 4.1.4 Discussion

The following discussion will focus on two main issues. First, the discrepancies with results concerning dissociative adsorption on silicon surfaces reported by other groups are addressed, followed by the implications of the new experimental findings for establishing a consistent reaction mechanism.

For the adsorption of $D_2$ on Si(001)2×1 using a supersonic molecular beam and detecting the coverage with TPD, sticking coefficients of the order of $10^{-5}$ were reported for temperatures below 650 K [32]. Since neither the differences in the dosing procedure (thermal gas versus molecular beam) nor an isotope effect could explain

the discrepancies of 2–3 orders of magnitude, it was speculated that these high values might be due to the high doping concentrations of the samples used in these experiments [26]. The segregation of the dopant on the surface could, in principle, alter the electronic structure of the silicon dangling-bond states in a way which might effectively lower the dissociation barrier. This would then explain not only the higher sticking coefficients but also the discrepancies between calculated [30,31,158] and measured [91–93] translational energy distributions of the desorbing $H_2$ molecules. Like the experiments of Kolasinski *et al.* [32], our experiments were performed on As-doped Si(001) with a similarly high dopant level. However, the sticking coefficients for the terrace adsorption determined from this sample indicate that doping concentrations of up to at least $n \sim 10^{19}$ cm$^{-3}$ do not significantly affect the surface reactivity.

For a detailed comparison the sticking coefficients for $D_2$ from the molecular beam experiments determined for a nozzle temperature of 300 K are shown in the Arrhenius plot of Fig. 4.7 (open triangles). Strikingly these values are very similar to the initial sticking coefficients determined for the surfaces which were slightly misoriented or not well prepared. In addition, in the temperature range investigated in the beam experiments the activation energy describing the surface temperature dependence of the sticking was found to be less than 0.07 eV, in qualitative agreement with the step adsorption behavior. Due to the limitations of the $D_2$ flux, deuterium uptake could only be measured up to total coverages of typically 0.1 ML. The deuterium uptake seemed to conform to a Langmuir adsorption behavior saturating at a total surface coverage of $\sim 0.14$ ML measured for a surface temperature of 630 K. This would be indicative that the reaction studied in the experiments of Kolasinski *et al.* corresponds to the sticking of hydrogen to minority sites rather than the ordered dimers on the terraces. The experiments described in the previous section showed that the surface quality sensitively depends on the preparation conditions, indicating that defect densities around the 10% level are feasible even for orientationally flat surfaces. Although this explanation is tempting, it should also be mentioned that, depending on the accuracy of the temperature measurements due to the long dosing times (up to 90 min) required, the apparent saturation behavior might also be explained by the onset of adsorption-desorption equilibrium.

The results reported by Hansen and Seebauer [155] do not only deviate by many orders of magnitude from our measurements of the sticking coefficients, as determined for identical vicinal surfaces. In addition, there are inconsistencies concerning the hydrogen diffusion activation barrier for Si(001) compared with the STM investigations of Owen *et al.* [159], Boland *et al.* [80], and our diffusion experiments described in the proceeding chapters. Having repeated their experiments under very carefully controlled conditions, the results would indicate that contaminants such as water might explain the high reactivities reported, although it is difficult to give a definite answer which would explain the discrepancies.

The high sticking coefficients of the different types of steps investigated, which



exceed the corresponding values for adsorption on the terraces, indicate that these minority sites present a comparatively small barrier towards the incoming hydrogen. Although this finding supports some theoretical models which suggest a higher reactivity of step or defect sites, it strongly argues against this process being also responsible for the adsorption on the ordered terrace dimers. In its simplest form, it has been suggested that after dissociation of the molecular hydrogen at highly reactive step or defect sites the terraces are filled by activated diffusion of the hydrogen atoms [81,102,110]. If terrace adsorption were mediated by steps and defects in that way, the measured sticking coefficients would scale as the step/defect density and would drop with a slope given by the barrier for hydrogen diffusion in the Arrhenius plot. Obviously, the sticking coefficients are independent of the miscut of the surface and the temperature dependence of the values attributed to terrace adsorption agree well with each other, the corresponding values determined for flat Si(001)2×1, and the previously reported values of Bratu *et al.* [26,27].

In the discussion thus far, it has been assumed that the number of minority sites is determined by misorientation and preparation of the surface but does not strongly depend on its temperature. Whereas the experiments indicate that this is indeed the case for the fast adsorption channel associated with steps and defects in the temperature range between 450–650 K, this does not exclude a more complicated defect-mediated adsorption channel with a temperature-dependent concentration of active sites as being responsible for terrace adsorption. It has been proposed that steps may serve as a source of isolated Si atoms which, once formed, migrate away from the step edges and facilitate $H_2$ dissociation on the terraces [103,106,110,111]. The barrier for such a defect migration was calculated to be of the order of 0.6 eV [103], which would be similar to the effective activation energy determined for the sticking. In fact, one might even view the adsorption via transient defects as an extreme case of phonon-assisted sticking. One argument against this particular dynamic effect is, of course, the observation that the terrace adsorption is independent of the step density. However, it is difficult to distinguish such a mechanism from phonon-assisted sticking by varying the surface temperature alone. More definite discrimination is possible by investigating sticking as a function of the kinetic energy of the incident $H_2$ molecules. Whereas in the dynamical model of phonon-assisted sticking $H_2$ dissociation is activated in both the lattice and the hydrogen degrees of freedom [28], an increased translational energy of the $H_2$ molecules is expected to have a much weaker effect in promoting sticking at single-atom defects. A very pronounced dependence of the sticking coefficient with kinetic energy of the hydrogen molecules has indeed been observed in recent molecular beam experiments [160,161] which are briefly discussed in section 4.2.2. These results fully support a direct reaction pathway compatible with the model of phonon-assisted sticking and clearly argue against the defect models.

### 4.1.5 Conclusion

The dissociative adsorption of molecular hydrogen on vicinal Si(001) and Si(111) surfaces could be decomposed into contributions from step/defect and terrace sites. The sticking coefficients for step adsorption on Si(001) are found to exceed the corresponding adsorption on the terrace sites by several orders of magnitude, reaching values of up to $10^{-4}$. Both the observation that the sticking coefficients for the terraces are independent of the step density and the observation that the adsorbed hydrogen is rather immobile up to surface temperatures of $\sim$600 K, rule out reaction mechanisms in which hydrogen adsorption on the ordered crystal faces of Si(001) and Si(111) proceeds via steps or other defect sites.



## 4.2 Hydrogen interaction with $D_B$ steps on vicinal Si(001)[1]

Understanding of the mechanistic aspects of hydrogen adsorption on the silicon dimers of Si(001)2×1 is still incomplete, in particular concerning the effect of Si-lattice geometry and electronic properties of the dangling bonds and their mutual interplay. In addition, as discussed in the previous chapter, the interaction of molecular hydrogen with silicon surfaces can be very site-specific. Although counterintuitive, this does not complicate matters. From the study of a new reaction pathway which is distinct from terrace dimer adsorption one can learn about the relevant parameters which govern the dynamics of the reaction. For more insight into the underlying processes a systematic investigation of the hydrogen interaction with a well-characterized type of active minority sites would be required. In that respect vicinal Si(001) misoriented towards [110] is particularly useful to serve that purpose. As discussed in section 2.1, double-height steps prevail for miscut angles $>2°$, with the rebonded $D_B$-type being energetically favorable.

In this section the hydrogen interaction behavior of Si(001) miscut by different angles is presented together with results of a theoretical study initiated by the experimental findings. The calculations were performed by P. Kratzer, E. Pehlke, and M. Scheffler as part of a collaborative effort to understand the reaction dynamics of hydrogen with silicon surfaces.

### 4.2.1 Adsorption kinetics

For Si(001)5.5°→[110] Fig. 4.10 shows a hydrogen adsorption experiment performed under conditions similar to those described in the previous chapter for a surface temperature of 575 K. A fast initial signal drop is followed by hydrogen uptake which proceeds at a rate in accordance with the sticking coefficient for terrace adsorption for that temperature. From the constant $\chi_s^{(2)}$ during interruption of the exposure and the absence of another fast signal drop after exposure is resumed, it can be seen that diffusion onto the terraces is negligible. The large differences in sticking probability between the steps and terraces allow selective saturation of the step sites with an appropriate dose of hydrogen while at the same time causing only inconsiderable adsorption on the terraces.

If it is assumed that the hydrogen sticks to the rebonded step-edge atoms, the saturation coverages of the steps would be a measure for deciding whether the hydrogen is adsorbed in the monohydride state or has formed a dihydride by breaking the Si–Si backbond to the upper terrace. In Fig. 4.11 corresponding temperature programmed desorption traces are shown for a fully and a partially step-saturated

[1] The results discussed in this chapter were published as an article in Physical Review: P. Kratzer, E. Pehlke, M. Scheffler; M. B. Raschke, and U. Höfer, *Phys. Rev. Lett.* **81**, 5596 (1998).

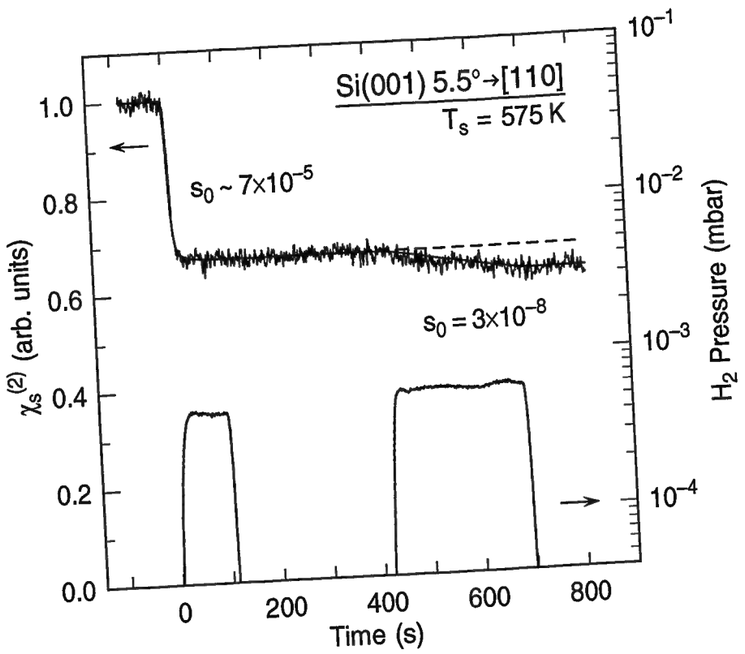


**Fig. 4.10:** Nonlinear response $\chi_s^{(2)}$ of Si(001)2×1 misoriented by 5.5° towards [110] during $H_2$ exposure for a surface temperature $T_s = 575$ K. Interrupting the hydrogen flux, one can test for the absence of hydrogen diffusion from the steps onto the terraces.

surface with miscut 5.5° → [110] prepared by dosing molecular hydrogen. A saturation coverage of $\theta_{step}^{sat} = 0.12 \pm 0.02$ ML is obtained from comparing with the fully monohydride-covered surface prepared by exposing to atomic hydrogen at $T_s \sim 600$ K. The additional desorption traces shown for the partially dihydride-covered surface prepared by exposing at a reduced temperature verify the saturation of the monohydride peak. For $T_s > 500$ K it is known that no dihydride is formed unless the surface is nearly monohydride-terminated [8].

By using the surface geometry depicted in Fig. 2.4 from the miscut angle $\alpha$ the number ratio of terrace to step dangling bonds can be calculated for an ideal surface:

$$\frac{\#db_{terr}}{\#db_{step}} = \frac{1}{2}\left(\frac{\sqrt{2}}{\tan\alpha} - 3\right). \tag{4.7}$$

With this relation the surface density of available step sites corresponding to the monohydride saturation coverage is given by

$$\theta_{step}^{theo} = \frac{1}{\left(1 + \frac{\#db_{terr}}{\#db_{step}}\right)}. \tag{4.8}$$



For $\alpha = 5.5°$, $\theta_{step}^{theo}$ amounts to 0.146 ML, which is agrees well with the experimental value determined by TPD. This correlation of the adsorbed amount of hydrogen in the fast reaction channel with the available number of step sites allows the rebonded step-edge atoms to be identified as the active sites with the hydrogen bound in the monohydride state. This interpretation is corroborated by a similarly good agreement between the expected step coverage as compared with the saturation coverage determined for the steps of the 2.5° misoriented sample. The corresponding experimental results are summarized in Tab. 4.1.

Less hydrogen than expected could be adsorbed on the surface misoriented by 10° towards [110]. This indicates a reduced number of reactive sites, which might be the result of faceting which is known to occur for larger miscut angles [62]. The steps coalesce and form multiple atomic high steps with faces of ⟨111⟩ orientation. This reconstruction might be induced here, in particular, since, with on average ~2.5 dimer units per terrace for the 10° miscut, this does not result in a low-index surface. However, as judged from the similar adsorption kinetics for both the step and terrace sites of that surface compared with the 2.5° and 5.5° samples, the nature of the

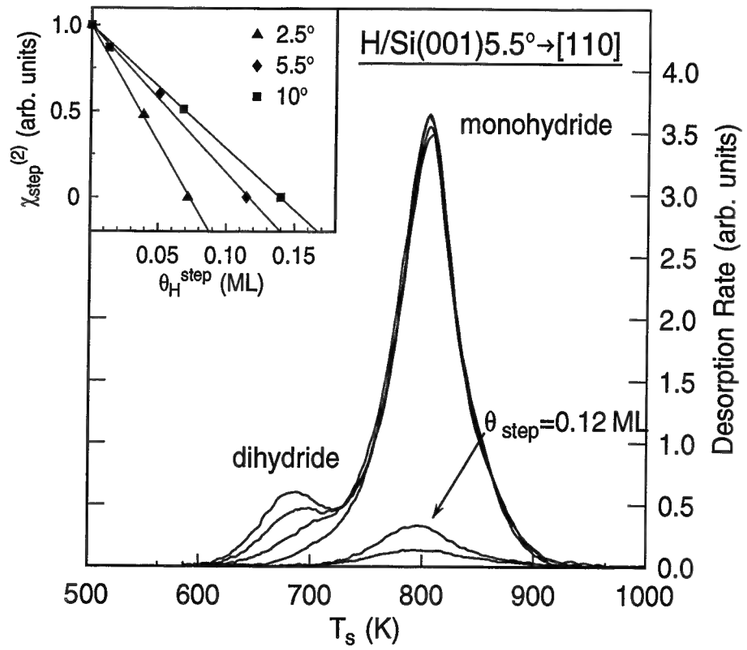


**Fig. 4.11:** Temperature programmed desorption of $H_2$ from H/Si(001) 5.5° → [110] for different coverages. Inset: calibration of the step contribution to the total nonlinear susceptibility $\chi_{s,step}^{(2)}$ with hydrogen coverage.

| $\alpha$ | $\frac{\#db_{\text{terr}}}{\#db_{\text{step}}}$ | $\theta^{theo}_{\text{step}}$(ML) | $\theta^{sat}_{\text{step}}$(ML) |
|---|---|---|---|
| 2.5° | 14.7 | 0.064 | $0.07 \pm 0.02$ |
| 5.5° | 5.9 | 0.146 | $0.12 \pm 0.02$ |
| 10° | 2.5 | 0.285 | $0.15 \pm 0.02$ |

**Tab. 4.1:** Calculated ratios of dangling bonds on the terraces compared with step sites and resulting maximal hydrogen coverage $\theta^{theo}_{\text{step}}$, in comparison with the measured saturation coverage of hydrogen at the steps.

available active sites still seems to be the same.

Temperature programmed desorption experiments have also been performed for different intermediate step coverages to calibrate the dependence of the step contribution to the nonlinear susceptibility on hydrogen coverage. As shown in the inset of Fig. 4.11, linear relations are found for the three different miscut angles up to saturation coverage. This can be understood because of the on average large separation of the individual adsorption sites, which reduces the nonlocal influence as discussed in chapter 2. From the near-resonant SHG from both the step and terrace dangling bond surface states only a small phase shift is expected between the two corresponding contributions.

To determine the kinetics of the step adsorption accurately, experiments were performed at a reduced hydrogen pressure of $2–3\times10^{-5}$ mbar, as shown in Fig. 4.12. The adsorption process can be well described by second-order Langmuir kinetics[2] and the numerical fit results in a sticking coefficient of $7\times10^{-5}$ in that case, given with respect to the total number of surface dangling bonds. For any given surface temperature this effective hydrogen sticking coefficient increases with increasing angle of miscut. With the sticking coefficient for step adsorption scaled relatively to the number of active sites as determined with TPD, within the uncertainty of the experiment these values converge for all three miscut angles.

For temperatures between 450 K and 600 K step and terrace adsorption could be investigated independently. This range is determined by the detection limit for sticking coefficients below $T_s \simeq 450\,\text{K}$ for terrace adsorption and the onset of diffusion from the steps onto the terraces for $T_s > 600\,\text{K}$. In contrast to the strong surface temperature dependence for terrace adsorption with sticking coefficients increasing from $10^{-10}$ to $10^{-7}$ in that temperature range, the corresponding step adsorption is

[2] For the one-dimensional system of the steps, however, on the assumption that the pairs of adsorption sites are equivalent under translation of one lattice constant along the step edge, one would expect deviations from Langmuir kinetics with increasing coverage. Assuming that the molecules adsorb randomly in pairs at the step edge sites and no diffusion takes place, this would result in a reduced hydrogen saturation coverage compared with the number of available sites. E. Pehlke performed a simulation of the step adsorption under these conditions and found a reduced saturation coverage of 85% of the number of step edge dangling bonds [162].



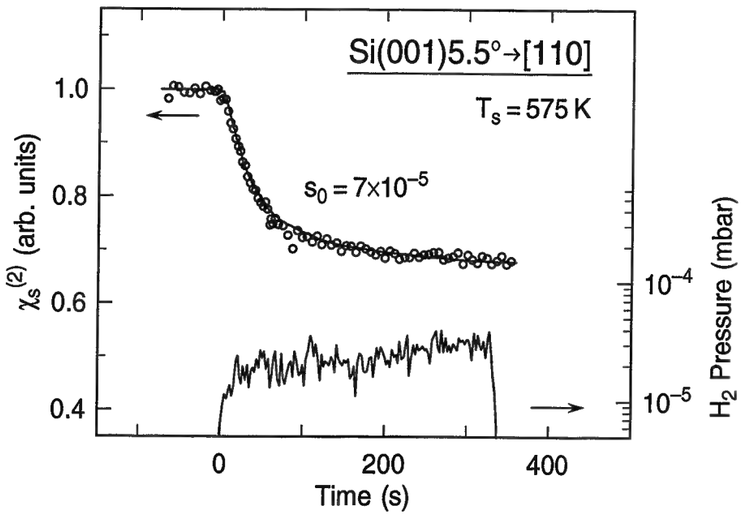


**Fig. 4.12:** Hydrogen adsorption at the steps of Si(001) 5.5° → [110] for a surface temperature $T_s = 575\,\text{K}$. Due to the low hydrogen pressure applied, terrace adsorption is negligible in this experiment.

essentially temperature-independent with nearly constant $s_0 \sim 10^{-4}$. Only for lower temperatures a gradual decrease of the reactivity of the steps is observed.

The resulting sticking coefficients for step and terrace adsorption for the different samples and various surface temperatures are summarized in the Arrhenius plot in Fig. 4.13, which covers the wide range of temperatures down to 90 K. In contrast to terrace adsorption, the weak effect of surface temperature on the dissociation at the steps can be described by the small activation energy of $E_a = 0.09 \pm 0.01$ eV. The narrow error bar of this value is due to the large range of surface temperatures covered in these experiments. For terrace adsorption the values determined for the different angles of miscut agree well with each other and the derived activation energy of 0.76 eV is very close to the value determined for flat Si(001) [26] and those discussed in the previous section.

### 4.2.2 Molecular beam experiments

During the course of this study a supersonic molecular beam experiment was established by M. Dürr. For details concerning the experimental setup and procedures the reader is referred to Ref. [160]. The ability to vary the kinetic energy of the gas molecules provides an additional experimental degree of freedom to gain more

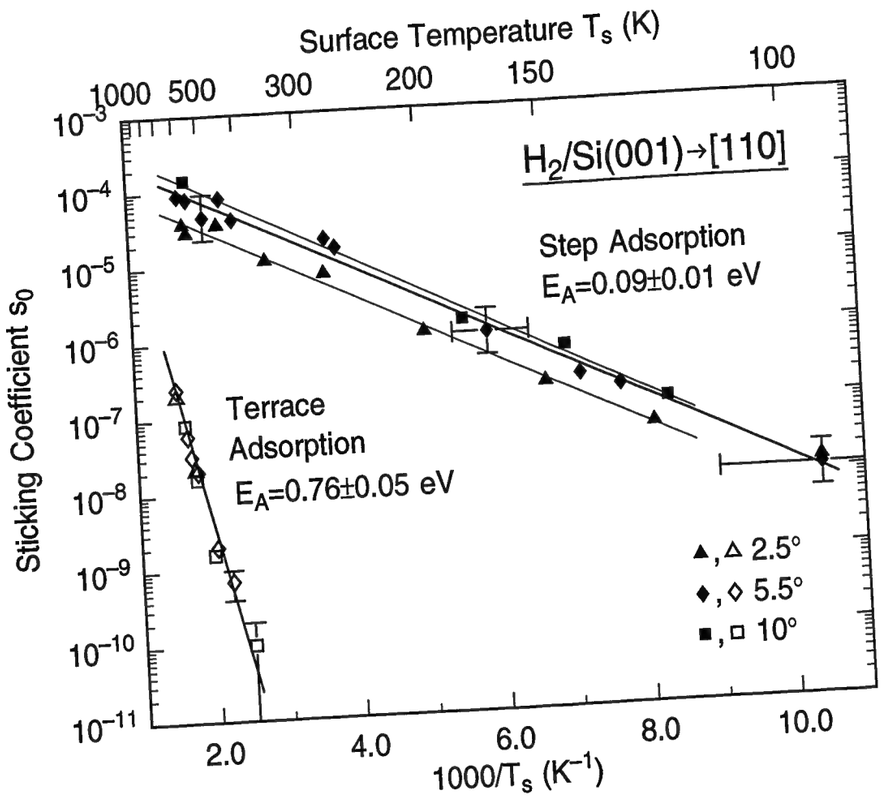


**Fig. 4.13:** Temperature dependence of the sticking coefficients $s_0$ for $H_2$ dissociative adsorption at the steps (solid symbols) and terraces (blank symbols) on vicinal Si(001) misoriented by 2.5°, 5.5°, and 10° towards [110]. The solid lines represent numerical fits to an Arrhenius law.

detailed information about the reaction kinetics. With the combination of the high sensitivity of SHG together with a high flux of hydrogen molecules of $2\times10^{16}$ $cm^{-2}s^{-1}$ on the sample, this experiment is two orders of magnitude more sensitive than previous molecular beam experiments [32]. It allows precise measurements of sticking coefficients down to $10^{-8}$.

In Fig. 4.14 hydrogen adsorption traces for Si(001)5.5°→[110] for a fixed surface temperature of 540 K and various nozzle temperatures are shown. The sticking coefficients for terrace adsorption strongly increase with increasing beam energy of the hydrogen molecules (average kinetic energy: 220 to 320 meV), as one would expect for an activated process. Due to the high directionality and the large mean energy of the $H_2$ molecules of the supersonic beam the sticking coefficients are in general larger than the experiments using thermal gas. The high sticking probabilities for the steps



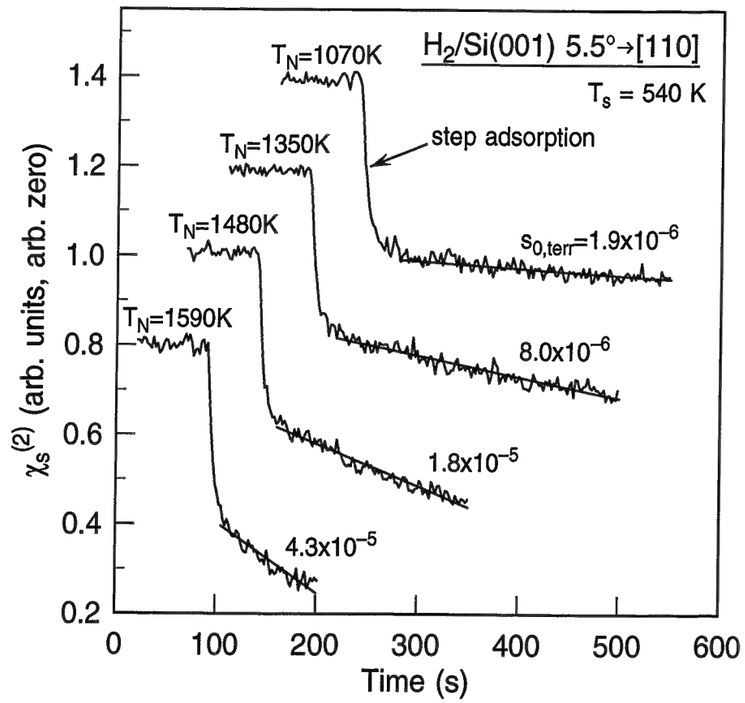


**Fig. 4.14:** Dissociative adsorption of $H_2$ from the supersonic molecular beam on Si(001)5.5° → [110] for different nozzle temperatures for the constant surface temperature of 540 K. Whereas the reactivity of the steps shows only a small variation with increasing kinetic energy of the hydrogen molecules, the sticking coefficients for terrace adsorption rise strongly. For details see Ref. [160,161].

are reproduced in the beam experiments and in contrast to terrace adsorption show only a small variation with the energy of the hydrogen molecules. This indicates that the kinetic energies in this experiment are already above the energy of the transition state for dissociation at the steps. Together with the high sticking coefficients, this result supports the conclusion of a small activation barrier for the step adsorption.

The results for terrace adsorption which are again found to be identical to the sticking on planar Si(001) fully support the conclusions drawn from the experiments discussed in section 4.1 that the dissociative adsorption is a direct rather than a defect- or step-mediated process.

### 4.2.3 Theory

At a surface temperature of 400 K the step sites exhibit a sticking probability six orders of magnitude in excess of the value for terrace adsorption. This would indicate that the local structure of the step edge is in a favorable configuration for dissociative adsorption compared with the silicon atoms of the terrace dimers. In addition, provided the relevance of lattice excitations to enable dissociation at the terrace dimers, the small dependence on surface temperature observed for the step adsorption supports this view. Since it is difficult to develop an atomistic model for the chemical reaction at the surface purely on the basis of the measured kinetic parameter, an in depth theoretical investigation could provide invaluable information.

For that purpose P. Kratzer, E. Pehlke, and M. Scheffler performed electronic structure calculations. Using density functional theory (DFT), they calculated the total energies and forces which act on the individual atoms. In brief, a plane-wave basis set was used and the generalized gradient approximation (GGA) was applied to the exchange-correlation functional. For the silicon atoms an *ab initio* pseudopotential was generated, and for hydrogen the Coulomb potential was taken. For details concerning the theoretical methods the reader is referred to Ref. [31,100,163] and references cited therein.

The $D_B$ step is modeled by a Si(117) slab with a thickness of about six atomic layers. In this geometry, periodically repeated $D_B$ steps are separated by two Si-dimer-wide terraces. In Fig. 4.15 the already optimized geometry with the resulting surface structure is shown. Characteristic are the unusually long bonds of the rebonded Si atoms formed with the atoms of the upper terrace, stressed by 6%. A Jahn-Teller-like distortion is responsible for buckling occurring at the step edge similarly to the terrace dimers making the surface semiconducting. For terrace adsorption both the location and energy of the transition state for the hydrogen molecule were calculated for adsorption on the upper and lower terrace dimers right next to the step edge ($T_1$ and $T_2$). Asymmetric transition states with the $H_2$ molecule dissociating above the lower atom of the Si dimer were found. This finding, together with the calculated barrier heights of 0.40 eV and 0.54 eV for sites $T_1$ and $T_2$, respectively, is very similar to results from calculations performed for flat Si(001) [99,112].

Since from the SHG and TPD experiments one could only indirectly infer that hydrogen indeed adsorbs at the step edge, this important first result of the calculations verifies that hydrogen does not simply bind, for example, to modified first dimers next to the step edge. The similar barriers calculated for adsorption on the terrace dimers of the stepped surface also reflect that the observed sticking coefficients for terrace adsorption are independent of the miscut angle.

In addition, the calculations directly reproduce the experimental finding that the hydrogen is adsorbed at the step edge in the monohydride state and that this state is favored both kinetically and thermodynamically. Although the backbond to the



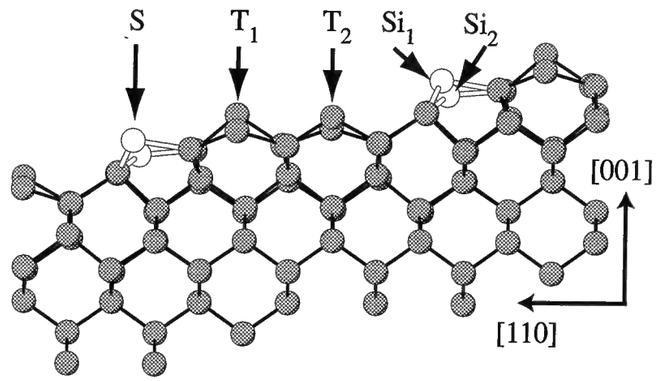


**Fig. 4.15:** Side view of the relaxed atomic geometry of double-height steps on Si(001). The orientation of the vicinal surface shown is (117), corresponding to a miscut angle of 11.4° towards [110] (by courtesy of P. Kratzer).

upper terrace is strained, the formation of the dihydride is found to be considerably less exothermic ($\sim 0.9\,\mathrm{eV}$) than monohydride formation ($\sim 2\,\mathrm{eV}$) with respect to $H_2$ adsorption. The calculations also find an activation barrier of 0.5 eV for the dihydride transition state, even somewhat higher than the monohydride formation on the terrace dimers. Thus, these results indicate that the high sticking coefficient is related to direct monohydride formation.

Performing *ab initio* molecular dynamics is computationally very demanding, and so only one trajectory was chosen for investigation for which the highest reaction probability would be expected. For that purpose the $H_2$ molecule approaches with its orientation parallel to the step edge at a position in between two neighboring dangling bonds.

For a slowly approaching molecule the concerted motion of the H atoms and the two rebonded Si atoms along the reaction path is shown in Fig. 4.16. The first thing to notice is that the buckling is released. The corresponding motion of the Si atoms ($Si_1$ and $Si_2$) is shown in the two insets in the figure. In addition to the vertical motion, the Si atoms temporarily approach each other as a result of an attractive interaction with the dissociating $H_2$ molecule. After complete dissociation the new Si–H groups swing back into their final symmetric positions. No transition state for this particular reaction pathway could be found, indicating that the adsorption barrier is zero. The calculations show that along this reaction path the total energy decreases monotonically as depicted in Fig. 4.17 (solid line). The second curve (dashed line) is the elastic energy stored in the lattice if, hypothetically, one were to remove the H atoms at the various distances instantaneously. This energy has therefore to be provided by the excess energy released by the new Si–H bond formation. For the barrier-

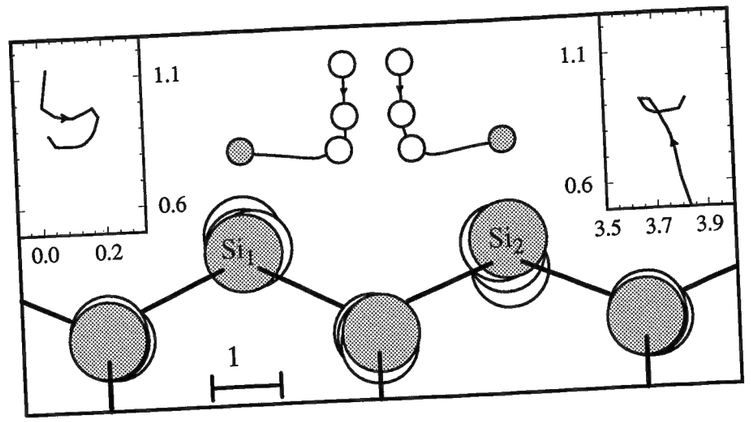


**Fig. 4.16:** Reaction path for $H_2$ dissociation at step atoms projected onto a (110) plane parallel to the $D_B$ step edge. Insets: corresponding motion of the rebonded Si atoms (by courtesy of P. Kratzer).

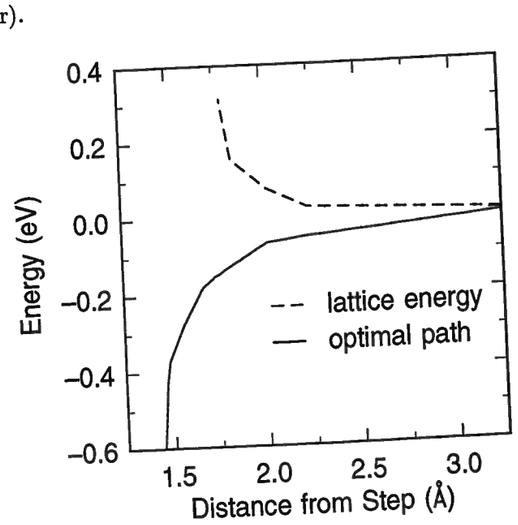


**Fig. 4.17:** Total energy of the $H_2$/surface system along the adsorption path shown in Fig. 4.16 (solid line). The dashed line corresponds to the elastic energy stored in the lattice after instantaneous abstraction of the hydrogen atoms (by courtesy of P. Kratzer).

free adsorption pathway this can be achieved for slowly approaching molecules which give the system sufficient time to relax. However, for fast approaching molecules the large mass difference of the reactants causes the relaxation to lag behind. In the



extreme case the molecule would have dissociated before the Si lattice has started to relax. For such a static lattice configuration the dissociation is likely to be activated. These findings explain not only the high reactivities of the steps, but also why additional thermal excitations of the step edge can facilitate the adsorption process: If a molecule approaches the step, then thermally induced release of the buckling allows the molecule to dissociate which would otherwise have been rejected. This explains the weak surface temperature dependence of the reaction observed experimentally.

Before proceeding, one comment should be added concerning the accuracy of the theoretical results. Uncertainties in energy arise from the use of empirical functionals and the finite unit cell size. Recent investigations comparing different first-principles calculation methods indicate that DFT might underestimate the energies by few hundred meV [107]. This would be compatible with the experimentally observed adsorption barriers, which when compared with the theoretical results seem to be underestimated by DFT. Therefore the existence of a small barrier for step adsorption would be within the limits of the theoretical uncertainty.

The finding of a barrier-free adsorption pathway for dissociative adsorption at the steps is in remarkable contrast to the large activation energies found both experimentally and theoretically for adsorption on the terrace dimers. The origin of this difference is likely due to a shift in energy of the dangling-bond-induced surface states at the step edge compared with the terrace dimers. The calculations showed that the Jahn-Teller effect leads to a splitting of the surface states from the dangling bonds of the rebonded step edge atoms into two bands separated by $\sim 1$ eV. As discussed in chapter 1, the energetically higher $p$ orbital at the lower Si atom is then unoccupied. However, if the two Si atoms were forced to equal height, this energy separation would reduce to 0.4 eV. This is in contrast to the terrace dimer, where the energy gap would only shrink to 0.7 eV [37]. In addition, for an equal-height configuration the formation of a $\pi$-bond would occur for the terrace dimer which is not possible at the steps.

Unoccupied surface states are required to interact with the hydrogen orbitals to facilitate dissociation. In the initial state, hybridization of the unoccupied hydrogen $\sigma^*$ with the unoccupied dangling-bond state occurs. This is accompanied by rehybridization involving the two surface states, resulting in charge transfer into the $sp^3$ orbitals of the Si atoms to form the new Si-H $\sigma$-bond. This can occur more easily at the steps due to smaller splitting of the electronic states.

The lower prefactor of $0.005 \pm 0.002$ with respect to the steps, in comparison with $0.5 \pm 0.3$ for terrace dimer adsorption, indicates more geometric constraints for the hydrogen molecules approaching the step sites. This means that, assuming a truly barrier-free adsorption pathway for the steps, molecules of certain translational and rotational energies might be steered into this adsorption pathway less efficiently than molecules approaching the terrace dimer, provided they have sufficient energy to overcome the barrier. Using pictorial language, one could say that, although the potential energy surface for the step has a hole, this hole might be narrow and has

steep walls. The energy minimum for the terrace dimer is high in energy but is broad and shallow.

The last interpretation is somewhat speculative since for a detailed description of the chemical response one would have to average over the many degrees of freedom of the systems. This is not possible unless one has calculated a sufficient number of trajectories, which would be an enormous effort.

### 4.2.4 Conclusion

The dissociative adsorption of $H_2$ into the monohydride state at well-ordered $D_B$ steps on Si(001) was found to be characterized by sticking coefficients several orders of magnitude in excess of the terrace adsorption. The increase from $10^{-8}$ to $10^{-4}$ in the investigated surface temperature range from 90 to 600 K corresponds to an activation energy of 0.09±0.01 eV. Density functional calculations of Kratzer, Pehlke, and Scheffler indicated the presence of a direct barrier-free dissociation pathway at the steps due to efficient rehybridization of the dangling-bond orbitals.



## 4.3 Inter-dimer reaction pathways for $H_2$ on Si(001)

The experiments discussed so far together with theoretical findings support the view that in addition to the molecular kinetic and internal energies, surface lattice excitations facilitate dissociative adsorption pathways for hydrogen with a reduced barrier and therefore lead to an increase in the probability of molecular adsorption. However, not only transient lattice distortions can reduce the adsorption barrier. The example of step adsorption shows that also equilibrium Si atom configurations such as the $D_B$ structure are possible which exhibits a reduced barrier height. These results discussed in the previous chapter have shown that the dissociative adsorption of hydrogen is highly sensitive towards the details of the silicon atom configuration and the related electronic structure. In addition to the adsorption site geometries provided by the initially clean planar and vicinal Si(001) surfaces, selective termination of silicon dangling bonds by atomic hydrogen on the ordered terrace dimers results in slightly altered geometric end electronic configurations of neighboring dangling bond pairs. This opens new adsorption pathways for terrace adsorption and thus enables a systematic study of the underlying parameter which govern the dissociation.

### 4.3.1 Theoretical predictions

Stimulated by the success of the DFT calculations made in order to explain the different reaction behavior of the $D_B$ steps as compared with the terrace dimers, E. Pehlke performed calculations of the adsorption energetics of molecular hydrogen with different dangling bond configurations on Si(001). Of particular interest were constellations of neighboring dangling bond sites on the terraces which in their initial state would appear similar in their geometric and electronic structure to the $D_B$ steps. For the purpose of this study, two dimers were chosen where selectively one of the dangling bonds on each dimer was initially terminated with a hydrogen atom in a *cis* configuration. The calculated potential energy surface for the dissociative adsorption of a hydrogen molecule on the resulting inter-dimer dangling bond configuration is depicted in Fig. 4.18. From the energy contours it can be seen that a hydrogen molecule approaching the surface can dissociate following a barrier-free adsorption pathway. This is again shown in Fig. 4.19, where the total energy of the $H_2$ molecule following its optimal reaction pathway is calculated.

In addition, a potential energy barrier search was performed for the case when only one of the two adjacent dimers carries a hydrogen atom. This pathway is not barrier-free and a value of ∼60 meV was found for a hydrogen molecule approaching the two inter-dimer dangling bond sites opposite the H atom. In the following discussion the two reaction pathways will be termed H4 and H3, respectively, according to the total number of hydrogen atoms (2+2) or (1+2) involved, as summarized in Fig. 4.20.

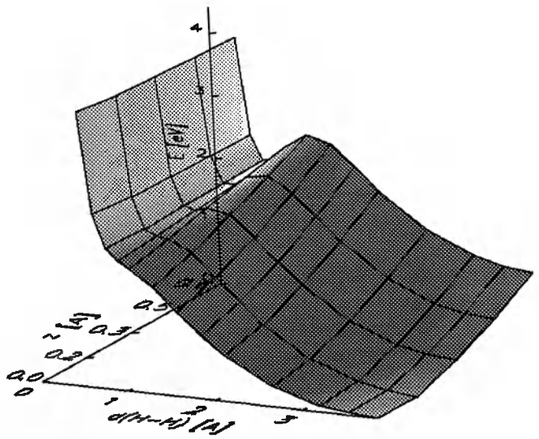

**Fig. 4.18:** Potential energy surface calculated for dissociative adsorption of molecular hydrogen across two inter-dimer dangling bond sites where the dimers are already half-saturated with hydrogen (*cis* configuration). The hydrogen molecules which would enter from the upper left can follow a barrier-free reaction pathway. The distance $d$(Si–H) is given with respect to the final monohydride configuration (by courtesy of E. Pehlke).

Parallel to these investigations Biedermann *et al.* were able for the first time to directly observe dissociative adsorption of $H_2$ on Si(001)2×1 with scanning tunneling microscopy [164]. Having exposed a hydrogen precovered surface with a small flux of molecular hydrogen they saw the selective disappearance of dangling-bond derived tunneling features adjacent to singly-occupied dimers. Having identified the adsorbed atoms as hydrogen with the help of TPD measurements this study provided direct evidence for the existence of the proposed H4 process discussed here.

### 4.3.2 Experiment

In order to verify both theory and experiment and for the purpose of a more in depth understanding of the relevant parameter governing the dissociative hydrogen adsorption, a systematic study of the related sticking coefficients and their temperature dependence was performed. For a detailed investigation of the H4 process and in order to test for the existence of the H3 reaction pathways proposed theoretically the surface hydrogen configurations described above have been realized experimentally by exposing a surface to atomic hydrogen at a sample temperature sufficiently low to inhibit diffusion. The high sticking probabilities for atomic hydrogen lead to a near random distribution of adsorbed hydrogen atoms resulting in the creation of the desired configurations with certain probabilities. In principle, a high initial coverage would be favorable in order to obtain a sufficiently large number of H4 sites. The



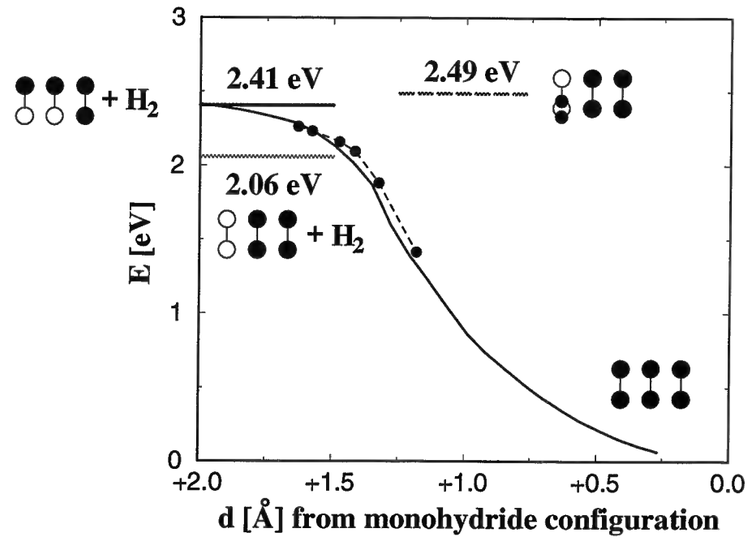


**Fig. 4.19:** Calculated energy for the hydrogen molecule dissociating along the optimal reaction path. The initial and final geometric configurations are depicted schematically (by courtesy of E. Pehlke).

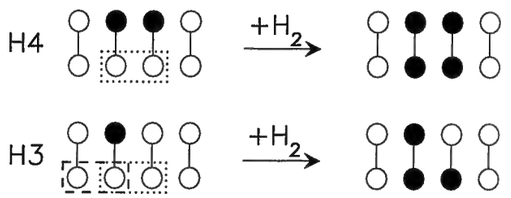


**Fig. 4.20:** Schematic of proposed inter-dimer reaction pathways. The blank (solid) circles represent clean (hydrogen-covered) silicon atoms.

drawback, however, is the decrease in relative sensitivity of the SH probe with coverage, as can be seen from the calibration curve shown in Fig. 3.5. As a compromise, for the purpose of the experiments the surface was precovered with ∼0.25 ML atomic hydrogen at 300 K. In this coverage regime the density of H4 sites can be roughly estimated as $\simeq\theta^2(1-\theta)^2$ to 3.5% ML. A somewhat higher laser fluence of 80 mJ/cm$^2$ was used compared with the previous experiments. This together with the lower surface temperature would lead to a sufficiently high sensitivity of SHG to resolve the expected changes in surface coverage.

The corresponding experiment is shown in Fig. 4.21. The surface is kept at a constant temperature of 300 K and the initial signal decrease is due to the exposure to atomic hydrogen. After this preparation procedure molecular hydrogen is dosed at a pressure of $\sim 3\times10^{-4}$ mbar, leading to a small but distinct signal drop. A blowup of the corresponding section is shown in the inset in the figure. Applying Langmuir adsorption kinetics, one derives a value of $(5\pm2)\times10^{-4}$ for the site-specific sticking probability. From the corresponding signal decrease a related change in hydrogen

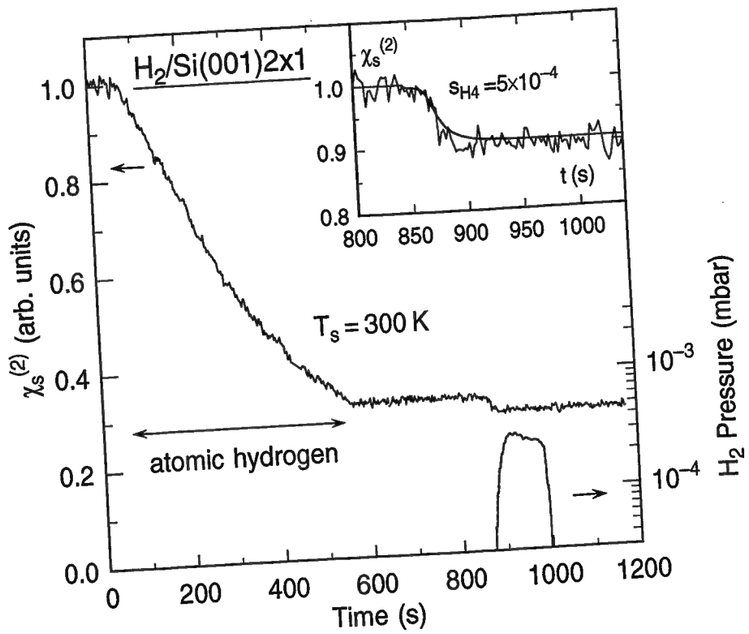


**Fig. 4.21:** Adsorption of molecular hydrogen on Si(001)2×1 at 300 K after preadsorption of ∼ 0.25 ML atomic hydrogen. Inset: blowup of the time period during $H_2$ exposure.

coverage of only ∼ 2% ML would be derived using the standard calibration. This would be at variance with the number of adsorption sites especially considering that each H4 site will be occupied by two hydrogen atoms. However due to the partial $H_2$ pressure of $\sim10^{-7}$ mbar during the initial atomic hydrogen dosing procedure the number of H4 sites would already be diminished. In addition the hydrogen distribution on the surface affects the SH-response. From temper experiments as discussed below it appeared that the SH-sensitivity towards the H4 sites is reduced, i.e. the dbs in the vicinity to adsorbed hydrogen contribute less to the SH-signal that free dangling bonds. These effects together with the possibility of a not purely random hydrogen distribution on the surface due to a site dependence in sticking probability for atomic hydrogen are likely to be responsible for the variation between SH-derived hydrogen



uptake and expected H4 site density.

In order to verify that the observed reaction is indeed the predicted H4 mechanism, the surface is annealed to 550 K for about 300 s after the preparation procedure. This thermal cycle completely quenches the H4 process. As discussed in the introductory chapter and as shown in Fig. 4.19, it is energetically favorable for the two hydrogen atoms to reside on the same dimer due to the intra-dimer interaction between the dangling bonds. Diffusion thus leads to annihilation of the initial H4 sites and consequently quenching of the fast reaction channel. Annealing at a temperature of 480 K for about 100 s is already found to be sufficient to reduce the amount of available H4 sites. The observed transition from the inter-dimer to the intra-dimer hydrogen configuration seems to occur at a rate about a factor of 10 higher than what one expects for single-atomic hydrogen diffusion.

Similarly, for the experiments testing for the existence of the H3 process an amount of 0.15 ML atomic hydrogen is preadsorbed at 300 K. The subsequent molecular hydrogen adsorption experiment is shown in Fig. 4.22 for a surface temperature of 395 K. The fast initial signal decrease can again be attributed to the H4 configurations, but, as apparent from the smaller signal drop, the corresponding sites are available at a reduced concentration compared with the H4 experiments described above. Then after the pressure is increased to $4\times10^{-3}$ mbar a continuous signal decrease can be observed.

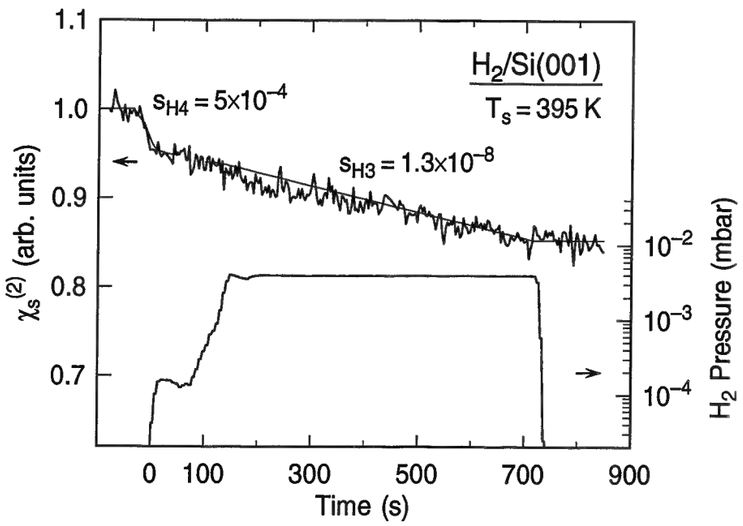


**Fig. 4.22:** Adsorption of molecular hydrogen on Si(001) at 395 K after preadsorption of ∼ 0.15 ML atomic hydrogen. The initial fast signal drop is due to a small number of H4 sites, followed by H3 adsorption with a significantly smaller sticking probability.

The corresponding rate of hydrogen uptake relates to a sticking probability of $1.3 \times 10^{-8}$ which can be attributed to the H3 process. Please note that this value is already given with respect to the expected number of H3 sites. Although their reactivity is considerably smaller than that of the H4 sites, this value still exceeds the initial sticking coefficient of the clean surface by more than two orders of magnitude for that specific surface temperature. Experiments carried out on the same surface and temperature without preadsorbing atomic hydrogen and exposure to a similar hydrogen dose show no signal decrease. This verifies that the presence of possible steps and defects can not be made responsible for the observed behavior.

For the evaluation of the sticking coefficient of the H3 sites it has been taken into account that the incoming $H_2$ molecule initially has two possibilities to interact with the site, as can be seen from the schematic in Fig. 4.20. The sticking probabilities are given here with respect to each of the two neighboring dangling bond pairs in order to directly compare the reactivities with other dangling bond configurations. One would expect that the H3 process does not saturate after the initially available number of sites would have reacted. Each adsorbing $H_2$ molecule would generate one new H3 site which would lead to a chain reaction. The hydrogen uptake would proceed along the dimer row in one direction until the growing chain encounters a defect or step or alternatively adsorbed hydrogen.

In Fig. 4.23 the sticking coefficients and their temperature dependences are summarized both for the H4 and H3 processes. Shown for comparison (dashed lines) are the results for both $D_B$-step adsorption and sticking on the initially clean terraces (termed H2 in this context), taken from the preceding chapter. For better comparison of the site-specific reactivities all sticking coefficients have been normalized to the number of available sites (compare section 3.4.3), i.e. all sticking coefficients are given with respect to the units containing two neighboring silicon atoms involved in the interaction.

With a sticking coefficient still as high as $2^{+2}_{-1} \times 10^{-4}$ for the H4 sites at a surface temperature of 100 K, for the activation of this process with surface temperature an upper limit for the barrier of 0.02 eV can be given. In contrast the H3 process can be described by an activation barrier of $0.17 \pm 0.05$ eV with a very low prefactor of $8 \times 10^{-6 \pm 1}$.

These results also serve to explain the adsorption behavior observed on the flat surface at temperatures above 580 K: With increasing coverage the signal decrease dropped at a rate faster than what one would expect from pure Langmuir adsorption behavior. This effect is already visible in the experiment shown in Fig. 4.4 for adsorption at 600 K. It is more pronounced for $H_2$ adsorption at higher surface temperatures, as seen in Fig. 4.24 for $T_s = 660$ K.

This reaction behavior can now readily be explained by invoking the H4 reaction pathway. For the initially clean surface only the intra-dimer H2 reaction pathway is available at first. Then with increasing coverage the dimerized hydrogen atoms can



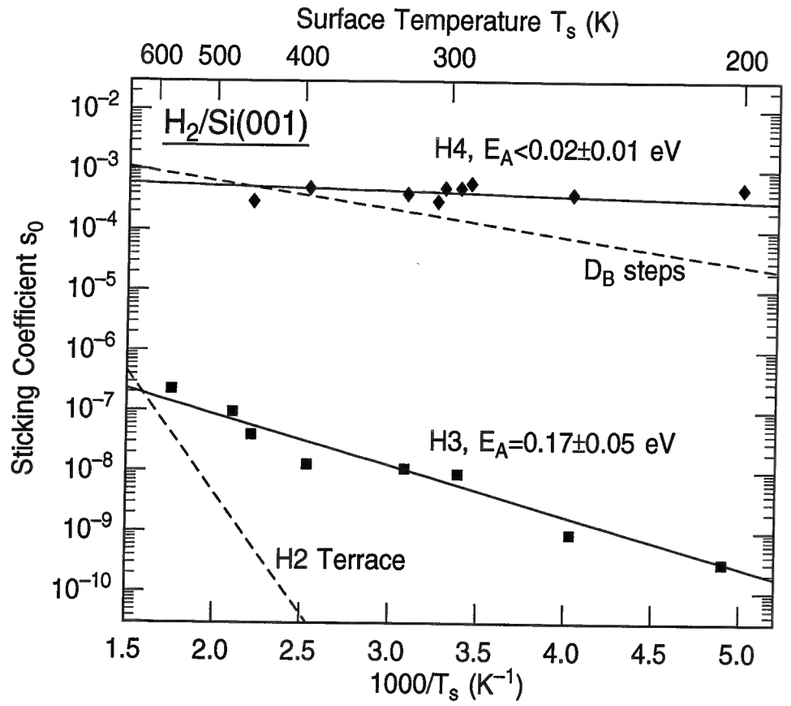


**Fig. 4.23:** Arrhenius plot describing the surface temperature dependence of the new H4 and H3 reaction pathways. The dashed lines represent the fit to the data for $D_B$-step and intra-dimer terrace adsorption (termed H2) pathways discussed in the previous chapter. Site normalized sticking coefficients are used for easier comparison.

split at a rate increasing with temperature. Before hopping back or - more rarely - diffusing along the dimer row to the next Si dimer, the hydrogen atoms can frequently change between the two silicon atoms on the same dimer [88,159]. H4 configurations can thus be created transiently. The contribution of the H3 sites to the observed reaction behavior is negligible because of the more than three orders of magnitude lower sticking coefficients. In addition as can be seen in the Arrhenius plot, their site-normalized sticking coefficients are already close to the values for the intra-dimer pathway for temperatures where hydrogen diffusion would be sufficiently large to lead to their creation.

To model the adsorption behavior a nonequilibrium reaction behavior is assumed. The creation of the H4 sites would then depend on the total surface hydrogen coverage and temperature. For small coverages the dependence would be approximately linear

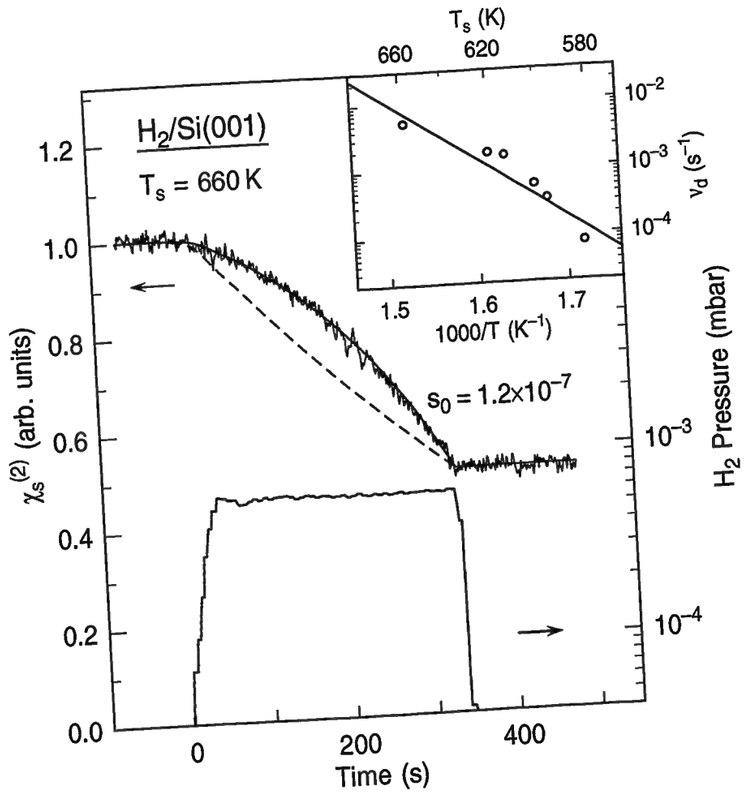


**Fig. 4.24:** Increase in rate of hydrogen adsorption with coverage on defect-free Si(001)2×1. This corresponds to a change in sticking coefficient from $1.2 \times 10^{-7}$ ($t = 0$ s) to $6.3 \times 10^{-7}$ ($t = 330$ s). The solid line is the result of a numerical fit performed according to the model described in the text. The dashed line represents Langmuir adsorption behavior assuming only one reaction pathway. Shown in the inset is the surface temperature dependence of the resulting fitting parameter $\nu_d$.

in $\theta$ and one can write

$$\frac{\mathrm{d}\theta_\mathrm{H}}{\mathrm{dt}} = \Phi \left\{ s_0(1-\theta_\mathrm{H}) + \hat{s}_{(\mathrm{H4})}\nu_d(T)\theta_\mathrm{H} \right\}. \tag{4.9}$$

The first term describes the standard Langmuir adsorption behavior for independent dissociative adsorption at the intra-dimer H2 sites without diffusion. The additional term takes the creation of and adsorption at the H4 sites into account. In the low-coverage limit the equation would simplify to $\mathrm{d}\theta/\mathrm{dt} = \Phi s_0$, i.e. from the initial signal decrease the sticking coefficient as derived in the previous experiments is obtained. Using $\hat{s}_{(\mathrm{H4})} = 5\times10^{-4}$, the data can be fit accurately with the additional free parameter $\nu_d$ as shown by the solid line in the figure. $\nu_d$ can be interpreted as the effective hopping frequency leading to the successful creation of H4 sites. An increase with temperature



is observed as depicted in the inset, derived from this and other measurements, and supports the initial non-equilibrium assumption made to describe the reaction. The values are a factor of about 10 lower than the diffusion rates for single hydrogen atoms. In the limited temperature range between 590 and 670 K accessible for these experiments the variation of $\nu_d$ with surface temperature is found to be compatible with typical diffusion barriers of 1.6–1.9 eV [12,159,165] for hydrogen on silicon.

A similar increase in sticking probability has been observed before in the case of Si(111)7×7 [27]. In contrast to the model proposed here for Si(001), the behavior was attributed to an effective decrease in the adsorption barrier with coverage, as will be discussed in some detail in chapter 5. This mechanism, however, is unlikely to be in operation on Si(001) because of the observed surface temperature dependence here. It should be noted, however, that the data shown in Fig. 4.24 can also be fit with satisfying accuracy by assuming the model used for Si(111).

### 4.3.3 Discussion

The experiments were able to verify the two new inter-dimer reaction pathways for dissociative adsorption of molecular hydrogen on Si(001) proposed on the basis of DFT calculations. With negligible barrier found experimentally for the H4 process and the slightly activated H3 adsorption by ∼0.17 eV there is excellent qualitative and even semiquantitative agreement between theory and experiment. Although no surface temperature dependence was investigated in the STM experiments of Biedermann *et al.* [164], the value derived for the site specific sticking coefficient for H4 of $(8\pm2)\times10^{-4}$ reported for 300 K in that study shows excellent agreement with the results presented above.

Inter-dimer transition states have been investigated theoretically before, but only for the initially clean surface [81,84]. The high activation barriers found for the corresponding dissociative adsorption as compared with the intra-dimer adsorption led to this process being rejected occurring under normal conditions.

The dramatic reduction of the inter-dimer adsorption barrier after preadsorbing atomic hydrogen is truly striking, but knowing the reaction behavior of the $D_\mathrm{B}$ steps, one might argue, that the high reactivity of the H4 sites does not come as a surprise, since in both cases similar geometric and electronic configurations prevail as could be concluded from the theoretical study. In the case of the H4 configuration the buckling angle of the two adjacent dimers is reduced to 2−4° [49] from its initial angle of 19°. The calculations show that the dimers buckle antisymmetrically which leads to a vertical Si atom displacement similar to the one observed for the rebonded $D_\mathrm{B}$-step-edge atoms. In contrast to the step adsorption with the still discernible temperature dependence, the reactivity of the H4 sites is virtually independent of surface temperature. This difference is likely to be correlated with the small variation in the geometric structure. The reaction is thus very sensitive to details of the resulting

electronic structure. The adsorption of one hydrogen atom on the Si dimer leads to the breaking of the weak $\pi$-like interaction and charge redistribution with the residual dangling bond half occupied. However, these dangling bonds can then interact inter-dimer-like and, similar to the steps, the dangling-bond state at the upper (lower) silicon atom becomes filled (depleted) with electrons, as the calculations show. Therefore in order to explain the difference in temperature dependence between the H4 and step sites, differences in the energetics of the corresponding Si-atom configurations might be responsible. The electronic configuration at the dangling bonds required to facilitate dissociation is tightly correlated with the lattice dynamics as discussed in section 2.2. As mentioned in section 2.1 the clean dimers on the terraces already at room temperature flip dynamically between their two asymmetric configurations [44,66]. This is in contrast to the $D_B$-step atoms, where from STM observations it is known that the alternating up-down configuration of the rebonded Si atoms is more stable [47,63]. This would be compatible with the calculated value of 0.3 eV for the energy which is stored in the lattice when two adjacent step edge atoms are brought to the same height. For the terrace dimers the corresponding energy is only of order 0.1 eV [44,98]. Hydrogen terminating one of the two silicon atoms is unlikely to increase this energy, in fact, from the reduced equilibrium buckling angle one would expect it to be even reduced.

The different activation energies determined from the temperature dependence of the H4 compared to the $D_B$-step sticking coefficient would qualitatively correlate with this difference in buckling energy barrier. As has been discussed in the previous section, since the energy required to release the step edge buckling has to come from the energy gain through Si-H bond formation, a concerted lattice motion can help dissociation of the $H_2$ molecule. The lattice distortions associated with the H4 dissociation require less energy compared to the corresponding process at the steps, therefore the temperature related activation of lattice excitations would only be a minor contribution to the dissociation. A possible consequence would be that more energy would be gained via $\sigma$-bond formation already at an earlier stage of the dissociation process for H4 compared to the steps after the first interaction of the hydrogen molecule with the unoccupied dangling bond. The dangling bonds can thus rehybridize effectively over a wider range of less ideal lattice distortions and related changes in electronic structure. If this model is correct this should manifest itself in the energetics along the ideal reaction path, where the gradient should then be larger for H4 compared with $D_B$-step adsorption.

With the activation energy determined from the surface temperature dependence of the sticking coefficient interpreted as the excitation energy required to distort the lattice to enable the incoming molecule to adsorb without experiencing a major barrier, the reduced sticking coefficient of the H3 process compared to H4 and $D_B$-step reaction could then be explained readily. Since the buckling of only one of the two dimers involved in the interaction is reduced in the case of H3, first energy has to be



provided to obtain a configuration similar to the H4 site before the molecule can dissociate effectively. In addition, on the clean dimer the intra-dimer $\pi$-like interaction has to be overcome. The small prefactor determined in the experiments indicates a strong effect of the surface corrugation. This means that only a small effective area is available for sticking and thus more geometric constraints would exist.

The absence of any discernible surface temperature dependence in the case of the H4 reaction provides an important contribution in the systematic of the relevance of the contribution of lattice excitations to the adsorption process in going from the H4 sites via the $D_B$-steps to the H3 configurations and finally to the intra-dimer H2 adsorption. Following the arguments given in section 2.2, the observed increase in surface temperature dependence can be thought to be related to an increase in the effective adsorption barrier which is reflected in different degrees of lattice distortions necessary to follow the energetically most favorable reaction path. The H3 process provides a suitable model system to test for the correlation of the adsorption barrier with the barrier determined from the surface temperature dependence of the sticking coefficient. The energy of 0.17 eV is readily accessible in molecular beam experiments varying the molecular degrees of freedom and related experiments are currently in progress.

The observed increase in sticking probability with coverage could be explained via a non-equilibrium process involving two reaction pathways with different kinetics. This behavior is inverse to the one discussed in section 4.1 where the presence of steps also provided a second reaction channel. In the case of the H4 process, however, the kinetically favorable sites are created with increasing coverage (autocatalytic process), whereas on the stepped surfaces the availability of the highly reactive sites decreases with surface hydrogen occupation.

### 4.3.4 Hydrogen desorption kinetics

In the experiments discussed so far only aspects concerning the site-selective dissociative adsorption of molecular hydrogen have been considered. However, the presence of energetically different sites on the surface would also affect the desorption kinetics. Therefore, the isothermal desorption from both flat as well as the Si(001)2×1 surfaces misoriented by 2.5°, 5.5° and 10° towards [110] have been investigated and the results have been compared to those described in section 2.2 and in Ref. [11]. However, the observed kinetic behavior disagrees with what one would expect from straight forward arguments and possible reasons are discussed here.

Representatively, in Fig. 4.25 two isothermal desorption measurements are compared for the 10° and 2.5° misoriented surfaces for similar surface temperatures of 730 and 725 K. Surprisingly, in spite of the variation in step density the desorption behavior looks very similar. Apparently for coverages $\theta > 0.03$ ML in both cases first order desorption kinetics is observed as indicated by the straight line. At lower coverages

the desorption deviates from first order and becomes second order.

Although the hydrogen is bound more strongly at the step sites (see proceeding section), this energy difference of $\leq 0.2$ eV does not compensate for the reduction of the barrier height for adsorption of $\geq 0.5$ eV. Therefore one expects a reduced desorption activation barrier for the steps compared to the terraces. Likewise, according to the principle of microscopic reversibility the hydrogen molecules should leave the surface via the step sites in the limits of low coverage. Under the conditions of the experiments hydrogen diffusion is fast so that the surface is in thermal equilibrium. Consequently for high coverages, as long as the steps are sufficiently occupied with hydrogen, one would expect zeroth order kinetics since the hydrogen would desorb via these sites. The behavior would gradually change to second order when the total surface hydrogen coverage falls below the step density and the combination of two isolated hydrogen atoms at the step sites becomes the rate limiting step. In contrast, within the uncertainty of the experiments the desorption behavior does not depend in a systematic way on step density and even looks very similar to the behavior observed for the flat surface in these and previous experiments [11]. The slightly higher onset of second order kinetics in the case of the 10° misoriented sample is too small to account for the expected effect and can at least be partly attributed to the 5 K higher temperature as discussed below. Both the derived desorption rates as well as the first and second order kinetics from the two experiments shown here, other data for the different misorientations and different temperatures, as well as the flat surface seem to agree within the experimental accuracy and lead to similar desorption activation energies.

In this picture, desorption from the terraces and thus an independence of the desorption rate from step density would only occur, if a larger adsorption barrier at the steps compared to the terrace sites would lead to an effectively reduced desorption barrier on the terrace dimers. Then, however, also the adsorption behavior would not be affected by the steps in contrast to the results discussed so far, and thus this explanation can be ruled out.

The observed desorption behavior is compatible with the TPD traces shown in Fig. 4.11. Both shape and peak temperature are found to be independent from step density. Compared to the direct information which can be obtained from isothermal measurements, the interpretation of TPD traces would be very model dependent.

Before considering different possibilities explaining this apparent discrepancy, comments should be made concerning the interpretation of the experimental data. It has already been mentioned that the calibration of the SHG response with coverage is truly valid only for the 600 K surface temperature where it has been performed. In addition, depending on the distribution of the hydrogen atoms on the surface (clustering or random) small changes in the SH signal occur. Furthermore in the case of the vicinal surfaces the step contribution to the overall SH signal can not be separated under the conditions of the desorption experiments. Thus, the conversion to



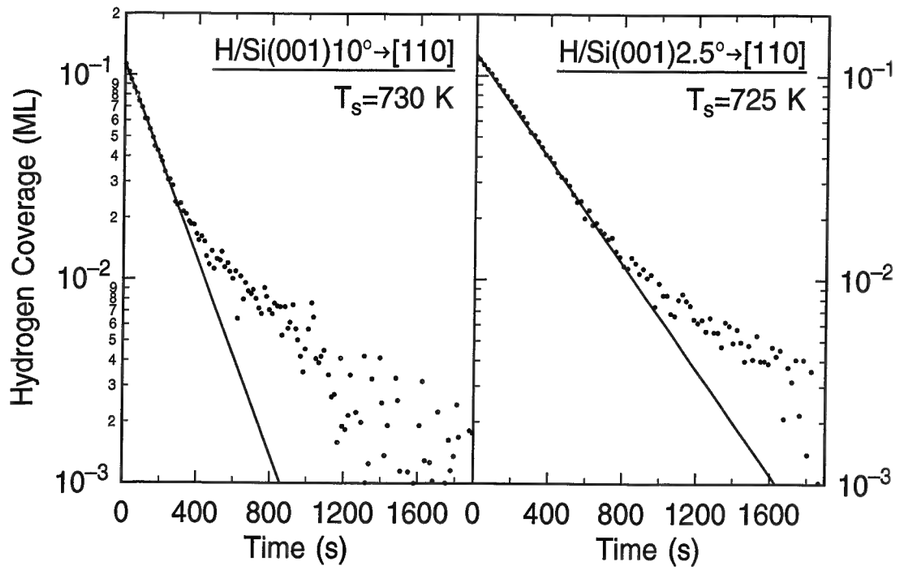


**Fig. 4.25:** Semilogarithmic plot of the isothermal desorption of hydrogen from Si(001) misoriented by 10° and 2.5° towards [110]. The straight lines correspond to first order kinetics. The different rates are due to the slightly different surface temperatures of 730 and 725 K, respectively.

coverage might be less accurate compared to the flat surface. For the desorption temperatures the $D_B$-steps might also already partially dissolve and meander. However, considering the expected dependence of the desorption kinetics on step density, these experimental uncertainties are unlikely to be sufficiently dominant to explain the apparent discrepancy. Therefore, judging also from the similar shape of the TPD traces an intrinsic effect of the surfaces under investigation seems likely.

For flat Si(001)2×1 the observed desorption behavior was explained with the very successful model of hydrogen pairing on the silicon dimers [11,48] which has been verified with STM experiments [8,80,165]. The second order kinetics comes out naturally from the entropy gain at low coverages exceeding the energy gain from the paring. For this desorption process an activation energy of 2.48±0.1 eV and a first order prefactor of $\sim 2\times 10^{15} s^{-1}$ were found [11].

When making the assumption, that also on the stepped surface the desorption proceeds via the terraces, one could think of two possible explanations: first, kinetic effects which lead to a reduced desorption prefactor for the steps, or other dominating favorable desorption channels on the terraces which are not present at lower surface temperatures. As the reduced prefactor for step adsorption discussed in the previous experiments indicated, the dissociation at these sites seems to be more sensitive to-

wards the molecular degrees of freedom such as orientation of the $H_2$ molecule upon approaching the surface. Assuming a prefactor for desorption from the steps to be similarly reduced by about three orders of magnitude compared to the flat surface, a desorption barrier of 2 eV would result in desorption rates compatible with those of the flat surface considering the desorption temperature range investigated from 670 to 800 K. However, this barrier of 2 eV would be below the experimental values found for desorption from the stepped surface.

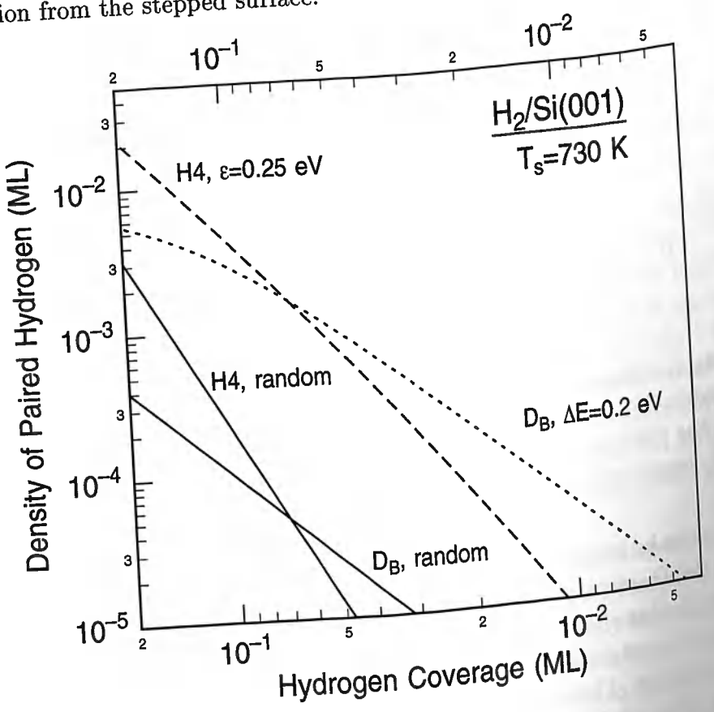


**Fig. 4.26:** Surface density of paired hydrogen for random H4-site or $D_B$-step occupation (solid lines, step density 0.1 ML). For comparison results are plotted for H4 assuming an inter-dimer pairing energy of $\epsilon$=0.25 eV and neighboring $D_B$-step occupation calculated for an binding energy difference of $\Delta E$=0.2 eV.

In view of the barrier-free adsorption pathway for terrace adsorption presented in the previous section here its possible effect also on the desorption is discussed. Whereas for high coverages one would expect the inter-dimer desorption pathway to contribute to the desorption process, at low coverages it would become negligible. For a pure random distribution of hydrogen on the surface in the low coverage limit, the number of H4 configurations would be $\propto \theta^4$ with $\theta$ the total surface hydrogen coverage as shown in Fig. 4.26. Applying a random distribution also for the stepped surface, the result for neighboring hydrogen atom population at the steps $\propto (\theta \cdot \theta_{step})^2$



for a density of $\theta_{step} = 0.1$ is shown for comparison. However as discussed in section 2.2, the hydrogen atoms on the terraces preferably occupy the same dimer which can be described by an effective attractive interaction of $\sim 0.25$ eV [11]. In addition, as will be discussed in the next chapter the steps are thermodynamically favored with a higher hydrogen binding energy for these sites of $0.1-0.2$ eV.

The equilibrium coverage of doubly-occupied dimers on the terraces, expressed in terms of the total hydrogen coverage, is given by [11,48]:

$$\theta_2 = \theta - \frac{\sqrt{1+4\alpha\theta(1-\theta)}-1}{2\alpha}, \tag{4.10}$$

with $\alpha = \exp(\epsilon/k_B T) - 1$ and $\epsilon$ the pairing energy. Assuming no other interactions between doubly-occupied dimers the probability of finding neighboring occupied dimers, i.e. H4 sites, is then $\propto (\theta_2)^2$ and the result is plotted as the dashed curve in the figure. The H4 process would then manifest itself in second order desorption under these conditions. First order behavior would require additional inter-dimer interactions which would favor the H4 quadruplet formation. Similarly for the steps applying eq. 4.17 which will be discussed in the next chapter, assuming the step sites to be favorable by 0.2 eV compared to the terrace sites, the density of paired hydrogen configurations at the steps with respect to the total number of surface sites has been calculated and is shown as the dotted line. Varying the pairing energy or the energy difference between step and terrace sites in can be shown that both occupation densities depend sensitively on the details of the energetics. Which of the different desorption channels would dominate would then not only depend on the relative surface densities of the required configurations, but also on the exact desorption activation barrier and prefactor for these pathways. The observed desorption kinetics would thus strongly depend on the surface hydrogen coverage.

In contrast to adsorption, where by varying surface temperature and dosing conditions the different reaction pathways can be separated, in the case of desorption, the interplay of the various reaction channels mediated by diffusion makes the question concerning the dominant process not a simple matter.

In the absence of isothermal investigations extending the coverage range above 0.2 ML as has been accessible in the SHG experiments discussed here, this issue can not yet be resolved. Attempts have been made applying reflectance anisotropy spectroscopy, however, the signal has not been calibrated with respect to the hydrogen coverage and a linear dependence has simply be assumed [166]. This however is very questionable for reasons similar to the ones discussed in section 3.4. The nonlocal effect of the adsorbate on the electronic structure in its vicinity alters the reflectivity in a way which can not be predicted by simple *a priori* arguments. Therefore further investigations are required to resolve this issue.

### 4.3.5 Conclusion

The existence of two new inter-dimer reaction pathways on Si(001) could be verified by performing hydrogen adsorption experiments on a randomly atomic hydrogen precovered surface. In contrast to the intra-dimer pathways on the clean surface the experiments indicate drastically reduced adsorption barriers for both processes. Based on the H4 pathway an observed increase in sticking probability with hydrogen coverage for adsorption on the initially clean surface could be explained. These additional reaction pathways might also be the key to understand the apparent independence of the desorption kinetics from step density for vicinal surfaces.



## 4.4 Equilibrium and non-equilibrium hydrogen coverages on vicinal Si(001)[1]

### 4.4.1 Thermodynamics of H/Si

It has been discussed in the previous sections that dissociative adsorption of molecular hydrogen on vicinal silicon surfaces is highly site-selective. In the following experiments, the particularly strong preference of the reaction for the double-height $D_B$-steps on Si(001) misoriented towards [110] is exploited to prepare non-equilibrium adsorbate layers. The differences in sticking coefficients of many orders of magnitude allow preparation of selectively hydrogen-saturated step-edges with essentially clean terraces in between. The resulting surface structure with the hydrogen adsorbed at the rebonded silicon step-edge atoms is shown schematically in Fig. 4.27. This surface

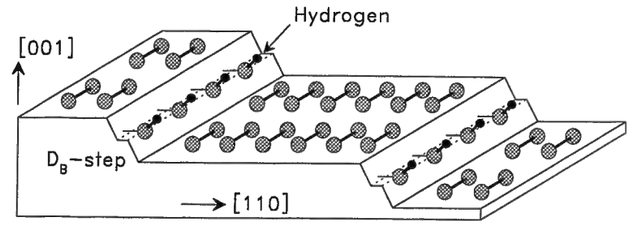


**Fig. 4.27:** Schematic representation of the vicinal Si(001) surface with atomic hydrogen-saturated rebonded $D_B$-steps. With six Si dimer units per terrace this corresponds to a miscut angle of $\simeq 5.5°$.

is not in thermodynamic equilibrium and can lower its free energy by partial hydrogen diffusion onto the terraces, leading to an increase in configurational entropy. The equilibrium distribution is then determined by the terrace size on the one hand, and possible energetic differences between the various adsorption sites on the other. The diffusion, however, is kinetically hindered for sufficiently low temperatures, making this configuration metastable. The relative stability of this structure for temperatures up to nearly 600 K for tens of minutes, as already discussed in the previous chapter, is a result of the large diffusion barriers for covalently bound chemisorbates on surfaces.

Here the ability to prepare these non-equilibrium adsorbate layers will be exploited for investigations of hydrogen diffusion and binding energy differences between the different adsorption sites on these surfaces. For that purpose the time evolution of the step depletion and corresponding filling of the terraces is monitored with SHG.

[1] The results discussed in this section were published as an article in Physical Review B: M. B. Raschke and U. Höfer, *Phys. Rev. B* **59**, 2783 (1999).

This experimental approach is essentially the reverse procedure applied by Reutt-Robey *et al.* studying CO diffusion on vicinal Pt(111) and Ni(100). Starting from an initially random distribution of CO on the surface prepared by rapid exposure, in these studies the diffusion *towards* the thermally favored step sites by infrared reflection absorption spectroscopy (IRAS) was monitored [167,168].

In contrast to metal surfaces, however, the diffusion activation energies for simple chemisorbates on semiconductor surfaces amount to a significant fraction of the binding energy. Due to this comparatively large barrier relative to the activation energy for desorption, there is only a narrow temperature range available for experiments. On the one hand, the surface temperature needs to be sufficiently large to promote a hopping rate detectable on the experimental time scale; on the other, the diffusion quickly competes with desorption.

Hydrogen diffusion on flat silicon surfaces has been investigated so far by means of optical second-harmonic diffraction on Si(111) [12] and, more recently, by STM on Si(001) [159]. In the first case the decay of concentration gratings created holographically by laser-induced desorption was monitored and provided information about the macroscopic mass transport diffusion process. Compared with the grating method operating on submicron length scales, and STM which probes on an atomic level, the method presented here yields kinetic information about the diffusion process on an intermediate mesoscopic scale involving only several atomic sites. Addressing the hydrogen diffusion on vicinal silicon surfaces, this gives insight into how the potential energy surface is modified in the vicinity of the steps.

Adsorbate-induced structural relaxations and charge redistributions on covalent surfaces do not allow an *a priori* estimate of the binding energies of different sites. From the equilibrium populations of the step and terrace sites one can deduce the binding energy differences, and a comparison can be drawn with the results from density functional calculations performed by E. Pehlke and P. Kratzer for that system.

### 4.4.2 Hydrogen diffusion

#### Experimental procedure

For the purpose of the experiments a surface is prepared where the steps are saturated with hydrogen. As in the experiments described in the previous section the initially clean surface is exposed to molecular hydrogen at a sample temperature where diffusion is negligible. The hydrogen adsorption behavior at the steps for a 2.5° misoriented sample can be seen in the first region of Fig. 4.28. The nonlinear susceptibility $\chi_s^{(2)}$ is monitored during hydrogen exposure at a pressure of $\sim 2\times10^{-5}$ mbar. With a site-specific sticking coefficient of $\sim 10^{-3}$ for the steps the exposure shown results in near saturation of the steps. A corresponding sticking probability of $10^{-8}$ for the terraces at the surface temperature of 555 K leads to negligible adsorption at the dimer sites.



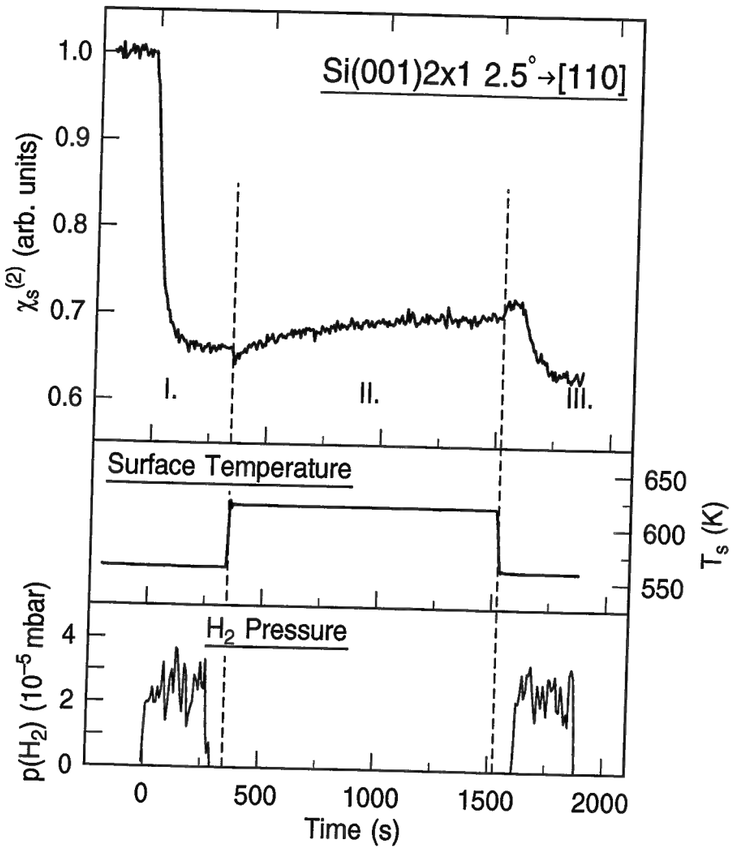


**Fig. 4.28:** Experimental procedure for determining both hydrogen diffusion and equilibrium properties on vicinal Si(001). Shown is the variation of the nonlinear susceptibility $\chi_s^{(2)}$ with hydrogen pressure and surface temperature during: I. Dissociative adsorption of molecular hydrogen at the steps until saturation for $T_s = 555$ K; II. Hydrogen diffusion onto the terraces at a temperature $T_s = 620$ K; III. After quenching the surface temperature hydrogen is readsorbed on the fraction of depleted step sites.

In the second step the surface temperature is stepped quickly within a few seconds to a value high enough to increase the hopping rate sufficiently to make it detectable on the experimental time scale. The temperature rise from 555 to 620 K is then followed by a continuous signal increase as shown in region II of the figure and is due to a net hydrogen transfer from the steps onto the terraces. The initial small signal decrease is the result of the negative temperature dependence of the nonlinear susceptibility and is fully reversible, as can be seen after quenching the surface temperature again. The

diffusion process eventually leads to an equilibrium distribution of hydrogen between the steps and terraces which is manifested as a constant SH signal. In the case of negligible desorption this situation is characterized by equal rates for hydrogen diffusion from and towards the steps.

Processes other than diffusion which could account for the observed signal increase would be either hydrogen desorption from the surface or adsorbate-induced surface reconstructions which affect the SH intensity. However, for both processes, for the investigated surface temperatures one expects much lower rates than those observed. With TPD spectra taken after saturation, and comparing the corresponding hydrogen coverages with those determined right after the signal has become essentially constant at the end of region II, it could be verified that the total surface coverage remained constant. After each diffusion experiment the sample is flash-annealed to 1250 K in order to desorb the hydrogen and produce well-ordered steps for the subsequent experiments. Identical diffusion experiments were performed for the 2.5°, 5.5°, and 10° misoriented samples. Representative for these experiments in Fig. 4.29, the time evolutions of the nonlinear susceptibility $\chi_s^{(2)}$ for the case of Si(001)5.5°→[110] during the diffusion process is shown for a number of different surface temperatures.

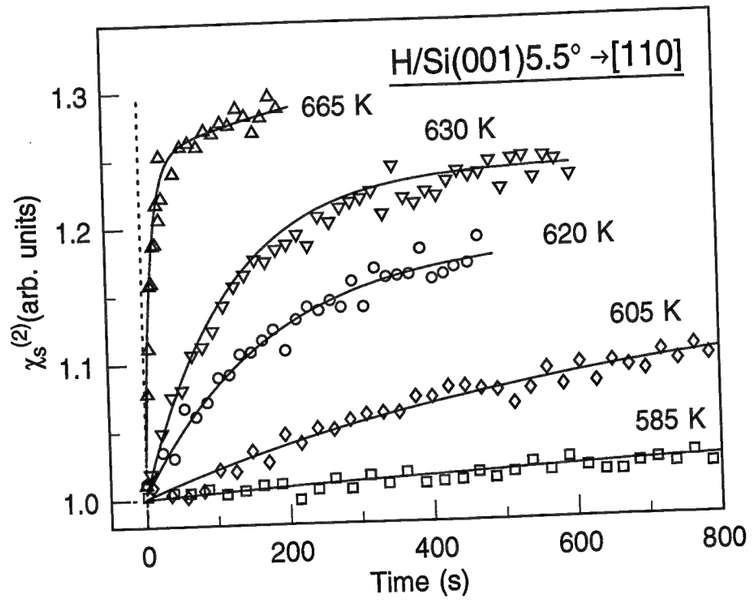


**Fig. 4.29:** Increase of the nonlinear susceptibility $\chi_s^{(2)}$ for the 5.5° sample during hydrogen diffusion from the initially saturated steps onto the terraces measured for different surface temperatures. The continuing signal increase at $T_s$=665 K is due to the onset of hydrogen desorption.



For temperatures in excess of 650 K hydrogen desorption becomes visible, leading to a continuing signal increase, as can be seen for the data taken at $T_s = 665$ K. Therefore, both the finite heating rate which has to be applied to reach the desired temperature value and the onset of hydrogen desorption determine the upper limit. The diffusion rate, however, is sufficiently distinct from the desorption process to allow its independent determination up to $T_s$=710 K.

The increase of the SH intensity during the diffusion process can be related to the changes in step and terrace coverage. For that purpose, as discussed in section 2.3 the total nonlinear response can be approximated as the sum of independent contributions from the steps $\chi^{(2)}_{s,step}$ and terraces $\chi^{(2)}_{s,terr}$ and a weakly coverage-dependent nonresonant term $\chi^{(2)}_{s,NR}$. Neglecting possible phase shifts and applying the linear relationships between $\chi_s^{(2)}$ and hydrogen coverage the corresponding expression reads:

$$\chi_s^{(2)}(\theta) = \chi^{(2)}_{s,step}(1 - \alpha_s\theta_s) + \chi^{(2)}_{s,terr}(1 - \alpha'_t\theta_t) + \chi^{(2)}_{s,NR}(\theta). \tag{4.11}$$

With the steps oriented perpendicular to the plane of incidence the s- and p-components of the incident light were chosen in order to maximize the signal, which is detected without a polarizer in the exit channel. Under these conditions, $\chi^{(2)}_{s,step}$ was approximately four times larger than $\chi^{(2)}_{s,terr}$ with respect to the number of dangling bonds, leading to the observed increase in SH intensity related to the net migration of hydrogen from the steps onto the terraces. Evaluating eq. 4.11 for constant total surface hydrogen coverage $\theta_0$, $\chi_s^{(2)}(\theta)$ can be converted to the temporal change of step or terrace coverage according to

$$\theta_s(t) = \theta_0 - \theta_t(t) = A\chi_s^{(2)}(t) + B \tag{4.12}$$

$$A = \left(\alpha_t\chi^{(2)}_{s,terr} - \alpha_s\chi^{(2)}_{s,step}\right)^{-1} \tag{4.13}$$

$$B = -A\left(\chi^{(2)}_{s,step} - \chi^{(2)}_{s,terr}(1 - \alpha_t\theta_0) - \chi^{(2)}_{s,NR}\right). \tag{4.14}$$

To obtain quantitative results, the SH temperature dependence has to be taken into account. This is done by linearly decreasing $\alpha_t$ from 3.1 to 2.8 over the corresponding surface temperature range from 600 to 680 K.

For the case of the 2.5° miscut sample the coverage-converted data are plotted in Fig. 4.30, showing the step depletion till equilibrium for three different surface temperatures. The conversion works reasonably well as judged from the resulting equilibrium distribution, which could be verified by an independent measure as discussed below. The conclusion drawn from these data is that both the high equilibrium step coverage and its temperature-dependent shift already indicate a higher binding energy for hydrogen at the step sites. For the larger misorientations this simple conversion method, however, could not be applied with sufficient accuracy. The probable cause might be that with decreasing terrace size the nonlinear contributions from the steps and terraces together with their temperature dependence interfere with each other more strongly.

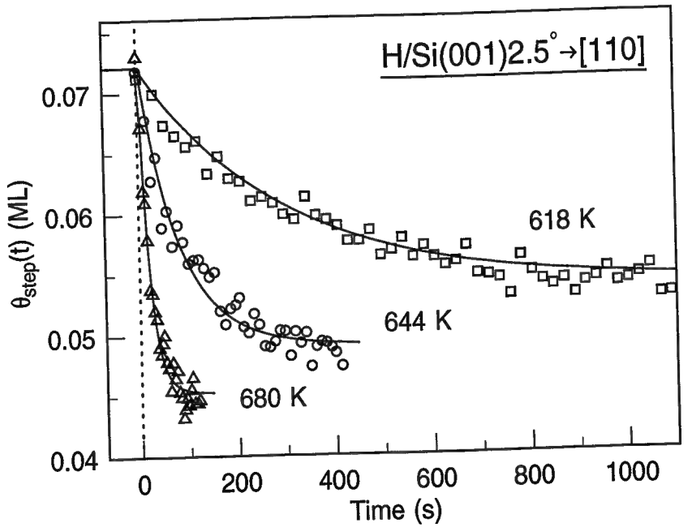


**Fig. 4.30:** Hydrogen population of the steps as a function of time obtained for the 2.5° misoriented surface. With higher temperatures one observes an increase in the rate for the step depletion and a decrease in equilibrium step coverage.

For an accurate analysis of the diffusion kinetics one would have to consider not only the rate for the initial step depletion process but also all the successive microscopic diffusion events between the adsorption sites on the terrace dimers. This would lead to an array of coupled linear differential equations and would require further assumptions about the diffusion dynamics both for the step-to-terrace diffusion and the terrace diffusion itself. For the following analysis it is therefore assumed that the diffusion on the terraces is fast compared with the migration from the steps, which can be justified because of the more tightly bound state at the step sites.

With only a comparatively small amount of hydrogen (<5% ML) actually involved in the net mass transfer, the deviation of the step coverage from equilibrium $\Delta\theta(t) = \theta_{step}(t) - \theta_{step}(t \to \infty)$ decreases exponentially:

$$R_\mathrm{d} = -\frac{d\Delta\theta(t)}{dt} = \Delta\theta(t)\nu_\mathrm{d}(T) = \Delta\theta(t)\nu_0 \exp\left(-\frac{E_\mathrm{A}}{k_\mathrm{B}T_\mathrm{s}}\right), \tag{4.15}$$

with the first-order rate constant $\nu_\mathrm{d}(T)$ and its temperature dependence expressed in terms of an activation energy $E_\mathrm{A}$ and a preexponential factor $\nu_0$. Since $\chi_\mathrm{s}^{(2)}$ depends to good approximation linearly on $\theta$ (eq. 4.11), the rate constants can be determined directly from the time-dependent change of the nonlinear susceptibility according to

$$\frac{\mathrm{d}\chi_\mathrm{s}^{(2)}(t)}{\mathrm{d}t} = \frac{\mathrm{d}\theta_\mathrm{s}(t)}{\mathrm{d}t}\left(\alpha_\mathrm{t}'\chi_{\mathrm{s,terr}}^{(2)} - \alpha_s\chi_{\mathrm{s,step}}^{(2)}\right). \tag{4.16}$$



The derived values are summarized in Fig. 4.31 in the form of an Arrhenius plot for all three misorientations investigated. As can be seen this method allows determination of diffusion rate constants over the comparatively wide range from below $10^{-3}\,\mathrm{s}^{-1}$ up to $\sim 1\,\mathrm{s}^{-1}$. Since adsorbates are known to affect the second harmonic signal already in very low concentrations, the low temperature limit is given by possible adsorption of residual gas.

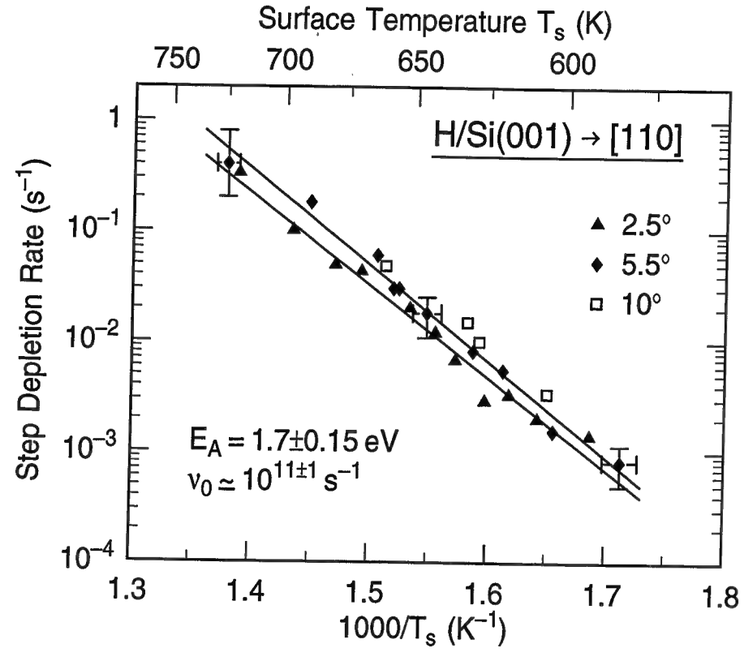


**Fig. 4.31:** Arrhenius plot of the measured diffusion rates for the three different surface orientations investigated. The data for the 2.5° and 5.5° miscut angle correspond to an activation energy of $1.7 \pm 0.15$ eV.

An activation energy $E_\mathrm{A} = 1.65 \pm 0.15\,\mathrm{eV}$ and a prefactor $\nu_0 = 1 \times 10^{11\pm1}\,\mathrm{s}^{-1}$ are deduced for the 2.5° sample. Nearly identical results of $E_\mathrm{A} = 1.7 \pm 0.1\,\mathrm{eV}$ and $\nu_0 = 5 \times 10^{11\pm1}\,\mathrm{s}^{-1}$ are obtained for both the 5.5° and 10° samples.

The errors of these values are dominated by the accuracy of the determination of the diffusion rate constants. However, even in case the assumption of rapid equilibration on the terraces does not hold, the initial behavior can still be described by an exponential equation similar to eq. 4.15. Therefore, this would only result in minor corrections of the activation energy since the rates change by three orders of magnitude in the temperature range investigated.

**Interpretation and discussion**

The mean activation energy of $1.7 \pm 0.15$ eV can be interpreted as the barrier for the hydrogen atoms to migrate from the step sites onto the first dimer of the lower terrace. The diffusion onto the upper terrace might also be possible, but seems less likely because of geometrical constraints and due to a lower value of the chemisorption energy calculated for the first dimer on the upper terrace [169], as shown later. Two cases have to be considered concerning the relation of the observed barrier height with the diffusion barrier for the terrace.

First a barrier for terrace diffusion significantly in excess of 1.7 eV would result in a preferred population of the terrace sites in the vicinity of the step-edge. This would lead to significantly different diffusion rates and step populations in successive diffusion cycles, which is in contrast to the experimental observations described below (see also Fig. 4.33). Thus a barrier for terrace diffusion equivalent to, or smaller than, the 1.7 eV is likely. For an actual activation barrier for step depletion slightly smaller compared with terrace diffusion one would have a direct measure of the barrier for the terrace diffusion. The difference, however, must not exceed a few tenths of an eV, because otherwise selective step saturation at $T_s = 550$ K as observed experimentally would not be possible. This conclusion agrees with the results of recent STM experiments that observed the hopping of single hydrogen atoms along the dimer rows of Si(001)2×1 [159] and deduced an activation barrier of $1.68 \pm 0.15$ eV, assuming an attempt frequency of $\nu_0 = 10^{13}\,s^{-1}$.

With a diffusion barrier for hydrogen of 1.7 eV, this value corresponds to roughly half of the Si–H binding energy and 2/3 of the activation energy for desorption [10–12,48,72,73,75]. This large lateral corrugation is not a specialty of the presence of the steps, rather being due to the localized nature of the covalent Si–H bond. Both for Si(001)2×1 [80,159,165] and Si(111)7×7 [12,170] similarly high values have been observed for the flat surface concentrated in the range of 1.5–2.2 eV. For Si(001), the diffusion was observed to be anisotropic with preferred motion along the dimer rows. For the concerted motion of paired hydrogen on the silicon dimers the barrier was estimated to be $1.95 \pm 0.2$ eV [165].

Theoretical investigations suggest that the diffusion of hydrogen on the terraces is mediated by substantial distortion of the silicon atoms from their equilibrium positions [76,88,89]. This enables the hydrogen to hop from one site to the other without completely breaking the original Si–H bond prior to formation of the new one. However, the calculated barriers vary over a considerably large range: For single hydrogen motion different calculations have assigned diffusion barriers of ~1.3 eV [88], 1.65 eV [89,159], and 2.25 eV [106] for the diffusion along the dimer rows and higher values ranging from 1.8 to 3.1 across them [88–90,159]. On the basis of our experiments the value of 2.25 eV seems to be unlikely, whereas the others are consistent within the limits set by these measurements.



This diffusion model provides a further argument supporting the assumption that diffusion from the step to the upper terrace is less likely to occur than the nearest site on the lower terrace. To transfer the hydrogen atom from the step-edge to the lower dimer would mainly require a stretching of the Si backbond of the rebonded Si atom. This generally requires less energy than compression of a bond over the same distance, as would be necessary to hand the H atom over to the upper dimer. In addition, the Si–H bond at the step-edge already points more towards the lower dimer.

As the diffusion process was investigated over only a few atomic sites, the results can be related to the microscopic processes discussed above. A topic of interest is how the experimental findings would relate to the diffusion coefficient that one would obtain from mass transport diffusion, i.e. hydrogen migration over macroscopic distances. Due to inherent difficulties applying laser-induced thermal desorption (LITD) for the generation of high resolution, sub-monolayer hydrogen gratings on Si(001) the method of second-harmonic diffraction which was used successfully in the case of hydrogen diffusion on Si(111)7×7 [12] is not directly applicable for Si(001). In order to circumvent this problem a new experimental technique which was proposed recently [171] has been established, making use of rare gas templates to produce a periodic hydrogen concentration profile which is subsequently detected by linear optical diffraction. The experimental procedure is described in the appendix and a very high resolution of this method could be demonstrated which makes it a promising tool for studying diffusion of strongly bound chemisorbates.

### 4.4.3 Chemisorption energy difference

The equilibrium hydrogen coverage, i.e. the distribution of the atoms between the available step and terrace sites, can, in principle, be directly read from the coverage-converted SH data shown in Fig. 4.30. However, there is a more direct and more precise method at hand that circumvents the uncertainties introduced by the necessary assumptions made when calculating the step coverage from the SH signal. In this procedure the number of depleted step sites is determined by titration, use again being made of their high reactivity. This is illustrated in region III of Fig. 4.28: The sample temperature is quickly quenched to the initial value of 555 K after reaching the hydrogen adlayer equilibrium, as indicated by the constant SH response. Decreasing the surface temperature at a rate much higher than the hydrogen diffusion rate preserves the original distribution by freezing out the hydrogen motion. The prerequisite for this experiment is, of course, that the total hydrogen coverage has not significantly decreased due to desorption during the time required for reaching equilibrium. As already mentioned, this was verified with TPD where the coverages were compared in separate experiments performed right after step saturation or after running a diffusion experiment. Then the surface is exposed to molecular hydrogen and the depleted step sites take up hydrogen, as indicated by the fast SH signal decrease. The site-specific

sticking coefficient derived from this second uptake is compatible with the value for the clean surface, indicating that the steps have not been altered during the diffusion anneal. The corresponding hydrogen uptake $\Delta\theta$ can be deduced directly from the SH response and has been verified by additional TPD experiments, as shown in Fig. 4.32 for the case of Si(001)5.5°→[110].

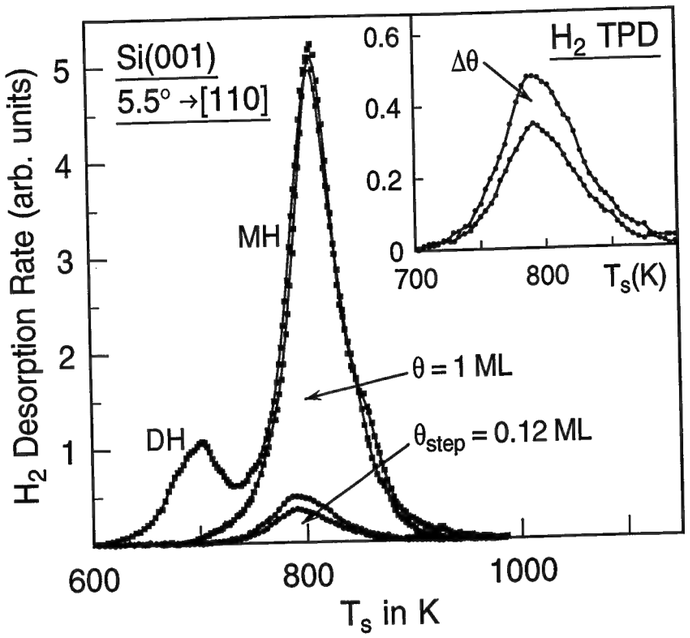


**Fig. 4.32:** Thermal desorption traces (heating rate $\sim 3\,\mathrm{Ks}^{-1}$) from Si(001)5.5° → [110]. Magnified in the inset are data taken right after saturation of the steps of the initially clean sample (lower curve) and data taken after filling the depleted step sites after an equilibration experiment at $T_s = 656\,\mathrm{K}$ (upper curve). For comparison, traces of the fully monohydride (MH) and partially dihydride (DH) covered surface are shown.

The amount of hydrogen which has diffused onto the terraces results as the areal difference between the trace acquired after readsorbing hydrogen at the partially depleted steps and the curve from the solely step-saturated surface. Again, to obtain absolute values the integrated areas have to be normalized with respect to the monohydride-saturated surface.

In Tab. 4.2 the equilibrium hydrogen distributions obtained for various equilibration temperatures are summarized. Here $\theta^0_{\mathrm{step}}$ denotes the hydrogen saturation coverage of the steps and $\Delta\theta$ is the secondary hydrogen uptake at the steps and corresponds to the amount of hydrogen which has diffused onto the terraces.

The step-terrace diffusion process is reversible. This can be seen by slowly de-



| $\alpha$ | $\theta^0_{\mathrm{step}}$ | $T_{\mathrm{dif}}(K)$ | $\Delta\theta$ | $\Delta E^*_{\mathrm{H}}$(eV) | $\Delta E^{\mathrm{chem}}_{\mathrm{H_2}}$(eV) |
|---|---|---|---|---|---|
| 2.5° | 0.074 | 618 | 0.017 | 0.28 | 0.24 |
| | 0.068 | 636 | 0.021 | 0.25 | 0.22 |
| | 0.072 | 643 | 0.023 | 0.24 | 0.21 |
| | 0.070 | 644 | 0.021 | 0.26 | 0.22 |
| | 0.072 | 680 | 0.026 | 0.24 | 0.22 |
| 5.5° | 0.115 | 656 | 0.038 | 0.22 | 0.15 |
| 10° | 0.14 | 628 | 0.016 | (0.32-0.35) | (0.18-0.23) |

**Tab. 4.2:** Results for the equilibrium hydrogen distribution for various temperatures for the three surface misorientations investigated. $\Delta E^*_{\mathrm{H}}$ is the effective energy difference with respect to single hydrogen atoms between the steps and terraces calculated with the simplified model described in the text. $\Delta E^{\mathrm{chem}}_{\mathrm{H_2}}$ is the difference in chemisorption energy for two hydrogen atoms as derived from the data by means of eq. 4.19.

creasing the surface temperature after reaching equilibrium, which leads to a partial back-migration of hydrogen towards the steps. A reduced amount of hydrogen could then be readsorbed at the steps compared with the experiments where the sample temperature is rapidly quenched as discussed above. A complete refilling of the steps, however, cannot be achieved because of the finite cooling rate and finite surface temperature.

The equilibrium occupation distribution between the step and terrace sites is determined by the minimum of the surface free energy. Unless the silicon lattice reconstructs, this is simply given by the adsorption enthalpy difference between the different adsorption sites on the one hand, and the entropy gain due to the scattering of hydrogen atoms across the terraces on the other. With average terrace widths of 14.7, 5.8, and 2.5 silicon dimers for the 2.5°, 5.5°, and 10° miscut angles, respectively, a preferential occupation of the step sites is observed compared with a purely random distribution. As already mentioned above, this together with the observed shift of the equilibrium distribution towards the terraces with increasing temperature indicates a higher binding energy for hydrogen at the steps.

In the following analysis, both a kinetic and a thermodynamic approach will be discussed to derive this energy difference between step and terrace sites from the equilibrium distribution. Whereas the purpose of the simplified kinetic model serves to illustrate the effect of the energy difference, the thermodynamic approach is less obvious but allows for a more accurate description.

In the kinetic model it is assumed that the different dangling bond sites both at the steps and on the terraces are independent, i.e. adsorption of a hydrogen atom on any one site does not affect the binding at neighboring silicon atoms. With equal rates

for both the step-to-terrace diffusion and vice versa, at equilibrium one can write

$$\frac{n_{\text{terr}}(1-n_{\text{step}})}{n_{\text{step}}(1-n_{\text{terr}})} = \exp\left(\frac{-\Delta E_{\text{H}}^{*}}{kT_{\text{s}}}\right). \tag{4.17}$$

In this equation $n_{\text{terr}}$ and $n_{\text{step}}$ are the relative occupation number densities for the specific adsorption sites. They can be expressed in terms of the observable coverages by the relations

$$n_{\text{terr}} = \frac{\Delta\theta}{1-\theta_{\text{step}}^{0}}, \quad \text{and} \quad n_{\text{step}} = 1 - \frac{\Delta\theta}{\theta_{\text{step}}^{0}}. \tag{4.18}$$

$\Delta E_{\text{H}}^{*}$ is the effective binding energy difference between the bonding of a hydrogen atom at a step and terrace site. For independent adsorption sites this is simply given by $\Delta E_{\text{H}}^{*} = E_{\text{terr}}^{\text{Si-H}} - E_{\text{step}}^{\text{Si-H}}$.

The resulting energy values as derived from the equilibrium hydrogen distributions are summarized in Tab. 4.2. Similar energies are found in the different experiments for the 2.5° and 5.5° misorientations with an average $\Delta E_{\text{H}}^{*} \simeq 0.25 \pm 0.05$ eV. The uncertainty arises from the accuracy of the absolute hydrogen coverages and the uncertainty in miscut angle. The difference between the measured hydrogen saturation coverage and the expected number of dangling bonds at the step-edge renders the interpretation of the 10° sample difficult and it will thus be omitted in the following discussion.

The estimate is based on the assumption that the hydrogen atoms are distributed evenly across the terraces without preference for particular terrace sites. Although there is no direct microscopic evidence, the following experiment can at least rule out that the hydrogen atoms, having left the step sites, predominantly populate the terrace dimers right next to the step-edge. This is shown in Fig. 4.33, where the cycle of diffusion and successively readsorbing hydrogen is repeated right after the first treatment has been performed. Within the accuracy of the experiment, the same diffusion rate is observed for the step depletion process, indicating that only few H atoms from the first cycle block sites on the dimers next to the step-edge. The higher initial terrace population prior to the second cycle reduces the entropy gain on the terrace and the equilibrium is shifted towards a higher relative step population. Therefore, as can be seen in the figure, slightly less hydrogen can be readsorbed after the second cycle.

The model discussed above, of course, only delivers a crude estimate since it is known that the dangling bonds on the terrace dimers interact. The $\pi$-like bonding with an interaction energy of $\sim 0.2-0.3$ eV [11,50] leads to preferential pairing of two hydrogen atoms on the same dimer, as discussed in the introductory chapter. In addition, because of possible restrictions in the free two-dimensional motion, e.g. due to the presence of the steps, the value of $\Delta E_{\text{H}}^{*}= 0.25$ eV should be regarded as an upper limit of the binding energy difference and rather be viewed in terms of an effective energy difference.



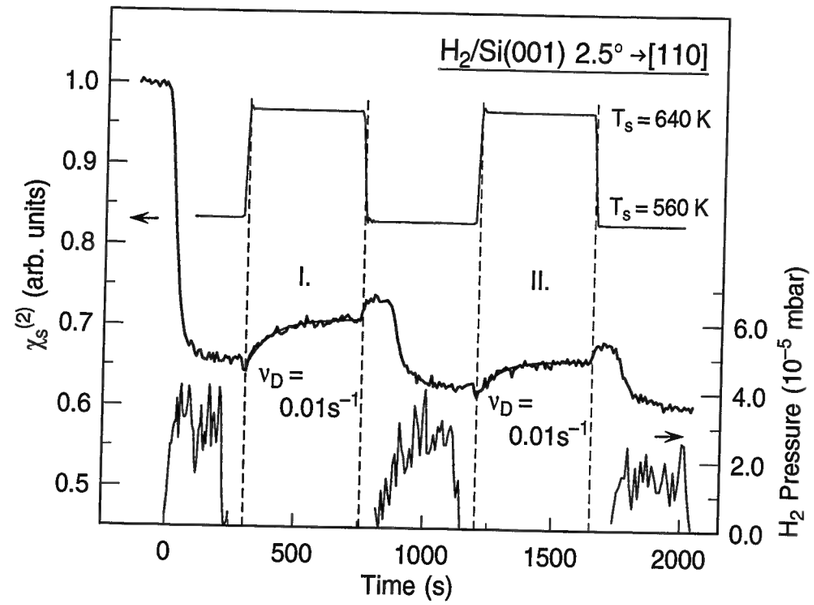


**Fig. 4.33:** Successive diffusion ($T_{\text{s}} = 640$ K) and titration ($T_{\text{s}} = 560$ K) experiments on Si(001)2.5° → [110]. A decreasing amount of hydrogen can be readsorbed at the steps with each cycle.

The constraint of the preferred pairing of the hydrogen atoms on the same dimer results in a reduced entropy gain for the hydrogen atoms on the terrace. Therefore, in order to explain the observed hydrogen distribution, a reduced binding energy difference would be required. The contribution from the pairing energy is quite substantial, as the following estimate indicates. For a pairing energy of 0.25 eV the fraction of hydrogen atoms which are paired on the terrace dimers can be calculated as 50–60% for hydrogen coverages between 0.02 and 0.04 ML[2]. This leads to an average contribution of $\sim 0.06 - 0.08$ eV per hydrogen atom to the effective energy difference. Expanding the kinetic model to account for the pairing energy thus gives a reduced value for the binding energy.

However, also accounting for the reduced diffusion phase space due to restrictions of the two-dimensional hydrogen motion makes the kinetic approach very complicated. Since one is only interested in the equilibrium properties of the hydrogen-covered

[2] The equilibrium coverage of hydrogen atoms occupying doubly-occupied dimers expressed in terms of the total hydrogen coverage $\theta_2 = \theta - \left\{\sqrt{1+4\alpha\theta(1-\theta)} - 1\right\}/2\alpha$ with $\alpha = \exp(\epsilon_{\text{pair}}/k_{\text{B}}T) - 1$ can be obtained from the equilibrium rate equation or simple statistical mechanics [11,48].

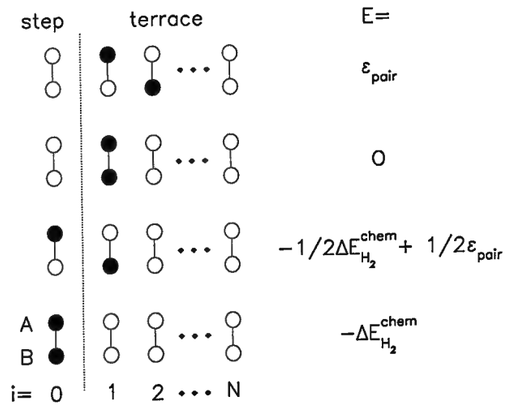


**Fig. 4.34:** Energies of the different hydrogen configurations between step-edge and dimer row. Note: the pairing energy at the step-edge is neglected.

surface, applying a thermodynamic model yields the energy differences in a rather direct way. For that purpose the following Hamiltonian is used [169] for describing the $H_2$ adsorption on a stepped surface:

$$H^{(D_B)} = -\frac{1}{2}\left(n_0^A + n_0^B\right)\Delta E_{H_2}^{chem} + \\ + \sum_{i=1}^{N}\left\{\frac{1}{2}\left(n_i^A\left(1-n_i^B\right) + n_i^B\left(1-n_i^A\right)\right)\epsilon_{pair}\right\}. \quad (4.19)$$

Assuming that all terrace sites have identical hydrogen chemisorption energies $\Delta E_{H_2}^{chem}$ is the chemisorption energy difference between two hydrogen atoms adsorbed either at the step-edge (index $i = 0$) or the terrace dimers ($i = 1...N$). $n_i^A$ and $n_i^B$ denote the occupation numbers (0 or 1) of the silicon atoms "A" and "B" of the $i$-th dimer. It is assumed that a pairing energy exists only for the terrace dimers and not between the step sites, but it can be shown that this assumption only has a small influence on the hydrogen distribution. On the basis of recent experimental [80,159] and theoretical results [88–90] it is further assumed that both inter-row diffusion and hopping across the steps is negligible for the temperatures of the experiment. The hydrogen motion is therefore restricted to single dimer rows of length $N$. This is included in this model Hamiltonian, and its validity to describe the situation correctly can be made obvious by writing down the resulting energies for the various hydrogen configurations possible as shown in Fig. 4.34. The blank (solid) circles correspond to clean (hydrogen-covered) silicon atoms. With $\sum_i n_i^A + \sum_i n_i^B = 2$, the resulting



partition function for this canonical ensemble can be written as

$$Z = \sum_{\substack{n_0^A=0,1\\ n_0^B=0.1}} \cdot \sum_{\substack{n_1^A=0,1\\ n_1^B=0.1}} \cdots \sum_{\substack{n_N^A=0,1\\ n_N^B=0.1}} e^{-\beta H} = e^{\beta\Delta E} + N + 2Ne^{\beta\frac{1}{2}(\Delta E-\epsilon_{pair})} + N(N-1)e^{-\beta\epsilon_{pair}}. \quad (4.20)$$

From that, the expectation values $\langle n_i^A\rangle = \langle n_i^B\rangle$, which relate to the measured relative coverages as $\langle n_0\rangle = n_{step}$ and $\langle n_i^{i\geq 1}\rangle = n_{terr}$, are calculated:

$$\langle n_0\rangle = \frac{e^{\beta\Delta E} + Ne^{\beta\frac{1}{2}(\Delta E-\epsilon_{pair})}}{Z}. \quad (4.21)$$

Using a pairing energy of $\epsilon_{pair} = 0.25$ eV and solving this equation numerically for $\Delta E$, one obtains the values for the chemisorption energy differences listed in the last column of Tab. 4.2.

Within the accuracy of the experiment, the values agree for the three different sample misorientations and an average of $\Delta E = 0.2 \pm 0.05$ eV can be given. With respect to the Si–H bond strength (see following chapter) this value relates to a less than 5% variation of the binding energy for the step versus terrace sites. The result is thus very similar to the typical energy differences found for chemisorbates on stepped metal surfaces [151,168,172].

### Theory

The experimental results can be directly compared with theoretical investigations of E. Pehlke and P. Kratzer, who calculated relaxed atomic geometries and chemisorption energies for hydrogen on vicinal Si(001) using density functional theory. The theoretical method used is similar to the one described in section 4.2 and the calculations discussed here were a continuation of that work. The outcome of these calculations will only be summarized here to the extent relevant for a deeper understanding of the experiments; for a more detailed account the reader is referred to Ref. [169]. Briefly, total energy minimizations and geometry optimizations were carried out for Si(1 1 11) slabs with a thickness of about six atomic layers. This corresponds to a miscut angle of 7.3° towards [110] with four dimers per terrace for the $D_B$ stepped surface, and the resulting relaxed atomic geometry is shown in Fig. 4.35.

In agreement with previous theoretical studies and experiments, the rebonded $D_B$-type step configuration turns out to be energetically favored. Similar to the pronounced buckling of the terrace dimers, rehybridization results in a height difference between neighboring rebonded step-edge atoms. In the following, the clean Si surface is used as the energy reference for the chemisorption energies. The relaxed geometries are now determined for two hydrogen atoms absorbed on the different surface dimers or at the two rebonded step Si atoms and are shown in Fig. 4.36. Upon hydrogen adsorption the buckling disappears for both step and terrace adsorption. The resulting

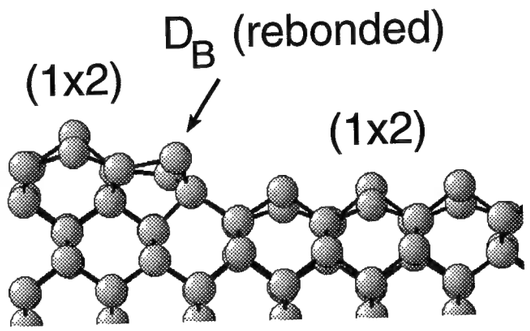


**Fig. 4.35:** Side view along [1$\bar{1}$0] of the relaxed atomic geometry of double-height steps on Si(001) (by courtesy of E. Pehlke).

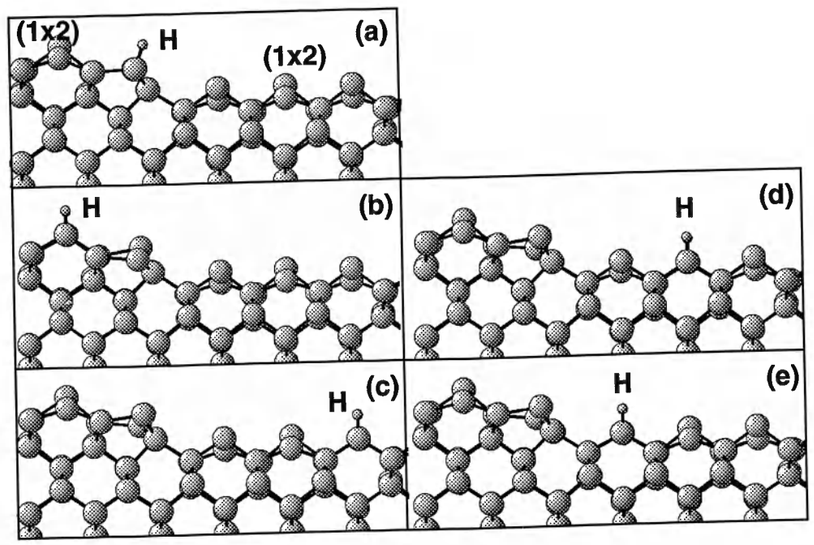


**Fig. 4.36:** Relaxed atomic geometries for two hydrogen atoms adsorbed at different sites of Si(1 1 11). Only one hydrogen atom is visible because of the view along the [1$\bar{1}$0] direction (from Ref. [169]).

chemisorption energies determined for these different configurations are summarized in Tab. 4.3 with the $H_2$ molecule at infinite distance from the surface defining zero energy.

For step adsorption the highest chemisorption energy is found compared with the terrace adsorption, reproducing the experimental findings. As a possible cause of this effect, it has been speculated that this might be due to both, the different relaxation energies and the $\pi$-like interaction between the dangling bonds of the dimer atoms, which might not be present at the steps [169]. Quantitatively the value for the chemisorption energy difference of 0.15 eV deduced from the measurement of the 5.5° miscut sample agrees well with the theory. Although the values for the 2.5° sample appear somewhat too large, the experimental uncertainty in this case is higher due to the small amount of hydrogen readsorbed in the titration experiment, consequently making these measurements more sensitive to systematic errors. However, the chemisorption energy difference between the step and a typical adsorption site in the middle of the terrace of $\sim$0.17 eV falls well within the range of experimental values of 0.15–0.22 eV.



| | Adsorption site | Chemisorption energy (eV) |
|---|---|---|
| (a) | H at rebonded $D_B$-step | -2.09 |
| (b) | H on (1×2) terrace, pos. 1 | -1.77 |
| (c) | H on (1×2) terrace, pos. 2 | -1.92 |
| (d) | H on (1×2) terrace, pos. 3 | -1.97 |
| (e) | H on (1×2) terrace, pos. 4 | -1.97 |

**Tab. 4.3:** Chemisorption energies for two hydrogen atoms adsorbed on Si(1 1 11). The corresponding adsorption geometries are shown in Fig. 4.36 (data from Ref. [169]).

### 4.4.4 Conclusion

The intrinsic chemical properties of vicinal Si(001) surfaces allowed formation of a periodic nonequilibrium hydrogen concentration profile. By taking advantage of the different adsorption energy barriers of the step compared with the terrace sites towards dissociative adsorption of molecular hydrogen, the steps could selectively be saturated with hydrogen. By monitoring the transition to thermal equilibrium of the surface hydrogen coverage an activation barrier for the step to terrace diffusion of 1.7±0.15 eV was determined. From the equilibrium hydrogen occupation the steps were found to be energetically favored and a chemisorption energy difference of $\sim$0.2 eV per $H_2$ could be derived. The preferred binding of the hydrogen atoms to the rebonded silicon step-edge atoms is in accordance with density functional calculations of Pehlke and Kratzer.

# Chapter 5

# Binding energy and detailed balance of hydrogen on silicon surfaces

## 5.1 Isosteric heat of adsorption

Due to its fundamental importance the adsorbate-surface bond strength has been determined for a number of chemisorption systems by means of equilibrium measurements [173–175]. In this standard technique the occupation density of the adsorbate is measured in equilibrium with its gas phase. However, the vast majority of these studies have been restricted to chemisorbates that do not have a sizeable barrier for adsorption, therefore making the heat of adsorption accessible under standard UHV conditions. For systems where equilibrium conditions are not applicable, in recent years the technique of adsorption microcalorimetry has advanced to studying adsorption on single-crystal surfaces by measuring directly the heat liberated in the reaction [176,177].

For dissociative chemisorption of hydrogen on silicon surfaces, in particular, the large activation barriers and related low sticking probabilities have thus far prevented the use of these methods to determine the hydrogen chemisorption energy on external surfaces. The general requirement – *in situ* determination of the surface coverage in equilibrium – renders the equilibrium experiments difficult. The ambient conditions, viz. elevated temperatures required to reach equilibrium and the related high pressures necessary to populate a significant fraction of the adsorption sites, call for special prerequisites concerning both the vacuum setup and the coverage determination in the presence of high $H_2$ pressures.

The virtue of the thermodynamic method is that no kinetic parameters of the reaction enter and it only requires static measurement of temperature, surface coverage, and gas pressure. The isosteric heat of the reaction related to the enthalpy of adsorption can easily be derived at equilibrium of the adsorbed species with its gas phase [146,173,178,179]:

$$\mathrm{d}\mu_\mathrm{g} = \mathrm{d}\mu_\mathrm{s}, \tag{5.1}$$

with $\mu_\mathrm{s}$ and $\mu_\mathrm{g}$ the chemical potentials of surface and gas environment. The corre-

sponding expressions for the gas phase and the surface, respectively, are:

$$\mathrm{d}\mu_\mathrm{g} = -s_\mathrm{g}\mathrm{d}T + v_\mathrm{g}\mathrm{d}p, \tag{5.2}$$

with entropy $s_\mathrm{g}$ and gas volume $v_\mathrm{g}$, and

$$\mathrm{d}\mu_\mathrm{s} = -\bar{s}_\mathrm{s}\mathrm{d}T + \bar{v}_\mathrm{s}\mathrm{d}p + \left.\frac{\partial\mu_\mathrm{s}}{\partial\theta}\right|_{p,T}\mathrm{d}\theta, \tag{5.3}$$

$\bar{s}_\mathrm{s}$ and $\bar{v}_\mathrm{s}$ being the partial molar quantities given with respect to the number of adsorbed particles. For constant adsorbate coverage $\theta$, defined as the occupation density of the surface, and $v_\mathrm{s} \ll v_\mathrm{g}$ the adsorbate chemical potential reduces to $\mathrm{d}\mu_\mathrm{s} = -\bar{s}_\mathrm{s}\mathrm{d}T$ and one obtains a two-dimensional analogon to the Clausius-Clapeyron equation [146,174]:

$$\left.\frac{\partial p}{\partial T}\right|_\theta = \frac{s_\mathrm{g} - \bar{s}_\mathrm{s}}{v_\mathrm{g}}. \tag{5.4}$$

For the ideal gas, and since $T(s_\mathrm{g} - \bar{s}_\mathrm{s}) = (h_\mathrm{g} - \bar{h}_\mathrm{s})$ at equilibrium with $h_\mathrm{g}$ and $\bar{h}_\mathrm{s}$ the corresponding enthalpies, the isosteric heat of adsorption, defined as $q_\mathrm{st} = (h_\mathrm{g} - \bar{h}_\mathrm{s})$, is given by

$$q_\mathrm{st} = k_\mathrm{B}T^2\left.\frac{\partial \ln p}{\partial T}\right|_\theta. \tag{5.5}$$

$q_\mathrm{st}$ can therefore be derived from the temperature dependence of the equilibrium isotherms. It is a differential molar quantity and is the heat involved when one molecule of $H_2$ is transferred to the adsorbed state under conditions such that the changes of $p$, $T$, and $\theta$ are negligible. Thus $q_\mathrm{st}$ can be interpreted in terms of an effective chemisorption energy [146,179]. For its relation to the corresponding bond energy, however, both adsorbate-induced changes in surface structure as well as adsorbate lateral interactions have to be taken into account.

## 5.2 Experiment

The focus of this section is on the special requirements concerning the equilibrium measurements. It is an extension of the general description of the experimental setup and procedures outlined in detail in chapter 2. In contrast to the UHV experiments described there, where room temperature $H_2$ gas is exposed to a sample at elevated temperature, here the silicon surface and surrounding gaseous atmosphere are kept at the same temperature. This thermal equilibrium is achieved in a special designed all-quartz UHV cell (Bahr, Manching, Germany) placed in a muffle furnace (Heraeus). This quartz chamber with inner diameter 50 mm and length ~25 cm loosely fills the muffle pipe and is connected to the stainless-steel UHV chamber via a quartz-metal transition located outside the oven.



The silicon sample ($11 \times 20\,\mathrm{mm}^2$) is loaded with the help of a pair of long tweezers through the flange opening onto a small all-quartz sample holder suspended from the top. With its polished side facing the front, the sample is held in place by two wedge-shaped forks on either side. For temperature measurements a NiCr/NiAl thermocouple contact is fed into the hollow sample holder tube open to the atmosphere. Photographs of the quartz cell utilized are displayed in Fig. 5.1: They show the bare cell with thermocouple wire and sample (top) and front view of the whole assembly connected with the main chamber with the open muffle (bottom).

Both pumping and hydrogen dosing proceed through the main chamber. To inhibit intermixing of the hot hydrogen gas inside the quartz vessel with the 300 K gas in the foreline, a quartz baffle is placed in the quartz tube leaving the muffle.

Figure 5.2 shows a schematic of the experiment. For details of the vacuum setup see also Fig. 3.1. The optical setup drawn is for SHG measurements under normal incidence of the pump light supplied by the Nd:YAG laser directed onto the sample surface through an optical quartz window at the front of the quartz cell. Under this geometry the anisotropic $\chi^{(2)}_{\mathrm{s},\xi\xi\xi}$-component of the Si(111)7×7 surface is probed. The signal is separated with a dielectric mirror (DM) coated as an edge filter, transparent for 1064 nm and highly reflective for 532 nm.

The quartz cell is baked at 400°C together with the dosing system and a base pressure of $\sim 1\times10^{-10}$ mbar is achieved. Since quartz is a rather porous material which tends to outgas at the elevated temperatures required for the measurements ($T > 750$ K), such high bakeout temperatures are necessary. This, however, prohibits the use of *ex situ* hydrogen terminated samples and therefore clean silicon surfaces have to be prepared *in situ* from the native-oxide-covered samples. Although quartz can easily be heated to above 1200 K, UHV conditions cannot be maintained because gas permeation through the walls becomes significant at these temperatures. Laser annealing of the crystal is therefore utilized with a cw Nd:YLF laser operating at 1053 nm with a maximal power of 27 W. The laser beam is incident a few degrees off-normal and is lightly focussed onto the sample to a diameter of ~ 2 mm. The reflected beam is directed into the beam dump (BD). For sample preparation the laser power is slowly increased to first outgas the sample after preheating the oven to 830 K. From e color of the annealed spot a surface temperature in excess of 1300 K could be estimated for the maximal power density of $500\,\mathrm{W/cm}^2$ applied.

The SH signal can be monitored *in situ* and in Fig. 5.3 the signal increase during thermal decomposition and removal of the native oxide is recorded. By slowly rastering the Nd:YLF laser vertically and horizontally across the surface an extended surface area can be cleaned. During this procedure the background pressure does not exceed $4\times10^{-10}$ mbar since essentially no heat load is exerted on other parts inside the system.

The quartz cell does not allow application of standard techniques to infer sample cleanliness and surface order. Therefore, different aspects concerning the nonlinear

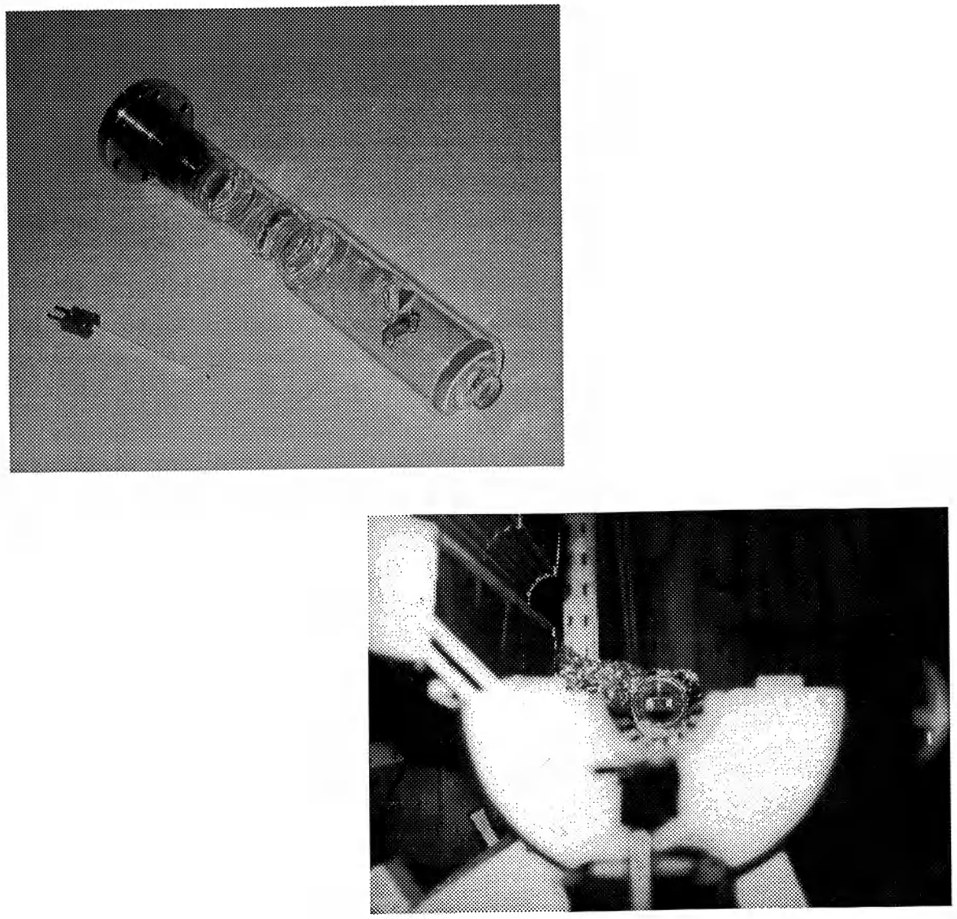

**Fig. 5.1:** The quartz cell with silicon sample: Chamber with front window for normal incidence annealing and SHG measurements (top). Thermocouple wires are fed into the hollow support tube of the sample holder. Front view of the mounted quartz cell inside the open muffle furnace (bottom).

susceptibility of the clean and hydrogen-covered surface, surface symmetry, reconstruction phase transition, and recombinative hydrogen desorption are addressed in these experiments, where the characteristics are well known for the clean Si(111)7×7 surface under standard UHV conditions.

Both the ultimate SH-signal intensity (data in Fig. 5.3) and the polarization dependence which reflects the $C_{3v}$-symmetry of the surface [180], were found to be identical to the behavior observed previously under the same conditions the laser was utilized.



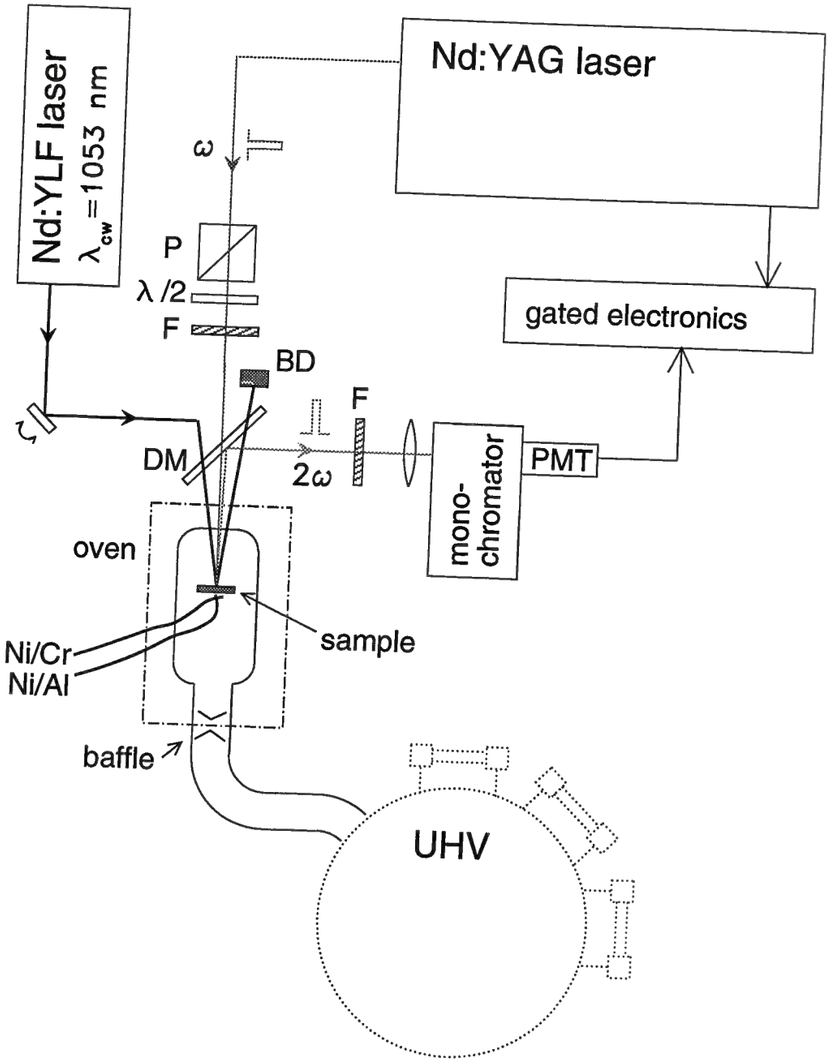


**Fig. 5.2:** Schematic of experimental setup: laser annealing using a 27 W cw Nd:YLF laser and second-harmonic generation with the Nd:YAG laser under near normal incidence in the quartz UHV cell.

In addition, by fully hydrogen terminating the sample at high $H_2$ pressures, it was possible to determine the contributions of the coverage-dependent resonant and non-resonant terms to the measured effective nonlinear susceptibility $\chi^{(2)}_{s,\xi\xi\xi}$. The obtained

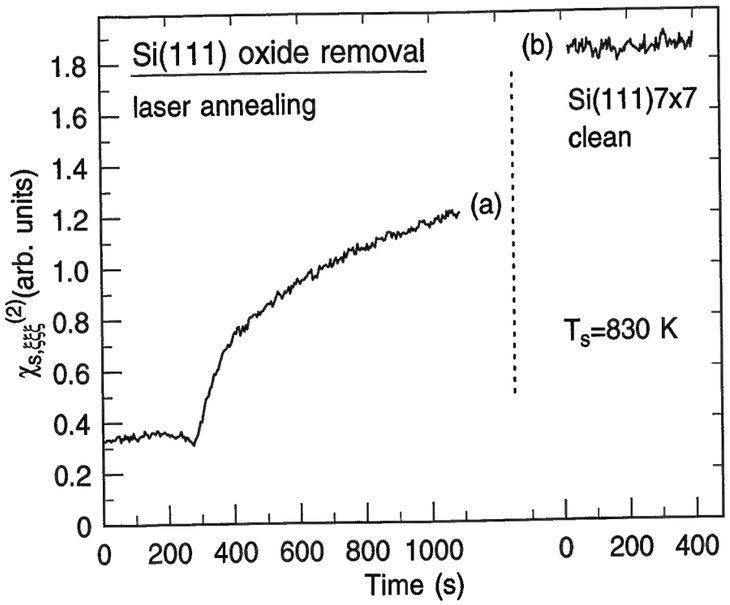


**Fig. 5.3:** Increase of the nonlinear susceptibility during thermal decomposition of the native oxide (a). After scanning the Nd:YLF laser a constant signal strength representative of the clean Si(111)7×7 surface (b) is achieved.

value for the ratio $\left|\chi^{(2)}_{s,db}\right| / \left|\chi^{(2)}_{s,NR}\right|$ of 0.18 is in good agreement with the value of 0.2 obtained for well-ordered Si(111)7×7 under standard UHV conditions [14].

Using SHG even allows one to conclude that the Si(111) surface in the quartz cell exhibits 7×7 reconstruction. This could be concluded from the observation of the reversible 7×7↔1×1 phase transition which is known to occur at $T_c \simeq 1130K$ [181,182]. The formation of the high temperature 1×1 phase is associated with an increase in the number of dangling bonds at the critical temperature. This is reflected in a corresponding rise of the nonlinear susceptibility [183,184]. The change of the anisotropic component $\chi^{(2)}_{s,\xi\xi\xi}$ while heating with the Nd:YLF laser is shown in Fig. 5.4. Ideally a 25% increase is expected [184]. This value is somewhat reduced here, which might be due to an inhomogeneous surface temperature distribution and superheating due to the comparatively high pump pulse fluence of 50 mJ/cm$^2$.

As discussed below, the kinetics determined for the associative desorption of hydrogen from the surface reproduces the behavior known from previous experiments. In general, the reaction kinetics towards establishing thermodynamic equilibrium is very sensitive to surface contaminants and disorder – in contrast to the coverage in equilibrium which in most cases is less affected by impurities.



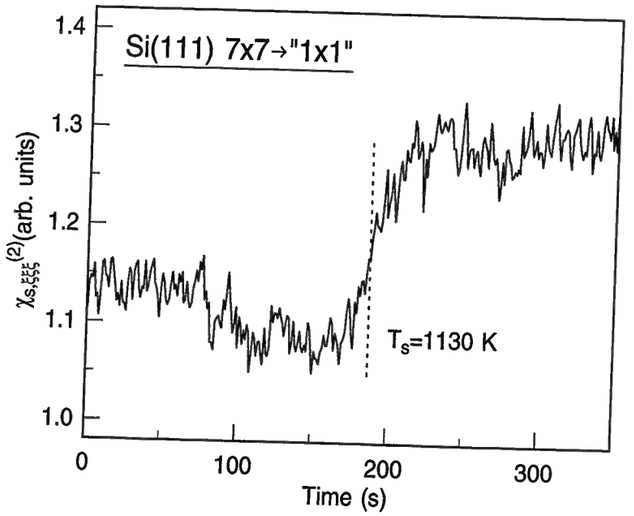


**Fig. 5.4:** Increase of the nonlinear susceptibility component $\chi^{(2)}_{s,\xi\xi\xi}$ during cw laser heating through the Si(111)7×7→1×1 phase transition at $T_c \simeq 1130\,\mathrm{K}$ as a result of the rise in dangling bond density.

## 5.3 Adsorption isotherms

For experimental convenience constant temperature adsorption isotherms $\theta_H = \theta_H(p)\Big|_T$ are recorded. This is achieved by keeping the oven at constant temperature and subsequently introducing hydrogen gas. During these experiments the muffle is flushed with a small argon flux to minimize sample contamination due to air permeation through the quartz, in particular at temperatures above 950 K. Both thermal equilibrium, i.e. same gas and sample temperature, and adsorption-desorption equilibrium have to be established. For that purpose the sample is exposed to a constant hydrogen pressure and the temporal behavior of the SH signal related to surface coverage is monitored while adjusting to its equilibrium value as shown in Fig. 5.5.

Whereas the thermalization of the hydrogen gas occurs rapidly due to its low pressure and heat capacity, the time required to eventually obtain a constant hydrogen coverage is determined by the kinetics of the adsorption and desorption processes and hence depends on $p(H_2)$ and $T$. As discussed in the previous chapter and as known from diffusion experiments on Si(111) [12,170], for the temperatures of these adsorption experiments hydrogen hopping across the surface occurs very rapidly. It can therefore safely be assumed that the final configuration of the adsorbed hydrogen is the equilibrium state. The desorption, which could be studied independently from the recovery of the SH signal after turning off the hydrogen flux, is found to well reproduce the behavior known from previous isothermal desorption experiments [12].

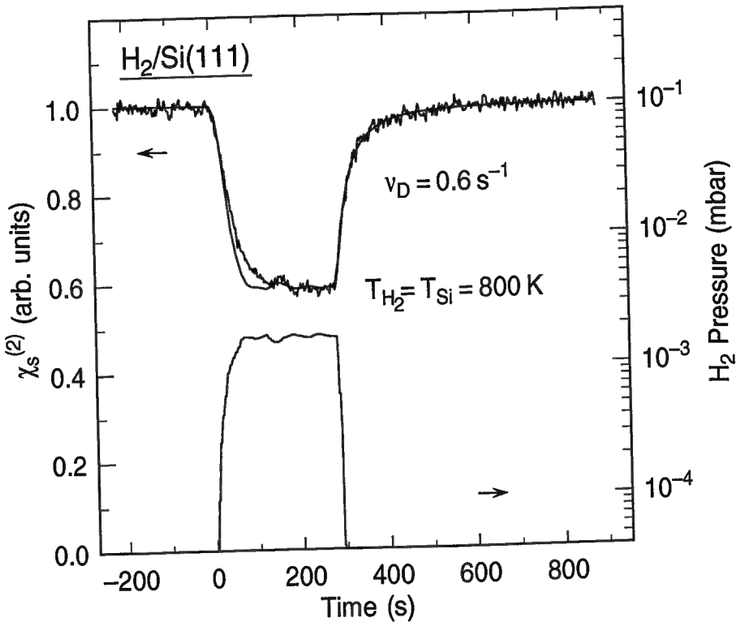


**Fig. 5.5:** Equilibrium experiment: nonlinear susceptibility $\chi^{(2)}_{s,\xi\xi\xi}$ and hydrogen pressure for $T_{H_2} = T_{Si} = 800$ K. The solid line represents a numerical fit assuming second order Langmuir kinetics.

Over the investigated temperature range the initial sticking coefficients are found to be a factor ranging from 3 to 12 higher, depending on temperature, than those in the experiments using hydrogen gas at 300 K [14] as is compatible with activated adsorption [26,28]. The adsorption behavior cannot be fit accurately over the whole coverage range from 0 to 0.3 ML in this experiment on the assumption of second order Langmuir kinetics. This is due to both a coverage dependence of the adsorption barrier and a variation of the isosteric heat and their interplay, as will be discussed below.

By varying the pressure stepwise discrete pairs of equilibrium coverage and pressure values are obtained. For temperatures above 800 K, where the equilibrium is established on a less than 1 s time scale, continuous isotherms can be recorded by applying slow pressure ramps. For that purpose the pressure is continuously increased from below $1\times10^{-5}$ mbar up to a maximal value of $\sim$1 mbar within a few hundred seconds. A representative result after transforming the SH signal into coverage values is shown in Fig. 5.6 for 850 K. By inverting the pressure ramp, i.e. decreasing the pressure from its maximal value, the reversibility and thus the existence of equilibrium at all times can been verified. In addition, this reversibility indicates that the surface



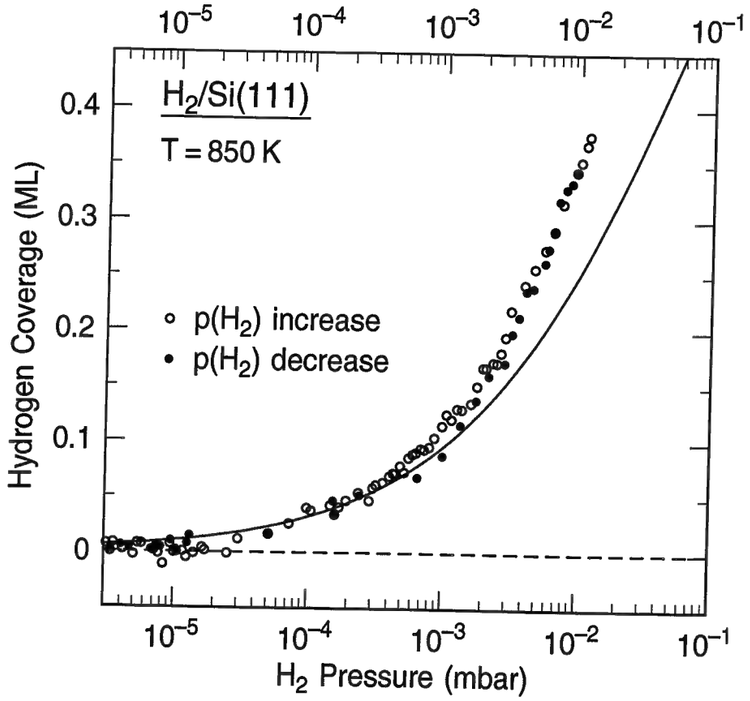


**Fig. 5.6:** Adsorption isotherm: hydrogen coverage vs. applied pressure recorded for $T = 850$ K, showing identical behavior for increasing or decreasing the pressure on a time scale of $\sim$ 600 s. The solid line represents a second order Langmuir adsorption isotherm for dissociative adsorption.

structure is not irreversibly altered during the adsorption/desorption process, which would be manifested in a change in SH intensity. A Langmuir isotherm for dissociative adsorption described by $p(H_2)^{1/2} \propto \theta/(1-\theta)$ for second order in both adsorption and desorption is plotted for comparison (solid line). The deviations towards higher coverages already indicate an increase in the isosteric heat with coverage, as will be discussed below.

Before proceeding, it should be mentioned that the absolute coverage calibration as described in chapter 3 is truly valid only for the particular surface temperature of 600 K. It is known that with increasing surface temperature the relative contribution of the dangling bonds to the total nonlinear susceptibility decreases with respect to the nonresonant term [17,123]. It can be shown, however, that the derived coverages in this experiment are at worst underestimated by 20% due to the resulting decrease in the initial slope $\alpha$. This uncertainty, however, would only affect the determination of the absolute values of the isosteric heat by negligible amounts. $q_{st}$ is derived from

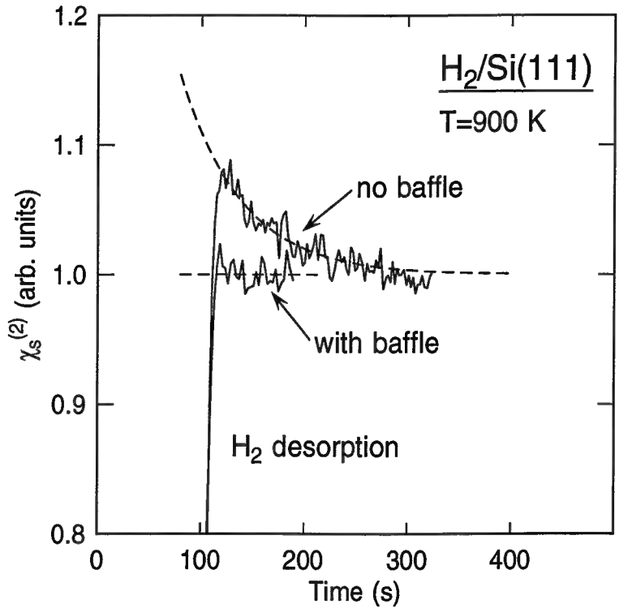


**Fig. 5.7:** SH signal dependence after desorption of hydrogen at $T = 900$ K: Hydrogen gas related cooling of the sample in the absence of the baffle is reflected in a comparatively higher SH signal for the clean surface after the hydrogen is pumped off and which decreases again as the sample rethermalizes.

the isochores and the relative variation of $\alpha$ in the temperature range between 800 and 1000 K is small. Therefore for the conversion of $\chi^{(2)}_{s,\xi\xi\xi}$ to hydrogen coverage the constant value of $\alpha = 1.3$ has been used which was determined in previous calibration experiments [14] described in section 3.4.

The gas-surface temperature equilibrium can be verified in a very simple fashion by making use of the negative temperature dependence of the SH signal. In Fig. 5.7 two experiments are compared with and without the use of a baffle in the inlet of the quartz cell for an initial temperature of 900 K. At $t = 100$ s the hydrogen is pumped off quickly which leads to a nearly instantaneous SH signal rise due to the high desorption rate for that temperature. In the absence of the baffle a higher signal intensity is recorded right after complete hydrogen desorption compared with the value measured before the beginning of the exposure and in contrast to the experiment where the baffle was introduced. This effect is due to the intermixing of the hot gas in the quartz cell with the hydrogen at room temperature in the foreline, which effectively leads to a reduced gas and sample temperature. The exponential re-thermalization with the oven leads to successive signal decrease to its original value. From the temperature dependence of $\chi^{(2)}_{s,\xi\xi\xi}$ [184] a 50 K sample temperature decrease can be estimated in this particular



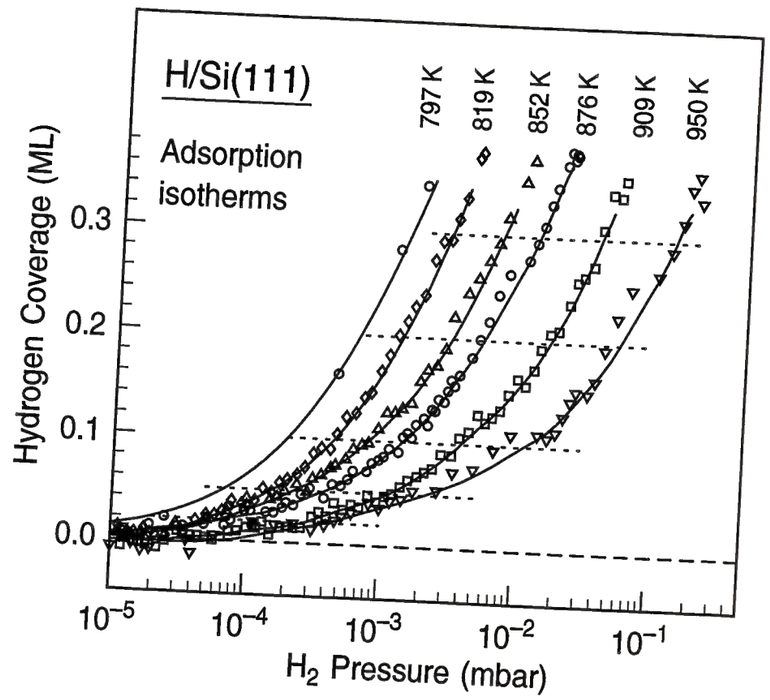


**Fig. 5.8:** Adsorption isotherms $\theta_H = f(p_{H_2})$ for hydrogen on Si(111)7×7 for different surface temperatures. For the to coverage conversion of $\chi^{(2)}_{s,\xi\xi\xi}$, $\alpha = 1.3 = const.$ has been used. The solid lines are plotted as a guide to the eye.

instance which is efficiently quenched by introducing the baffle. The accuracy of the equilibrium temperature could then be estimated to be ±20 K.

In Fig. 5.8 a series of adsorption isotherms $\theta_H = f(p_{H_2})$ recorded for different temperatures is reproduced. In order to derive $q_{st}$, isosteres are obtained from interpolating $p$ and $T$ values at constant hydrogen coverage from the set of isotherms. The results are shown in Fig. 5.9 as an isosteric plot and with eq. 5.5 rewritten as

$$\left.\frac{\partial \ln p}{\partial \frac{1}{T}}\right|_{\theta} = -\frac{q_{st}}{k_B}, \tag{5.6}$$

the slopes of these curves directly yield the isosteric heat of adsorption. The corresponding values and their coverage dependence are summarized in Fig. 5.10. After an initial increase $q_{st}$ takes an approximately constant value of 1.75±0.15 eV for $\theta > 0.15$ ML. The various data points in this figure are the results of best fits to the whole set of data available. If more than one data point is given for the same coverage, the evaluation is restricted to the most accurate isotherms, and the two extremal values of $q_{st}$ still compatible with these data are plotted. The absolute error of $q_{st}$ is determined

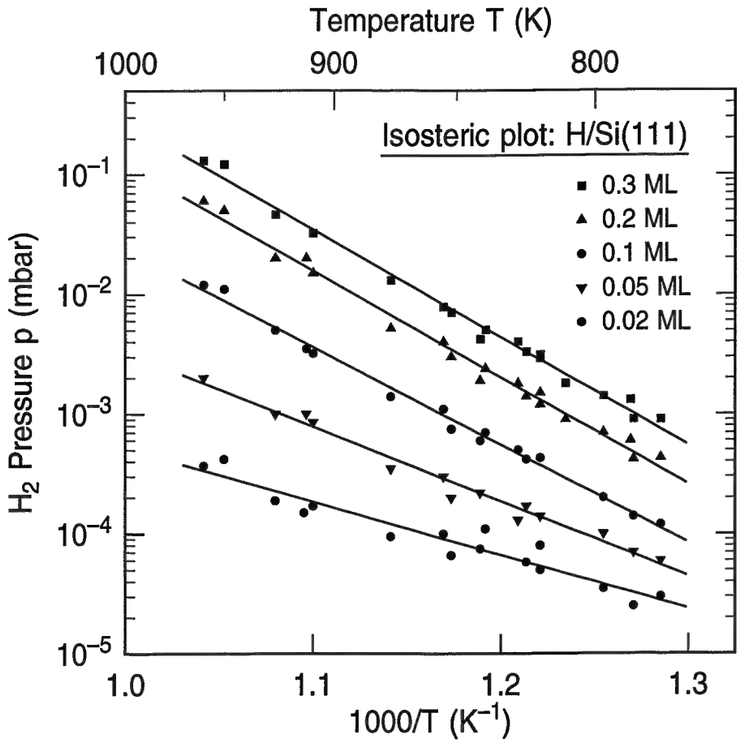


**Fig. 5.9:** Isosteric plot as derived from the measured isotherms shown in Fig. 5.8 for different hydrogen coverages. From the slopes an increase of $q_{st}$ with coverage is apparent.

by the accuracy of the temperature determination and the temperature range covered by the isosteric plot. The 20 K temperature uncertainty would correspond to a $\pm 0.1$ eV error in $q_{st}$.

The isosteric heat of adsorption, which is equivalent to the chemisorption energy, i.e. the total energy change resulting from the dissociative adsorption, relates to the binding energy by

$$E_{\mathrm{Si-H}} = \frac{1}{2}(q_{st} + E_{\mathrm{H-H}}), \tag{5.7}$$

where $E_{\mathrm{H-H}}$ is the dissociation energy of the $H_2$ molecule of 4.52 eV [157,185]. The corresponding values can be read from the converted right-hand scale of Fig. 5.10. Strictly speaking, since $q_{st}$ is equal to the sum of all energy changes related to the adsorption process, this relation is valid only for noninteracting adsorbates and if, given that after the Si–H bonds have formed, no relaxations of the local geometry and changes in the electronic structure occur. However, although hydrogen adsorption on silicon leads to substantial charge redistributions and related relaxation of the H-



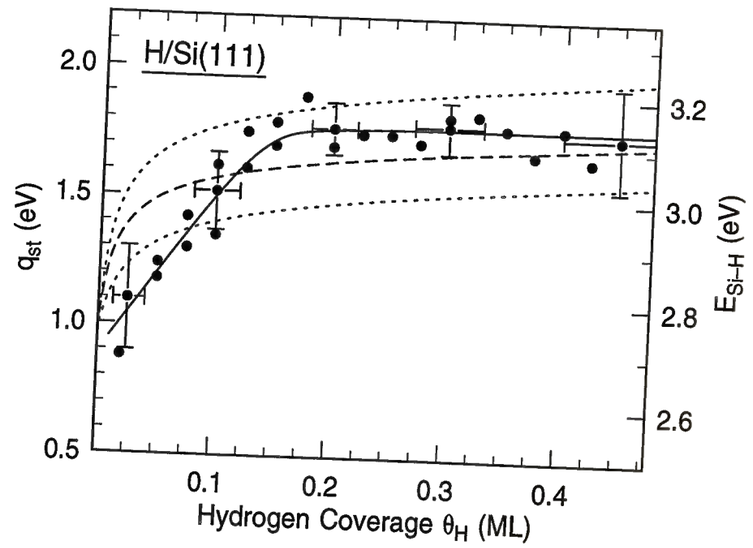


**Fig. 5.10:** Variation of the isosteric heat of adsorption $q_{st}$ for $H_2$/Si(111)7×7 with coverage. The curves represent a guide to the eye (solid line) and the coverage dependence expected for attractive adsorbate interaction according to eq. 5.8 with the parameter $z=3$ and $\epsilon=0.25$ eV (dashed line). For comparison the dependence is also plotted for $z=3$ and $\epsilon=0.2$ eV ($z=4$, $\epsilon=0.25$ eV) with the lower (upper) dotted line.

terminated Si atoms compared to the initial Si positions, the effect on the bond energy as derived from this equation does not exceed $\sim\pm 0.1$ eV, as will be discussed below.

It would be highly desirable to also determine the bond strength of hydrogen on the Si(001) surface. Symmetry reasons for SH measurements, however, require a conventional off-normal geometry in this case. In addition, due to the smaller nonlinear susceptibility of Si(001) in particular at elevated temperatures a reduced signal intensity is expected. Attempts have been made with a second quartz cell equipped with two small additional windows at 45° to the surface normal. The laser annealing procedure, however, could not yet be applied successfully in order to obtain a clean well-ordered silicon surface as in the case of Si(111)7×7. No sufficient surface sensitivity has been achieved which might be the result of surface disorder or even roughening which would reduce the SH intensity drastically. Since the (001) low-index plane on silicon does not have the lowest free energy, the surface might be sensitive to the inhomogeneous temperature distribution due to the Gaussian laser profile.

## 5.4 Discussion

The discussion begins by comparing the results from the present experiments with previous efforts to determine the Si–H bond energy. Then the measurements of $E_{\mathrm{Si-H}}$ are compared with predictions from theoretical first-principles calculations. Finally, $q_{\mathrm{st}}$ allows a consistency check of the energetics of the $H_2$/Si system.

Myers *et al.* replaced the investigation of adsorption on external surfaces with the study of hydrogen interaction with the internal walls of closed hollow microcavities in a silicon crystal produced by helium-ion implantation and subsequent annealing [186–188]. By nuclear reaction analysis the amount of hydrogen chemisorbed in equilibrium could be determined. In previous studies the release of hydrogen from D- and H-implanted specimens was observed and bond energies of 2.5±0.2 eV were inferred [186,187]. In the most recent paper a slightly modified approach led to a bond strength of 2.67±0.1 eV [188]. Clearly, the structure of the walls of these cavities is different from ordered primitive silicon single-crystal surfaces, rendering the interpretation difficult. In addition, however, since all experiments were carried out at only one sample temperature, additional estimates were necessary concerning e.g. thermodynamic aspects of hydrogen in bulk silicon to infer the bond strength values, which recently led to reinterpretations of the experiments resulting in values between 2.49 eV on the one hand [189] and 2.99 and 3.15 eV on the other [190]. Covering this large range of possible values depending on the model employed to evaluate the data, these experiments could not yet give a definite answer for the Si–H bond strength. Similarly difficult is the transfer of the bond strength determined for hydrogen adsorbed at defects of the $Si/SiO_2$ interface of 2.56±0.06 eV [191,192].

The gas phase dissociation energies for the first Si–H bond for $SiH_4$ and $Si_2H_6$ are 3.92 eV and 3.74 eV respectively [185,193,194]. In different studies it has been referred to these values in an attempt to estimate the surface bond strength [9,13,15,95,195]. It was assumed that due to the covalent nature of the Si–H bond the molecular analogs have bond energies similar to the bonding to the silicon surface. The energies of the silane molecules, however, do not account for surface strain and interactions such as those between the dangling bonds. Clearly, in the light of the new experiments these values turn out much larger compared to the surface bond strength. Interestingly, by successive replacement of hydrogen by silyl groups the energy of the Si–H bond at the substituted silicon atom substantially decreases, reaching 3.42 eV for $(H_3Si)_3Si$–H [196]. Likewise for the SiH molecule a dissociation energy of only 3.04 eV has been reported [193].

For the Si–H bond on a Si(111)1×1 surface a bond energy of 3.60 eV was predicted theoretically [197], but, because of the complexity of the 7×7 reconstruction, calculations taking this large unit cell into account have not been performed until recently. Whereas in the DFT slab calculations of Vittadini and Selloni [76,96] reduced $4 \times 2$ supercells were used to represent the ad- and rest-atoms, Joannopoulos and



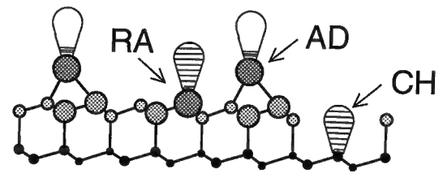


**Fig. 5.11:** Section of the Si(111)7×7 reconstruction, with AD, RA, and CH indicating the adatom, rest-atom and corner hole. The shading of the dangling bonds schematically represents the different electron charge distributions.

co-workers treated the full 7×7 reconstruction, including the dangling bonds of the adatoms, rest-atoms and the corner hole [77,97,198].

For the $H_2$ chemisorption energy with an adatom/rest-atom pair Vittadini *et al.* find 1.42 eV using the general gradient approximation (GGA) (local density approximation (LDA): 1.74 eV) [96]. Despite the difference between the GGA and LDA values these results would be well consistent with the experimental values. For the 7×7 reconstruction, calculations were performed for single hydrogen atom adsorption on the adatom, the rest-atom, and the corner hole sites, resulting in adsorption energies of 2.9, 3.2 and 3.5 eV, respectively [77]. These differences in bond energy were interpreted to be due to strongly nonlocal changes of the surface electronic structure induced by hydrogen adsorption [76,77]. As shown schematically in Fig. 5.11, charge transfer towards the corner holes and rest-atoms on the intrinsic surface results results in substantially depleted adatom dangling bonds (∼0.5 electrons per dangling bond). When hydrogen interacts with any of these dangling bonds, this leads to reverse charge transfer and the differences in adsorption energies reflect the corresponding energies required. In addition, the outward (inward) displacement of the rest-atom (adatom) is released. The differences in occupation density also leads to different reactivities of the various sites which has been directly observed for the Ge(111)$c(2\times8)$ surface together with the corresponding reverse charge transfer [199].

Most recently, also the chemisorption energy for $H_2$ on the adatom-rest-atom pair of sites on Si(111)7×7 was calculated and found to be 1.6 eV, which is equal to the energy for single hydrogen atom adsorption $(2.9 + 3.2 - 4.5)$ eV [97]. This would indicates that no relaxations upon adsorption or no interaction between the dangling bonds of these sites occur. In contrast the chemisorption energy of 2.1 eV for the adatom-corner hole pair would correspond to a nonlocal attractive interaction energy of +0.2 eV.

The differences in binding energy for the different sites on Si(111) have also been found in the calculations of Vittadini *et. al.* [76] mentioned above for a surface which consists of an equal number of adatoms and rest-atoms. Taking the adatom/rest-atom ratio of two for the Si(111)7×7 unit cell into account, the energy difference of 0.80 eV

(LDA: 0.74 eV) with the hydrogen at the rest-atom bound more strongly compared to the adatom would reduce to $\sim 0.2$ eV. This value is in good agreement with the calculations from Lim *et. al.* [77]. These energy differences which have already been proposed on the basis of the isothermal measurements of the desorption kinetics [10] have recently been verified with STM diffusion experiments [170] and the calculations reproduce well the values found in these two experiments.

On the basis of these findings the observation of an increase of the chemisorption energy of hydrogen with coverage comes as a surprise. In equilibrium one would expect, that the hydrogen atoms on the surface would preferably occupy the sites with the highest binding energy. Therefore with increasing coverage the hydrogen would successively also adsorb at the less favorable sites and the measured chemisorption energy would decrease. In principle the experimentally observed increase in the chemisorption energy with coverage could be explained by the presence of attractive interactions between the adsorbed particles. Equivalently, attractive interactions between the dangling bonds would lead to preferential pairing (or clustering) of the hydrogen atoms on the surface.

In order to illustrate the consequences of such a model, for a surface with equal adsorption sites the variation of the heat of adsorption with coverage for dissociative adsorption is given by [200,201]

$$\frac{q_{\mathrm{st}} - q_{\mathrm{st},0}}{z\epsilon} = -\left[1 - \frac{1-2\theta}{\sqrt{1-4(1-\eta)\theta(1-\theta)}}\right]. \tag{5.8}$$

Here $\eta = \exp(\epsilon/k_{\mathrm{B}}T)$, and $q_{\mathrm{st},0}$ denotes the heat of adsorption at zero coverage. Shown as the dashed curve in Fig. 5.10 is the behavior of $q_{\mathrm{st}}$ that one would expect for a positive i.e. attractive interaction energy $\epsilon = 0.25$ eV and for $z = 3$ as the number of nearest-neighbor sites. For comparison and to illustrate the sensitivity of the energy changes involved the dependence is also shown for $\epsilon = 0.2$ eV and $z = 3$ ($\epsilon = 0.25$ eV, $z = 4$) as the lower (upper) dotted line. Although this could only qualitatively explain the observed increase in bond energy with coverage, it would agree with the calculations which found either no (adatom/rest-atom) or attractive (adatom/corner hole) interaction between the dangling bonds.

The adsorption of hydrogen atoms on the various dangling-bond sites is associated with charge redistributions and the related energy enters the calculated bond strengths. Charge would have to be either attracted to form a covalent bond (adatom) or distributed onto neighboring sites from the rest-atom and corner hole with nearly one electron surplus each. The differences in the calculated values for the bond strength on these sites indicate that for both processes energy is required. The least energy for the charge redistribution seems to be required for the corner holes explaining their high hydrogen bond energy. However, for a nearly fully hydrogen saturated surface the remaining dangling bonds would all carry exactly one electron, just the amount required to form a $\sigma$-bond together with the single $1s$ electron provided from



the hydrogen atom. With increasing coverage, less charge transfer would therefore be required and one would thus expect a higher chemisorption energy for higher coverages.

In this model the experimental value determined for small coverages of $\sim 2.8$ eV would then correspond to hydrogen atoms bound to the surface sites with the highest initial energy. In view of the high values of 3.5 and 3.2 eV calculated for the corner hole and rest-atom sites that value however would not be in particularly good agreement with the theory. The fast increase observed with coverage as seen in Fig. 5.10 would also require that the at first less favorable sites would be very sensitive concerning their reactivity for already small charge redistributions. Concerning this microscopic interpretation of the experimental results it should be noted that they would rely on the assumption that the surface structure is not affected during the adsorption experiment. It is known for example that the critical temperature for the $7\times7 \leftrightarrow 1\times1$ phase transition can be lowered by up to 100 K upon hydrogen exposure of up to 1 mbar [202]. Whereas this process is unlikely to occur for the temperatures of the experiments an enhanced mobility of the adatoms can not be excluded which would at least transiently create new adsorption sites. In addition it is likely that due to the high adsorption/desorption flux during exposure in particular for temperatures above 900 K silicon atoms might be etched.

Nevertheless, since the calculations on Si(111)7×7 were performed for the low coverage limit with only single atoms or molecules adsorbed on the unit cell, investigations for higher coverages would be interesting. In the case of $H_2$ adsorption on Si(001), recent theoretical investigations found the chemisorption energies to be higher by $\sim 0.1$ eV for the chemisorption on the dimers of an otherwise fully hydrogen-covered surface [169]. Due to the more pronounced nonlocal effect of the adsorption on Si(111) a more pronounced coverage dependence would be feasible.

## 5.5 Energy balance

With the heat of adsorption determined for $H_2$ on Si(111)7×7 these experiments provides the last yet unknown parameter to check for the consistency of the energetics of the $H_2$/Si system. In accordance with energy conservation the heat of adsorption $q_{\mathrm{st}}$, equivalent to the reaction enthalpy $\Delta H_{\mathrm{r}}$, is related to the barrier for adsorption $E_{\mathrm{a}}$ and desorption $E_{\mathrm{d}}$ by

$$q_{\mathrm{st}} \simeq \Delta H_{\mathrm{r}} = E_{\mathrm{d}} - E_{\mathrm{a}}. \tag{5.9}$$

This relation can be directly applied to the energy changes of the $H_2$/Si system along the reaction coordinate, as shown in Fig. 5.12. Using the value of 0.87±0.1 eV [14] for $E_{\mathrm{a}}$, i.e. interpreting the resulting activation energy for the temperature dependence of the sticking coefficient in terms of an effective adsorption barrier. Substituting this value together with $E_{\mathrm{d}} = 2.40 \pm 0.1$ eV [10], both obtained for coverages around

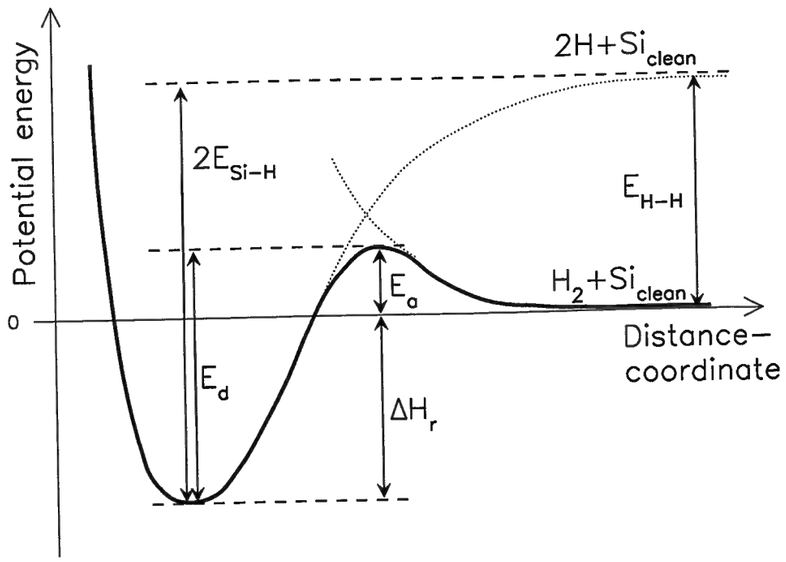


**Fig. 5.12:** Potential energy diagram for dissociative adsorption of hydrogen on silicon surfaces involving an activation barrier of height $E_a$ and a desorption barrier $E_d$.

0.1–0.2 ML, in this equation, one would expect $q_{st}=1.53\pm0.15$ eV. This result would be in excellent agreement with the experimentally derived values $q_{st}=1.4-1.7$ eV for that coverage regime. Equally good agreement can be achieved by using the slightly higher desorption activation energies obtained for coverages above 0.2 ML with TPD of $E_d=2.54$ eV [24] and $E_d=2.47$ eV [75] and from LITD experiments of $E_d=2.65\pm0.2$ eV [72]. These results qualitatively reflect the increase of $q_{st}$ with coverage.

In addition, for higher coverages an apparent increase in sticking probability was observed as mentioned in section 4.3. Since an interpretation in terms of additional reaction channels as observed for Si(001) seems unlikely on Si(111) this behavior was interpreted in terms of a slight reduction of the adsorption barrier according to $E_a = E_{a,0}(1-\beta\theta)$ with parameter $\beta \simeq 0.25$ [26]. This effective decrease of the adsorption barrier also goes along well with the coverage dependence of $q_{st}$ and might have its origin in charge redistributions induced by neighboring adsorbed hydrogen leading to an electronically more favorable configuration for the incoming molecule to dissociate.

This consistency check can be viewed as an independent source of evidence for the large adsorption barrier of $\sim$0.9 eV, as determined from the surface temperature dependence of the sticking reaction [14]. This value had been questioned by some



authors [15,95] not only because of the low sticking probabilities involved but also because of its inconsistency with the energy distribution of the desorbing hydrogen molecules, as discussed in section 2.2. The lack of knowledge of $q_{st}$ has led to the erroneous assumption that due to the covalent nature of the Si–H bond, the molecular analogs have bond energies similar to the bonding of hydrogen to the silicon surface. These molecular values have often been invoked to argue against the high barriers found for dissociative adsorption [15,95]. However, neither the high silicon-hydrogen bond strength of silanes nor the low values of the experiments on the microcavities can accomplish the energy balance. The model of phonon-assisted sticking conceptually and the experiments described here experimentally verify qualitatively and quantitatively the high value for the adsorption barrier.

## 5.6 Conclusion

In a novel experimental approach, a bakeable all-quartz UHV apparatus was used to establish thermal equilibrium between molecular hydrogen and the well-defined Si(111)7×7 surface at gas pressures of $10^{-5}-1$ mbar and temperatures of $770-980$ K. Under these conditions the equilibrium surface hydrogen coverage was detected with SHG. From the resulting adsorption isotherms the hydrogen binding energy and its coverage dependence could be derived. For Si(111)7×7 the binding energy was found to increase from 2.8 to 3.1 eV in the coverage range from 0.05 to 0.4 ML. The Si–H surface bond is thus considerably weaker that hydrogen bonding in silanes (3.7–3.9 eV). The values are compatible with the large barrier (0.9 eV) for phonon-assisted sticking of $H_2$/Si and are in good agreement with theoretiacal predictions.

# Chapter 6

# Desorption kinetics of SiO from Si(001)[1]

The interaction of oxygen with silicon surfaces plays a crucial role in the fabrication of semiconductor devices and is of continuous interest from a fundamental scientific viewpoint [203]. At low temperatures sufficiently high pressures of oxygen result in oxide growth with the adsorption of oxygen to be essentially dissociative and preceded by a short-lived molecular precursor [145,204–206]. At elevated temperatures the oxygen interaction is characterized by two regimes: etching at low pressures proceeds via formation of volatile SiO, whereas for exposures above a critical oxygen pressure oxide clusters nucleate and oxidation competes with etching [206–210]. The thermal decomposition of the oxide is known to be spatially inhomogeneous, progressing via growing voids or shrinking oxide islands without thinning of the remaining oxide [211–213]. For a detailed atomistic description of this complicated process, the determination of the structure of thin oxide layers with the scanning tunneling microscope (STM) provide invaluable information [208,214,215]. Equally important the kinetic parameters of the reaction steps are of interest in deriving the underlying dynamics.

Having used SHG as the major probe to study the elementary reaction steps of hydrogen on silicon surfaces one is tempted to demonstrate its applicability also as a quantative probe for reactions with more complex chemisorbates. In the case of oxygen adsorption on Si(111), the sensitivity of this technique has been demonstrated in several previous experiments [132,180,210,216,217]. However, no definite relation between SH signal and oxygen coverage has yet been established by calibration.

Here the elementary reaction steps of oxide layer decomposition, i.e. SiO desorption from Si(001), are addressed quantitatively. The coverage and temperature dependences of this process are investigated in detail by performing isothermal measurements. Calibration of the SH response with temperature programmed desorption (TPD) as described in section 3.4 is used to obtain quantitative results over a wide range of coverages.

[1] The results discussed in this chapter were published as an article in Surface Science: M. B. Raschke, P. Bratu and U. Höfer, *Surf. Sci.* **410**, 351 (1998).

## 6.1 Isothermal desorption

For the preparation of the oxide layer on Si(001)2×1, the sample is exposed to molecular oxygen at $T_s = 530$ K. Then the sample temperature is rapidly increased to the desired value for the isothermal desorption measurements, and the change in SH signal is monitored as a function of time. After complete desorption of the oxide, the nonlinear susceptibility approaches its initial value measured for the clean surface for that particular temperature. After each desorption experiment, the sample is annealed at 1300 K and cooled at a rate of $1-2\,\mathrm{Ks}^{-1}$ in order to prepare a well-ordered substrate for the subsequent measurements.

As shown in chapter 2 for small oxygen coverages $\theta \leq 0.1$ ML, $\chi_s^{(2)}$ decreases linearly with coverage and then saturates at a value that is five times less than that of the clean surface. With the observed linear relationship, the time dependence $\chi_s^{(2)}(t)$ can be directly related to $\theta(t)$. For higher initial coverages beyond 0.1 ML the detailed functional dependence $\chi_s^{(2)}(\theta)$ has been taken into account in order to convert $\chi_s^{(2)}(t)$ to coverage. Strictly speaking, since the SH experiments described in section 3.4 were performed at $T_s = 530$ K, the calibration is only valid for that surface temperature. At the excitation wavelength of 1064 nm, the ratio $\chi^{(2)}_{s,db}/\chi^{(2)}_{s,NR}$ is known to decrease with increasing temperature [184]. In the analysis of the isothermal desorption data, this effect is taken into account and the ratio of the SH signal is adjusted before and after desorption. Any temperature dependence of $\alpha$, $\beta$, or the phase difference has been neglected. Since the desorption rates below change by several orders of magnitude, a small uncertainty of the calibration procedure is of negligible influence on the derived kinetic parameters.

Fig. 6.1 shows the resulting temporal change of the surface coverage for a number of different temperatures, starting with the same initial coverage of $\theta_0 \simeq 0.1$ ML. Data corresponding to different initial coverages but fixed desorption temperatures are collected in Fig. 6.2. For the purpose of data analysis, first-order kinetics is assumed for the desorption process:

$$R_d = -\frac{d\theta}{dt} = \theta(t)\nu_d(\theta, T_s) = \theta(t)\nu_0(\theta)\exp\left(-\frac{E_A(\theta)}{k_B T_s}\right) \qquad (6.1)$$

with a coverage- and temperature-dependent rate constant $\nu_d(\theta, T_s)$. Its (exponential) temperature dependence is expressed in terms of an activation energy $E_A(\theta)$ and pre-exponential factor $\nu_0(\theta)$.

The signal-to-noise ratio of the individual desorption traces does not allow an independent, accurate determination of the coverage and temperature dependence of $\nu_d(\theta, T_s)$. In order to deduce the activation energy and prefactor, we compare data with the same initial coverage $\theta_0$ (Fig. 6.1), neglect the coverage dependence (i.e. $\nu_d(\theta) = \text{const.}$), and determine the rate constant from numerical fits to the resulting simple exponential time evolution $\theta(t) = \theta_0 \exp(-\nu_d t)$. The resulting Arrhenius



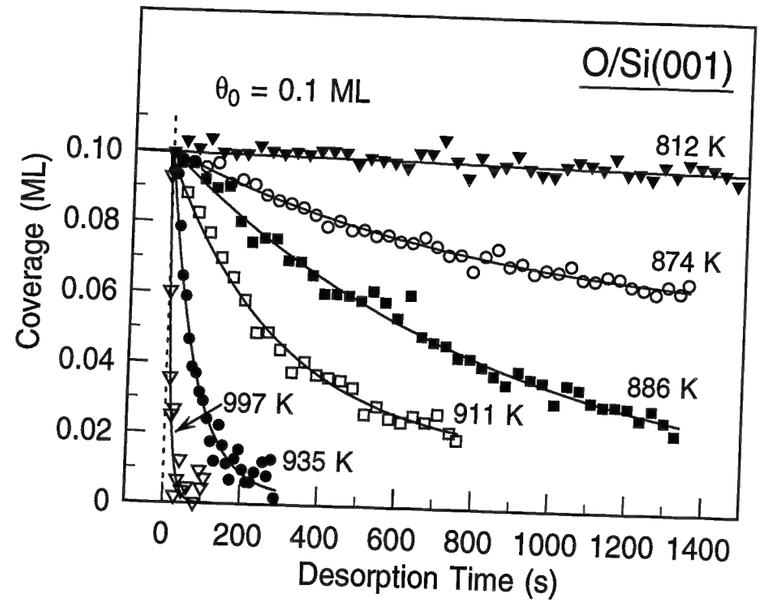


**Fig. 6.1:** Isothermal desorption from the Si(001) surface with an initial oxygen coverage of $\theta_0 \simeq 0.1$ ML. The solid curves represent numerical fits applying first order desorption kinetics.

plot will be discussed in the following section. The coverage dependence of the rate constants is determined from sets of data with varying initial coverages taken at fixed desorption temperatures. The rate constants deduced from the data displayed in Fig. 6.2, from other data at $T_s = 925$ K, and from a set of data obtained at a desorption temperature $T_s = 876$ K are collected in Fig. 6.3.

In this figure the rate constants $\nu_d = R_d/\theta$ are plotted as a function of the inverse initial coverage $1/\theta_0$. In this representation $\nu_d$ would be constant for a first-order desorption process ($-d\theta/dt \propto \theta$), but would increase linearly for zeroth-order kinetics ($d\theta/dt = \text{const}$). As can be seen from the figure, the latter behavior seems to be the case for coverages $\theta_0 > 0.1$ ML. For $\theta_0 \leq 0.1$ ML the coverage dependence can be described by an apparent kinetic order of one half ($-d\theta/dt \propto \theta^{1/2}$). Such behavior is typical of desorption from the boundaries of two-dimensional islands [218]. With the mean island area proportional to coverage, the number of atoms at the boundaries scales like $\theta^{1/2}$. Using the corresponding temporal dependence of $\theta(t) = \theta_0(1-at)^2$, the individual desorption traces can also be fit reasonably accurate within the experiment uncertainties. For higher coverages the desorption traces can be described neither by simple first- nor half-order kinetics. In the case of the highest initial coverage used in the present investigation ($\theta_0 = 0.6$ ML) the desorption starts with an almost

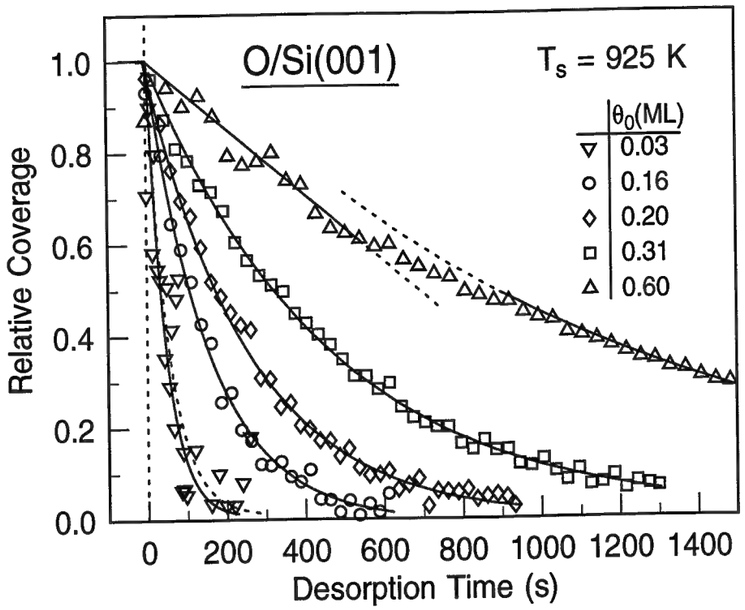


**Fig. 6.2:** Isothermal desorption from the Si(001) surface at constant surface temperature of $T_s = 925$ K for different initial coverages. For a better comparison, the normalized coverages $\theta(t)/\theta_0$ are plotted. The solid lines represent numerical fits described in the text.

coverage-independent rate as can be seen in Fig. 6.2. The line through the data for the initial decay ($t < 600\,\mathrm{s}$) indicates a constant desorption rate. Desorption at later times ($1000\,\mathrm{s} < t < 3400\,\mathrm{s}$), however, is again found to be compatible with $\theta(t) \propto \exp(-\nu_d t)$. This behavior is in qualitative agreement with earlier isothermal desorption measurements having used of X-ray photoelectron spectroscopy (XPS) which showed a transition from apparent zero-order to first-order kinetics for coverages between 0.7 and 1 ML [141].

From STM studies it is known that during desorption the surface undergoes substantial roughening [213]. In order to address the question to what extent surface roughening during the desorption process influences the desorption kinetics, the following experiments were conducted: In the first step 0.2 ML oxygen was adsorbed on the well-prepared surface and then desorbed isothermally at $T_s = 925$ K. Without prior annealing of the surface, 0.03 ML was then adsorbed at 530 K in the subsequent experiment. The desorption trace of the so prepared oxide layer is shown by the dotted line in Fig. 6.2. The same experiments were repeated with the same pre-dose coverage but different subsequent coverages of 0.02 and 0.06 ML. The resulting desorption rate constants for the three experiments are shown in Fig. 6.3 as blank square symbols. Obviously, within the accuracy of the experiment there are no observable



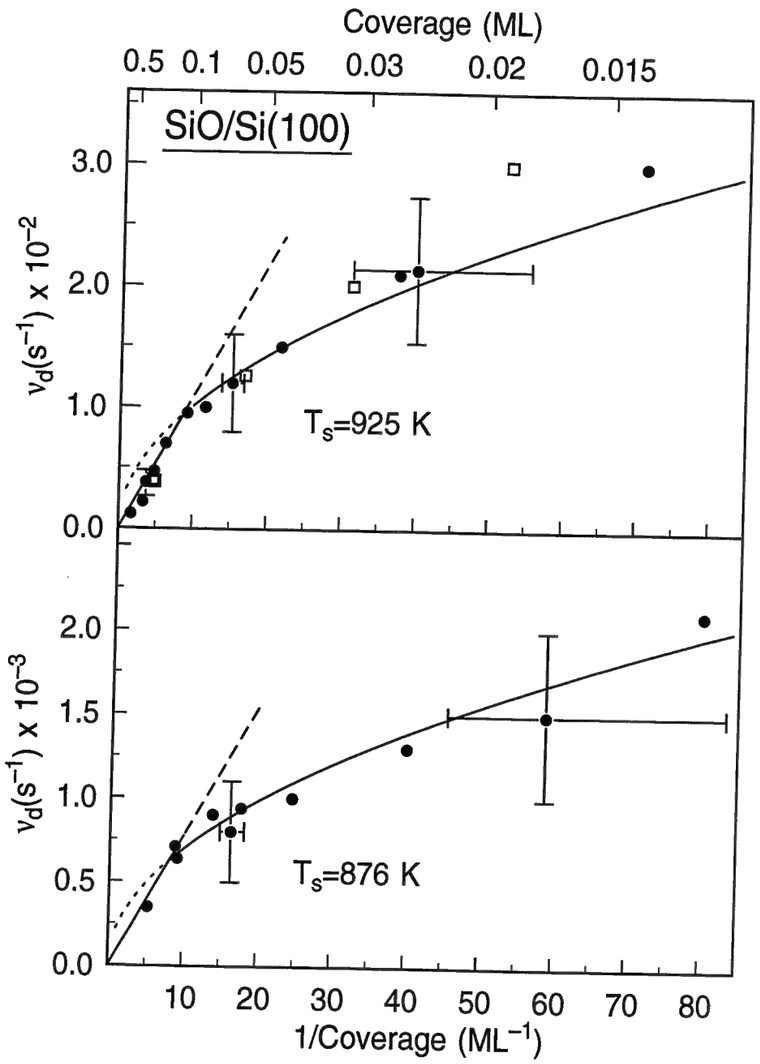


**Fig. 6.3:** Desorption rate constants $\nu_d = R_d/\theta$ for isothermal desorption experiments from the Si(001) surface as a function of the inverse initial oxygen coverage $1/\theta_0$. The straight and the curved solid lines indicate the behavior expected for apparent kinetic orders of 0 and 1/2, respectively. The square symbols at coverages of 0.02, 0.03, and 0.06 ML represent data obtained without annealing the surface after the desorption of 0.2 ML oxygen.

differences between the desorption behavior from the initially well-prepared surface and that from the slightly roughened surface.

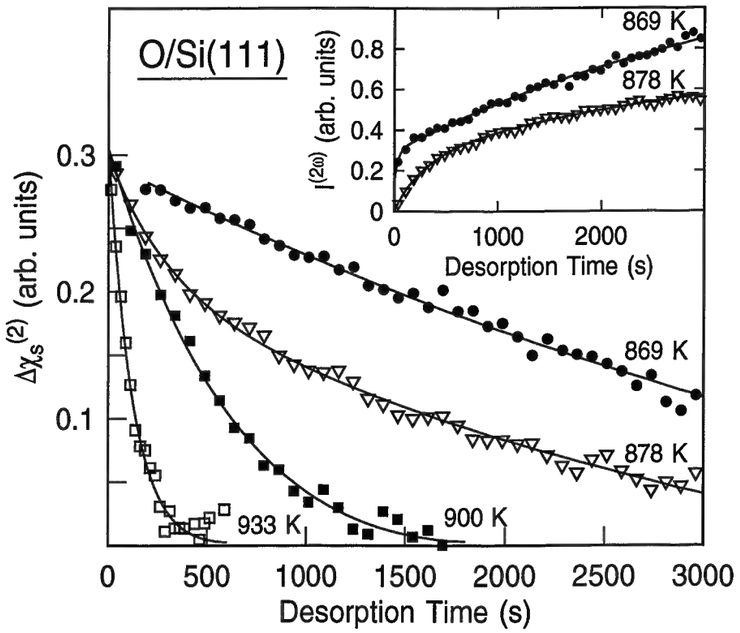


**Fig. 6.4:** Relative change of the nonlinear susceptibility of Si(111) during isothermal desorption of $\sim 0.3$ ML oxygen at various temperatures. The inset shows two representative SH intensity traces as a function of time, measured at different surface temperatures. The fast initial signal increase is associated with rearrangement processes, while the subsequent slower change is related to desorption (from [130]).

An interesting difference is found by comparing these isothermal desorption measurements from Si(001)2×1 with similar experiments from Si(111)7×7. P. Bratu measured the SH response during isothermal desorption from Si(111) [130] and obtained the result shown in Fig. 6.4.

In contrast to Si(001), the desorption process from Si(111) is associated with a more complex time dependence, in particular for temperatures below 900 K. This can be seen from the temporal change of the SH signal shown in the inset for two different surface teperatures. Here, the decay of $\Delta\chi_s^{(2)}(\theta) \equiv \chi_{s(0)}^{(2)} - \chi_s^{(2)}(\theta)$ is characterized by two time constants. For the purposes of analysis, the decay of $\Delta\chi_s^{(2)}$ was described by two exponentials and the slow time constant was identified with the desorption rate of SiO. Between 800 K and 880 K the rates associated with the fast process vary from $10^{-3}\,s^{-1}$ to $5\times10^{-2}\,s^{-1}$, whereas in the same temperature range the desorption rates lie between $10^{-6}$ and $3\times10^{-4}\,s^{-1}$.

The fast initial increase of the SH signal is likely caused by a rearrangement process of the oxide layer prior to desorption which leads to an increased number



of dangling bonds. This interpretation is suggested by previous XPS results. After oxygen exposure at room temperature the Si 2p core levels show satellites that are commonly interpreted in terms of different silicon oxidation stages ($Si^{1+}$ to $Si^{4+}$) [219,220]. After annealing at 750 K the intensity of the $Si^{3+}$ and $Si^{4+}$ is observed to increase at the expense of $Si^{1+}$ and $Si^{2+}$ [219]. STM investigations have related this behavior to oxygen island formation on the surface [209].

Oxygen adsorption on Si(111)7×7 is preceded by a metastable molecular precursor [204,215,221]. An interesting question that arises from recent work concerning this system is whether the rearrangement process is in fact caused by diffusion of molecular rather than atomic oxygen. Using a variable-temperature STM, Tsong *et al.* [222] recently observed diffusive motion of so-called "bright" oxygen-induced sites on Si(111)7×7 and suggested that this is caused by the diffusion of the $O_2$ precursor. The observation that the rearrangement process occured only for the Si(111) but not for the Si(001) surface would be consistent with $O_2$ diffusion driving the clustering of oxygen on the surface.

However, it seems unlikely that molecular oxygen is able to persist on the surface at temperatures as high as 900 K. We consistently find that molecular oxygen quickly dissociates at surface temperatures above 500 K [132,145]. Similar findings have been reported by others [223,224]. On the other hand, STM results showed that oxide growth on Si(001) preferably nucleates at defect sites, whereas no such preference is seen for Si(111) [225]. Although this might indicate that the oxygen adsorbed on Si(001) at low temperatures is already closer to its equilibrium configuration than adsorption on Si(111), further experiments will be necessary in order to give a definite answer to the origin of the rearrangement process.

## 6.2 Arrhenius parameter

The desorption rates obtained for Si(001) with initial oxygen coverage of $\theta_0 \simeq 0.1$ ML are displayed in Fig. 8 in the form of an Arrhenius plot. As a result of the high adsorbate sensitivity of SHG the desorption could already be monitored for temperatures as low as 780 K. As can be seen from the figure, isothermal desorption measurements allow evaluation of desorption rate constants over five orders of magnitude ranging from $10^{-6}\,s^{-1}$ to $10^{-1}\,s^{-1}$. Higher values can hardly be obtained in those isothermal desorption experiments because of the finite heating rate which has to be applied to reach the desired temperature. Provided the experimental conditions are stable the low-temperature limit is, in principle, only governed by the background pressure in the chamber. From the data an activation energy for SiO desorption from Si(001) of $E_A = 3.4 \pm 0.2$ eV with prefactor $\nu_0 = 10^{16\pm1}\,s^{-1}$ can be deduced. The error of these values is dominated by the accuracy of the temperature measurement.

For comparison, results from a modulated molecular beam reactive scattering

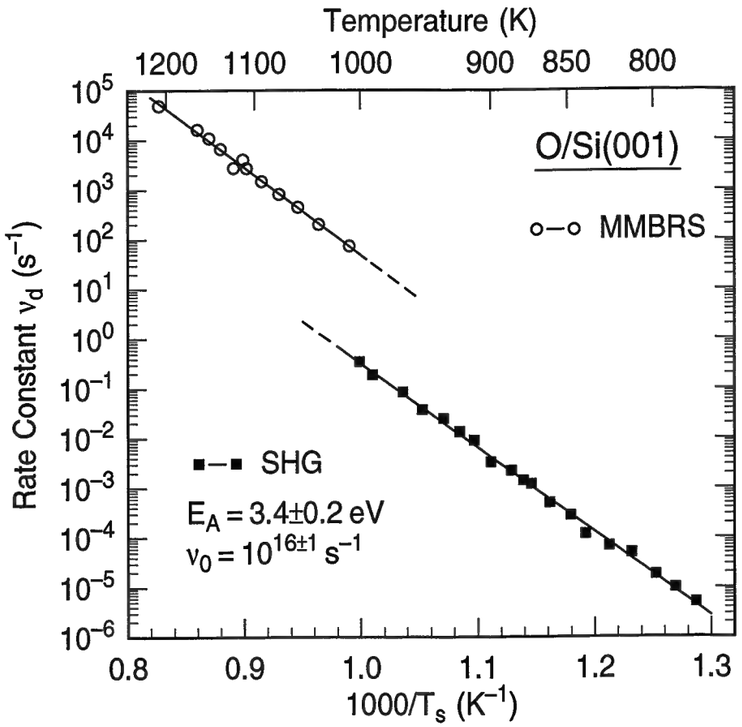


**Fig. 6.5:** Arrhenius plot of the measured first-order rate constant $\nu_d$ for SiO desorption from Si(001) for an initial oxygen coverage $\theta_0 = 0.1$ ML (solid squares). The data marked with blank dots represent results obtained from molecular beam scattering experiments [141].

(MMBRS) experiment [141] are included in the figure. The SHG data extend the range of rate constants obtained so far with MMBRS and TPD [226] by more than four orders of magnitude towards lower temperatures. Considering the whole temperature range between 780 K and 1200 K, in which the desorption process was investigated, the rates for SiO desorption vary over nearly 11 orders of magnitude. Strikingly, over this whole range the desorption reaction obeys the Arrhenius law.

The activation energies $E_A$ obtained using the different techniques of SHG, TPD and MMBRS are found to be in fairly good agreement with each other and seem to vary only little with initial coverage. For Si(001) the TPD values concentrate in the range of 3.5–3.9 eV [203,226]; from MMBRS values of 4.0±0.4 [227], 3.5±0.1 [141], 3.4±0.1 [207] and 3.0 eV [228] are reported. 2.8±0.05 eV was reported by Ohkubo *et al.* [229] both for Si(001) and Si(111), using the scattering technique. This energy appears to be too small in relation to our values and those from other studies.



In a recent investigation TPD was used to study SiO desorption from Si(001) after dissociative adsorption of water [230]. The obtained activation energies of 3.3 eV and 3.5 eV for initial $D_2O$ coverages of 0.05 and 0.4 ML, respectively, are in excellent agreement with the 3.4 eV from our experiment for 0.1 ML.

Although the activation energies are quite similar, the pre-exponential factors $\nu_0$ deduced from the scattering experiments are 2–4 orders of magnitude larger than those obtained by TPD and from the SHG measurements. Judged by the observed coverage dependence of the desorption rate constants as discussed above, this is likely a consequence of the different oxygen coverages in these experiments. Whereas most of the TPD studies were carried out from oxidized surfaces with high oxygen coverages ($> 0.1$ ML), the coverages in the MMBRS experiments are typically $10^{-3}$ ML and below [203]. Quantitatively, the prefactors reported in the literature vary between $10^{16}\,s^{-1}$ [228,229] and $10^{20}\,s^{-1}$ [141]. Our value of $10^{16}\,s^{-1}$ for the Si(001) surface obtained for an initial oxygen coverage of 0.1 ML again agrees well with that from the TPD study [230] which reported a range between $2.5\times10^{17}\,s^{-1}$ and $2.5\times10^{16}\,s^{-1}$ for $D_2O$ coverages of 0.05–0.4 ML.

Unanimously, the observed pre-exponentials are remarkably large and exceed the values for most other adsorbate systems by two or more orders of magnitude [231]. Within the framework of transition state theory (TST) a high frequency factor $\nu_0$ would require desorption to occur via the excitation of a strongly localized initial state into a highly mobile transition state. The pre-exponential factor for the rate constant of a given process is expressed via the partition functions of the reactants and of the activated complex. For a unimolecular reaction $\nu_0$ would then be given by

$$\nu_0 \simeq \frac{k_B T}{h}\frac{k^\#}{k}, \tag{6.2}$$

with the ratio of the total partition function of the activated complex and adsorbate, $k^\#/k$, expressed as the product of the ratios of the translational, rotational and vibrational contributions [231–233]. This gives an upper limit for $\nu_0$ with the rotational and translational degrees of freedom contributing most strongly. In the absence of both translation and rotation, $\nu_0 \simeq 10^{13}s^{-1}$ for a surface temperature of 800 K and $k_{vib} \approx 1$. The classical partition function for rotation for a two-atomic molecule and translation are given by

$$k_{rot} = \frac{8\pi^2 TI}{h^2\sigma}, \quad \text{and} \quad k_{trans} = \frac{\sqrt{2\pi m k_B T}}{h} l, \tag{6.3}$$

with $l$ the average distance between adjacent adsorption sites, $m$ the mass of the molecule, $I$ the moment of inertia and $\sigma$ a symmetry number. On the assumption that the activated complex can be represented solely by a rotating SiO, $\nu_0$ would already be of the order of $10^{16}\,s^{-1}$ when calculated for a temperature of 800 K. If, in addition, two-dimensional motion or another rotational contribution is taken into

account, $\nu_0$ can easily reach values of $10^{19}\,s^{-1}$. Alternatively, by using three bending modes in addition to one free internal rotation of the SiO, the frequency factor can be calculated to be of the order of $10^{17}\,s^{-1}$.

## 6.3 Discussion of the desorption mechanism

Comparing the desorption from the Si(001) surface with Si(111) [132,227] shows the kinetic parameters concerning both activation energy and prefactor to be quite similar. Apparently, microscopic details due to the different surface orientations do not strongly affect the desorption process. This is supported by recent

REMPI spectroscopy experiments addressing the dynamics of the SiO desorption in reactive oxygen scattering experiments [234,235]. Here very similar behavior for Si(001) and Si(111) was observed with the vibrational and rotational energies of the desorbing SiO molecules being in near thermal equilibrium with the silicon surface. This would indicate that the desorption follows a reaction path going through a state in which SiO is almost freely rotating [235]. The results thus support the estimate of the prefactor given above. Furthermore, from the validity of the Arrhenius law over nearly 11 orders of magnitude it may be concluded that there is a common underlying microscopic mechanism in the desorption process, regardless of whether the reaction occurs upon interaction of individual oxygen atoms with the bare surface at high temperature (as in the scattering experiments), or at finite coverages and temperature below the critical temperature for surface etching (TPD and isothermal SHG measurements).

For further discussion of the microscopic reaction steps involved in SiO desorption it is important to take the information into account that has been obtained from spatially resolved investigations using scanning microscopy techniques [211–213]. The thermal decomposition of thick (50–500 Å) as well as ultrathin oxide films was found to proceed inhomogeneously from the perimeters of circular voids or shrinking oxide islands without thinning of the remaining oxide [211,212]. Even for monolayer desorption from Si(001) the formation of these growing voids which expose the bare silicon substrate could clearly be observed by Johnson and Engel with STM [213]. The growth rate of the voids seemed to scale as their area, which led to the conclusion that the formation of mobile silicon monomers inside the void area is the rate limiting step of the desorption process. These monomers were suggested to diffuse to the void perimeter, react with oxygen, and form volatile SiO [213].

Such a mechanism, however, is very unlikely to be operative at small oxygen coverages. It would lead to apparent zero-order kinetics ($R_d \propto (1-\theta) \approx$ const, for $\theta \to 0$), which we can clearly exclude for $\theta < 0.3$ ML. Furthermore, and in contrast to the experimental observations discussed above, one would expect an enhanced desorption rate when oxygen is desorbed from a pre-roughened surface, where monomers



should form more readily. The creation of Si monomers at the steps and likewise also at defects of a rough surface is likely to require considerably less activation energy [236,237] than the 3.4 eV measured for SiO desorption. In contrast, previous beam experiments actually showed that the rate even decreases somewhat with increasing etch of the surface [141].

In the model proposed here the actual oxygen binding configuration is the key to understanding the highly complex desorption behavior of SiO. As a result of the insertion reaction of oxygen between two silicon atoms [204,219], the average coordination number equivalent to the oxidation stages of the silicon atoms increases with increasing coverage, as discussed above. This has a stabilizing effect on the oxide layer and therefore results in a reduced desorption rate of aggregated as compared with isolated oxygen species. Here it is assumed that the desorption at finite coverages occurs at the boundaries of the oxygen islands and is preceded by the formation of the least coordinated isolated Si–O–Si species with a formal oxidation state of +1. Then fission of Si–O and Si–Si bonds leads to the activated SiO(a) state and desorption of gas phase SiO(g):

$$Si^{(2+,3+,4+)}O \rightleftharpoons Si^{1+}O \rightleftharpoons SiO(a) \longrightarrow SiO(g). \qquad (6.4)$$

The overall activation barrier for this process would clearly be dominated by the reaction enthalpy of the second process. Otherwise the activation energy determined by MMBRS where only isolated oxygen species are present on the surface would be much lower than the values determined by SHG or TPD. On the other hand, the error bars of ± (0.2–0.3) eV of the activation energies given above are still compatible with an energy difference between high and low coordinated species that is sufficient to prevent small oxygen islands from dissolving at low coverages. Furthermore, oxygen clusters conceivably become stabilized kinetically with increasing size.

Within the framework of this model the coverage dependence of the desorption rate can be explained in a straightforward way: Even at low coverages of a few percents of a monolayer, oxygen forms two-dimensional islands with an average circumference that is proportional to the square root of the coverage. This leads to apparent half-order desorption kinetics. When the coverage increases to half a monolayer and beyond, the oxygen coordination of silicon increases within the islands, as seen in an increase of the relative amount of the most stable $Si^{4+}O$ in XPS [219]. Then the desorption rate from the boundaries of these thicker islands becomes even less dependent on the total oxygen coverage. Since oxygen islands are not formed under the conditions of the beam experiments, the rate-constants are appreciably higher in this case.

An alternative explanation for the STM results of Johnson and Engel is possible on the assumption that the layers are not in thermal equilibrium before desorption. In this case, there will be not only desorption during the time the sample is heated. Oxygen rearrangement and aggregation within the oxidized area is likely to occur simultaneously. This might contribute to the faster void growth reported in Ref. [213].

The fact that diffusional equilibrium is not readily achieved under the conditions of typical desorption experiments was actually demonstrated with TPD studies using isotopically labeled oxygen [226]. The SHG experiments of Shklyaev *et al.* [210] having investigated the critical oxidation conditions on Si(111) corroborate such an interpretation. In the temperature regime between 880 and 1070 K it was found that slowly grown oxides are more stable to decomposition than less equilibrated oxygen layers formed rapidly under conditions of high oxygen pressures.

In order to reach a more definite conclusion about the microscopic reaction mechanism it would e.g. be highly desirable to conduct oxygen diffusion experiments. Making use of the rare gas template technique as discussed in the Appendix, it could be shown that the formation of an oxygen adsorbate grating is feasible. The high sensitivity of linear diffraction would make the coverage dependence of the diffusion process accessible.

## 6.4 Conclusion

The isothermal desorption of SiO from the Si(001) surface was studied by SHG over a wide range of temperatures and initial oxygen coverages. The rates obey an Arrhenius law with an activation barrier $E_A = 3.4 \pm 0.2$ eV. Whereas the activation energy exhibits little or no dependence on the initial oxygen coverage, the first-order rate constants are found to increase by more than an order of magnitude when the initial oxygen coverage is decreased from 0.6 ML to 0.02 ML. The observed behavior is compatible with a model where isolated SiO units are formed at the boundaries of oxygen islands. This study has demonstrated the applicability of SHG to obtain quantitative results for complex chemisorbates, opening insight into desorption and related processes not easily accessible with other techniques.

# Appendix A

# Linear optical diffraction from adsorbate gratings

The performance of diffusion experiments for covalently bound adsorbates on surfaces is in general difficult due to the large diffusion barriers [85]. Therefore for hydrogen on silicon surfaces, at the beginning of this thesis's work only the diffusion on Si(111)7×7 has yet been investigated [12]. This was achieved having made use of the then newly developed technique of second-harmonic diffraction from a submonolyer grating, generated by laser-induced thermal desorption (LITD) of adsorbed hydrogen. For reasons discussed below, however, this method could not be applied to Si(001). With the discovery of the high reactivity of the steps on Si(001) as discussed in chapter 4 an alternative method was at hand to produce a lateral concentration profile by making use of intrinsic surface properties. The related diffusion experiments discussed in section 4.4 provided microscopic insight into the diffusion process on Si(001). In addition STM studies have started to address this issue [80,159,165]. For that reason the experiments described here, which make use of a new method to produce a concentration gradient [171] and detect it with linear optical diffraction have not been the primary goal of our studies. Nevertheless, its applicability to obtain macroscopic diffusion rate constants is demonstrated here. The technique shows unprecedented sensitivity and is capable to study a large number of adsorbate systems.

### Introduction

When two incident laser beams interfere on an adsorbate-covered surface, a periodic modulation of the adsorbate density can be achieved by laser-induced thermal desorption (LITD). The resulting micron-scale grating can be detected by using diffraction of second-harmonic generation [12,238–242] or linear optical diffraction [243,244] and from the decay of the concentration profile the diffusion coefficients can be extracted.

However, high-resolution patterning of strongly bound chemisorbates such as hydrogen on silicon using LITD has the following limitation: On the one hand, sufficient desorption during the duration $\tau_p$ of the incident laser pulse requires a pulse of enough intensity to reach a sufficiently high surface temperature. However, the maximal temperature rise is determined by the onset of substrate damage or adsorbate decomposi-

tion. On the other hand, due to the lateral heat diffusion for a (sub-)micron resolution the pulse width must not exceed a few ns [245,246]. This difficulty has prevented for example application of the second-harmonic diffraction technique to study the hydrogen diffusion on Si(001) because laser intensities sufficient to form a sub-micron grating already cause irreversible substrate damage.

In order to circumvent this problem, the experiments described here use weakly bound layers of inert gas, as was recently suggested [171]. A grating generated by laser-induced desorption of a physisorbed adlayer of a rare gas can be used as a template for the chemisorbate as shown schematically in Fig. A.1. Provided it sufficiently passivates the substrate towards interaction with the chemisorbate, a secondary grating can be produced and the rare gas can easily be removed afterwards by thermal desorption. Having determined the corresponding experimental parameters, the applicability of this method will be demonstrated here to study diffusion of even strongly bound chemisorbates.

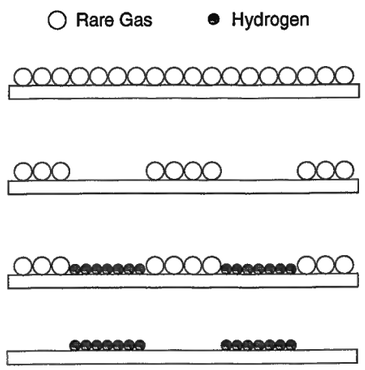


**Fig. A.1:** Scheme for patterning of adsorbed monolayer by the template technique: The troughs of a LID-generated rare gas grating are filled via selective adsorption of hydrogen. Subsequent desorption of the rare gas leaves the hydrogen grating on the surface

## Experiment

In the first step the grating is prepared with a single 3 ns pulse at 532 nm provided by the frequency-doubled Nd:YAG laser, split symmetrically at a holographic grating into two beams as shown in Fig. A.2. These two beams ($s$ polarized, $\emptyset$= 5 mm, $E \simeq 1$ mJ) then overlap on the sample at an angle $\theta = \pm 2.6°$ with respect to the surface normal. To form a spatially homogeneous grating, the flat-top beam profile provided at the outcoupling mirror of the laser is relay-imaged with a $4f$ system onto the sample surface. The modulation depth can be estimated from LITD mass spectroscopy



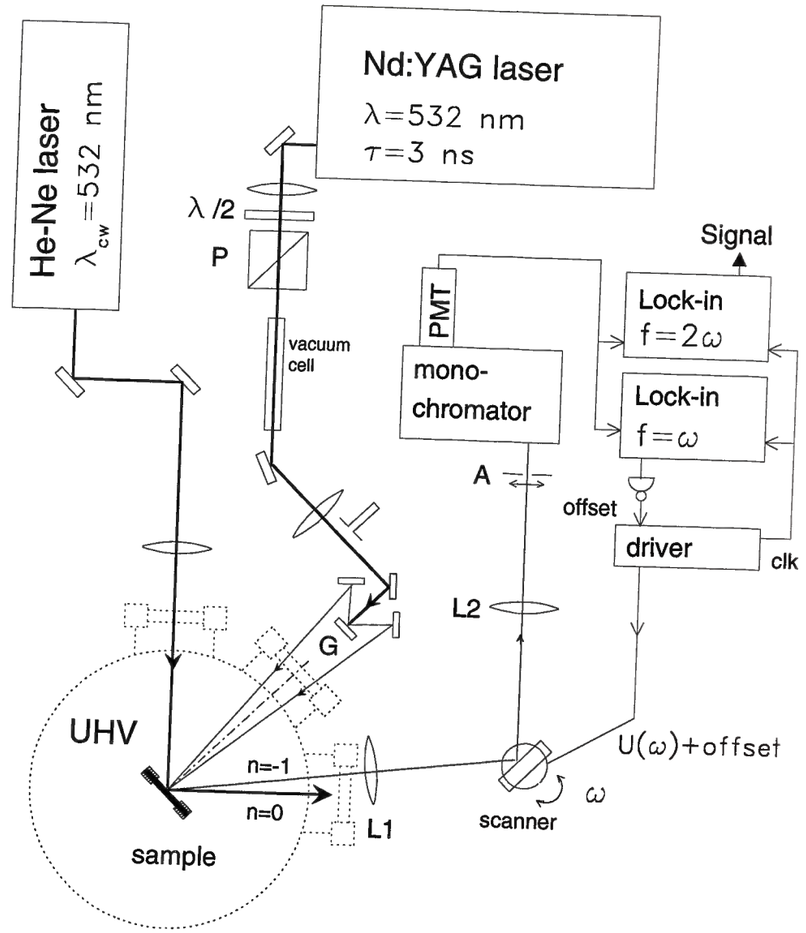


**Fig. A.2:** Schematic of optical setup: Laser-induced desorption (LID) generation of adsorbate grating and detection using linear optical diffraction, together with modulation and lock-in scheme for stray light suppression.

experiments by comparing the desorbed amount during grating formation with the signal obtained by removing the full layer with a single intense laser pulse.

For grating detection the advantage of the orders of magnitude higher signal intensity of linear diffraction over SHG is in general undermined by a high background due to diffuse scattering usually comparable to, or even larger than the diffracted signal [243]. Here a refined modulation technique for background suppression is applied and its high sensitivity is demonstrated. The grating with periodicity $l_g = \lambda/2\sin\theta = 5.9\mu m$ is irradiated with the 5 mW cw output of a He-Ne laser at 543.5 nm and under 45°

incidence (alternatively, 10 mW at 532 nm from a diode pumped cw Nd:$YVO_4$ laser was utilized). To separate the minus first-order diffracted beam with a typical intensity of order $10^{-6}$ of the incident beam [243] from the diffusely scattered background, a modulation scheme is applied. The underlying idea is that the scattered light is radiated in all solid angle directions with smooth angular distribution, whereas the diffracted light is highly directional. By modulating the detection angle one thus obtains a DC offset from the scattering and an AC contribution from diffraction which can be separated by lock-in detection. For that purpose the sample surface is 1:1 imaged (L1) onto the mirror mounted on a scanner motor which dithers around its axis. With the ability to control both frequency and amplitude, this method also greatly simplifies the procedure used in previous experiments where for the purpose of signal modulation sample oscillations were induced by exciting a torsional resonance mode of the UHV manipulator [171].

The scanner mirror is then imaged onto the entrance aperture of the monochromator with the photomultiplier tube. For that purpose a 200 mm camera lens (L2) is utilized to compensate imaging distortions due to the varying angle of incidence. The signal modulation is then achieved with a narrow slit aperture (A) placed in the focal point, and the modulation amplitude is adjusted so as to obtain a near sinusoidal signal at twice the modulation frequency $\omega$. For a properly adjusted system the signal modulation of the background could be nearly completely suppressed.

In addition, a second lock-in amplifier detects the $\omega$ signal component, which is zero as long as the focal point of the diffracted light scans across the slit aperture symmetrically. Small thermal drifts of the sample holder induced by heating the silicon crystal would thus reduce the $2\omega$ signal. A negative feedback loop was therefore established with the $\omega$ signal and the scanner driver electronics, continuously correcting the mirror position for these drifts.

To good approximation the first-order diffracted signal $S(t)$ is proportional to the square of the first spatial Fourier component of the monolayer grating as derived from Fick's law [238,244]. Its time variation resulting from surface diffusion is then given by

$$S(t) = S_0 \exp\left(\frac{-8\pi D t}{l_g^2}\right) = S_0 \exp\left(-2\alpha_g t\right), \qquad \text{(A.1)}$$

where $l_g$ is the grating period and $D$ the temperature-dependent diffusion coefficient. Note that this expression is only valid if $D$ is independent from coverage.

### Rare-gas adsorption on Si(001)2×1

The rare-gas layers adsorbed on Si(001)2×1 were characterized by using TPD and desorption traces for krypton on both clean and hydrogen-terminated Si(001) are shown in Fig. A.3. The spectra are characterized by several features which saturate one after the other except for the low-temperature multilayer peak. After hydrogen-



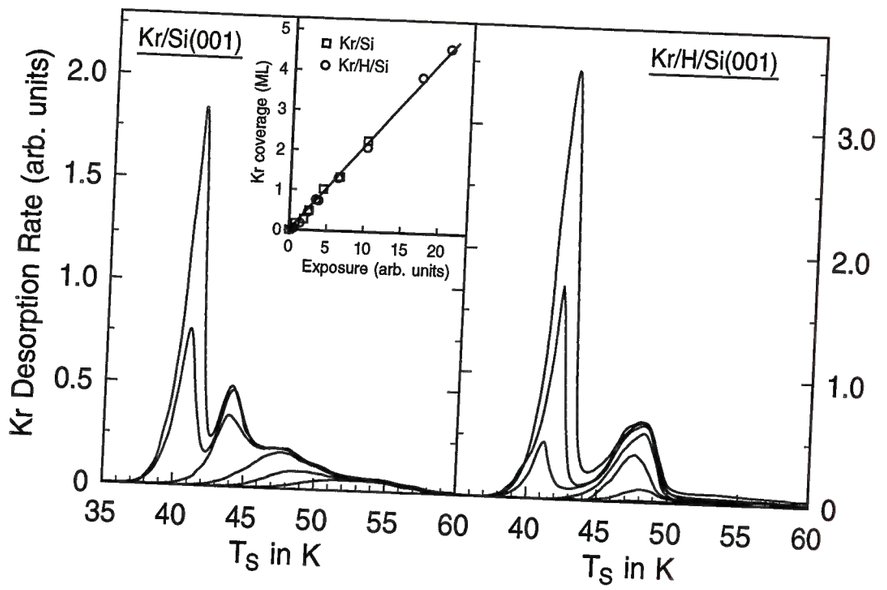


**Fig. A.3:** TPD desorption traces for Kr from clean Si(001)2×1 (0.17, 0.34, 0.6, 0.89, 1.5, and 2.2 ML) and from hydrogen-terminated Si(001)2×1 (0.18, 0.46, 0.80, 1.3, 2.1, and 3.9 ML); obtained for a heating rate of $0.6 - 0.7\,\mathrm{Ks}^{-1}$.

terminating the sample the desorption behavior becomes dominated by only a single high-temperature peak. By comparing the exposures necessary to saturate the Kr monolayer on H/Si(001) the broad feature in the left figure could be attributed to the monolayer desorption on clean Si(001). In the plot of the coverage-converted integrated peak areas versus exposure (inset), the data from both experiments are shown and agree excellently.

In Fig. A.4 representative data are shown for argon and xenon adsorption on clean Si(001). In both cases the desorption peaks are structurally very similar to krypton desorption.

Few studies have yet addressed rare-gas adsorption on Si(111)7×7 [247–249] and Si(001)2×1 [250,251], and no structure analyses of rare-gas layers have been performed to date. The various features of the monolayer desorption peak indicate the presence of different binding sites and the adsorption of Xe on Si(001)2×1 has been discussed in terms of two different binding geometries and formation of an incommensurate hexagonal structure for coverages above 0.85 ML [250,251]. One site would be a pedestal position on the dimer row between two adjacent dimers, the other a cave position between the dimer rows.

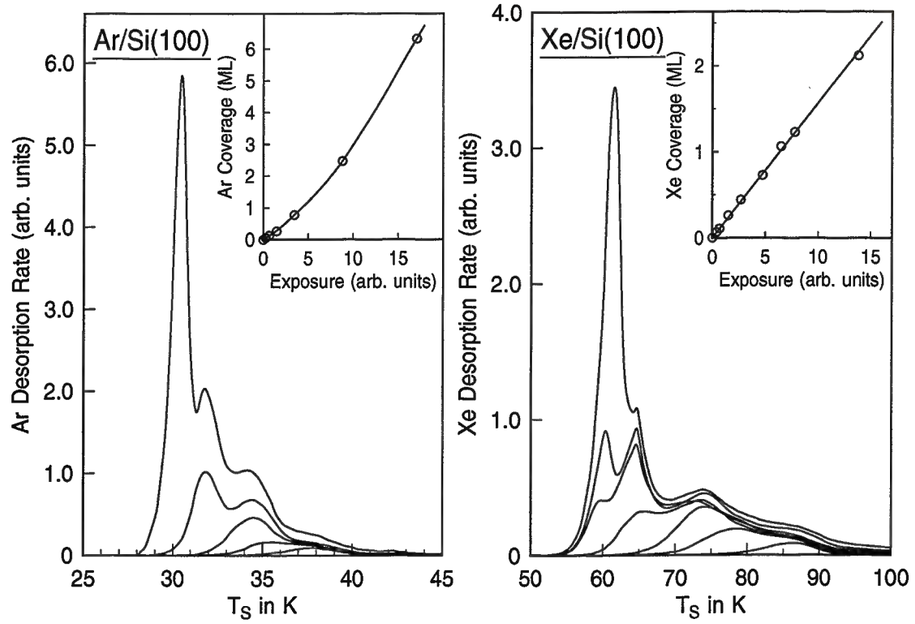


**Fig. A.4:** TPD desorption traces for Ar (left, heating rate $0.4 - 0.5\,\mathrm{Ks}^{-1}$) and Xe (right, heating rate $1.3 - 1.4\,\mathrm{Ks}^{-1}$) from clean Si(001)2×1.

### Rare-gas silicon passivation

The effectivity of the rare-gas layer in protecting the silicon substrate below from the impinging secondary adsorbate atoms was investigated for both Kr and Xe layers. For that purpose a rare-gas layer of desired thickness is prepared and successively exposed to a constant flux of, for example atomic hydrogen. By using SHG, and comparing the signal intensity before and after that procedure the amount of hydrogen adsorbed could be deduced, and thus the effective change in sticking probability compared with an initially clean silicon sample is derived. Since one ML of Kr or Xe also quenches the SH intensity by about 10 to 20%, the rare gas is removed prior to determining the adsorbed quantity of hydrogen[1]. The resulting sticking coefficients were also verified by TPD. In addition, similar experiments were performed for oxygen adsorption on Kr-precovered Si(001), and the results are summarized in Fig. A.5.

A moderate initial decrease is followed by a sharp drop by nearly a factor of 10 around completion of the monolayer, similar to the results reported for Xe on Si(111)7×7 [171]. This behavior would be compatible with the rare-gas atoms sitting

[1] This strong effect on the SH intensity is surprising for only weakly physisorbed adsorbates. It indicates a significant interaction of the closed shell rare-gas atoms with the dangling bond surface states.



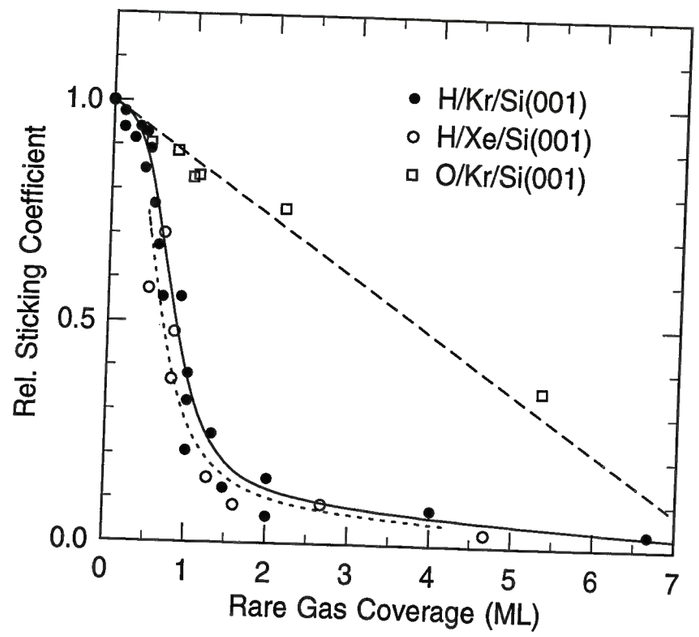


**Fig. A.5:** Relative sticking coefficient of atomic hydrogen and molecular oxygen as a function of rare-gas layer thickness of Kr and Xe on Si(001)

at the hollow sites formed by the silicon dangling bonds. As long as a commensurate layer is formed the dangling bonds can still be attacked, whereas only the incommensurate layer places rare-gas atoms close to or atop the dangling bonds, shielding them more efficiently from the incoming hydrogen atoms. Xe atoms seem to be somewhat more efficient, which might simply be due to the larger atom size. The hydrogen atoms impinging on the rare-gas-covered surface can either be backscattered or diffuse into the layer. Depending on thickness and initial energy, they might eventually be trapped or reach a dangling bond and react. This would explain the exponential decrease for coverages above one ML.

Quite different behavior is found in the case of oxygen. The oxygen molecules, although they might initially be more efficiently blocked by the rare-gas atoms due to their larger size compared to hydrogen, are likely to physisorb on top of the rare-gas layer rather than being backscattered into the vacuum. Then upon heating the film additional oxygen molecules can interdiffuse with the rare-gas layer and reach the silicon surface prior to being removed together with the rare-gas atoms.

These findings have the important consequence for the patterning experiments that whereas 1 ML of rare gas would already be sufficient to produce a well-modulated hydrogen grating, thicker layers are required, for example for oxygen patterning.

### Rare-gas diffusion

Another criterion for successful transfer of the rare-gas grating to hydrogen is to suppress its diffusion sufficiently. From experiments on metal surfaces it is known that rare-gas atoms readily diffuse already for temperatures well below the onset of desorption [85]. The behavior of a Kr grating at a surface temperature of 26 K, inscribed into an initially 2 ML thick layer, is shown in Fig. A.6. Exponential decay on a time scale of about 100 s can be attributed to diffusion eventually washing out the initial structure.

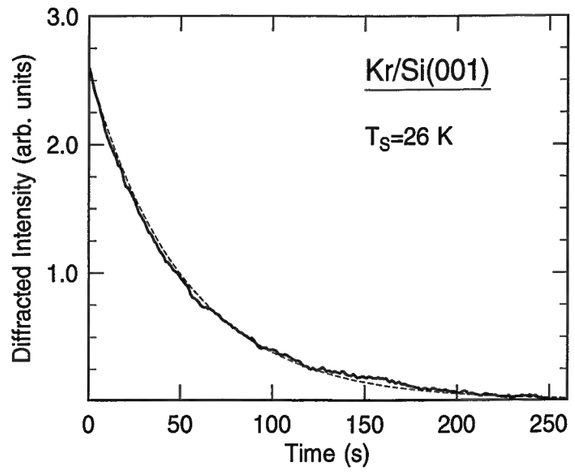


**Fig. A.6:** Multilayer Kr diffusion at a surface temperature of 26 K. The dashed line is the result of a single exponential fit with $D = 1.7 \times 10^{-10}\,\mathrm{cm^2 s^{-1}}$.

Similar experiments were conducted for Xe gratings both for monolayer and multilayer adsorption. The resulting Arrhenius plot for multilayer diffusion is shown in Fig. A.7, indicating that for temperatures below 40 K gratings can be made sufficiently long-lived to be used as a template. Since the multilayer of Xe is less strongly bound than the monolayer on silicon, the obtained activation energy of 36 meV can probably be interpreted as a Xe-Xe diffusion barrier. The decay of the grating would then occur by Xe flow from the top of the ridges into the empty troughs.

Strikingly, there is a dramatic enhancement of the diffusion rate with decreasing coverage. For submonolayer diffusion of Xe as much as two orders of magnitude higher diffusion coefficients were found for surface temperatures below 35 K. A similar behavior has been observed e.g. for Xe diffusion on Pt(111) [252]. There it was attributed to formation of a two-dimensional condensed phase in the form of islands with increasing coverage, and the combined effect of intrinsic lateral corrugation and attractive interactions effectively reduces the diffusion rate. Rare-gas diffusion on



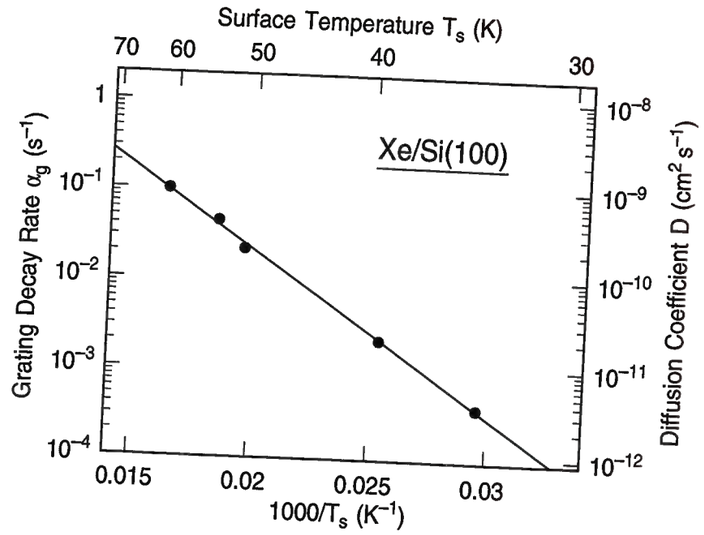


**Fig. A.7:** Grating decay rate $\alpha_g$ and corresponding diffusion coefficients $D$ for multilayer Xe diffusion.

silicon has not yet been investigated and by exploiting the sensitivity of this method one could obtain a wealth of information concerning both coverage dependence and diffusion anisotropy. These results would be interesting to be compared with rare-gas diffusion on metal surfaces.

### Rare-gas template for hydrogen patterning

From the rare-gas diffusion experiments it is concluded that for patterning more than one monolayer thick films are most suitable. The corresponding experimental steps can be seen from Fig. A.8, where the recorded first-order diffracted signal is plotted: A fully modulated multilayer Kr grating is exposed to atomic hydrogen, leading to a pronounced signal increase. This increase is due to the higher contrast of the dielectric function as a result of the strongly interacting chemisorbate with the surface electronic states, which decreases the surface polarizability. Since Kr increases the surface polarizability, both gratings add up in phase. Consequently, when the surface temperature is increased the onset of rare-gas diffusion and successive desorption leads to a signal drop and the remaining diffracted intensity is purely due to the secondary hydrogen grating. For continuous hydrogen exposure the diffracted signal passes through a maximum (see dashed line) and drops off subsequently since hydrogen penetrates the rare-gas layer and the grating is deleted out.

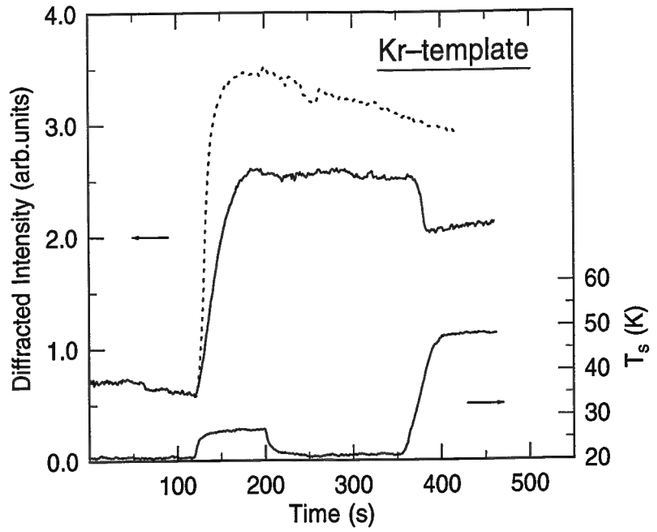


**Fig. A.8:** Change of diffraction intensity during the patterning process. The slight temperature rise during H exposure is due to the hot filament facing the sample surface. The signal instabilities occured because of vibrations of the chamber during gas handling.

### Hydrogen diffusion on Si(001)2×1

The following experiments demonstrate the capabilities of the new technique performing high-resolution diffusion experiments with hydrogen on Si(001).

Typical results for the decay of a weakly modulated hydrogen grating are shown in Fig. A.9 for a surface temperature of 760 K. In that experiment the hydrogen exposure was stopped after the signal increased by 10% in relation to the rare-gas grating intensity. To appreciate the full capability of the method, data from a fully coverage-modulated hydrogen grating are shown in Fig. A.10. Above 2200 s the diffusion experiment was stopped and the temperature has been increased to desorb the hydrogen. The residual signal from the clean surface is more than three orders of magnitude lower than the initial intensity. It does not show any directionality towards the diffracted minus first-order direction, thus indicating that the grating could be completely removed. The remaining background is due to the speckle pattern and could, in principle, be even further suppressed by applying additional polarization modulation.

Both diffusion and desorption lead to a decay of the diffracted signal and the two contributions cannot be distinguished *a priori*. In the case of rare gases, where the adsorbate becomes mobile far below the desorption temperature, the desorption could be neglected. For hydrogen on silicon however, due to its large lateral corrugation



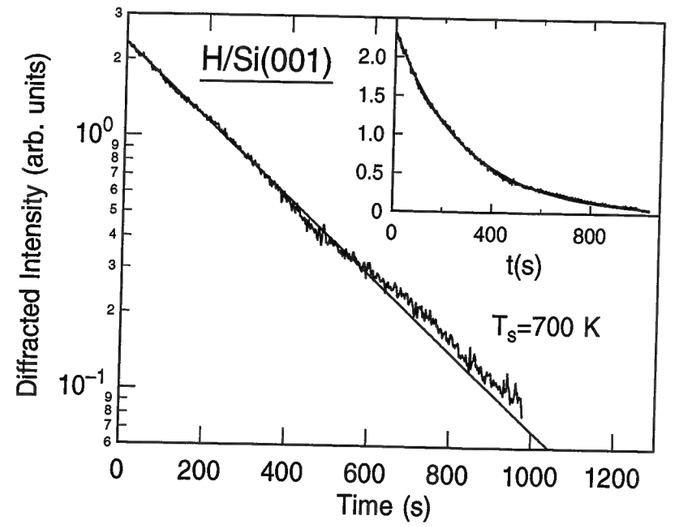


**Fig. A.9:** Exponential decay of a weakly modulated hydrogen grating with a total hydrogen coverage of $\sim$0.05 ML. for a surface temperature of 700 K. Inset: linear plot of the same data.

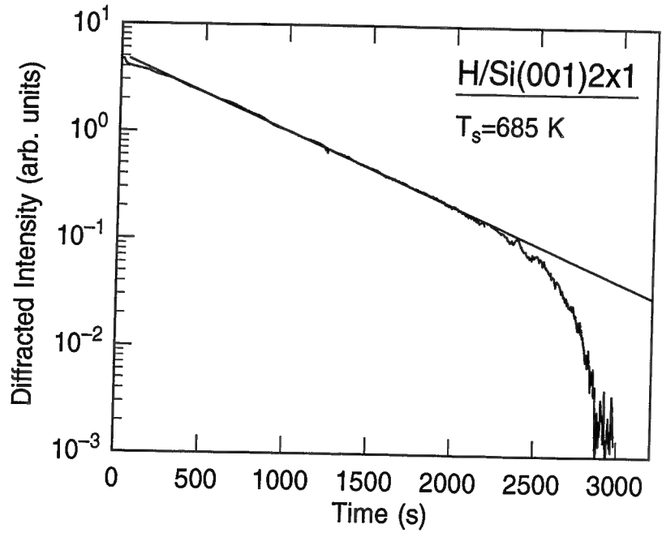


**Fig. A.10:** Decay of a fully modulated grating for $T_s = 685$ K. The initial signal drop is likely to be due to the desorption of dihydride. For $t > 2200$ s the temperature was increased to desorb the residual hydrogen.

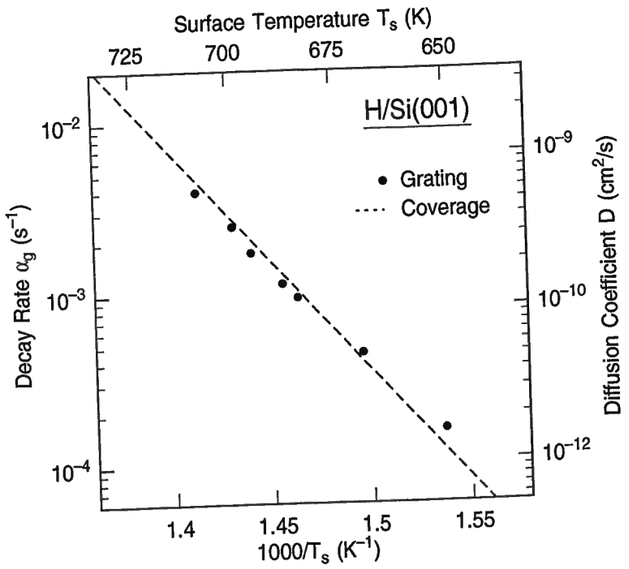


**Fig. A.11:** Comparison of the measured grating decay rates (filled symbols) with the hydrogen desorption rates (dashed line, from Ref. [11]). Due to the large grating spacing of $l_g = 5.9\,\mu$m the diffusion rate can not be deduced

with respect to the desorption energy the corresponding rates have to be determined independently. In Fig. A.11 both the measured decay rates for the grating $\alpha_g$ (solid circles), and, for comparison, the first order desorption time constant $\alpha_{\rm des} = \frac{1}{\theta}\frac{{\rm d}\theta}{{\rm d}t}$ determined from these and previous experiments [11] are plotted. However, and in contrast to the rare gas diffusion experiments, due to the large grating spacing $l_g = 5.9\,\mu m$ the decay of the grating is dominated by desorption. The equation $\alpha_g = \alpha_{\rm D} + \alpha_{\rm des} = \frac{4D}{(l_g/\pi)^2} + \alpha_{\rm des}$ interrelates the contributions from desorption and diffusion to the overall grating decay rate. It is thus apparent that a reduced grating periodicity would have to be utilized to increase the diffusion term. A grating periodicity of 1 $\mu$m or below would be desirable which can easily be achieved by changing the angle of incidence of the two laser beams which generate the rare-gas grating.

In summary, the applicability of a new way of generating a periodic concentration profile for strongly bound adsorbates has been demonstrated. The rare gas template technique was used to generate a hydrogen grating on Si(001) without any effect on the substrate. The signal-to-noise of up to $\sim 10^{-4}$ achieved by using a simple, but highly sensitive detection scheme makes this technique a very promising probe for surface diffusion.

# Bibliography

[1] J. T. Law, *Adsorption of hydrogen on silicon*, J. Chem. Phys. **30**, 1568 (1959).

[2] H. Ibach and J. E. Rowe, *Hydrogen adsorption and surface structure of silicon*, Surf. Sci. **43**, 481 (1974).

[3] J. A. Appelbaum and D. R. Hamann, *Self-consistent quantum theory of chemisorption: H on Si(111)*, Phys. Rev. Lett. **34**, 806 (1975).

[4] J. A. Appelbaum and D. R. Hamann, in *Topics in Current Physics, Theory of Chemisorption*, edited by J. R. Smith (Springer, Berlin, 1980), Vol. 19, p. 43.

[5] K. C. Pandey, *Realistic tight-binding model for chemisorption: H on Si and Ge (111)*, Phys. Rev. B **14**, 1557 (1976).

[6] Y. J. Chabal and K. Raghavachari, *Surface infrared study of Si(100)-(2 × 1)H*, Phys. Rev. Lett. **53**, 282 (1984).

[7] Y. J. Chabal, A. L. Harris, K. Raghavachari, and J. C. Tully, *Infrared spectroscopy of H-terminated silicon surfaces*, Int. J. Mod. Phys. B **7**, 1031 (1993).

[8] J. J. Boland, *Scanning tunneling microscopy of the interaction of hydrogen with silicon surfaces*, Adv. Phys. **42**, 129 (1993).

[9] K. Sinniah, M. G. Shermann, L. B. Lewis, W. H. Weinberg, J. J. T. Yates, and K. C. Janda, *New mechanism for hydrogen desorption from covalent surfaces: The monohydride phase on Si(100)*, Phys. Rev. Lett. **62**, 567 (1989).

[10] G. A. Reider, U. Höfer, and T. F. Heinz, *Desorption kinetics of hydrogen from the Si(111)7 × 7 surface*, J. Chem. Phys. **95**, 4080 (1991).

[11] U. Höfer, L. Li, and T. F. Heinz, *Desorption of hydrogen from Si(100)2 × 1 at low coverages: The influence of π-bonded dimers on the kinetics*, Phys. Rev. B **45**, 9485 (1992).

[12] G. A. Reider, U. Höfer, and T. F. Heinz, *Surface diffusion of hydrogen on Si(111)7 × 7*, Phys. Rev. Lett. **66**, 1994 (1991).

[13] K. W. Kolasinski, W. Nessler, A. de Meijere, and E. Hasselbrink, *Hydrogen adsorption and desorption from Si: Considerations on the applicability of detailed balance*, Phys. Rev. Lett. **72**, 1356 (1994).

[14] P. Bratu and U. Höfer, *Phonon-assisted sticking of molecular hydrogen on Si(111)-(7 × 7)*, Phys. Rev. Lett. **74**, 1625 (1995).

[15] K. W. Kolasinski, *Dynamics of hydrogen interactions with Si(100) and Si(111) surfaces*, Int. J. of Mod. Phys. B **9**, 2753 (1995).

[16] H. N. Waltenburg and J. J. T. Yates, *Surface chemistry of silicon*, Chem. Rev. **95**, 1589 (1995).

[17] U. Höfer, *Nonlinear optical investigations of the dynamics of hydrogen interaction with silicon surfaces*, Appl. Phys. A **63**, 533 (1996).

[18] D. J. Doren, *Kinetics and dynamics of hydrogen adsorption and desorption on silicon surfaces*, Adv. Chem. Phys. **95**, 1 (1996).

[19] M. R. Radeke and E. A. Carter, *Ab initio dynamics of surface chemistry*, Annu. Rev. Phys. Chem. **48**, 243 (1997).

[20] J. M. Jasinski, B. S. Meyerson, and B. A. Scott, *Mechanistic studies of chemical vapor deposition*, Ann. Rev. Phys. Chem. **38**, 109 (1987).

[21] J. M. Jasinski and S. M. Gates, *Silicon chemical vapor deposition one step at a time: fundamental studies of silicon hydride chemistry*, Acc. Chem. Res. **24**, 9 (1991).

[22] M. Copel and R. M. Tromp, *H coverage dependence of Si(001) homoepitaxy*, Phys. Rev. Lett. **72**, 1236 (1994).

[23] Z. Zhang and M. G. Lagally, *Atomistic Processes in the early stages of thin-film growth*, Science **276**, 377 (1997).

[24] G. Schulze and M. Henzler, *Adsorption of atomic hydrogen on cleaved silicon (111)*, Surf. Sci. **124**, 336 (1983).

[25] M. Liehr, C. M. Greenlief, S. R. Kasi, and M. Offenberg, *Kinetics of silicon epitaxy using $SiH_4$ in a rapid thermal chemical vapor deposition reactor*, Appl. Phys. Lett. **56**, 629 (1990).

[26] P. Bratu, K. L. Kompa, and U. Höfer, *Optical second-harmonic investigations of $H_2$ and $D_2$ adsorption on Si(100): the surface temperature dependence of the sticking coefficient*, Chem. Phys. Lett. **251**, 1 (1996).



[27] P. Bratu, W. Brenig, A. Groß, M. Hartmann, U. Höfer, P. Kratzer, and R. Russ, *Reaction dynamics of molecular hydrogen on silicon surfaces*, Phys. Rev. B **54**, 5978 (1996).

[28] W. Brenig, A. Gross, and R. Russ, *Detailed balance and phonon assisted sticking in adsorption and desorption of $H_2$/Si*, Z. Phys. B **96**, 231 (1994).

[29] W. Brenig, A. Gross, U. Höfer, and R. Russ, *Adsorption-desorption of $H_2$/Si: A 5-D dynamical model*, phys. stat. sol. (a) **159**, 75 (1997).

[30] A. C. Luntz and P. Kratzer, *$D_2$ dossociative adsorption on and assocciative desorption from Si(100): Dynamic consequences of an ab initio potential energy surface*, J. Chem. Phys. **104**, 3075 (1996).

[31] A. Gross, M. Bockstedte, and M. Scheffler, *Ab initio molecular dynamics study of the desorption of $D_2$ from Si(100)*, Phys. Rev. Lett. **79**, 701 (1997).

[32] K. W. Kolasinski, W. Nessler, K.-H. Bornscheuer, and E. Hasselbrink, *Beam investigations of $D_2$ adsorption on Si(100): On the importance of lattice excitations in the reaction dynamics*, J. Chem. Phys. **101**, 7082 (1994).

[33] W. Mönch, *Semiconductor surfaces and interfaces* (Springer, Berlin, 1995).

[34] V. G. Lifshits, A. A. Saranin, and A. V. Zotov, *Surface phases on silicon* (Wiley, Chichester, 1994).

[35] D. Haneman, *Surfaces of silicon*, Rep. Prog. Phys. **50**, 1045 (1987).

[36] J. A. Kubby and J. J. Boland, *Scanning tunneling microscopy of semiconductor surfaces*, Surf. Sci. Rep. **26**, 61 (1996).

[37] J. Pollmann, P. Krüger, M. Rohlfing, M. Sabisch, and D. Vogel, *Ab initio calculations of structural and electronic properties of prototype surfaces of group IV,III-V and II-VI semiconductors*, Appl. Surf. Sci. **104**, 1 (1996).

[38] R. E. Schlier and H. E. Farnsworth, *Stucture and adsorption characteristics of clean surfaces of germanium and silicon*, J. Chem. Phys. **30**, 917 (1959).

[39] R. M. Tromp, R. J. Hamers, and J. E. Demuth, *Si(001) dimer structure observed with scanning tunneling microscopy*, Phys. Rev. Lett. **55**, 1303 (1985).

[40] R. I. G. Uhrberg, G. V. Hansson, J. M. Nichols, and S. A. Flodström, *Experimental studies of the dangling- and dimer-bond-related surface electron bands on Si(100)2 × 1*, Phys. Rev. B **24**, 4684 (1981).

[41] L. S. O. Johansson, R. I. G. Uhrberg, P. Matrensson, and G. V. Hansson, *Surface-state band structure of the Si(100)2×1 surface studied with polarization-dependent angle-resolved photoemission on single-domain surfaces*, Phys. Rev. B **42**, 1305 (1990).

[42] P. Krüger and J. Pollmann, *Dimer reconstruction of diamond, Si, and Ge(001) surfaces*, Phys. Rev. Lett. **74**, 1155 (1995).

[43] R. A. Wolkow, *Direct observation of an increase in buckled dimers on Si(001) at low temperature*, Phys. Rev. Lett. **68**, 2636 (1992).

[44] J. Dąbrowski and M. Scheffler, *Self-consistent study of the electronic and structural properties of the clean Si(001)(2 × 1) surface*, Appl. Surf. Sci. **56-58**, 15 (1992).

[45] J. Fritsch and P. Pavone, *Ab initio calculations of the structure, electronic states, and the phonon dispersion of the Si(100) surface*, Surf. Sci. **344**, 159 (1995).

[46] A. I. Shkrebtii, R. D. Felice, C. M. Bertoni, and R. D. Sole, *Ab initio study of structure and dynamics of the Si(100) surface*, Phys. Rev. B **51**, 11201 (1995).

[47] R. J. Hamers, R. M. Tromp, and J. E. Demuth, *Scanning tunneling microscopy of Si(001)*, Phys. Rev. B **34**, 5343 (1986).

[48] M. P. D'Evelyn, Y. L. Yang, and L. F. Suctu, *π-bonded dimers, preferential pairing, and first-order desorption kinetics of hydrogen on Si(100)-2 × 1)*, J. Chem. Phys. **96**, 852 (1992).

[49] A. Vittadini, A. Selloni, and M. Casarin, *Pairing of hydrogen atoms on the Si(100)-2 × 1 surface: the role of interactions among dimers*, Phys. Rev. B **49**, 11191 (1994).

[50] J. E. Northrup, *Theoretical studies of arsine adsorption on Si(100)*, Phys. Rev. B **51**, 2218 (1995).

[51] B. S. Swartzentruber, Y.-W. Mo, R. Kariotis, M. G. Lagally, and M. B. Webb, *Direct determination of step and kink energies on vicinal Si(001)*, Phys. Rev. Lett. **65**, 1913 (1990).

[52] B. S. Swartzentruber, Y.-W. Mo, M. B. Webb, and M. G. Lagally, *Scanning tunneling microscopy studies of structural disorder*, J. Vac. Sci. Technol. A **7**, 2901 (1989).

[53] V. A. Ukraintsev, Z. Dohnalek, and J. J. T. Yates, *Electronic characterization of defect sites on Si(001)-(2 × 1) by STM*, Surf. Sci. **388**, 132 (1997).



[54] R. J. Hamers and U. K. Köhler, *Determination of the local electronic structure of atomic-sized defects on Si(001) by tunneling spectroscopy*, J. Vac. Sci. Technol. A **7**, 2854 (1989).

[55] M. Chander, Y. Z. Li, J. C. Patrin, and J. H. Weaver, *Si(100)-2 × 1 surface defects and dissociative and nondissociative adsorption of $H_2O$ studied with scanning tunneling microscopy*, Phys. Rev. B **48**, 2493 (1993).

[56] L. Andersohn and U. Kohler, *In situ observation of water adsorption on Si(100) with scanning tunneling microscopy*, Surf. Sci. **284**, 77 (1993).

[57] J. Wang, T. A. Arias, and J. D. Joannopulos, *Dimer vacancies and dimer-vacancy complexes on the Si(100) surface*, Phys. Rev. B **47**, 10497 (1993).

[58] J. J. Boland, *Role of bond-strain in the chemistry of hydrogen on the Si(100) surface*, Surf. Sci. **261**, 17 (1992).

[59] D. J. Chadi, *Stabilities of single-layer and bilayer steps on Si(001) surfaces*, Phys. Rev. Lett. **59**, 1691 (1987).

[60] O. L. Alerhand, A. N. Berker, J. D. Joannopoulos, D. Vanderbilt, R. J. Hamers, and J. E. Demuth, *Finite-temperature phase diagram of vicinal Si(100) surfaces*, Phys. Rev. Lett. **64**, 2406 (1990).

[61] T. W. Poon, S. Yip, P. S. Ho, and F. F. Abraham, *Equilibrium structure of Si100) stepped surfaces*, Phys. Rev. Lett. **65**, 2161 (1990).

[62] E. Schröder-Bergen and W. Ranke, *Steps on Si(001) vicinal surfaces tilted by various angles in the* [110]-, [100]- *and* [210]-*zones, investigated by high-resolution LEED*, Surf. Sci. **259**, 323 (1991).

[63] H. Itoh, S. Narui, Z. Zang, and T. Ichonokawa, *Structure of double-atomic-height steps in Si(001) vicinal surfaces observed by scanning tunneling microscopy*, Surf. Sci. Lett. **277**, L70 (1992).

[64] E. Pehlke and J. Tersoff, *Phase diagramm of vicinal Si(001) surfaces*, Phys. Rev. Lett. **67**, 1290 (1991).

[65] O. L. Alerhand and E. J. Mele, *Surface reconstruction and vibrational excitation of Si(100)*, Phys. Rev. B **35**, 5533 (1987).

[66] P. E. Wierenga, J. A. Kubby, and J. E. Griffith, *Tunneling images of biatomic steps on Si(001)*, Phys. Rev. Lett. **59**, 2169 (1987).

[67] R. E. Schlier and H. E. Farnsworth, *Semiconductor surface physics* (Pennsylvania University Press, Pennsylvania, 1957).

[68] K. Takayanagi, Y. Tanishiro, S. Takahashi, and M. Takahashi, *Structural analysis of Si(111)-7 × 7 by UHV-transmission electron diffraction and microscopy*, J. Vac. Sci. Technol. A **3**, 1502 (1985).

[69] R. D. Meade and D. Vanderbilt, *Adatoms on Si(111) and Ge(111) surfaces*, Phys. Rev. B **40**, 3905 (1989).

[70] G. S. Higashi, R. S. Becker, Y. J. Chabal, and A. J. Becker, *Comparison of Si(111) surfaces prepared using aqueous solutions of $NH_4F$ versus HF*, Appl. Phys. Lett. **58**, 1656 (1991).

[71] P. Jakob and Y. J. Chabal, *Chemical etching of vicinal Si(111): dependence of the surface structure and the hydrogen termination on the pH of the etching solution*, J. Chem. Phys. **95**, 2897 (1991).

[72] B. G. Koehler, C. H. Mak, D. A. Arthur, P. A. Coon, and S. M. George, *Desorption kinetics of hydrogen and deuterium from Si(111)-7 × 7 studied using laser-induced thermal desorption*, J. Chem. Phys. **89**, 1709 (1988).

[73] M. L. Wise, B. G. Koehler, P. Gupta, P. A. Coon, and S. M. George, *Comparison of hydrogen desorption kinetics from Si(111)7 × 7 and Si(100)2 × 1*, Surf. Sci. **258**, 166 (1991).

[74] M. C. Flowers, N. B. H. Jonathan, Y. Lui, and A. Morris, *Temperature programmed desorption of molecular hydrogen from a Si(111) surface: Theory and experiment*, J. Chem. Phys. **102**, 1034 (1995).

[75] M. C. Flowers, N. B. H. Jonathan, A. Morris, and S. Wright, *The desorption of molecular hydrogen from Si(100)-2 × 1 and Si(111)-7 × 7 surfaces at low coverages*, J. Chem. Phys. **108**, 3342 (1998).

[76] A. Vittadini and A. Selloni, *Binding Sites, Migration Paths, and Barriers for Hydrogen on Si(111)7 × 7*, Phys. Rev. Lett. **75**, 4756 (1995).

[77] H. Lim, K. Cho, I. Park, J. D. Joannopoulos, and E. Kaxiras, *Ab initio study of hydrogen adsorption on the Si(111)-(7 × 7) surface*, Phys. Rev. B **52**, 17231 (1995).

[78] M. C. Flowers, N. B. H. Jonathan, Y. Lui, and A. Morris, *Temperature programmed desorption of molecular hydrogen from Si(100)2 × 1 surface: Theory and experiment*, J. Chem. Phys. **99**, 7038 (1993).

[79] J. J. Boland, *Evidence of pairing and its role in the recombinative desorption of hydrogen from the Si(100)2 × 1 surface*, Phys. Rev. Lett. **67**, 1539 (1991).



[80] M. McEllistrem, M. Allgeier, and J. J. Boland, *Dangling bond dynamics on the silicon (100)-2 × 1 surface: dissociation, diffusion, and recombination*, Science **279**, 545 (1998).

[81] C. J. Wu and E. A. Carter, *Adsorption of hydrogen atoms on the Si(100)2 × 1 surface: implications for the $H_2$ desorption mechanism*, Chem. Phys. Lett. **185**, 172 (1991).

[82] P. Nachtigall, K. D. Jordan, and C. Janda, *Calculations of the Si-H bond energies for the monohydride phase*, J. Chem. Phys. **95**, 8652 (1991).

[83] S. Pai and D. Doren, *First principles calculations of prepairing mechanism for $H_2$ desorption from Si(100)-2 × 1*, J. Chem. Phys. **103**, 1232 (1995).

[84] A. Vittadini and A. Selloni, *Density functional study of $H_2$ desorption from monohydride and dihydride Si(100) surfaces*, Chem. Phys. Lett. **235**, 334 (1995).

[85] R. Gomer, *Diffusion of adsorbates on metal surfaces*, Re. Prog. Phys. **53**, 917 (1990).

[86] D. C. Sorescu, D. L. Thompson, and L. M. Raff, *Diffusion of hydrogen atoms on a Si(111)-(7×7) reconstructed surface: Monte Carlo variational phase-space theory*, J. Chem. Phys. **101**, 1638 (1994).

[87] B. M. Rice, L. M. Raff, and D. L. Thompson, *Diffusion of H atoms on a Si(111) surface with partial hydrogen coverage: Monte Carlo variational phase-space theory with tunneling correction*, J. Chem. Phys. **88**, 7221 (1988).

[88] A. Vittadini, A. Selloni, and M. Casarin, *Energetics of atomic hydrogen diffusion on Si(100)*, Surf. Sci. Lett. **289**, L625 (1993).

[89] C. J. Wu, I. V. Ionova, and E. A. Carter, *First-principles-derived rate constants for H adatom surface diffusion on Si(100)-2×1*, Phys. Rev. B **49**, 13488 (1994).

[90] P. Nachtigall and K. D. Jordan, *Barriers for hydrogen atom diffusion on the Si(100)-2 × 1 surface*, J. Chem. Phys. **102**, 8249 (1995).

[91] K. W. Kolasinski, S. F. Shane, and R. N. Zare, *Internal-state distribution of recombinative hydrogen desorption from Si(100)*, J. Chem. Phys. **96**, 3995 (1992).

[92] S. F. Shane, K. W. Kolasinski, and R. N. Zare, *Recombinative desorption of $H_2$ on Si(100)-(2 × 1) and Si(111)-(7 × 7): Comparison of internal state distributions*, J. Chem. Phys. **97**, 1520 (1992).

[93] S. F. Shane, K. W. Kolasinski, and R. N. Zare, *Internal-state distribution of $H_2$ desorbed from mono- and dihydride species of Si(100)*, J. Chem. Phys. **97**, 3704 (1992).

[94] A. Pusel, U. Wetterauer, and P. Hess, *Photochemical hydrogen desorption from H-terminated silicon(111) by VUV photons*, Phys. Rev. Lett. **81**, 645 (1998).

[95] K. W. Kolasinski, W. Nessler, K.-H. Bornscheuer, and E. Hasselbrink, *Investigations of the adsorption dnamics of $D_2$ on Si(100)*, Surf. Sci. **331**, 458 (1995).

[96] A. Vittadini and A. Selloni, *$H_2$ adsorption/desorption at Si(111)7 × 7: a density functional study*, Surf. Sci. Lett. **383**, L779 (1997).

[97] K. Cho, E. Kaxiras, and J. D. Joannopoulos, *Theory of adsorption and desorption of $H_2$ Molecules on the Si(111)-(7 × 7) surface*, Phys. Rev. Lett. **79**, 5078 (1997).

[98] P. Kratzer, B. Hammer, and J. K. Nørskov, *The coupling between adsorption dynamics and the surface structure: $H_2$ on Si(100)*, Chem. Phys. Lett. **229**, 645 (1994).

[99] P. Kratzer, B. Hammer, and J. K. Nørskov, *Direct pathway for sticking/desorption of $H_2$ on Si(100)*, Phys. Rev. B **51**, 13432 (1995).

[100] E. Pehlke and M. Scheffler, *Theory of adsorption and desorption of $H_2$/Si(100)*, Phys. Rev. Lett. **74**, 952 (1995).

[101] C. J. Wu and E. A. Carter, *Anisotropic diffusion of hydrogen atoms on the Si(100)2 × 1 surface*, Phys. Rev. B **46**, 4651 (1992).

[102] C. J. Wu, I. V. Ionova, and E. A. Carter, *Ab initio $H_2$ desorption pathways for H/Si(100): the role of $SiH_{2(a)}$*, Surf. Sci. **295**, 64 (1993).

[103] M. R. Radeke and E. A. Carter, *A dynamically and kinetically consistent mechanism for $H_2$ adsorption/desorption from Si(100)*, Phys. Rev. B **54**, 11803 (1996).

[104] M. R. Radeke and E. A. Carter, *Ab initio explanation of the apparent violation of detailed balance for $H_2$ adsorption/desorption from Si(100)*, Surf. Sci. **355**, L289 (1996).

[105] A. J. R. da Silva, M. R. Radeke, and E. A. Carter, *Ab initio molecular dynamics of $H_2$ desorption from Si(100)-2 × 1*, Surf. Sci. **381**, L628 (1997).

[106] P. Nachtigall, K. D. Jordan, and C. Sosa, *Theoretical study of the mechanism of recombinative hydrogen desorption from the monohydride phase of Si(100): The role of defect migration*, J. Chem. Phys. **101**, 8073 (1994).



[107] P. Nachtigall, K. D. Jordan, A. Smith, and H. Jonsson, *Investigations of the reliability of density functional methods: Reaction and activation energies for Si-Si bond cleavage and $H_2$ elimination from silanes*, J. Chem. Phys. **104**, 148 (1996).

[108] Z. Jing and J. L. Whitten, *Ab initio studies of H chemisorption on Si(100)*, Phys. Rev. B **46**, 9544 (1992).

[109] Z. Jing, G. Lucovsky, and J. L. Whitten, *Mechanism of $H_2$ desorption from monohydride Si(100)2 × 1H*, Surf. Sci. Lett. **296**, L33 (1993).

[110] Z. Jing and J. L. Whitten, *Theoretical studies of $H_2$ desorption from Si(100)-2 × 1H*, J. Chem. Phys. **98**, 7466 (1993).

[111] Z. Jing and J. L. Whitten, *Multiconfiguration self-consistent-field treatment of $H_2$ desorption from Si(100)-2 × 1H*, J. Chem. Phys. **102**, 3867 (1995).

[112] E. Penev, P. Kratzer, and M. Scheffler, *Effect of the cluster size in modelling the $H_2$ desorption and dissociative adsorption on Si(001)*, J. Chem. Phys. (submitted).

[113] Y. R. Shen, *Surfaces probed by second-harmonic and sum-frquency generation*, Nature **337**, 519 (1989).

[114] Y. R. Shen, *Surfaces probed by nonlinear optics*, Surf. Sci. **299**, 551 (1994).

[115] Y. R. Shen, *Nonlinear optical studies of surfaces*, Appl. Phys. A **59**, 541 (1994).

[116] N. Bloembergen, R. K. Chang, S. S. Jha, and C. H. Lee, *Optical second-harmonic generation in reflection from media with inversion symmetry*, Phys. Rev. **174**, 813 (1968).

[117] Y. R. Shen, *The principles of nonlinear optics* (Wiley, New York, 1984).

[118] Y. R. Shen, *Optical second harmonic generation at interfaces*, Annu. Rev. Phys. Chem. **40**, 327 (1989).

[119] T. F. Heinz, in *Nonlinear surface electromagnetic phenomena*, edited by H.-E. Ponath and G. I. Stegeman (North-Holland, Amsterdam, 1991), p. 353.

[120] G. A. Reider and T. F. Heinz, in *Photonic probes of surfaces*, edited by P. Halevi (Elsevier, Amsterdam, 1995), pp. chap.9, p.1.

[121] J. F. McGilp, *Optical characterisation of semisonductor surfaces and interfaces*, Prog. Surf. Sci. **49**, 1 (1995).

[122] K. Pedersen and P. Morgen, *Dispersion of optical second-harmonic generation from Si(111)*7 × 7, Phys. Rev. B **52**, R2277 (1995).

[123] G. Schmitt, *Untersuchung der nichtlinearen optischen Eigenschaften von Siliziumoberlächen im nahen Infrarot: Frequenzabhängigkeit und mikroskopische Mechanismen*, Dissertation, Technische Universität München, 1996.

[124] J. I. Dadap, Z. Xu, X. F. Hu, M. C. Downer, N. M. Russel, J. G. Ekerdt, and O. A. Aktsipetrov, *Second-harmonic spectroscopy of a Si(001) surface during calibrated variations in temperature and hydrogen coverage*, Phys. Rev. B **56**, 13367 (1997).

[125] S. Hollemann and F. Rebentrost, *Tight-binding modle calculations of the nonlinear optical response of free and hydrogenated Si(111) surfaces*, Surf. Sci. **331**, 1342 (1995).

[126] V. I. Gavrilenko and F. Rebentrost, *Nonlinear optical susceptibility of the (111) and (001) surfaces of silicon*, Appl. Phys. A **60**, 143 (1995).

[127] B. S. Mendoza, A. Gaggiotti, and R. D. Sole, *Microscopic theory of second harmonic generation at Si(100) surfaces*, Phys. Rev. Lett. **81**, 3781 (1998).

[128] T. F. Heinz and U. Höfer, *Nonlinear optical processes at semiconductor surfaces*, Surf. Sci. Rep. (in preparation).

[129] G. Lüpke, D. J. Bottomley, and H. M. van Driel, *Second- and third-harmonic generation from cubic centrosymmetric crystals with vicinal faces: phenomenological theory and experiment*, J. Opt. Soc. Am. B **11**, 33 (1994).

[130] P. Bratu, *Optische Frequanzverdopplung an Si(111)*7 × 7*: Adsorption, Dissoziation und Desorption von Sauerstoff*, Dissertation, Ludwig-Maximilians-Universität, 1993.

[131] C. Wittenzellner, *Untersuchungen zum Adsorptionsverhalten von Ammoniak auf Silizium und Rhenium mit Second-Harmonic Generation*, Dissertation, Ludwig-Maximilians-Universität, München, 1993.

[132] P. Bratu, K. L. Kompa, and U. Höfer, *Kinetics of oxygen dissociation on Si(111)*-(7×7) *investigated with optical second-harmonic generation*, Phys. Rev. B **49**, 14070 (1994).

[133] P. Feulner and D. Menzel, *Simple ways to improve "flash desorption" measurements from single crystal surfaces*, J. Vac. Sci. Technol. **17**, 662 (1980).

[134] H. Schlichting and D. Menzel, *Techniques for wide range, high resolution and precision, thermal desorption measurements*, Surf. Sci. **285**, 209 (1993).



[135] *Thermocouple calibration tables and alloy data*, Omega Engeneering Inc., Stanford, 1971.

[136] J. J. Boland, *Scanning tunneling microscopy study of the adsorption and recombinative desorption of hydrogen from the Si(100)*2 × 1 *surface*, J. Vac. Sci. Technol. A **10**, 2458 (1992).

[137] A. Ishizaka and Y. Shiraki, *Low temperature surface cleaning of silicon and its application to silicon MBE*, J. Electrochem. Soc. **133**, 666 (1986).

[138] G. Ertl and J. Küppers, *Low energy electrons and surface chemistry* (VCH, Weinheim, 1985).

[139] M. A. van Hove, W. H. Weinberg, and C.-M. Chan, in *Springer series in surface science 6*, edited by G. Ertl and R. Gomer (Springer, Berlin, 1986).

[140] T. F. Heinz, M. M. T. Loy, and W. A. Thompson, *Study of Si(111) surfaces by optical second-harmonic generation: reconstruction and surface phase transformation*, Phys. Rev. Lett. **54**, 63 (1985).

[141] M. P. D'Evelyn, M. M. Nelson, and T. Engel, *Kinetics of the adsorption of $O_2$ and of the desorption of SiO on Si(100): A molecular beam, XPS, and ISS study*, Surf. Sci. **186**, 75 (1987).

[142] W. Ranke and D. Schmeisser, *Adsorption of water on a cylindrical silicon crystal*, Surf. Sci. **149**, 485 (1985).

[143] M. Kuchler and F. Rebentrost, *Adsorbate-induced changes of linear and nonlinear electronic-response properties and second-harmonic generation at simple metal surface*, Phys. Rev. B **50**, 5651 (1994).

[144] U. Höfer, A. Puschmann, D. Coulman, and E. Umbach, *Adsorption of molecular oxygen on Si(111)*, Surf. Sci. **211**, 948 (1989).

[145] U. Höfer, P. Morgen, W. Wurth, and E. Umbach, *Initial stages of oxygen adsorption on Si(111). II. The molecular precursor*, Phys. Rev. B **40**, 1130 (1989).

[146] F. C. Tompkins, *Chemisorption of gases on metals* (Academic Press, London, 1978).

[147] U. Höfer, *Documentation APS: Analyse and Plot Spectra*, Physik-Department E20, Technische Universität München, 1986.

[148] U. Höfer, *Hochauflösende Photoelektronen-Spektroskopie an Oberflächen: Linienform, Verlustprozesse und Anwendungen*, Dissertation, Technische Universität München, 1989.

[149] A. Zangwill, *Physics at surfaces* (Cambridge Universtiy Press, Cambridge, 1988).

[150] G. A. Somorjai, *Introduction to surface chemistry and catalysis* (Wiley, New York, 1994).

[151] K. D. Rendulic, *The influence of surface defects on adsorption and desorption*, Appl. Phys. A **47**, 55 (1988).

[152] J. H. G. Owen, K. Miki, D. R. Bowler, C. M. Goringe, I. Goldfarb, and G. A. D. Briggs, *Gas-source growth of group IV semiconductors: I. Si(001) nucleation mechansims*, Surf. Sci. **394**, 79 (1997).

[153] J. H. G. Owen, K. Miki, D. R. Bowler, C. M. Goringe, I. Goldfarb, and G. A. D. Briggs, *Gas-source growth of group IV semiconductors: II. Growth regimes and the effect of hydrogen*, Surf. Sci. **394**, 91 (1997).

[154] R. S. Becker, G. S. Higashi, Y. J. Chabal, and A. J. Becker, *Atomic scale conversion of clean Si(111):H-*$1 \times 1$ *to Si(111)-*$2 \times 1$ *by electron-stimulated desorption*, Phys. Rev. Lett. **65**, 1917 (1990).

[155] D. A. Hansen, M. R. Halbach, and E. G. Seebauer, *Experimental measurements of fast adsorption kinetics of* $H_2$ *on vicinal Si(100) and Si(111) surfaces*, J. Chem. Phys. **104**, 7338 (1996).

[156] R. J. Phaneuf and E. D. Williams, *Surface phase separation of vicinal Si(111)*, Phys. Rev. Lett. **58**, 2563 (1987).

[157] R. C. Weast, *in CRC Handbook of Chemistry and Physics* (CRC Press, Boca Raton, Florida, 1987).

[158] P. Kratzer, R. Russ, and W. Brenig, *Ab initio quantum dynamics of* $H_2$*/Si(100) adsorption/desorption on a 3-D potential*, Surf. Sci. **345**, 125 (1996).

[159] J. H. G. Owen, D. R. Bowler, C. M. Goringe, K. Miki, and G. A. D. Briggs, *Hydrogen diffusion on Si(100)*, Phys. Rev. B **54**, 14153 (1996).

[160] M. Dürr, *Untersuchung der dissoziativen Adsorption von Wasserstoff auf gestuften Silizium(001)-Oberflächen mittels Molekularstahl und optischer Frequenzverdoppelung*, Diploma thesis, Technische Universität München, 1997.

[161] M. Dürr, M. B. Raschke, and U. Höfer, *Dissociative adsorption of molecular hydrogen on silicon surfaces: A SHG/molecular beam investigation*, J. Chem. Phys. (submitted).

[162] E. Pehlke, private communication.



[163] A. Gross, *Reactions at surfaces studied by ab initio dynamics calculations*, Surf. Sci. Rep. **32**, 291 (1998).

[164] A. Biedermann, E. Knoesel, Z. Hu, and T. F. Heinz, *Direct observation of dissociative adsorption of* $H_2$ *on Si(100) induced by atomic H*, Phys. Rev. Lett. (*in press*).

[165] D. R. Bowler, J. H. G. Owen, K. Miki, and G. A. D. Briggs, *Diffusion of paired hydrogen on Si(100)*, Phys. Rev. B **57**, 8790 (1998).

[166] J. Zhang, A. K. Lees, A. G. Taylor, M. H. Xie, B. A. Joyce, Z. Sobiesierksi, and D. I. Westwood, *New hydrogen desorption kinetics from vicinal Si(001) surfaces observed by reflectance anisotopy spectrocopy*, J. Cryst. Growth **175**, 477 (1997).

[167] J. E. Reutt-Robey, D. J. Doren, Y. J. Chabal, and S. B. Christman, *CO diffusion on Pt(111) with time-resolved infrared-pulsed molecular beam methods: Critical tests and analysis*, J. Chem. Phys. **93**, 9113 (1990).

[168] K. Sinniah, J. E. Reutt-Robey, A. R. Brown, and D. J. Doren, *Kinetics of step-site filling for CO/Ni(9,1,1): A pulsed molecular beam-surface infrared study*, J. Chem. Phys. **101**, 764 (1994).

[169] E. Pehlke and P. Kratzer, *Density-functional study of hydrogen chemisorption on vicinal Si(100) surfaces*, Phys. Rev. B **59**, 2790 (1999).

[170] R.-L. Lo, I.-S. Hwang, M.-S. Ho, and T. T. Tsong, *Diffusion of single hydrogen atoms on Si(111)-*$(7 \times 7)$ *surfaces*, Phys. Rev. Lett. **80**, 5584 (1998).

[171] P. A. Williams, G. A. Reider, L. Li, U. Höfer, T. Suzuki, and T. F. Heinz, *Physisorbed template for spatial patterning of adsorbates*, Phys. Rev. Lett. **79**, 3459 (1997).

[172] S. H. Payne and H. J. Kreuzer, *Adsorption and thermal desorption on stepped surfaces*, Surf. Sci. **399**, 135 (1998).

[173] S. Čern y and V. Ponec, *Determination of heat of adsorption on clean solid surfaces*, Catal. Rev. **2**, 249 (1969).

[174] K. Christmann, *Introduction to surface physical chemistry* (Steinkopf, Damstadt, Springer, New York, 1991).

[175] K. Christmann, O. Schober, G. Ertl, and M. Neumann, *Adsorption of hydrogen on nickel single crystal surfaces*, J. Chem. Phys. **60**, 4528 (1974).

[176] S. Černỳ, *Adsorption microcalorimetry in surface science studies. Sixty years of its development into a modern powerful method*, Surf. Sci. Rep. **26**, 1 (1996).

[177] D. A. King, *Femtomole adsorption calorimetry on single-crystal surfaces*, Chem. Rev. **98**, 797 (1998).

[178] S. Černỳ, in *The chemical physics of solid surfaces and heterogeneous catalysis*, edited by D. A. King and D. P. Woodruff (Elsevier, Amsterdam, 1983), Vol. 2, p. 1.

[179] D. M. Young, *Physical adsorption of gases* (Butterworth, London, 1962).

[180] T. F. Heinz, M. M. T. Loy, and W. A. Thompson, *Study of symmetry and disordering of Si(111)*$7 \times 7$ *surfaces by optical second harmonic generation*, J. Vac. Sci. Technol B. **3**, 1467 (1985).

[181] J. J. Lander, *Chemisorption and ordered surface structures*, Surf. Sci. **1**, 125 (1964).

[182] W. Telieps and E. Bauer, *The* $((7 \times 7) \leftrightarrow (1 \times 1)$ *phase transition on Si(111)*, Surf. Sci **162**, 163 (1985).

[183] T. Suzuki and Y. Hirabayashi, *First observation of the Si(111)*-$7 \times 7 \leftrightarrow 1 \times 1$ *phase transition by the optical second harmonic generation*, Jpn. J. Appl. Phys. **32**, L610 (1993).

[184] U. Höfer, L. Li, G. A. Ratzlaff, and T. F. Heinz, *Nonlinear optical study of the Si(111)*$7 \times 7$ *to* $1 \times 1$ *phase transition: Superheating and the nature of the* $1 \times 1$ *phase*, Phys. Rev. B **52**, 5264 (1995).

[185] R. T. Sanderson, *Chemical bonds and bond energies* (Academic Press, New York, 1971).

[186] S. M. Myers, D. M. Follstaedt, H. J. Stein, and W. R. Wampler, *Deuterium bonding at internal surfaces in silicon*, Phys. Rev. B **45**, 3914 (1992).

[187] S. M. Myers, D. M. Follstaedt, H. J. Stein, and W. R. Wampler, *Hydrogen interaction with cavities in helium-implanted silicon*, Phys. Rev. B **47**, 13380 (1993).

[188] W. R. Wampler, S. M. Myers, and D. M. Follstaedt, *Surface silicon-deuterium bond energy from gas-phase equilibration*, Phys. Rev. B **48**, 4492 (1993).

[189] W. R. Wampler, S. M. Myers, and D. M. Follstaedt, *Reply to "Comment on 'Surface silicon-deuterium bond energy from gas-phase equilibration'"*, Phys. Rev. B **55**, 13319 (1996).

[190] C. Herring and C. G. V. de Walle, *Comment on "Surface silicon-deuterium bond energy from gas-phase equilibration"*, Phys. Rev. B **55**, 13314 (1996).



[191] K. L. Brower and S. M. Myers, *Chemical kinetics of hydrogen and (111)Si-*$SiO_2$ *interface defects*, Appl. Phys. Lett. **57**, 162 (1990).

[192] A. H. Edwards, *Interaction of H and* $H_2$ *with the silicon dangling orbital at the* $\langle 111 \rangle$ *Si/*$SiO_2$ *interface*, Phys. Rev. B **44**, 1832 (1991).

[193] R. Walsh, *Bond dissociation energy values in silicon-containing compounds and some of their implications*, Acc. Chem. Res. **14**, 246 (1981).

[194] R. Walsh, in *The chemistry of organic silicon compounds*, edited by S. Patai and Z. Rappoport (Wiley, New York, 1989).

[195] K. Sinniah, M. G. Shermann, L. B. Lewis, W. H. Weinberg, J. J. T. Yates, and K. C. Janda, *Hydrogen desorption from the monohydride phase on Si(100)*, J. Chem. Phys. **92**, 5700 (1990).

[196] S. Pai and D. Doren, *Substituent effects in silicon hydrides: Implications for models of surface sites*, J. Phys. Chem. **98**, 4422 (1994).

[197] C. G. V. de Walle, *Energies of various configurations of hydrogen in silicon*, Phys. Rev. B **49**, 4579 (1994).

[198] K. D. Brommer, M. Galván, J. D. Dal Pino, and J. D. Joannopoulos, *Theory of adsorption of atoms and molecules on Si(111)*-$(7 \times 7)$, Surf. Sci. **314**, 57 (1994).

[199] T. Klitsner and J. S. Nelson, *Site-specific hydrogen reactivity and reverse charge transfer on Ge(111)*-$c(2 \times 8)$, Phys. Rev. Lett. **67**, 3800 (1991).

[200] A. R. Miller, *The adsorption of gases on solids* (Cambridge University Press, Cambridge, 1949).

[201] J. H. D. Boer, *Adsorption phenomena*, Adv. in Catal. **8**, 17 (1956).

[202] M. Hartmann. et al., (in preparation).

[203] T. Engel, *The interaction of molecular and atomic oxygen with Si(100) and Si(111)*, Surf. Sci. Rep. **18**, 91 (1993).

[204] U. Höfer, P. Morgen, W. Wurth, and E. Umbach, *Metastable molecular precursor for the dissociative adsorption of oxygen on Si(111)*, Phys. Rev. Lett. **55**, 2979 (1985).

[205] N. F. Mott, S. Rigo, F. Rochet, and A. M. Stoneham, *Oxidation of silicon*, Philos. Mag. B **60**, 189 (1989).

[206] H. C. Lu, E. P. Gusev, E. Garfunkel, and T. Gustafsson, *An ion scattering study of the interaction of oxygen with Si(111): surface roughening and oxide growth*, Surf. Sci. **351**, 111 (1996).

[207] J. R. Engstrom, D. J. Bonser, M. M. Nelson, and T. Engel, *The reaction of atomic oxygen with Si(100) and Si(111)*, Surf. Sci. **256**, 317 (1991).

[208] A. Feltz, U. Memmert, and R. J. Behm, *High temperature scanning tunneling microscopy studies on the interaction of $O_2$ with Si(111)-(7 × 7) surfaces*, Surf. Sci. **314**, 34 (1994).

[209] Y. Ono, M. Tabe, and H. Kageshima, *Scanning-tunneling-microscopy observation of thermal oxide growth on Si(111)7 × 7 surfaces*, Phys. Rev. B **48**, 14291 (1993).

[210] A. A. Shklyaev and T. Suzuki, *Branching of critical conditions for Si(111)-(7 × 7) oxidation*, Phys. Rev. Lett. **75**, 272 (1995).

[211] M. Liehr, J. E. Lewis, and G. W. Rubloff, *Kinetics of high-temperature thermal decomposition of $SiO_2$ on Si(111)*, J. Vac. Sci. Technol. A **5**, 1559 (1987).

[212] G. W. Rubloff, *Defect microchemistry in $SiO_2$/Si structures*, J. Vac. Sci. Technol. A **8**, 1857 (1990).

[213] K. E. Johnson and T. Engel, *Direct measurement of reaction kinetics for the decomposition of ultrathin oxide on Si(001) using scanning tunneling microscopy*, Phys. Rev. Lett. **69**, 339 (1992).

[214] J. V. Seiple and J. P. Peltz, *Scanning tunneling microscopy study of oxide nucleation and oxidation-induced roughening at elevated temperatures on the Si(001)-(2 × 1) surface*, Phys. Rev. Lett. **73**, 999 (1994).

[215] R. Martel, P. Avouris, and I.-W. Lyo, *Molecularly adsorbed oxygen species on Si(111)-(7 × 7): STM-induced dissociative attachment studies*, Science **272**, 385 (1996).

[216] H. W. K. Tom, X. D. Zhu, Y. R. Shen, and G. A. Somorjai, *Investigations of the Si(111)-(7 × 7) surface by second-harmonic generation: Oxidation and the effects of surface phosphorus*, Surf. Sci **167**, 167 (1986).

[217] K. Nakamura, A. Kurokawa, and S. Ichimura, *Comparison of initial oxidation of Si(111)7 × 7 with ozone and oxygen investigated by second harmonic generation*, J. Vac. Sci. Technol. A **15**, 2441 (1997).

[218] J. R. Arthur and A. Y. Cho, *Adsorption and desorption kinetics of Cu and Au on (0001) graphite*, Surf. Sci. **36**, 641 (1973).



[219] G. Hollinger, J. F. Morar, F. J. Himpsel, G. Hughes, and J. J. Jordan, *Si(111) surface oxidation: O 1s core-level study using synchrotron radiation*, Surf. Sci. **168**, 609 (1986).

[220] P. Morgen, U. Höfer, W. Wurth, and E. Umbach, *Initial stages of oxygen adsorption on Si(111): the stable state*, Phys. Rev. B **39**, 3720 (1989).

[221] G. Dujardin, G. Comtet, L. Hellner, T. Hirayama, M. Rose, L. Philippe, and M. J. Besnard-Ramage, *Site specific and state selective photofragmentation of molecular oxygen on Si(111)-(7 × 7)*, Phys. Rev. Lett. **73**, 1727 (1994).

[222] I.-S. Hwang, R.-L. Lo, and T. T. Tsong, *Site hopping of single chemisorbed oxygen molecules on Si(111)-(7 × 7) surfaces*, Phys. Rev. Lett. **78**, 4797 (1997).

[223] P. Avouris, I.-W. Loy, and F. Bozso, *Atom resolved surface chemistry: The early steps of Si(111)-7 × 7 oxidation*, J. Vac. Sci. Technol. B **9**, 424 (1991).

[224] C. Silvestre and M. Shayegan, *Observation of a metastable precursor for adsorption of oxygen on Si(111) and the activation energy for chemisorption*, Phys. Rev. B **37**, 10432 (1988).

[225] M. Udagawa, Y. Umetani, H. Tanaka, M. Itoh, T. Uchiyama, Y. Watanabe, T. Yokotsuka, and I. Sumitra, *The initial stages of the oxidation of Si(100)2 × 1 studied by STM*, Ultramicroscopy **42**, 946 (1992).

[226] Y.-K. Sun, D. J. Bonser, and T. Engel, *Thermal decomposition of ultrathin oxide layers on Si(100)*, J. Vac. Sci. Technol. A **10**, 2314 (1992).

[227] U. Memmert and M. L. Yu, *Comparison between Si(100) and Si(111) in the reaction with oxygen at high temperatures*, Surf. Sci. Lett. **245**, L185 (1991).

[228] M. L. Yu and B. N. Eldridge, *Real-time study of oxygen reaction on Si(100)*, Phys. Rev. Lett. **58**, 1691 (1987).

[229] K. Ohkubo, Y. Igari, S. Tomoda, and I. Kusunoki, *SiO production from Si(100) and (111) surfaces by reaction with $O_2$ beams*, Surf. Sci. **260**, 44 (1992).

[230] M. C. Flowers, N. B. H. Jonathan, A. Morris, and S. Wright, *The adsorption and reaction of water on Si(100)-2 × 1 and Si(111)-7 × 7 surfaces*, Surf. Sci. **351**, 87 (1996).

[231] V. P. Zhdanov, *Arrhenius parameters for rate processes on solid surfaces*, Surf. Sci. Rep. **12**, 183 (1991).

[232] S. Glasstone, K. J. Laidler, and H. Eyring, *The theory of rate processes* (McGraw-Hill, New York, 1941).

[233] K. J. Laidler, *Theories of chemical reaction rates* (McGraw-Hill, New York, 1969).

[234] K. G. Nakamura and M. Kitajima, *Reactive scattering of $O_2$ with the Si(111) surface: Resonance enhanced multiphoton ionization of SiO*, J. Chem. Phys. **102**, 8569 (1995).

[235] K. G. Nakamura, I. Kamioka, and M. Kitajima, *Dynamics of SiO desorption in reactive scattering of $O_2$ with a silicon surface*, J. Chem. Phys. **104**, 3403 (1996).

[236] B. S. Swartzentruber and M. Schacht, *Kinetics of atomic-scale fluctuations of steps on Si(001) measured with variable-temperature STM*, Surf. Sci. **322**, 83 (1995).

[237] C. Pearson, B. Borovski, M. Krueger, R. Curtis, and E. Ganz, *Si(001) step dynamics*, Phys. Rev. Lett. **74**, 2710 (1995).

[238] X. D. Zhu, T. Rasing, and Y. R. Shen, *Surface diffusion of CO on Ni(111) studied by diffraction of optical second-harmonic generation off a monolayer grating*, Phys. Rev. Lett. **61**, 2883 (1988).

[239] X. D. Zhu and Y. R. Shen, *Generation and detection of a monolayer grating by laser desorption and second-harmonic generation: CO on Ni(111)*, Opt. Lett. **14**, 503 (1989).

[240] G. A. Reider, M. Huemer, and A. J. Schmidt, *Surface second harmonic generation spectroscopy without interference of substrate contributions*, Opt. Commun. **68**, 149 (1988).

[241] T. Suzuki and T. F. Heinz, *Second-harmonic diffraction from a monolayer grating*, Opt. Lett. **14**, 1201 (1989).

[242] W. Zhao, R. W. Verhoef, and M. Ascher, *Diffusion of potassium on Re(001) investigated by coverage grating-optical second-harmonic diffraction*, J. Chem. Phys. **107**, 5554 (1997).

[243] X. D. Zhu, A. Lee, and Y. R. Shen, *Detection of monolayer gratings of adsorbates by linear optical diffractions*, Phys. Rev. B **52**, 317 (1991).

[244] X.-D. Xiao, Y. Xie, and Y. R. Shen, *Surface diffusion probed by linear optical diffraction*, Surf. Sci. **271**, 295 (1992).

[245] J. D. Burgess, P. C. Stair, and E. Weitz, *Calculations of the surface temperature rise and desorption temperature in laser-induced thermal desorption*, J. Vac. Sci. Technol. A **4**, 1362 (1986).



[246] C. H. Mak, J. L. Brand, A. A. Deckert, and S. M. George, *Surface diffusion of hydrogen on Ru(001) studied using laser-induced thermal desorption*, J. Chem. Phys. **85**, 1676 (1986).

[247] E. Conrad and M. B. Webb, *Xe and Kr adsorption on the Si(111)7 × 7 surface*, Surf. Sci. **129**, 37 (1983).

[248] J. E. Demuth and A. J. Schnell-Sorokin, *Rare gas titration studies of Si(111) surfaces*, J. Vac. Sci. Technol. A **2**, 808 (1984).

[249] J. W. Bartha, U. Barjenbruch, and M. Henzler, *Surface structure and thermal desorption spectroscopy on Si(111)*, J. Phys. Chem. **19**, 2459 (1986).

[250] E. G. Michel, P. Pervan, G. R. Castro, R. Miranda, and K. Wandelt, *Structural and electronic properties of K/Si(100)2 × 1*, Phys. Rev. B **45**, 11811 (1992).

[251] L. Utrera and R. Ramirez, *Molecular dynamics simulation of Xe diffusion on the Si(100)2 × 1 surface*, J. Chem. Phys. **96**, 7838 (1992).

[252] D. L. Meixner and S. M. George, *Surface diffusion of xenon on Pt(111)*, J. Chem. Phys. **98**, 9115 (1993).

# Acknowledgements

I am pleased to acknowledge Karl-Ludwig Kompa for the continuous and generous support, much scientific freedom, and research opportunities that he provided. Thanks are due to Dietrich Menzel as my advisor at the Technische Universität.

I am indebted to Ulrich Höfer, who is a dedicated scientist. His high standard for the research we have done and published together have contributed to my growth as a scientist in ways too numerous to count. I had many intense and animated discussions with him, and I learned that his steady advice was of great value as I struggled to take advantage of it.

Deep gratitude goes to Georg Reider, a truly amazing scientist and person, I had the chance to collaborate with. He introduced me to the linear-optical diffraction technique, and his encouragement, patience, and guidance will be a model for my future.

Much is owed to Eckhard Pehlke, who has enriched my understanding of the physics we investigated by putting my intuition on solid theoretical ground. I greatly profited from enlightening discussions in the fruitful collaboration between experiment and theory we had.

I am also obliged to Peter Kratzer and Takanori Suzuki for valuable advice.

In particular I thank Michael Dürr for the great time we had together setting up his molecular-beam experiment under unconventional circumstances. I wish to express sincere appreciation for his encouragement and for many discussions and critical stimuli that I have benefited from.

Of the many other members of the group, our institute, and the university, I am particularly grateful to Karl Bauer, Ralf Ernstdorfer, Peter Feulner, Christoph Gebhardt, Michael Hartmann, Georg Schmitt, Carsten Voelkmann, and Jochen Wanner, all of whom I could rely on at all times.

The Laser Chemistry Division has provided an excellent environment for learning about the various aspects of scientific life. Every taxpayer ultimately payed for this research and I will try to give them a good return on their investment.

# Vita

**Markus B. Raschke**

| | |
|---|---|
| October 19, 1970 | Born in Pegnitz, Germany |
| 1981–90 | Gymnasium in Bayreuth |
| 1990–93 | Universität Bayreuth, majoring in Chemistry and Physics |
| 1992 | Universität Bayreuth, B. S. in Chemistry |
| 1993 | Universität Bayreuth, B. S. in Physics |
| 1994–95 | Graduate School, Department of Physics & Astronomy, Rutgers, The State University of New Jersey, USA |
| 1995 | Rutgers, M. S. in Physics |
| 1995–99 | Max-Planck Insitut für Quantenoptik, Garching, Germany |
| 1999 | Ph. D. in Physics, Technische Universität München, Munich |
| Since Aug. 1999 | University of California at Berkeley, USA |